

BIOMECHANICAL LOADS IN RUNNING-BASED SPORTS:  
ESTIMATING GROUND REACTION FORCES FROM SEGMENTAL  
ACCELERATIONS

Johannes Petrus Verheul

A thesis submitted in partial fulfilment of the requirements of Liverpool John Moores  
University for the degree of Doctor of Philosophy

March 2019

---

## Abstract

---

Training loads are monitored in sports as part of a process which aims to enhance performance whilst simultaneously reducing the risk of injury. Although physiological loads have been investigated extensively, biomechanical loading is still poorly quantified and, therefore, largely unexplored. Ground reaction force (GRF) is a well-established measure of external whole-body biomechanical loading, which drives and contributes to the internal stresses on e.g. muscles, tendons and bones. GRF might thus be used to further understand the relationship between whole-body biomechanical loads and performance and injuries, but valid methods for accurately estimating GRF outside laboratory settings are currently unavailable. However, since GRF is determined by the accelerations of the body's different segments, currently popular body-worn accelerometers might allow for estimating GRF in the field. Therefore, the aim of this thesis was to investigate if GRF can be estimated from segmental accelerations, especially for dynamic and high-intensity running tasks that are frequently performed during running-based sports.

The first two studies showed that a two mass-spring-damper model can be used to accurately reproduce overall GRF profiles and impulses for various high-intensity running tasks, but that this model cannot be used to predict GRF from trunk accelerometry. These results suggest that trunk accelerations alone are insufficient to accurately predict GRF in this manner, but additional information about accelerations of other segments allows for alternative approaches to be explored. Therefore, the third study aimed to estimate GRF from multiple segmental accelerations using a direct mechanical approach. GRF profiles from full-body segmental accelerations were estimated reasonably across dynamic and high-intensity running tasks, but errors substantially increased when the number of segments was reduced. Since these results further support the suggestion that one or several segmental accelerations are unlikely sufficient to estimate whole GRF waveforms, the fourth study aimed to identify key segmental contributions to distinct GRF features using principal component analysis. However, this study showed that dominant segmental acceleration characteristics and associated GRF features, as well as the relative importance of these features, are highly complex and task-specific.

---

Together these findings show that it is unlikely that one or several segmental accelerations can provide accurate and meaningful estimates of GRF across different running activities. These outcomes warrant caution when using body-worn accelerometers to estimate GRF and monitor whole-body biomechanical loads during running-based sports in the field.

---

## Acknowledgements

---

This PhD thesis would not have been possible without the help, advice, guidance, knowledge and support of so many incredible people. I would, therefore, like to use this opportunity to show my appreciation to those who have been a crucial part of my journey to completing this PhD.

First of all, I would like to thank my director of studies, Dr Mark Robinson, for your invaluable guidance and advice throughout my PhD. I appreciate the confidence and interest you have shown in me, the many meetings and discussions on biomechanics and beyond, and your ability to channel my often-overflowing thoughts into a simple summary. I would also like to express my gratitude to my co-supervisors, Professor Paulo Lisboa, for your ability to provide mathematical solutions to all my biomechanical and mathematical problems, and Professor Warren Gregson, for your practical advice and applied input to my research, as well as the reflective discussions about training load monitoring in the field.

My sincere appreciation also goes out to Dr Jos Vanrenterghem, for the interest you have shown in my work, your sharp biomechanical analyses and your ability to always see the relevance of my research. I would like to thank Dr Niels Nedergaard, for your crucial preparatory research and guidance on the two mass-spring-damper model, Dr Mark Pogson, for your tireless help with the Python optimisation script and the numerous mass-spring-damper model experiments, Dr Mark Lake, for the informal discussions and feedback on the use of accelerometry in biomechanics, and Dr Ian Poole, for your technical assistance during my data collections. Furthermore, I would like to thank all my lab mates in the LJMU biomechanics labs throughout the years, without whom my PhD journey would not have been as enjoyable.

Finally, I want to thank my parents, Jan and Petra, for your confidence and belief in me throughout my life, and your endless support in all my academic and sports ambitions. To my beautiful wife, Hannah, for all your love, support, encouragement and patience. To my Lord Jesus Christ, for giving me life, for saving it and keeping it. “For in Him we live and move and have our being” (Acts 17:28).

---

## Publications

---

### Journal articles

- Verheul J., et al. (2019) “Biomechanical loading during running: can a two mass-spring-damper model be used to evaluate ground reaction forces for high-intensity tasks?”. *Sports Biomechanics*.
- Verheul J., et al. (2018) “Whole-body biomechanical load in running-based sports: the validity of estimating ground reaction forces from segmental accelerations”, *Journal of Science and Medicine in Sport*.
- Verheul J., et al. “Identifying key segmental contributions to ground reaction force features across different running tasks”. (Under review).

### Conference papers

- Verheul J., et al. “Mechanical load monitoring in sports: predicting ground reaction forces from segmental accelerations for high-intensity and dynamic tasks”, *The 8<sup>th</sup> World Congress of Biomechanics*, Dublin, Ireland, 8<sup>th</sup> to 12<sup>th</sup> July 2018. (Oral presentation).
- Verheul J., et al. “Mechanical load monitoring: can accelerometers really estimate whole-body stresses?”, *The XXVII Isokinetic Medical Group Conference: Football Medicine Outcomes*, Barcelona, Spain, 2<sup>nd</sup> to 4<sup>th</sup> June 2018. (Oral presentation).
- Verheul J., et al. “Load monitoring in sports: can accelerometers really estimate whole-body mechanical stresses?”, *The annual BASES Biomechanics Interest Group Meeting*, University of Salford, Salford, UK, 4<sup>th</sup> April 2018. (Oral presentation, **award for best podium presentation**).
- Verheul J., et al. “Training load monitoring in soccer: can a mass-spring-damper model reproduce ground reaction forces during dynamic tasks?”, *The 26<sup>th</sup> Congress of the International Society of Biomechanics*, Brisbane, Australia, 23<sup>rd</sup> to 27<sup>th</sup> July 2017. (Oral presentation).
- Verheul J., et al. “Training load monitoring in football: can trunk accelerations predict ground reaction forces using a mass-spring-damper model?”, *The Faculty of Science*

---

*Postgraduate Research Day*, Liverpool John Moores University, Liverpool, UK, 19<sup>th</sup> June 2017. (Oral presentation).

- Verheul J., et al. “Training load monitoring in football: can trunk accelerations predict ground reaction forces using a mass-spring-damper model?”, *The annual BASES Biomechanics Interest Group Meeting*, University of Portsmouth, Portsmouth, UK, 19<sup>th</sup> April 2017. (Poster presentation).
- Verheul J., et al. “Predicting whole-body loading from accelerometry in football”, *The Faculty of Science Postgraduate Research Day*, Liverpool John Moores University, Liverpool, UK, 20<sup>th</sup> June 2016. (Poster presentation).

---

# Table of contents

---

<b>Abstract</b> .....	<b>II</b>
<b>Acknowledgements</b> .....	<b>IV</b>
<b>Publications</b> .....	<b>V</b>
<b>Table of contents</b> .....	<b>VII</b>
<b>List of figures</b> .....	<b>X</b>
<b>List of tables</b> .....	<b>XVI</b>
<b>Symbols and acronyms</b> .....	<b>XVII</b>
<b>Chapter 1: General introduction</b> .....	<b>1</b>
<b>Chapter 2: Literature review</b> .....	<b>5</b>
2.1 Training load monitoring .....	6
2.1.1 <i>Load differentiation: external vs internal – physiological vs biomechanical</i> ..	8
2.2 Body-worn sensors.....	9
2.2.1 <i>Global positioning systems</i> .....	10
2.2.2 <i>Accelerometers</i> .....	11
2.3 Ground reaction forces.....	14
2.3.1 <i>Ground reaction forces as a measure of biomechanical loading</i> .....	17
2.3.2 <i>Measuring ground reaction forces in the field</i> .....	19
2.4 Mass-spring models .....	21
2.4.1 <i>The mass-spring model</i> .....	21
2.4.2 <i>Multi-body mass-spring-damper models</i> .....	23
2.5 Summary .....	26
2.6 Thesis aim and objectives .....	27
<b>Chapter 3: Using a two mass-spring-damper model to reproduce ground reaction forces for high-intensity running tasks</b> .....	<b>28</b>
3.1 Introduction.....	29
3.2 Methods.....	31
3.2.1 <i>Participants and protocol</i> .....	31
3.2.2 <i>Kinetic data collection</i> .....	31
3.2.3 <i>Modelling ground reaction forces</i> .....	32
3.2.4 <i>Data processing and analysis</i> .....	33
3.3 Results.....	34
3.4 Discussion.....	40
3.5 Conclusion .....	43
<b>Chapter 4: Predicting ground reaction forces from trunk accelerations with a two mass-spring-damper model</b> .....	<b>44</b>

---

4.1	Introduction.....	45
4.2	Methods.....	46
	4.2.1 <i>Participants and protocol</i> .....	46
	4.2.2 <i>Kinetic and accelerometry data collection</i> .....	47
	4.2.3 <i>Directly predicting ground reaction forces from trunk accelerations</i> .....	47
	4.2.4 <i>Indirectly predicting ground reaction forces from trunk accelerations</i> .....	48
	4.2.5 <i>Data processing and analysis</i> .....	49
4.3	Results.....	49
	4.3.1 <i>Direct ground reaction force predictions</i> .....	49
	4.3.2 <i>Indirect ground reaction force predictions</i> .....	52
4.4	Discussion.....	53
	4.4.1 <i>Directly predicting ground reaction forces from trunk accelerations</i> .....	53
	4.4.2 <i>Indirectly predicting ground reaction forces from trunk accelerations</i> .....	54
	4.4.3 <i>Using trunk accelerations for biomechanical load monitoring purposes</i> .....	57
	4.4.4 <i>Limitations</i> .....	58
4.5	Conclusion .....	58
<b>Chapter 5: Validating ground reaction forces estimated from multiple segmental accelerations .....</b>		<b>60</b>
5.1	Introduction.....	61
5.2	Methods.....	62
	5.2.1 <i>Participants and protocol</i> .....	62
	5.2.2 <i>Kinematic and kinetic data collection</i> .....	63
	5.2.3 <i>Data processing and analysis</i> .....	64
5.3	Results.....	67
	5.3.1 <i>Estimated ground reaction force from fifteen segments</i> .....	67
	5.3.2 <i>Segment reductions</i> .....	69
5.4	Discussion .....	72
	5.4.1 <i>Estimating ground reaction forces from fifteen segments</i> .....	72
	5.4.2 <i>Segment reductions</i> .....	74
	5.4.3 <i>Using accelerometers to estimate ground reaction forces</i> .....	75
5.5	Conclusion .....	76
<b>Chapter 6: Identifying key segmental contributions to ground reaction force features ...</b>		<b>77</b>
6.1	Introduction.....	78
6.2	Methods.....	79
	6.2.1 <i>Data</i> .....	79
	6.2.2 <i>Normalisation and scaling</i> .....	79
	6.2.3 <i>Principal component analysis</i> .....	81

---

6.2.4	<i>Principal accelerations and principal ground reaction forces</i> .....	82
6.3	Results.....	83
6.4	Discussion.....	89
6.4.1	<i>Implications for load monitoring purposes</i> .....	90
6.4.2	<i>Limitations</i> .....	93
6.5	Conclusion.....	94
<b>Chapter 7:</b>	<b>General discussion</b> .....	<b>95</b>
7.1	Introduction.....	96
7.2	Implications for biomechanical load monitoring practice.....	96
7.2.1	<i>The two mass-spring-damper model approach</i> .....	97
7.2.2	<i>Trunk accelerations to assess biomechanical loading?</i> .....	98
7.3	The value of ground reaction force as a biomechanical load measure.....	100
7.3.1	<i>Ground reaction forces in running-based sports</i> .....	101
7.3.2	<i>How good is good enough?</i> .....	101
7.3.3	<i>External vs internal biomechanical loads</i> .....	103
7.3.4	<i>Cumulative biomechanical loading</i> .....	104
7.4	Future applications and technologies.....	105
7.4.1	<i>Body-worn accelerometers</i> .....	106
7.4.2	<i>Implantable sensors</i> .....	107
7.4.3	<i>Markerless motion capture</i> .....	108
7.4.4	<i>Machine learning</i> .....	109
<b>Chapter 8:</b>	<b>Conclusion</b> .....	<b>111</b>
<b>Appendices</b> .....		<b>113</b>
Appendix A:	The two mass-spring-damper model.....	114
Appendix B:	Comparing solving methods: gradient descent vs. numerical optimisation.....	116
Appendix C:	The relationship between measured trunk accelerations and the two mass-spring-damper model's upper mass acceleration.....	120
Appendix D:	Bounding the two mass-spring-damper model's parameter search spaces.....	125
Appendix E:	Fixing the two mass-spring-damper model's parameter values.....	129
Appendix F:	Simultaneously modelling trunk accelerations and ground reaction forces.....	133
Appendix G:	Marker attachment locations.....	137
Appendix H:	Marker trajectory filter cut-off frequencies.....	138
Appendix I:	Measuring segmental accelerations: motion capture vs. accelerometers.....	141
Appendix J:	Task specific principal component analysis.....	145
<b>References</b> .....		<b>149</b>

---

## List of figures

---

<b>Figure 1.1</b> The multi-layered biomechanical load sphere, in which the core reflects biomechanically meaningful, field-based, and valid and reliable biomechanical load measurements. Current accelerometry derived load measures are easily measurable in the field but have limited biomechanical meaning, while biomechanical research relies on relevant load metrics but is primarily laboratory based.....	3
<b>Figure 2.1</b> <i>A</i> : Training stimuli followed by a sufficient recovery period leads to supercompensation and increased physical capacity/health. <i>B</i> : Insufficient recovery or excessive loads can lead to negative adaptations. These maladaptations can cause an athlete to have a reduced capacity/health to withstand training loads, and an increased risk of injury. ( <i>This figure was taken and adjusted from figures 1 and 2 in Soligard et al. (2016) and figure 2.1 in Meeusen and de Pauw (2013)</i> ).....	6
<b>Figure 2.2</b> <i>A</i> : A commercial GPS device (OptimEye S5, Catapult Innovations, Scoresby, Australia) with an in-built tri-axial accelerometer sampling at 100 Hz. GPS devices are typically worn in a tight-fitting vest on the back of the upper trunk. <i>B</i> : A tri-axial accelerometer (DTS 3D 518, Noraxon Inc, Scottsdale, AZ, USA) sampling at 1000 Hz. These units can be used for laboratory- or field-based research and can be attached to different body segments.....	11
<b>Figure 2.3</b> The biomechanical load-response-adaptation chain with ground reaction forces as the external biomechanical load measure. (note: internal musculoskeletal responses and adaptations are examples and are not exhaustive). .....	16
<b>Figure 2.4</b> <i>A</i> : the single mass-spring model consisting of the total body mass BM on a spring with stiffness k and length y without ( $y_1$ ) and with ( $y_2$ ) external loading respectively. <i>B</i> : a typical measured ground reaction force profile for running at $4 \text{ m}\cdot\text{s}^{-1}$ (black solid line) and predicted force profile from the mass-spring model (red dashed line).....	22
<b>Figure 3.1</b> Representative examples of measured (black solid line) and modelled (red dotted line) ground reaction forces (GRF) including the root mean square error (RMSE) between both	

---

curves. GRF curves for accelerations and running at high speeds did not always contain a distinct impact peak (A, G).....	37
<b>Figure 3.2</b> Measured, modelled and error values for the impulses, impact peaks and loading rates. Negative and positive errors are a respective underestimation and overestimation of the measured value.....	38
<b>Figure 3.3</b> Model parameter values for the different tasks including means (black dotted line) and standard deviations (SD; grey dashed line) for accelerations, decelerations, and low, moderate and high-speed running. For visualisation purposes, extreme individual outliers have been removed from the plots.....	39
<b>Figure 4.1</b> Diagram of how measured trunk accelerations (TA) were used to directly predict ground reaction forces (GRF) with the two mass-spring-damper model.....	48
<b>Figure 4.2</b> Diagram of how measured trunk accelerations (TA) were used to indirectly predict ground reaction force (GRF) via a regression analysis. If there was a correlation between the modelled upper mass acceleration $a_1$ (replicated TA) and GRF parameter values, this relationship was used to recalculate the parameter before calculating the predicted GRF profiles.....	49
<b>Figure 4.3</b> Representative examples of measured trunk accelerations (TA; black solid line) with modelled $a_1$ curves (blue dotted line) on the left, and the measured ground reaction force (GRF; black solid line) and directly predicted GRF profiles (red dotted line) on the right, including the root mean square error (RMSE) between both curves. ....	51
<b>Figure 4.4</b> Scatter plots of the eight model parameters for each individual acceleration (blue circles), deceleration (red triangles) and low, moderate and high-speed running (light grey, dark grey and black crosses respectively) trial. Parameter values required to model trunk accelerations (TA) or ground reaction force (GRF) are plotted on the x-axes and y-axes respectively.....	52
<b>Figure 5.1</b> <i>A</i> : A seventy-six retroreflective marker set was attached to anatomical landmarks and marker trajectories were recorded during the trials. <i>B</i> : Tracked marker trajectories in the Qualisys Tracking Manager (QTM) software for an example running trial (top) and static calibration trial (bottom). <i>C</i> : Marker trajectories were used to build a fifteen-segment kinematic model in Visual3D. ....	64

---

**Figure 5.2** To maintain total body mass, segment masses not included in a combination were redistributed. Body parts were defined as the core (head, trunk, pelvis), the left and right arm (hand, forearm, upper arm), and the left and right leg (foot, shank, thigh). For example, if a combination did not include the shank, its mass was equally distributed over the foot and thigh (1), core segments if neither the thigh or foot were included (2), or all segments in the combination if no core segments were included either (3). ..... 65

**Figure 5.3** Swarm plot of the root mean square errors (RMSE) for ground reaction force (GRF) curves estimated from fifteen segmental accelerations. *Inset:* representative measured (black solid line) and estimated (red dashed line) GRF profiles, together with RMSE values for all acceleration (n=167), deceleration (n=162), 90° cut (n=171), low (n=158), moderate (n=157) and high-speed running (n=141) trials. .... 67

**Figure 5.4** Correlation (A-C) and Bland-Altman (D-F) plots between measured and estimated GRF loading characteristics impulse, impact peak and loading rate, from fifteen segments. ... 69

**Figure 5.5** Root mean square errors (RMSE), impulse, impact peak and loading rate errors for estimated GRF profiles for each task. Bars represent the percentage of trials (primary y-axis) within the very low (<1 N·kg<sup>-1</sup>), low (1-2 N·kg<sup>-1</sup>), moderate (2-3 N·kg<sup>-1</sup>), high (3-4 N·kg<sup>-1</sup>) or very high (>4 N·kg<sup>-1</sup>) error boundaries, and black dots represent the mean errors (secondary y-axis), for each given number of segments. .... 71

**Figure 6.1** Representative example of individual and summed ground reaction force (GRF) profiles reconstructed from the first five principal components (PCs), for a single participant running at a constant moderate speed. Individual principal GRFs (PGRFs; grey dotted lines) were added together as the summed PGRFs ( $\sum$ PGRFs; grey solid lines) for the first k PCs and compared to the measured GRF (black solid line) by the curve root mean square error (RMSE). ..... 85

**Figure 6.2** Mean principal ground reaction forces (PGRFs) calculated from the first five principal components (PCs), for each task. PGRFs were calculated from principal accelerations (PAs) reconstructed from either the k<sup>th</sup> PC (top row), or the sum of the first k PCs ( $\sum$ PGRF<sub>1-k</sub>; middle row). Root mean square errors (RMSE; bottom row) are mean errors for the  $\sum$ PGRF

---

profiles and the horizontal black line represents the RMSE for $\sum$ PGRFs from all 45 PCs (i.e. the original data).....	86
<b>Figure 6.3</b> Principal accelerations (PAs) from the first five principal components (rows) for accelerations (blue), decelerations (red) and 90° cuts (green). PA profiles are mean $\pm$ standard deviation (shaded) curves from 0-100% of stance, for all fifteen segments (columns).....	87
<b>Figure 6.4</b> Principal accelerations (PAs) from the first five principal components (rows) for running at constant low (light grey), moderate (grey) and high speeds (black). PA profiles are mean $\pm$ standard deviation (shaded) curves from 0-100% of stance, for all fifteen segments (columns).....	88
<b>Figure 7.1</b> The multi-layered biomechanical load sphere. While the two mass-spring-damper model (2MSD) studies were located towards the surface of the sphere, ground reaction forces estimated from multiple segments demonstrated the potential for moving towards the core of the sphere. The complexity revealed by the principal component analysis (PCA) highlights the difficulty of moving towards the core.....	98
<b>Figure A.1</b> The two mass-spring-damper model.....	114
<b>Figure C.1</b> Representative examples of trunk accelerations (TA) and upper mass accelerations ( $a_1$ ), and measured, predicted and modelled ground reaction forces (GRF) for different tasks. Although TA could be replicated well by the model's $a_1$ (blue dashed line), the predicted GRFs (red dashed line) were poor. Required $a_1$ (blue dotted line) to accurately model GRF (red dotted line) strongly deviated from the TA for all tasks.....	121
<b>Figure C.2</b> Quadratic fitted trunk acceleration ( $TA_Q$ ) signals were used as input for the model's upper mass acceleration ( $a_1$ ) to predict GRF. General TA curve shapes showed different shapes between the different tasks (A, D, G, J). Although the model was able to accurately fit the modelled $a_1$ to the $TA_Q$ (B, E, H, K), predicted GRF was still very poor (C, F, I, L).....	123
<b>Figure D.1</b> Scatter plots of the eight model parameters for each individual acceleration (blue circles), deceleration (red triangles) and low, moderate and high-speed running (light grey, dark grey and black crosses respectively) trial. Parameter values required to model trunk accelerations (TA) or ground reaction force (GRF) are plotted on the x-axes and y-axes respectively.....	127

---

<b>Figure E.1</b> Example of scatter plots of the eight model parameter values required to model TA and GRF when three parameters ( $\omega_1$ , $\omega_2$ , $\lambda$ ) were fixed at a constant value. Scatter plots include each individual acceleration (blue circles), deceleration (red triangles) and low-, moderate- and high-speed (light grey, dark grey and black crosses respectively) trial. Parameter values required to model trunk accelerations (TA) or ground reaction force (GRF) are plotted on the x-axes and y-axes respectively.....	131
<b>Figure F.1</b> Diagram of how measured trunk accelerations (TA) and ground reaction forces (GRF) were simultaneously modelled with the two mass-spring-damper model.....	134
<b>Figure F.2</b> Representative examples of measured trunk accelerations (TA; black solid line) and modelled $a_1$ (blue dotted line) on the left, and the measured ground reaction force (GRF; black solid line) and predicted GRF (red dotted line) on the right, when simultaneously modelled. Across the different tasks TA and GRF could not both be reproduced well at the same time, using the same set of model parameters.....	136
<b>Figure G.1</b> Attachment locations of segment tracking markers (blue), segment defining markers (red) and markers used for both (black).....	137
<b>Figure H.1</b> Representative examples of measured ground reaction force (GRF; black solid line) profiles and GRF estimated from marker trajectories filtered at 25 Hz (blue dotted line), 20-10 Hz (red dashed line) or 10 Hz (green dashed line), for each task.....	139
<b>Figure I.1</b> Attachment of the Noraxon DTS 3D accelerometer to the marker cluster plate (A), back of the pelvis (B), and medial side of the thigh (C) and shank (D).....	142
<b>Figure I.2</b> Representative examples of segmental accelerations from motion capture-based marker trajectories (MoCap; black solid line) and accelerometry (Acclrm; blue dotted line). Columns represent the segmental accelerations of the left/right shank and thigh, and pelvis, while rows represent the different tasks.....	143
<b>Figure J.1</b> Mean principal ground reaction forces (PGRFs) calculated from the first five principal components (PCs), for each task. PGRFs were calculated from principal accelerations (PAs) reconstructed from either the $k^{\text{th}}$ PC (top row), or the sum of the first $k$ PCs ( $\sum \text{PGRF}_{1-k}$ ; middle row). Root mean square errors (RMSE; bottom row) are mean errors for the $\sum \text{PGRF}$	

---

profiles and the horizontal black line represents the RMSE for  $\sum$ PGRFs from all 45 PCs (i.e. the original data). ..... 147

**Figure J.2** Root mean square error (RMSE) values for ground reaction forces (GRFs) reconstructed from k summed principal components ( $PC_k$ ). Mean and standard deviations (SD) of RMSEs for summed principal GRFs were compared between the task-specific (blue solid line and shaded area) principal component analysis (PCA) or a PCA on all data combined (red solid line and shaded area). ..... 148

---

## List of tables

---

<b>Table 3.1</b> Modelled ground reaction force curve and loading characteristics errors .....	36
<b>Table 3.2</b> Mean $\pm$ standard deviation values for the eight model parameters for the different tasks .....	39
<b>Table 4.1</b> Modelled upper mass acceleration and ground reaction force errors.....	50
<b>Table 4.2</b> Linear regressions for the eight model parameters .....	53
<b>Table 5.1</b> Estimated ground reaction force curve and loading characteristics errors.....	68
<b>Table 5.2</b> Combinations of segments with the lowest root mean square errors for each number of segments .....	70
<b>Table 6.1</b> Principal components and ground reaction forces for the different tasks .....	83
<b>Table A.1</b> Equations describing the eight natural parameters of the two mass-spring-damper model .....	115
<b>Table B.1</b> Modelled ground reaction force curve and loading characteristics errors.....	118
<b>Table B.2</b> The eight numerical solvers.....	119
<b>Table D.1</b> Modelled trunk acceleration and ground reaction force curve errors using a free and bound parameter search space.....	127
<b>Table E.1</b> Linear regressions for the eight model parameters with free, bound and fixed parameters .....	131
<b>Table F.1</b> Modelled curve errors for $a_1$ and ground reaction force.....	134
<b>Table H.1</b> Marker trajectory filter cut-off frequency comparison.....	140

---

## Symbols and acronyms

---

$a_1$	Acceleration of the upper mass in the two mass-spring-damper model
$a_2$	Acceleration of the lower mass in the two mass-spring-damper model
$c$	Damping coefficient of the damper in the two mass-spring-damper model
CoM	Centre of mass
$g$	Gravitational acceleration ( $-9.81 \text{ m}\cdot\text{s}^{-2}$ )
GPS	Global positioning system
GRF	Ground reaction force
$\text{GRF}_{\text{estimated}}$	Ground reaction force estimated from multiple segmental accelerations
$\text{GRF}_{\text{measured}}$	Ground reaction force measured with a force platform embedded in the ground
$\text{GRF}_{\text{modelled}}$	Ground reaction force modelled using the two mass-spring-damper model
$k$	Stiffness of the spring in a single mass-spring model
$k_1$	Stiffness of the upper spring in the two mass-spring-damper model
$k_2$	Stiffness of the lower spring in the two mass-spring-damper model
$l_1$	Natural length of the upper spring in the two mass-spring-damper model
$l_2$	Natural length of the lower spring in the two mass-spring-damper model
$\lambda$	Mass ratio of the lower mass relative to the total body mass in the two mass-spring-damper model
$\lambda_k$	Eigenvalue of the $k^{\text{th}}$ eigenvector in the principal component analysis
BM	Total body mass
$m_1$	Mass of the upper mass in the two mass-spring-damper model
$m_2$	Mass of the lower mass in the two mass-spring-damper model

---

$\omega_1$	Natural frequency of the upper spring in the two mass-spring-damper model
$\omega_2$	Natural frequency of the lower spring in the two mass-spring-damper model
PA	Principal acceleration
PC	Principal component
PCA	Principal component analysis
PGRF	Principal ground reaction force
RMSE	Root mean square error
TA	Trunk accelerations measured with an accelerometer embedded in a commercial trunk-worn GPS device
$v_1$	Velocity of the upper mass in the two mass-spring-damper model
$v_2$	Velocity of the lower mass in the two mass-spring-damper model
$x_1$	Position of the upper mass in the two mass-spring model without external loading
$x_2$	Position of the lower mass in the two mass-spring model without external loading
$y_1$	Length of the spring in a single mass-spring model without external loading
$y_2$	Length of the spring in a single mass-spring model when externally loaded
$\zeta$	Damping ratio of the damper in the two mass-spring-damper model

---

## **Chapter 1: General introduction**

---

---

Sport outcomes are largely determined by the training an athlete has been exposed to. Training loads are, therefore, monitored to enhance performance whilst reducing the risk of injury. This practice of training load monitoring has developed rapidly since the mid-1970s and is a well-established and widely applied concept amongst sport-scientists, coaches and practitioners today. However, training load measures predominantly aim to quantify and assess the physiological demands of training and/or competition. The biomechanical loads athletes experience on the other hand, are still poorly quantified and are, therefore, relatively unexplored and not well understood (Vanrenterghem et al., 2017). Since the external and internal forces working on the different hard- and soft-tissues of the body are known to damage these structures, sound measures of biomechanical load are required to further investigate the underlying mechanisms of musculoskeletal injuries in running-based sports.

For a biomechanical load measure to be useful for training load monitoring practice, there are three essential components to consider: biomechanical meaning, feasibility for field-based measurement, and validity and reliability of these measurements. Given the interdependence of these requirements, biomechanical load monitoring can be described as a multi-layered sphere (figure 1.1) of which researchers and practitioners should aim to reach the core.

*Biomechanical meaning.* First, it is essential that the measured variable is biomechanically meaningful. For example, heart-rate can be used to assess metabolic training loads but cannot quantify the forces acting on the musculoskeletal system.

*Field-based measurements.* Secondly, it is crucial that the variable can be measured in the field on a daily basis. For example, muscle and tendon stresses can be estimated using motion capture, force platform and musculoskeletal modelling techniques, but these are not typically available in the field, are laborious and time consuming, and thus unfeasible to be used outside laboratory settings.

*Validity and reliability.* Thirdly, consistently accurate measurements are required. For example, overuse injuries are the result of small repetitive structure-specific loads (on

e.g. muscles, bones), and the accumulation of excessive measurement inaccuracies can considerably limit a metric's usability.

In short, training load metrics used for biomechanical load monitoring require a biomechanically meaningful foundation, should allow for day-to-day measurement outside laboratory settings, and need sufficient measurement validity and reliability. However, the multifactorial nature of these requirements makes measuring and evaluating biomechanical loads in running-based sports highly complex.

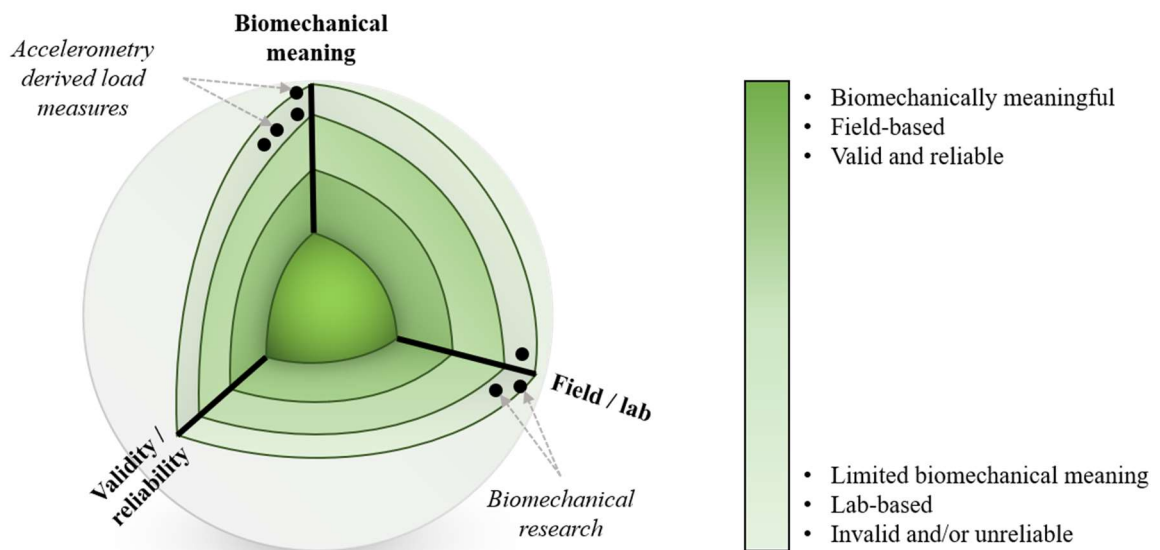


**Figure 1.1** The multi-layered biomechanical load sphere, in which the core reflects biomechanically meaningful, field-based, and valid and reliable biomechanical load measurements. Current accelerometry derived load measures are easily measurable in the field but have limited biomechanical meaning, while biomechanical research relies on relevant load metrics but is primarily laboratory based.

Current load monitoring methods use accelerometry-based load measures such as PlayerLoad or Body Load to quantify the overall (external) biomechanical loads on the body (Boyd et al., 2011; Ehrmann et al., 2016). These metrics are typically derived from accelerometers embedded in trunk-worn GPS devices, which are commonly used in running-based sports. Consequently, trunk acceleration-based variables are easily measurable in the field and have also been shown to have reasonable reliability and validity (Barrett et al., 2015, 2014). However, a biomechanical

---

underpinning of these load metrics is yet lacking and hence, their biomechanical meaning and usefulness is questionable. Therefore, despite their field-based nature, accelerometry derived load measures are thus at the surface of the biomechanical load sphere (figure 1.1).

Biomechanical research relies heavily on the precise quantification of forces acting in and on the body during movement (Winter, 2009). These forces are typically measured directly with force platforms (external forces) or can be estimated in combination with kinematics measured from three-dimensional motion capture systems (internal forces) (Damsgaard et al., 2006; Seth et al., 2018). These techniques thus allow for valid and reliable measurement of biomechanically meaningful variables. However, force platform and motion capture technologies are not typically available in field settings (e.g. running track, football pitch), which limits their use to laboratories only. Therefore, despite their biomechanical relevance and high accuracy, force measures are also at the surface of the biomechanical load measure sphere (figure 1.1).

Researchers and practitioners use different measures of biomechanical load to evaluate the musculoskeletal demands of sports. Nevertheless, techniques for accurately and reliably measuring biomechanically meaningful metrics in the field are yet unavailable. However, given the direct relationship between forces and accelerations, as described by Newton's second law ( $F=m \cdot a$ ), accelerations of individual segments might allow for estimating forces acting in and on the body. With the current popularity of body-worn accelerometers especially, this might eventually allow for more meaningful biomechanical load monitoring in running-based sports. It is, however, still largely unexplored whether segmental accelerations can provide meaningful measures of biomechanical load in the field, while maintaining sufficient accuracy for their application. This thesis sets out to get to the core of this problem.

---

## **Chapter 2: Literature review**

---

The aim of this review is to provide a summary of the existing literature associated with the topics of this thesis. First, the concept of monitoring training loads in sports will be explained and its importance emphasised. Several training load aspects will be discussed including the load-adaptation paradigm and the differentiation between internal/external and physiological/biomechanical loads. Secondly, an overview of currently available methods for measuring and monitoring training loads in the field will be provided. The use of popular global positioning systems and accelerometers especially, will be discussed and the strengths and weaknesses of these technologies highlighted. Thirdly, the use of ground reaction forces as a measure of external whole-body biomechanical load will be introduced. The usefulness of ground reaction force measurements outside laboratory settings, as well as the shortcomings of current technologies to do this, will be explained. Fourthly, an overview of mass-spring models that have been used to predict and evaluate ground reaction forces in sport contexts will be presented. Several applications of these models, including their limitations, will be described and the novel use of a two mass-spring-damper model in a training load context will be presented. Finally, the aim and objectives of this thesis will be specified to set the scene for the studies described in the following chapters.

## 2.1 Training load monitoring

Performance in sports is largely determined by the training an athlete has been exposed to. Systematic exposure to different training stimuli can lead to responses in the aerobic, cardiovascular and musculoskeletal system, which can lead to positive physical adaptations and ultimately enhanced sporting performance (figure 2.1 A). Distance running for example, has been shown to lead to an increased aerobic capacity ( $VO_2$  max) resulting in faster running times (Daniels et al., 1978). However, inadequate or excessive training loads, in combination with insufficient recovery times, could lead to no or even negative adaptations (maladaptation) and a reduced capacity to withstand training loads, causing an athlete to be at increased risk of injury or illness (Drew and Finch, 2016; Eckard et al., 2018; Kibler et al., 1992; Soligard et al., 2016; Windt and Gabbett, 2017) (figure 2.1 B). A well-designed training programme therefore requires a balanced periodization of adequate training frequency, volume and intensity to trigger positive adaptations, as well as sufficient recovery times (Bompa and Buzzichelli, 2019).

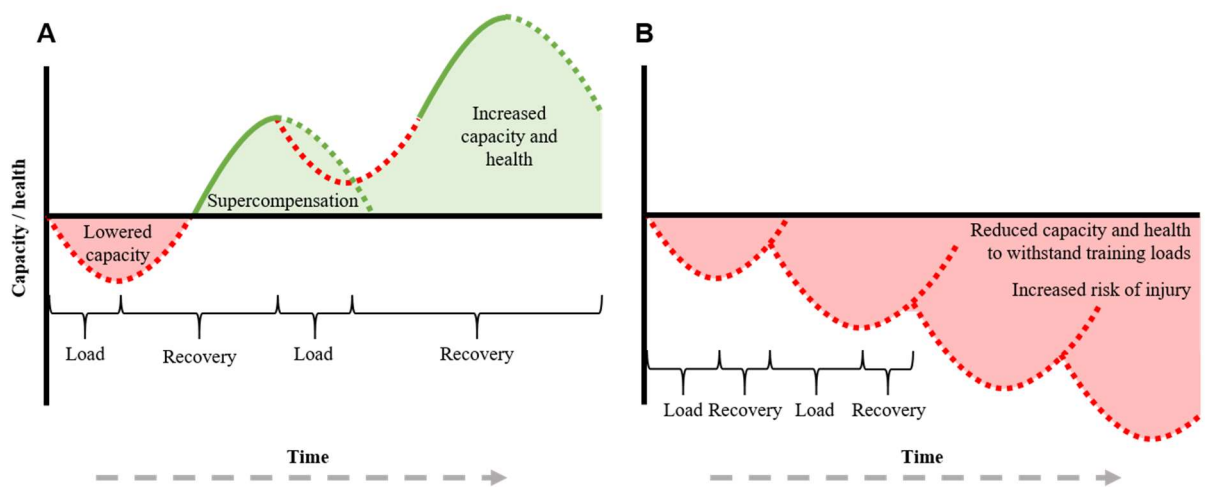


**Figure 2.1 A:** Training stimuli followed by a sufficient recovery period leads to supercompensation and increased physical capacity/health. **B:** Insufficient recovery or excessive loads can lead to negative adaptations. These maladaptations can cause an athlete to have a reduced capacity/health to withstand training loads, and an increased risk of injury. (This figure was taken and adjusted from figures 1 and 2 in Soligard et al. (2016) and figure 2.1 in Meeusen and de Pauw (2013)).

---

Optimal training prescription mainly aims to enhance athletic performance, whilst simultaneously reducing the risk of injury. To achieve this, a thorough understanding of the applied stimuli and desired outcomes, as well as the dose-response relationships between these factors, is essential. Although this association between the training loads imposed on an athlete (dose) and the resulting physical reaction (response) is a well-established concept (Eckard et al., 2018), dose-response relationships are often nonlinear and multifactorial, and therefore difficult to predict (McLaren et al., 2018; Weston, 2013). The importance of accurately quantifying the loads experienced during training, together with monitoring these loads over time, has therefore been highlighted as critical for attaining positive adaptations and subsequent performance improvements (Foster et al., 2001; Mujika, 2013).

Training loads are monitored in sports as part of a process which aims to determine if and how (individual) athletes adapt to the prescribed training stimuli, predict performance, fitness and fatigue outcomes, and reduce the risk of injury and illness (Bourdon et al., 2017). Although simple measures of time, distance and heart-rate are known to have been used for training load monitoring purposes since the 1930s (Foster et al., 2017), the first attempts to describe the effects of physical training on athletic performance were made in the mid-1970s (Banister et al., 1975; Calvert et al., 1976). These authors suggested a training impulse (TRIMP) model based on systems theory to predict performance outcomes from several fitness and fatigue parameters. Over the last four decades, training load monitoring has rapidly gained popularity and numerous TRIMP-like approaches (Busso, 2003; Morton et al., 1990; Wood et al., 2005), as well as other models (Hellard et al., 2006; Hulin et al., 2016; Jobson et al., 2009; Noakes, 2000) have been suggested and applied to guide training programmes and predict performance, fitness and fatigue outcomes. Today, training load monitoring is a well-established and widely applied concept amongst sport-scientists (Bourdon et al., 2017), and perceived as beneficial and worthwhile by the majority of coaches and practitioners (Weston, 2018).

---

### 2.1.1 *Load differentiation: external vs internal – physiological vs biomechanical*

Due to the recognised value of training load monitoring for evaluating specific dose-response relationships, together with the increased knowledge and technological improvements, an abundance of load measures have been used to assess the physical demands of training (Akenhead and Nassis, 2016; Cardinale and Varley, 2017; Mujika, 2017). This large amount of load metrics can, however, make it difficult to interpret and distinguish between the different aspects of training. Therefore, a separation between external load, which can be defined as the work and activities performed by the athletes, and internal load, which is the physiological stress induced by this training and is essential for mediating adaptations to exercise, has been suggested (Akubat et al., 2013; Impellizzeri et al., 2005). Since external loads are relatively easy to measure, external load metrics have been investigated for their ability to assess the more difficult to measure internal loading. For example, given the relationship between running volume and intensity, and energy expenditure, external measures of running distance, velocity and acceleration have been used to estimate and assess the internal metabolic demands of soccer training (Bangsbo et al., 2006; Gaudino et al., 2014). Moreover, simple and non-invasive rating of perceived exertion (RPE), which is the self-reported level of intensity of a training session, has been used to evaluate internal loads. RPE has been shown to be related to measures of external loading (Foster et al., 2001; McLaren et al., 2018) and has been used to assess the internal loading in various different sports (Casamichana et al., 2013; Gaudino et al., 2015; Impellizzeri et al., 2004; Lovell et al., 2013; McGuigan and Foster, 2004; Wallace et al., 2009; Weston et al., 2015).

Besides internal and external aspects, training loads can be further differentiated into distinct physiological and biomechanical load-adaptation (or dose-response) pathways (Vanrenterghem et al., 2017). In this separation, the physiological loads include all the biochemical stresses of training that affect the state of the cardiovascular system (e.g. heart, lungs). Examples of internal physiological load parameters include heart rate, oxygen uptake and blood lactate, while metabolic power or distance covered describe the external loads. Biomechanical loading on the other hand, are the forces and stresses acting on/in the different hard- and soft-tissues of the body

---

(e.g. muscles, tendons, ligaments, bones, cartilage), typically resulting from the repetitive collisions with the ground, and pushing off during running. These musculoskeletal stresses can be quantified as either the external ground reaction forces, or the internal joint contact forces and muscle-tendon forces. In contrast to physiological measures, however, techniques to measure the biomechanical demands of training are still lacking and these loads are thus difficult to assess in the field. In short, therefore, differentiating between internal-external and physiological-biomechanical loads can allow for a more detailed and structured evaluation of the physical demands of training, providing that the loading characteristics of interest can be accurately quantified.

## **2.2 Body-worn sensors**

To quantify numerous different loading parameters, body-worn sensors have quickly gained popularity in sports and exercise during recent years. In an annual survey of worldwide fitness trends, wearable technologies went from not being on the list in 2015 to being the most popular fitness trend in 2016, 2017 and 2019 (Thompson, 2018, 2016, 2015), and was in the top three in 2018 (Thompson, 2017). Consequently, a wide range of body-worn sensors has become available for use in sports, including heart rate monitors (HRMs), near-infrared spectroscopy (NIRS), electromyographic (EMG) sensors, global positioning systems (GPS), and micro-electrical mechanical systems (MEMS) or inertial measurement units (IMUs), such as accelerometers, magnetometers and gyroscopes (Camomilla et al., 2018; Cardinale and Varley, 2017; Cummins et al., 2013; Düking et al., 2016). The commercial availability of these sensors at a relatively low cost provides athletes, coaches, practitioners and researchers with an abundance of information to assess training and fitness. Therefore, much research in the field of sport and exercise has focussed on the use of wearable technologies to quantify and monitor the internal and external training loads to which athletes are exposed. Body-worn GPS devices and accelerometers especially, have received a lot of attention for their ability to measure the external loads of training and competition.

---

### 2.2.1 *Global positioning systems*

GPS is a satellite-based navigation network which provides measurements of location and time, which was originally developed by the American Department of Defence for military use. Technological improvements have, however, allowed for relatively cheap commercial availability of wearable GPS devices. As a result, GPS been introduced in a wide range of sports and has become increasingly popular to assess the external loads of training today. The compact GPS units (e.g. 95x52 mm for a Catapult OptimEye S5) are typically worn on the back of the upper trunk in a pocket of a tight-fitting vest (figure 2.2 A), and continuously measure an athlete's positional data during training or competition. Since their first use in sports in the early 2000s, GPS sampling frequencies have improved from 1 Hz in the original systems to 10 Hz or even 15 Hz today. With this increased sampling frequency the validity and reliability of GPS units has also improved considerably (Johnston et al., 2014; Rampinini et al., 2015; Scott et al., 2015) and GPS devices have been shown to be an accurate and reliable means to measure total distance and running velocity (Coutts and Duffield, 2010; Johnston et al., 2014; Rampinini et al., 2015; Varley et al., 2012). Therefore, a wide variety of metrics including total distance covered, running velocity, accelerations and decelerations, and distance covered within specific speed and/or acceleration threshold zones are currently derived from GPS and used to assess external training loads (Akenhead and Nassis, 2016; Cummins et al., 2013). However, it has also been suggested that 10 Hz might be the optimum sampling frequency when using GPS in highly dynamic sports (Johnston et al., 2014; Scott et al., 2015), and that accuracy can be comprised for movements at higher speeds (e.g. accelerating  $>4 \text{ m}\cdot\text{s}^{-2}$ ) (Akenhead et al., 2014; Coutts and Duffield, 2010; Rampinini et al., 2015; Varley et al., 2012). The additional use of IMUs embedded in current GPS devices to assess training loads has, therefore, been explored.



**Figure 2.2** *A*: A commercial GPS device (OptimEye S5, Catapult Innovations, Scoresby, Australia) with an in-built tri-axial accelerometer sampling at 100 Hz. GPS devices are typically worn in a tight-fitting vest on the back of the upper trunk. *B*: A tri-axial accelerometer (DTS 3D 518, Noraxon Inc, Scottsdale, AZ, USA) sampling at 1000 Hz. These units can be used for laboratory- or field-based research and can be attached to different body segments.

### 2.2.2 Accelerometers

Besides GPS, the use of IMUs to monitor training loads in sports has become increasingly popular. Technological developments have allowed IMUs to substantially reduce in size as well as cost, and most current GPS devices now contain built-in accelerometers, gyroscopes and/or magnetometers. Of these IMUs, sport scientists and practitioners have mainly focussed on the accelerometer, which provides a measure of acceleration in one (uni-axial) or three directions (tri-axial). These local accelerations provide a means to track real-time changes in velocity of the segment to which the unit is attached (figure 2.2 B) and are characterised by the frequency and intensity of the segmental movements. Since their first applications in human movement

---

studies in the 1950s, accelerometers have been used in laboratory based, as well as field studies, to analyse human gait (Saunders et al., 1953; Seel et al., 2014; Tao et al., 2012), quantify movement patterns (Cavagna et al., 1961; Kavanagh and Menz, 2008), monitor physical activity and energy expenditure (Bouten et al., 1994; Troiano et al., 2014), assess running mechanics (Buchheit et al., 2015; Lafortune, 1991; McGregor et al., 2009; Reenalda et al., 2016), estimate the physiological demands of running (McGregor et al., 2009; Murray et al., 2017), and detect and evaluate sport-specific movements (Blair et al., 2018; Chambers et al., 2015; Nedergaard et al., 2014).

One of the main reasons for the recent growth in popularity of accelerometers in sports is that they overcome some limitations of GPS. Accelerometers do not require the use of a satellite, allowing their use indoors, and typically have a much higher sampling frequency (100 Hz or more) compared to GPS units. Despite studies that have questioned the reliability and validity of different types of accelerometers (Nicolella et al., 2018; Sperlich and Holmberg, 2016), other studies have shown these units to be reliable and accurate in a laboratory environment, as well as on the field (Boyd et al., 2011; Hollville et al., 2016; Kelly et al., 2015; Simons and Bradshaw, 2016). In addition, accelerometers embedded within GPS devices have been found to provide valid measures of distinct acceleration characteristics such as the peak acceleration during walking, jogging and running (Rowlands and Stiles, 2012; Wundersitz et al., 2015a), jumping and landing tasks (Rowlands and Stiles, 2012; Simons and Bradshaw, 2016; Tran et al., 2010), and team sports movements (Wundersitz et al., 2015b). However, other findings suggest that certain GPS-embedded accelerometers might have a reduced reliability and validity when measuring the absolute acceleration magnitudes or peak accelerations, especially for movements at higher intensities (Kelly et al., 2015; Wundersitz et al., 2015a; Ziebart et al., 2017).

In contrast to GPS, which measures an athlete's global movements, accelerometry can be used to assess local segmental motion. Various studies have, therefore, investigated the ability of accelerometers to detect sport-specific actions and evaluate performance (Camomilla et al., 2018; Chambers et al., 2015; Dellaserra et al., 2014). The aim of such research is to understand

---

specific movements in more detail and/or provide coaches with a tool to analyse and assess technique. Examples of sport-specific activity evaluations, includes the detection of tackles and physical collisions in rugby (Gabbett et al., 2010; Wundersitz et al., 2015c), bowling in cricket (McNamara et al., 2015) and throwing in baseball (Koda et al., 2010), quantification of kicking biomechanics in different football codes (Blair et al., 2018), classification of strokes and serves in tennis (Ahmadi et al., 2009; Connaghan et al., 2011), differentiation of swing patterns in golf (Lai et al., 2011), quantification of swimming technique (Beanland et al., 2014; Stamm et al., 2013), and movement identification in snowboarding (Harding et al., 2008), cross-country skiing (Marsland et al., 2012) and running-based team sports (Nedergaard et al., 2014; Wundersitz et al., 2015d). Although most studies have focused on using a single unit, others have investigated the use of multiple accelerometers (e.g. Ahmadi et al. (2017), Lai et al. (2011)), or a combination of accelerometers with other IMUs (e.g. gyroscopes and magnetometers) (McNamara et al., 2015; Wundersitz et al., 2015d). Despite the large number of studies that have shown the capability of accelerometers to provide information about specific actions in different sports, others have found contrasting results (Gabbett, 2013; Gastin et al., 2014; Mitschke et al., 2018; Ziebart et al., 2017). These authors have suggested that measured biomechanical parameters might be strongly dependent on the type of sensor, operating range and detection algorithms used. Similarly, Chambers et al. (2015) highlighted that the manufacturer and sampling rate of IMU devices used to detect sport-specific movements is a crucial factor for the quality of research and translation to the field.

Several (trunk-) accelerometry derived training load measures have been used to assess external biomechanical loading. These parameters include PlayerLoad (Barrett et al., 2014; Boyd et al., 2011; Scott et al., 2013), (New) Body Load (Ehrmann et al., 2016; Lovell et al., 2013; McLean et al., 2018; Weaving et al., 2014), Force Load (Colby et al., 2014) and Dynamic Stress Load (Gaudino et al., 2015). However, the measure that has arguably received the most of attention is PlayerLoad. This external load parameter is typically derived from accelerations measured at the back of the upper trunk and is defined as the square root of the sum of the squared rate of change of accelerations of the three accelerometer axes, scaled by a factor 100 and given in

---

arbitrary units. Some studies have found PlayerLoad to have a strong relationship with external load measures such as total distance covered (Casamichana et al., 2013; Gallo et al., 2015; Green, 2018; Polglaze et al., 2015; Scott et al., 2013), as well as internal load measures like oxygen uptake ( $\text{VO}_2$ ) and energy expenditure (Walker et al., 2016), heart rate (Barrett et al., 2014) and ratings of perceived exertion (RPE) (Casamichana et al., 2013; Gallo et al., 2015; Scott et al., 2013). PlayerLoad has therefore been suggested to be used as a replacement for other load metrics that cannot be measured. For example, PlayerLoad might be used as a substitute for the total distance covered in situations where GPS is not available (e.g. indoor sport facilities), or to assess fatigue and/or injury risk (Akenhead et al., 2017; Barrett et al., 2016). However, other studies have suggested that PlayerLoad might not be an accurate loading metric for comparisons between different athletes due to its large inter-athlete variability (Barrett et al., 2014), which might be due to differences in the way the accelerometers are worn. Differences in accelerometer fitting has for instance been found to strongly affect accumulated trunk-accelerometry derived loads of running, agility and tackling activities (McLean et al., 2018). Moreover, it has also been suggested that lower-limb movement strategies cannot be well assessed and/or altered based on the PlayerLoad metric (Barrett et al., 2015, 2014), likely due to the placement of accelerometers between the Scapulae, and thus away from the lower limbs. For the same reason, caution should be taken when using PlayerLoad or similar accelerometry derived load measures from a single accelerometer as a measure of whole-body biomechanical loading, which is the result of the body's centre of mass (CoM) movement and not the trunk or any other individual segment.

### **2.3 Ground reaction forces**

Despite the abundance of currently available load metrics to assess the physical demands of training (Akenhead and Nassis, 2016), most parameters primarily aim to quantify physiological loads. Biomechanical load measures on the other hand, are still limited and have, therefore, been relatively unexplored (Vanrenterghem et al., 2017). Ground reaction forces (GRFs), resulting from the repetitive collisions with the ground during running, are a well-established measure of whole-body biomechanical loading. These external forces cause internal stresses to the different

---

hard- and soft-tissues of the body (Edwards, 2018; Loundagin et al., 2018; Scott and Winter, 1990) and are known trigger several internal responses which play a critical role in the adaptation process of for instance bones (Frost, 1987; Rosa et al., 2015), muscles (Timmins et al., 2016; Wisdom et al., 2015) and tendons (Bohm et al., 2015; Wang et al., 2013), from the molecule to the organ. In the biomechanical load-response-adaptation pathway described by Vanrenterghem et al. (2017), external GRFs can thus be understood as the first step in a chain of internal responses, which lead to musculoskeletal (mal)adaptations (figure 2.3). GRF could, therefore, be a good candidate to further investigate the role of external biomechanical loading in relation to internal responses and adaptations, which might eventually be used in sports for a variety of purposes such as performance enhancement, injury prevention and rehabilitation.

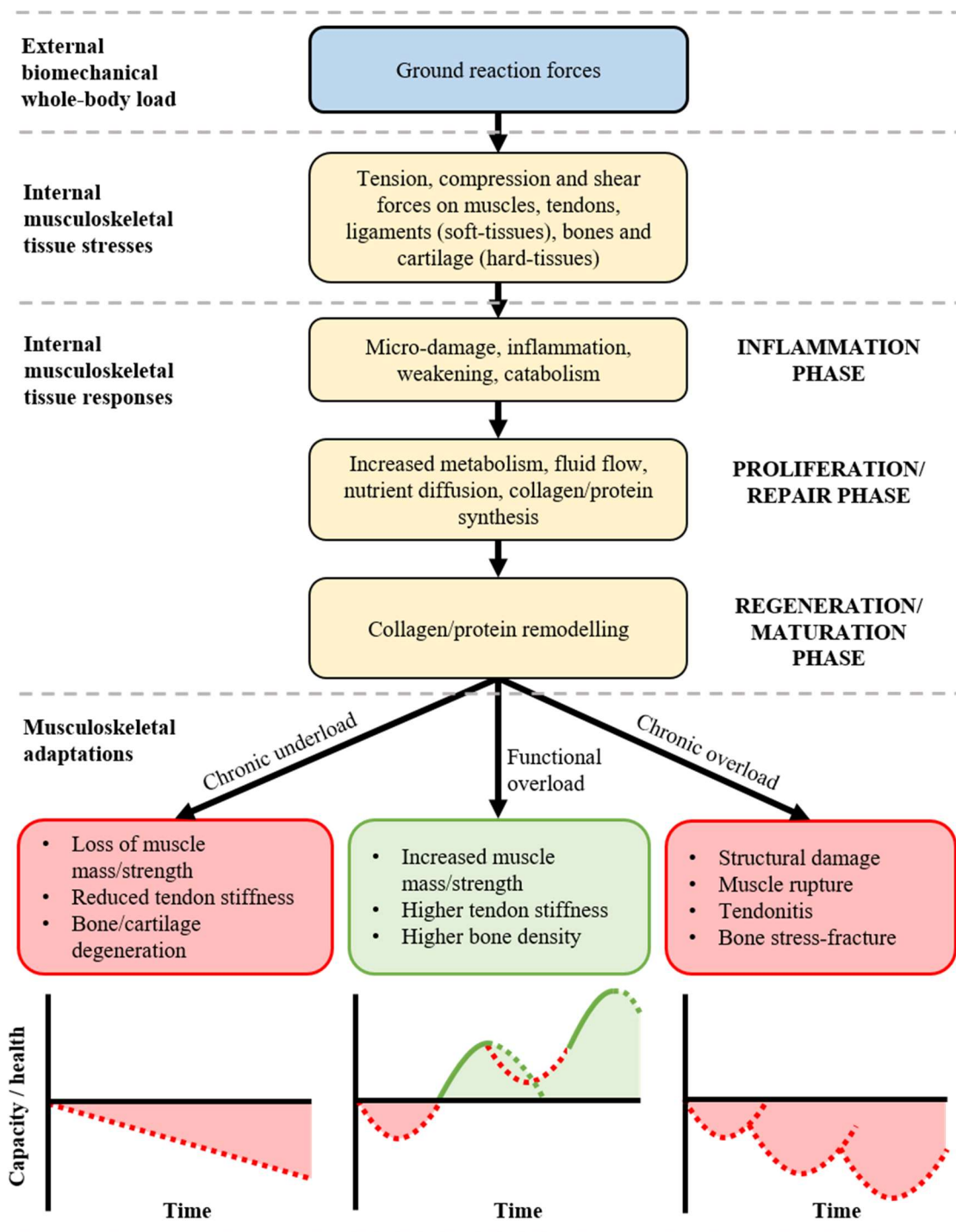


**Figure 2.3** The biomechanical load-response-adaptation chain with ground reaction forces as the external biomechanical load measure. (note: internal musculoskeletal responses and adaptations are examples and are not exhaustive).

---

### 2.3.1 *Ground reaction forces as a measure of biomechanical loading*

To start with, measurement of GRF in the field could provide a novel tool for performance assessment and optimisation. For example, GRF profiles could be used to evaluate running technique, based on which athletes could be given direct technical feedback in the field to optimise their performance. Previous studies have shown that GRF might be used to assess and optimise sprint performance in (team sport) athletes (Bezodis et al., 2017; Hunter et al., 2005; Kugler and Janshen, 2010; Nagahara et al., 2017; Rabita et al., 2015), identify leg asymmetries in sprinters (Udofa et al., 2017), improve running economy (Heise and Martin, 2001; Kyröläinen et al., 2001; Moore, 2016) or reduce injury-related GRF loading characteristics in runners (Clansey et al., 2014; Willy et al., 2016). In addition, since the relationships between external and internal stresses are yet difficult to determine (McLaren et al., 2018; Weston, 2013), monitoring GRF could lead to a more in-depth understanding of the biomechanical dose-response relationship. With GRF as an external measure of biomechanical loading, the relationship with internal responses of muscles, tendons, bones, ligaments and cartilage could be further explored, which would allow for investigating the required external biomechanical dose required to achieve the desired positive internal responses and adaptations. This might eventually aid the optimisation of training prescription and ultimately performance enhancements.

Secondly, monitoring GRF and specific (injury-related) loading characteristics could help to identify abnormalities and the potential risk of injury. Numerous studies have suggested several aspects of the GRF to be related to musculoskeletal overuse injuries, including vertical impact force peaks (Cavanagh and LaFortune, 1980; Clement and Taunton, 1981; Grimston et al., 1993; Hreljac, 2004; Hreljac et al., 2000), vertical loading rates (Bredeweg et al., 2013; Davis et al., 2016; Hreljac, 2004; Milner et al., 2006; van der Worp et al., 2016; Zadpoor and Nikooyan, 2011a) and horizontal braking forces (Gottschall and Kram, 2005; Napier et al., 2018). In addition, the magnitude of such loading characteristics has been shown to be directly affected by fatigue (Bazuelo-Ruiz et al., 2018; Christina et al., 2001; Degache et al., 2016; Grimston et al., 1994; Lazzer et al., 2015; Morin et al., 2011; Paquette and Melcher, 2017), while spectral

---

analyses of GRF profiles have been shown to be able to highlight (leg specific) running-induced fatigue in real-time (Halabi et al., 2017). Specific characteristics of the GRF, as well as the whole curve, could thus be used as markers to indicate whether an athlete is at increased risk of injury. Therefore, access to continuous measurements of GRF in applied sport settings would offer a powerful tool for injury prevention.

Thirdly, monitoring and evaluating GRF as discussed above would provide further insight and understanding of the biomechanical demands of different tasks performed during training and competition. As a result, rehabilitation programmes and return-to-sport decisions can be based on whether an athlete is able to produce required forces and withstand biomechanical loads experienced during these activities. Based on their personal GRF data, athletes suffering from injury can be prescribed a sufficient biomechanical workload to strengthen the injured tissues, whilst avoiding overload of other tissues or the risk of re-injury (Ardern et al., 2016; Blanch and Gabbett, 2016). For example, it has been reported that load distribution in the lower limbs during running can be influenced by altering foot-strike pattern (Almeida et al., 2015; Dickinson et al., 1985; Hamill et al., 2014; Williams III et al., 2012), footwear (Dickinson et al., 1985; Firminger and Edwards, 2016; Nigg et al., 1987), step frequency (Firminger and Edwards, 2016; Heiderscheit et al., 2011; Hobara et al., 2012) or running volume and speed (Nagel et al., 2008; Verheul et al., 2017), which might thus be used to emphasise (un)loading of the injured tissues. Moreover, the ability of an athlete to tolerate the cumulative GRF loading typically experienced during competition could form an important part of return-to-sport criteria. Therefore, GRF measurements could also be a valuable tool after injury has occurred, to guide rehabilitative training and aid return-to-sport decision making.

In summary, accurate GRF measurements could be used in various sport contexts. Measuring and monitoring GRF would allow for separating the physiological and biomechanical load-adaptation pathways (Vanrenterghem et al., 2017) and hence, further investigation and a more detailed understanding of the biomechanical demands of training and competition.

---

Consequently, training prescription could be further optimised to enhance performance, prevent injuries, inform rehabilitation programmes and/or aid return-to-sport decision.

### 2.3.2 *Measuring ground reaction forces in the field*

In laboratory settings, GRF is typically measured with force platforms embedded in the ground. The first attempts of such measurements date back to the first half of the 20<sup>th</sup> century (Amar, 1920; Fenn, 1930, 1924) and mainly focussed on direct quantifications of anteroposterior shear components of the GRF. A few decades later, when more advanced force platforms became available, the first systematic studies investigating GRF of running were performed (e.g. Cavagna et al., 1964; Cavanagh and Lafortune, 1980; Munro et al., 1987). Today, force platforms are highly accurate and are generally used as the ‘gold-standard’ for GRF measurements (Winter, 2009). However, force platforms are expensive, can only measure GRF for a single step at a time and are not typically available outside laboratory settings. Hence, other approaches are required to measure or estimate GRF in the field for GRF to be used as a training load monitoring tool.

Alternative methods exist to estimate GRF without the use of force platforms. For example, various types of instrumented insoles, which measure the pressure the foot exerts on the ground, have been used to estimate GRF for different tasks (Ramirez-Bautista et al., 2017). However, the validity of pressure insoles to measure GRF is typically restricted to walking only (Forner Cordero et al., 2004; Jung et al., 2014; Liu et al., 2010), since the accuracy of estimated GRFs decreases for more sport-specific tasks such as running and jumping (Park et al., 2016; Ramirez-Bautista et al., 2017). Furthermore, issues such as restricted movement due to limited sole flexibility and added mass in the shoe, battery life, the number of sensors required, sensor signal coverage, high cost and the inability to measure the shear components of GRF, still limit the extensive use of pressure insoles (Ramirez-Bautista et al., 2017). Other studies have suggested that GRF might be estimated from flight time, vertical acceleration of the lower limb during landing and ground contact time (Clark et al., 2017, 2014; Udofa et al., 2016). However, the validity of this approach has currently only been verified for straight running at constant speeds

---

and requires highly accurate spatiotemporal input which is not typically available in the field. More recently, several studies have aimed to use machine learning and/or neural network approaches to predict GRF from marker trajectory data (Johnson et al., 2018b, 2018a) or body-worn accelerometers (Pogson et al., n.d.; Wouda et al., 2018) for a variety of running tasks. Despite the promising results, however, computational methods typically do not allow for exploring the underlying physical mechanisms of the predicted GRF profiles which might limit their use for e.g. explaining injury mechanisms or defining performance enhancing criteria. In short, these different methods are thus not feasible to be used to estimate and monitor GRF in non-laboratory settings.

A simple mechanical approach to estimate GRF is by using whole-body CoM accelerations. Based on Newton's second law, which states that the force acting on an object equals the mass of that object multiplied by its acceleration ( $F=m \cdot a$ ), GRF could be predicted as the product of an athlete's mass and CoM acceleration. Given the widespread use and relatively easy accessibility of body-worn accelerometers in sports, this simple method might open the door for measuring CoM, and consequently, estimating GRF in non-laboratory settings. However, due to the CoM constantly changing position during movement it is virtually impossible to attach an accelerometer unit on, or even close to the body's CoM. Nevertheless, several studies have investigated whether body-worn accelerometers can be used to either provide reasonable estimates of the whole-body CoM acceleration (Edwards et al., 2018; Nedergaard et al., 2017; Schütte et al., 2015; Wundersitz et al., 2013), or directly estimate GRF (Gurchiek et al., 2017; Neugebauer et al., 2014; Raper et al., 2018). Some of these studies have suggested that fatigue induced deviations in dynamic CoM motion might be detected (Schütte et al., 2015) or GRF directly predicted (Gurchiek et al., 2017; Neugebauer et al., 2014) for several straight walking and running tasks, using a trunk- or pelvis-mounted accelerometer respectively. However, given the reported errors of GRF estimates in these studies, their application for load monitoring purposes is questionable. Moreover, other studies have shown that accelerometers placed on the shank, pelvis or trunk all substantially overestimated the actual CoM (Edwards et al., 2018; Nedergaard et al., 2017), and that shank accelerometers cannot provide valid and reliable

---

measures of GRF (Raper et al., 2018). These authors, therefore, suggested that individual body-worn accelerometers should be used with caution for evaluating GRF and whole-body biomechanical loads. Consequently, other more complex methods (e.g. accelerometry driven biomechanical models) are likely required to estimate GRF from accelerometers in the field.

## **2.4 Mass-spring models**

Since continuous and accurate measurements of GRFs for running-based sports are yet unavailable outside laboratory settings, it is very difficult to investigate how isolated anatomical, kinematic or external parameters affect the GRF (and vice versa) in the field. Therefore, musculoskeletal modelling methods such as OpenSim (Delp et al., 2007; Seth et al., 2018) and AnyBody (Damsgaard et al., 2006) have been used to investigate the relationships between specific aspects of the dynamics of human movement and the external or internal forces acting on the body. These approaches are, however, complex and often require a substantial amount of kinematic and/or kinetic input. A relatively simple method that has been used to describe human motion in relation to GRF on the other hand, is by using mass-spring(-damper) models. In these models, which are based on the spring-like (elastic) nature of human running, one or several masses are used to represent the inertial characteristics of various body segments, while springs and dampers represent the energy returning (elastic) and absorbing (damping) properties of the different body tissues respectively. Given their simplicity and adaptability, mass-spring models have been used extensively to study motion of the human body and predict GRF during different activities.

### *2.4.1 The mass-spring model*

The simplest (but arguably the most commonly used) mass-spring model is that of an individual point mass representing the body's total mass, on top of a single spring (Blickhan, 1989; McMahon and Cheng, 1990) (figure 2.4). This mass-spring model assumes a linear vertical downward motion of the body's CoM after touch-down, which is reversed during the second half of ground-contact (Bobbert et al., 1991; Cavanagh and LaFortune, 1980). Following

Hooke's law, which states that the force in a spring is linearly related to its stiffness and compression (or extension), GRF can be calculated according to equation 2.1.

$$\text{GRF} = -k \cdot (y_2 - y_1) + \text{BM} \cdot g \quad (2.1)$$

In which  $k$  represents the linear stiffness of the spring,  $y_1$  and  $y_2$  are the length of the spring without and with external loading respectively,  $\text{BM}$  the total body mass and  $g$  the gravitational acceleration. This equation can be rewritten to determine either the vertical stiffness ( $k_{\text{vert}}$ ) or leg stiffness ( $k_{\text{leg}}$ ) according to equations 2.2 and 2.3.

$$k_{\text{vert}} = \frac{\text{GRF}_{\text{max}}}{\Delta y_{\text{max}}} \quad (2.2)$$

$$k_{\text{leg}} = \frac{\text{GRF}_{\text{max}}}{\Delta L_{\text{max}}} \quad (2.3)$$

In which  $\text{GRF}_{\text{max}}$  is the maximal GRF during ground-contact,  $\Delta y_{\text{max}}$  is the maximal vertical displacement of the body's CoM (mass) and  $\Delta L_{\text{max}}$  the maximal vertical displacement of the leg (spring).

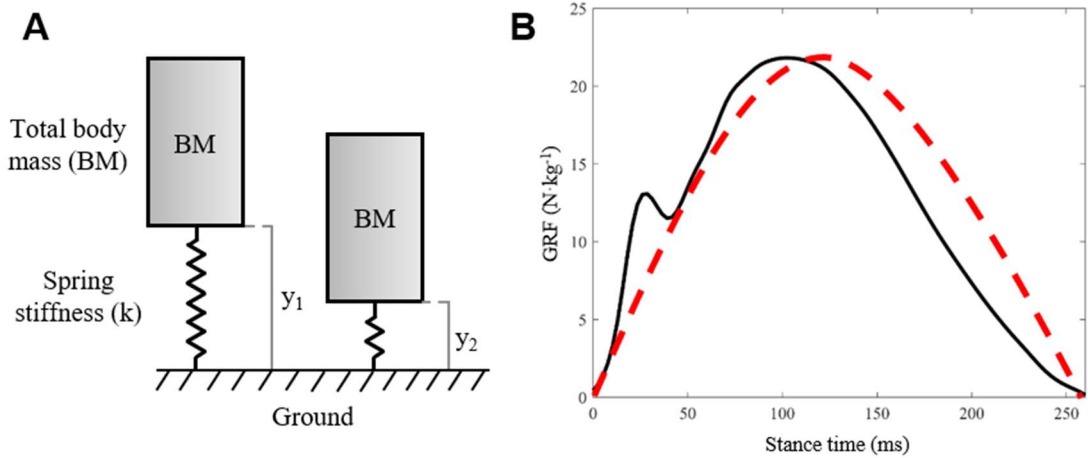


**Figure 2.4** *A*: the single mass-spring model consisting of the total body mass  $\text{BM}$  on a spring with stiffness  $k$  and length  $y$  without ( $y_1$ ) and with ( $y_2$ ) external loading respectively. *B*: a typical measured ground reaction force profile for running at  $4 \text{ m} \cdot \text{s}^{-1}$  (black solid line) and predicted force profile from the mass-spring model (red dashed line).

Although the mass-spring model has mainly been applied to predict GRF and determine vertical and/or leg stiffness for running and hopping (Farley and González, 1996; Geyer et al., 2006; Girard et al., 2017, 2011; McMahan and Cheng, 1990; Morin et al., 2005; Pappas et al., 2014a),

---

this model has also been used to describe various other characteristics of running at different constant speeds, including running economy (Dalleau et al., 1998; Heise and Martin, 1998; McMahon, 1987), stride length, frequency and duration (Blickhan, 1989; Bullimore and Burn, 2007), sprint performance (Arampatzis et al., 1999; Girard et al., 2017, 2016, 2011; Hobara et al., 2010; Morin et al., 2006; Taylor and Beneke, 2012), fatigue effects (Dutto and Smith, 2002; Girard et al., 2011; Morin et al., 2006) and the influence of different surfaces (Ferris et al., 1998; Kerdok et al., 2002). However, despite these various applications of the single mass-spring model, multiple studies have shown that the simple sinusoidal GRF profiles predicted by this model (figure 2.4) are not an accurate representation of the actual asymmetrical GRF of running and impact characteristics associated with landing (Alexander et al., 1986; Bullimore and Burn, 2007; Cavagna, 2006; Clark and Weyand, 2014). High-frequency impact force peaks related to support leg motion typically occur after touch-down, while the rest of the body accounts for a larger active force peak. Changes in these specific GRF loading characteristics have been related to injury, as discussed in section 1.3.1, and have been shown to be directly affected by running speed (Bobbert et al., 1991; Hamill et al., 1983; Kuitunen et al., 2002; Nilsson and Thorstensson, 1989), foot-strike pattern (Clark et al., 2014; Lieberman et al., 2010), footwear (Liu and Nigg, 2000; Zadpoor and Nikooyan, 2010) and surface incline (Gottschall and Kram, 2005). Given the importance of GRF in relation to these aspects, multi-body mass-spring-damper models have been used to model the distinct force characteristics of the GRF more accurately.

#### *2.4.2 Multi-body mass-spring-damper models*

To describe and study the complex behaviour of the human body in more detail, several multi-body mass-spring-damper models have been used. The simplest of these are the models with two masses, such as the two mass model (Clark et al., 2017, 2014; Udofa et al., 2016) and various variations of a two mass-spring-damper model (Alexander et al., 1986; Derrick et al., 2000; Mizrahi and Susak, 1982; Nedergaard, 2017; Ozgüven and Berme, 1988) (see appendix A for a detailed example of the two mass-spring-damper model used in this thesis). In these models, the upper and lower mass typically represent the upper body and support leg respectively, while multiple springs and dampers represent the energy returning and absorbing characteristics of the

---

different body tissues. These studies have shown that two mass-spring-damper models can indeed estimate GRF profiles more accurately (i.e. including the separate impact and active peaks) than the single mass-spring model, for running at different constant speeds up to  $5 \text{ m}\cdot\text{s}^{-1}$  (Derrick et al., 2000; Nedergaard, 2017), different stride lengths (Derrick et al., 2000), changes in direction (Nedergaard, 2017) and jumping (Mizrahi and Susak, 1982; Ozgüven and Berme, 1988). In addition to two mass-spring-damper models, other (more complex) models which consist of three, four or even five masses and a large number of spring and damper elements have been suggested. Such models have mainly been used to investigate GRF and specific physical or external aspects related to running, including different footwear properties (Ly et al., 2010), muscle activity (Nigg and Liu, 1999; Nikooyan and Zadpoor, 2012; Zadpoor and Nikooyan, 2010), mass distributions (Liu and Nigg, 2000), ground stiffness (Ly et al., 2010) and even prosthetic feet (Klute and Berge, 2004). Despite the benefits of more complex and detailed models, however, the added elements also require more model parameters to be estimated, which makes it increasingly difficult to determine parameter values and interpret their physical meaning.

Although mass-spring-damper models have been comprehensively used to study different types of movements, some modelling assumptions are known to violate important characteristics of human motion. For example, the constant stiffness of the springs (and other constant mechanical properties) during the ground contact phase do not accurately represent the variable stiffness of the different body parts, which changes throughout the ground contact phase due to muscular activation (muscle tuning) before and after touch-down (Blickhan, 1989; Nigg and Wakeling, 2001; Santello, 2005; Wakeling et al., 2001). Moreover, the muscles are known to produce a substantial amount of work when pushing the body off the ground (Cavagna, 2006; Winter, 1983), which is not taken into account by any of the elements in the mass-spring-damper models. The absence of energy producing elements is thus a major limitation of the above described passive models. Therefore, some attempts have been made to include active elements representing muscle activity into a four-body model (Nikooyan and Zadpoor, 2012; Zadpoor and Nikooyan, 2010). These studies have, however, shown that mass-spring-damper models are

---

too simplistic to allow for an accurate representation and investigation of the complex coordinated activation of different muscles.

Another limitation of mass-spring-damper models is that they require experimental data not typically available outside a laboratory. For example, the majority of studies have used GRFs measured with a force platform or marker trajectory data to determine the different model parameters and examine the features of interest. However, several studies have investigated the use current body-worn sensors to estimate the parameters of the single mass-spring model. Trunk-mounted GPS devices and the embedded accelerometers especially, have been used to simultaneously determine running velocity ( $v$ ) flight time ( $t_f$ ) and ground contact time ( $t_c$ ). From these variables, the maximal GRF and maximal displacements of the CoM ( $\Delta y_{\max}$ ) and leg ( $\Delta L_{\max}$ ) are then estimated according to equations 2.4-2.6 (Morin et al., 2005).

$$\text{GRF}_{\max} = \frac{\pi}{2} \cdot \left( \frac{t_f}{t_c} + 1 \right) \cdot \text{BM} \cdot g \quad (2.4)$$

$$\Delta y_{\max} = \frac{\text{GRF}_{\max} \cdot t_c^2}{\text{BM} \cdot \pi^2} + g \cdot \frac{t_c^2}{8} \quad (2.5)$$

$$\Delta L_{\max} = L - \sqrt{L^2 - \left( \frac{v \cdot t_c}{2} \right)^2} + \Delta y_{\max} \quad (2.6)$$

In which  $L$  is the initial leg length,  $\text{BM}$  is the total body mass and  $g$  is the gravitational acceleration. Subsequently,  $\Delta y_{\max}$  and  $\Delta L_{\max}$  are then typically used to calculate and evaluate an athlete's vertical and leg stiffness according to equations 2.2 and 2.3. This method has for instance been used to investigate the effects of running on different surfaces (Gaudino et al., 2013), assess sprint performance and fatigue (Girard et al., 2011; Morin et al., 2006), or identify stride imbalances (Buchheit et al., 2015). The reliability and validity of this approach has, however, also been questioned (Eggers et al., 2018) and it remains to be determined how suitable stiffness measures following from an accelerometer driven mass-spring model are. Furthermore, due to the simplicity of the single mass-spring model this method is limited to the investigation of vertical and leg stiffness only.

---

Despite the use of a mass-spring model to assess training load variables, this simple model cannot accurately predict the characteristics of the task-specific GRF profiles for various movements. Multi-body mass-spring-damper models have, however, been shown to be capable of accurately replicating GRFs for different tasks, as discussed above. Since the motion of the masses in these more complex models are typically described by their accelerations, a similar accelerometer-based approach might be used to determine the parameters for these models. For example, commonly trunk-worn accelerometers have been suggested to be used as input for the upper mass in a two mass-spring-damper model and predict GRF (Nedergaard, 2017). However, although initial results for straight running and side-stepping tasks look promising, further research is required to examine whether this novel mass-spring-damper model approach can indeed allow for accurately estimating GRF profiles from body-worn accelerometers in the field.

## **2.5 Summary**

Training loads are monitored in sports as part of a process which primarily aims to enhance athletic performance, whilst reducing the risk of injury. Current body-worn sensors, such as GPS devices and accelerometers, are a popular means to measure a wide variety of external training load metrics. In contrast to physiological loads, however, the biomechanical demands of training and competition are difficult to quantify and are, therefore, still not well understood. GRF is a well-established measure of whole-body biomechanical loading and could thus provide further insight in the biomechanical loads imposed on athletes but cannot currently be measured outside laboratory settings. However, since GRF is determined by the accelerations of the body's different segments, body-worn accelerometers might be used to estimate and assess GRF in the field. Previous studies have for instance shown that simple biomechanical features can be obtained from a single mass-spring model for straight running at constant speeds, using accelerometry input. However, methods to accurately estimate GRF across tasks typically performed during running-based sports are still unavailable. Therefore, if body-worn accelerometers can be used to accurately estimate GRF (e.g. by using a mass-spring-damper model or a direct mechanical approach) this would allow for monitoring whole-body biomechanical loading in the field.

---

## 2.6 Thesis aim and objectives

The overall aim of this thesis was to investigate if GRF can be estimated from segmental accelerations, especially for dynamic and high-intensity running tasks that are frequently performed during running-based sports. The specific objectives of the studies in this thesis were:

- *Study 1*: to examine if a two mass-spring-damper model can be used to accurately reproduce GRF profiles and loading characteristics for high-intensity running tasks.
- *Study 2*: to investigate whether a two mass-spring-damper model can be used to accurately predict GRF from trunk accelerometry.
- *Study 3*: to validate GRF estimated from multiple segmental accelerations using a direct mechanical approach and establish the minimal number of segments required.
- *Study 4*: to identify key segmental contributions to specific GRF features, using a principal component analysis.

The outcomes of these studies will provide further insight in the feasibility of using body-worn accelerometers to measure GRF and monitor whole-body biomechanical loading during running-based sports in the field.

---

## **Chapter 3: Using a two mass-spring-damper model to reproduce ground reaction forces for high-intensity running tasks**

---

*Abstract:* Running impact forces expose the body's hard- and soft-tissues to biomechanical loads leading to beneficial adaptations, but also risk of injury. High-intensity running tasks especially, are deemed highly demanding for the musculoskeletal system, but stresses experienced during these actions have been relatively unexplored. To eventually predict ground reaction forces (GRFs) and understand the biomechanical loads experienced during such activities in greater detail, this study aimed to determine whether a two mass-spring-damper model can be used to accurately reproduce GRF profiles and loading characteristics for high-intensity running tasks. This model, based on eight model parameters, was used to replicate GRFs for rapid accelerations and decelerations, constant speed running and maximal sprints. GRF profiles and impulses could be reproduced with low to very low errors across tasks. However, the more subtle loading characteristics (impact peaks and loading rates) were modelled less accurately with moderate to very high errors. These results show that a two mass-spring-damper model can be used to reproduce overall GRFs for different high-intensity running tasks. If information from body-worn sensors (e.g. accelerations of the upper trunk) can be used to estimate the model parameters, this approach might open the door to predicting GRFs (whole-body biomechanical loading) in the field and could help to understand the biomechanical demands of training and competition in greater detail.

*This study was accepted for publication in Sports Biomechanics (Verheul et al., 2019).*

---

### 3.1 Introduction

During human running the body is repetitively exposed to collisions with the ground. Ground reaction forces (GRFs) resulting from these impacts are absorbed by the different hard- and soft-tissues of the lower limbs and returned in a spring-like manner. Several mass-spring(-damper) models have, therefore, been used to further understand movement, as well as anatomical and mechanical aspects, in relation to the GRF (Nikooyan and Zadpoor, 2011). The simplest model suggested is that of a single point mass, representing the body's centre of mass (CoM), attached to a spring (Blickhan, 1989; McMahon and Cheng, 1990) (figure 2.4 A). This mass-spring model, which is based on the elastic nature of running and assumes a linear vertical downward CoM motion which is reversed during the second half of stance (Bobbert et al., 1991; Cavanagh and Lafortune, 1980), has been applied to describe various running characteristics including vertical and leg stiffness (Farley and González, 1996; Girard et al., 2017, 2011; McMahon and Cheng, 1990; Morin et al., 2005; Pappas et al., 2014b), running economy (McMahon, 1987), stride length, frequency and duration (Blickhan, 1989; Bullimore and Burn, 2007) and fatigue effects (Dutto and Smith, 2002; Girard et al., 2011; Morin et al., 2006). However, multiple studies have shown that GRF profiles following from the mass-spring model are not an accurate representation of the actual GRF of running (Alexander et al., 1986; Bullimore and Burn, 2007; Clark and Weyand, 2014).

During ground contact, a mass-spring model assumes vertical motion of the mass (body's CoM) and linear compression of the spring, resulting in a sine shaped GRF profile with a single force peak at mid-stance (figure 2.4 B). However, it is well known that this basic GRF curve does not well describe the asymmetrical force application and impact characteristics associated with landing (Alexander et al., 1986; Bullimore and Burn, 2007; Cavagna, 2006; Clark and Weyand, 2014). High-frequency impact force peaks typically occur after touch-down, and are affected by running speed (Bobbert et al., 1991; Hamill et al., 1983; Kuitunen et al., 2002; Nilsson and Thorstensson, 1989), foot-strike pattern (Clark et al., 2014; Lieberman et al., 2010), footwear (Liu and Nigg, 2000; Zadpoor and Nikooyan, 2010) and surface incline (Gottschall and Kram, 2005). These impact peaks have been shown to be primarily be related to support leg motion,

---

while the upper body accounts for the larger active peak (Bobbert et al., 1991; Clark et al., 2017). Therefore, a two mass-spring-damper model has been used to describe the distinct force characteristics due to upper and lower mass behaviour (Alexander et al., 1986; Derrick et al., 2000). Previous studies have shown that this model can indeed replicate GRF profiles, including the impact and active peaks, for running at different speeds up to  $5 \text{ m}\cdot\text{s}^{-1}$  (Derrick et al., 2000; Nedergaard, 2017), different stride lengths (Derrick et al., 2000), and changes in direction (Nedergaard, 2017). However, the ability of this simple model to replicate GRF profiles for more sport-specific running tasks is yet completely unknown.

During running-based sports, athletes typically perform a wide variety of different movements. These activities can be divided into low-intensity (e.g. walking, jogging) and high-intensity (e.g. rapidly accelerating, sprinting) movements, as well as sport-specific actions (e.g. shooting, jumping, tackling) (Bloomfield et al., 2007). The external forces experienced during these activities exposes the musculoskeletal system to various biomechanical loads, leading to beneficial tissue adaptations (Bohm et al., 2015; Rosa et al., 2015; Wisdom et al., 2015), but also the risk of injuries (Drew and Finch, 2016; Gabbett and Ullah, 2012). High-intensity activities, such as rapid accelerations and decelerations  $>1 \text{ m}\cdot\text{s}^{-2}$  or sprinting, are deemed especially demanding for the musculoskeletal system (Buchheit and Simpson, 2017; Duhig et al., 2016; Harper and Kiely, 2018; Vanrenterghem et al., 2017). Moreover, high-intensity running has been found to account for up to 31% of the total distance covered in professional sports (Akenhead et al., 2013; Bradley et al., 2009; Dalen et al., 2016; Di Salvo et al., 2009; Vigh-Larsen et al., 2018). If the task-specific (double peak) GRF profiles of these activities can be accurately quantified, this could help to understand the mechanical demands of training and competition in greater detail. Therefore, to eventually predict GRF in the field, this study aimed to determine whether a two mass-spring-damper model can be used to accurately reproduce GRF profiles and loading characteristics for high-intensity running tasks that are frequently performed during running-based sports.

---

## 3.2 Methods

Ethical approval for this study was granted by Liverpool John Moores University ethics committee, with reference number 16/SPS/017. Data from the cohort and data collection described below were used for the studies described in this chapter, as well as chapter 4.

### 3.2.1 *Participants and protocol*

Fifteen team sports athletes participated in this study (10 males and 5 females, age  $23\pm 1$  yrs, height  $174\pm 8$  cm, body mass  $74\pm 9$  kg). All participants were healthy at the time of testing and were physically active for at least three hours per week (sports participation  $8.5\pm 3$  hrs per wk). Prior to data collection, participants provided written informed consent according to Liverpool John Moores University ethics regulations.

After a short warm-up which consisted of easy jogging and stretching, participants performed a variety of high-intensity running tasks. Participants were instructed to land with one foot on a force platform embedded in the ground for a single step during each trial. Acceleration trials were performed from standstill to sprinting speed while force data were collected for the first, second and third step of separate trials. Decelerations included the first and second steps of rapidly decelerating from sprinting to immediate standstill, as well as gradual decelerating from sprinting to easy jogging. Constant speed running trials were performed at speeds ranging from  $2\text{ m}\cdot\text{s}^{-1}$  to maximal sprinting speed ( $\sim 7\text{-}9\text{ m}\cdot\text{s}^{-1}$ ; participant-specific), with stepwise increases of  $1\text{ m}\cdot\text{s}^{-1}$ . Running speeds were measured with photocell timing gates (Brower Timing Systems, Draper, UT, USA) which were positioned at 3 m apart at 1.5 m before and after the force platform. To control running speed, verbal feedback to speed up or slow down was given after each trial, and only trials within a  $\pm 5\%$  range of the target speed were included. Three consecutive trials were performed for each task and speed in a different randomised order for each participant.

### 3.2.2 *Kinetic data collection*

For each trial, GRF data were collected for a single step on the force platform (9287B, 90x60 cm, Kistler Holding AG, Winterthur, Switzerland) at a sampling frequency of 3000 Hz.

---

Measured GRF were exported to Matlab (version R2016a, The MathWorks, Inc., Natick, MA, USA) where touch-down, and take-off from the force platform were identified by a 20 N threshold of the vertical GRF. GRF data were then filtered using a 2<sup>nd</sup> order Butterworth low-pass filter with a cut off frequency of 50 Hz, and resultant GRF was calculated from the three individual force components ( $F_x$ ,  $F_y$ ,  $F_z$ ).

### 3.2.3 Modelling ground reaction forces

A two mass-spring-damper model (appendix A), described by eight natural model parameters ( $p_1$ ,  $v_1$ ,  $p_2$ ,  $v_2$ ,  $\lambda$ ,  $\omega_1$ ,  $\omega_2$  and  $\zeta$ ), was used to replicate the measured GRF (Alexander et al., 1986; Derrick et al., 2000). The motion of the model was described by the acceleration of its upper and lower mass according to equations 3.1 and 3.2.

$$a_1 = -\omega_1^2 \cdot (p_1 - p_2) + g \quad (3.1)$$

$$a_2 = -\omega_2^2 \cdot p_2 + \omega_1^2 \cdot \lambda \cdot (p_1 - p_2) - 2 \cdot \zeta \cdot \omega_2 \cdot v_2 + g \quad (3.2)$$

In which  $a_1$  and  $a_2$  are the acceleration of the upper and lower mass respectively,  $g$  is the gravitational acceleration,  $p_1$  is the relative position of the upper mass  $m_1$ ,  $p_2$  and  $v_2$  are the relative position and initial velocity of the lower mass  $m_2$ ,  $\lambda$  is the ratio of the upper mass relative to the lower mass ( $m_1/m_2$ ),  $\omega_1$  and  $\omega_2$  are the natural frequencies of the upper and lower spring respectively, and  $\zeta$  is the damper's damping ratio. From these parameters, the modelled GRF was then calculated according to equation 3.3.

$$\text{GRF}_{\text{modelled}} = -\frac{\text{BM} \cdot \omega_2}{1 + \lambda} \cdot (\omega_2 \cdot p_2 + 2 \cdot \zeta \cdot v_2) \quad (3.3)$$

In which BM is the total body mass. The eight initial parameters of the mass-spring-damper model were optimised to fit the modelled GRF to the resultant measured GRF. For each trial, a unique optimal set of the eight parameters was defined from which the modelled GRF was calculated. Modelled GRF was always forced to start from 0 N at touch-down (which is a necessity for a physically realistic representation of the GRF during stance) by calculating the lower mass position  $p_2$  from its initial velocity  $v_2$ ,  $\omega_2$  and  $\lambda$  according to equation 3.4.

$$p_2 = \frac{-2 \cdot \zeta \cdot v_2}{\omega_2} \quad (3.4)$$

The optimisation process for the parameters to model GRF was based on solving the model's differential equations using a numerical method (appendix B). The two 2<sup>nd</sup> order differential equations for the upper and lower mass accelerations  $a_1$  and  $a_2$  (equations 3.1 and 3.2) were rewritten to four 1<sup>st</sup> order equations and solved with numerical solvers. For this, a purpose written Python script (Python, 2017) with a numerical optimisation algorithm (SciPy, 2017) was used. Measured GRF curves were down-sampled to 100 Hz in order to reduce computation time and starting conditions for the optimisation process were based on the model parameters as described by Nedergaard (2017). The resulting parameters from the optimisation process were then used to calculate the modelled GRF according to equation 3.3. The best combination of model parameters was selected by minimising the root mean square error (RMSE; equation 3.5), in combination with the gradient error between the modelled and measured GRF curve over the duration of ground contact.

$$\text{RMSE} = \sqrt{\frac{\sum_{t=0}^n (\text{GRF}_{\text{modelled}}(t) - \text{GRF}_{\text{measured}}(t))^2}{n}} \quad (3.5)$$

In which  $t$  is each individual time point of the GRF curve and  $n$  the total duration of stance.

#### 3.2.4 Data processing and analysis

Measured and modelled GRF curves were normalised to each participant's body mass. Accuracy of the modelled GRF profiles was evaluated by the absolute (equation 3.5) and relative (equation 3.6) curve RMSE compared to the measured GRF. Relative RMSEs (as well as GRF loading characteristics) were determined to allow for comparison between tasks with different GRF magnitudes.

$$\text{RMSE}_{\text{relative}} = \sqrt{\frac{\sum_{t=0}^n \left( \frac{\text{GRF}_{\text{modelled}}(t) - \text{GRF}_{\text{measured}}(t)}{\text{GRF}_{\text{measured}}(t)} \right)^2}{n}} \cdot 100\% \quad (3.6)$$

In addition, errors of relevant GRF loading characteristics impulse, impact peak and loading rate were examined to further evaluate modelled GRF accuracy. Impulse was defined as the area

---

under the whole GRF curve and was normalised to the duration of ground contact. Impact peak was defined as the initial force peak during the first 30% of stance. Loading rate was defined as the average gradient of the GRF curve between touch-down and the impact peak and was normalised to the time to the impact peak. RMSE and GRF loading characteristic errors were then averaged across trials and participants for each task, i.e. accelerations, decelerations, and constant speed running at a low (2-3 m·s<sup>-1</sup>), moderate (4-5 m·s<sup>-1</sup>) and high (>6 m·s<sup>-1</sup>) speed. RMSE was rated as being very low (<1 N·kg<sup>-1</sup>), low (1-2 N·kg<sup>-1</sup>), moderate (2-3 N·kg<sup>-1</sup>), high (3-4 N·kg<sup>-1</sup>) or very high (>4). Based on meaningful performance or injury related differences (Bazuelo-Ruiz et al., 2018; Bezodis et al., 2017; Hunter et al., 2005), the magnitude of GRF loading characteristic errors was rated as being very low (<5%), low (5-10%), moderate (10-15%), high (15-20%) or very high (>20%). Furthermore, linear correlation analyses were performed between modelled and measured impulses, impact peaks and loading rates, and rated as very weak (R<sup>2</sup><0.1), weak (R<sup>2</sup>=0.1-0.3), moderate (R<sup>2</sup>=0.3-0.5), strong (R<sup>2</sup>=0.5-0.7), very strong (R<sup>2</sup>=0.7-0.9) or extremely strong (R<sup>2</sup>=0.9-1) (Hopkins et al., 2009).

### 3.3 Results

The two mass-spring-damper model was able to accurately replicate measured GRF profiles across tasks (figure 3.1; table 3.1). RMSE was very low for accelerations, as well as low- and moderate speed running. Despite the slightly increased modelled GRF errors for the higher intensity tasks, RMSE was still low for the highest running speed but moderate for decelerations. Impulses were modelled with very high accuracy (table 3.1). Relative impulse errors for modelled GRF profiles were smaller than 1% for accelerations, decelerations and running at different constant speeds. Consequently, the correlation between the measured and modelled GRF impulses were extremely strong (R<sup>2</sup>=1, p<0.001) across running tasks (figure 3.2 A). Moreover, absolute as well as relative impulse errors were independent of task or the magnitude of the area under the GRF curve (figure 3.2 B and C).

Since not all trials included a distinct impact peak (e.g. for accelerations (figure 3.1 A) or when participants ran with a forefoot strike during high-speed running (figure 3.1 G)) and for several

---

trials the impact peak could not be modelled (see figure 3.1 B, F and H), only a select number of trials was included in the impact peak and loading rate analysis (table 3.1). For the trials in which the measured GRF included an impact peak, the model could reproduce these peaks for 34%, 99% and 48% of the acceleration, deceleration and constant speed running trials respectively. Impact peaks were modelled with low to moderate errors for constant speed running (table 3.1). However, for accelerations (18.92%) and decelerations (20.64%) the relative modelled impact peak errors were high to very high. Despite this, the modelled impact peak values had an extremely strong correlation ( $R^2=0.97$ ,  $p<0.001$ ) with the measured force peaks across the different tasks (figure 3.2 D). The model typically underestimated the measured impact peaks and the absolute error significantly ( $p<0.001$ ) increased when the measured impact peak increased (figure 3.2 E). However, the relative error remained constant regardless of task and the magnitude of the impact peak (figure 3.2 F).

**Table 3.1** Modelled ground reaction force curve and loading characteristics errors

	RMSE		Impulse error		Impact peak error		Loading rate error	
	N·kg <sup>-1</sup>	%	N·s·kg <sup>-1</sup>	%	N·kg <sup>-1</sup>	%	N·kg <sup>-1</sup> ·s <sup>-1</sup>	%
Accelerations (n=189)	0.69	9.9	0.01	0.6	2.43	18.9	487	31.3
	±0.47	±6.4	±0.01	±0.5	±1.49	±11.7	±342	±19.9
Decelerations (n=240)	2.48	33.9	0.01	0.7	7.43	20.6	431	18.7
	±1.17	±28.3	±0.01	±0.5	±4	±13.7	±276	±9.4
Constant speed running								
Low (2-3 m·s <sup>-1</sup> ; n=126)	0.48	7.6	0.01	0.4	1.53	10.2	200	19.1
	±0.22	±5.8	±0	±0.3	±1.25	±8.5	±116	±9.8
Mod. (4-5 m·s <sup>-1</sup> ; n=126)	0.78	9.4	0.01	0.3	1.54	7.5	254	20.8
	±0.25	±3.9	±0	±0.2	±0.86	±4.2	±101	±6.9
High (>6 m·s <sup>-1</sup> ; n=176)	1.21	13.6	0.01	0.3	2.99	12	287	18.4
	±0.56	±7.1	±0	±0.2	±1.74	±8.1	±156	±9.7
All tasks (n=857)	1.28	17	0.01	0.5	5.74	17.4	385	20.3
	±1.06	±19.1	±0.01	±0.4	±3.85	±12.2	±247	±10.7

Mean ± standard deviations for root mean square errors (RMSE), impulse, impact peak and loading rate errors of the modelled GRF profiles for different tasks. Values are either absolute or relative errors compared to the measured GRF. Impact peak and loading rate (grey shaded) was modelled for 34%, 99% and 48% of the acceleration, deceleration and constant speed running trials respectively.

Modelled loading rate values were high to very high across the different tasks (table 3.1). Similar to the impulse and impact peak however, the correlation between measured and modelled loading rates was extremely strong ( $R^2=0.96$ ,  $p<0.001$ ) (figure 3.2 G). The model typically underestimated the loading rate and the absolute errors significantly ( $p<0.001$ ) increased when the measured loading rate increased (figure 3.2 H). The relative loading rate errors on the other hand, were independent of task and magnitude (figure 3.2 I).

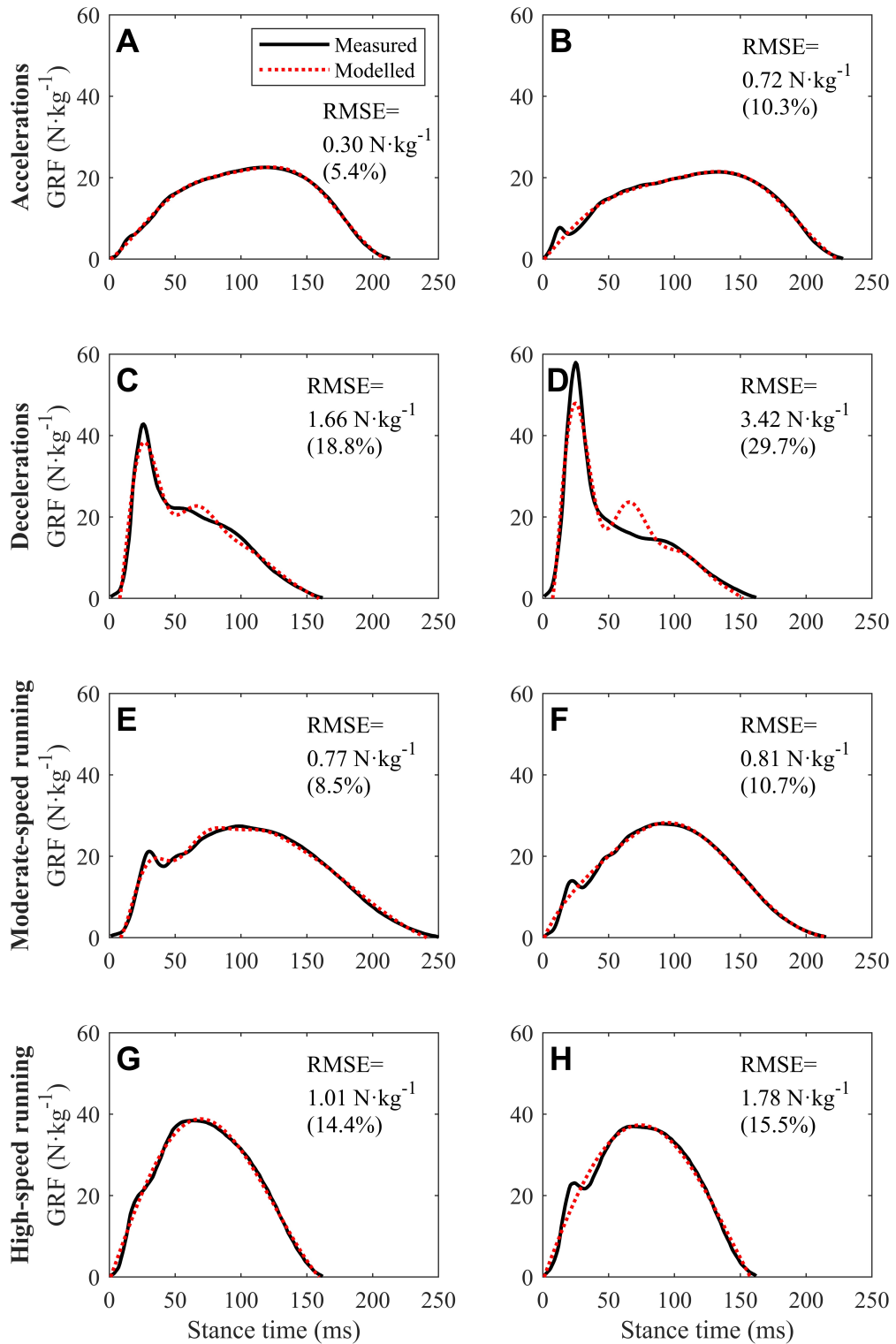


**Figure 3.1** Representative examples of measured (black solid line) and modelled (red dotted line) ground reaction forces (GRF) including the root mean square error (RMSE) between both curves. GRF curves for accelerations and running at high speeds did not always contain a distinct impact peak (A, G).

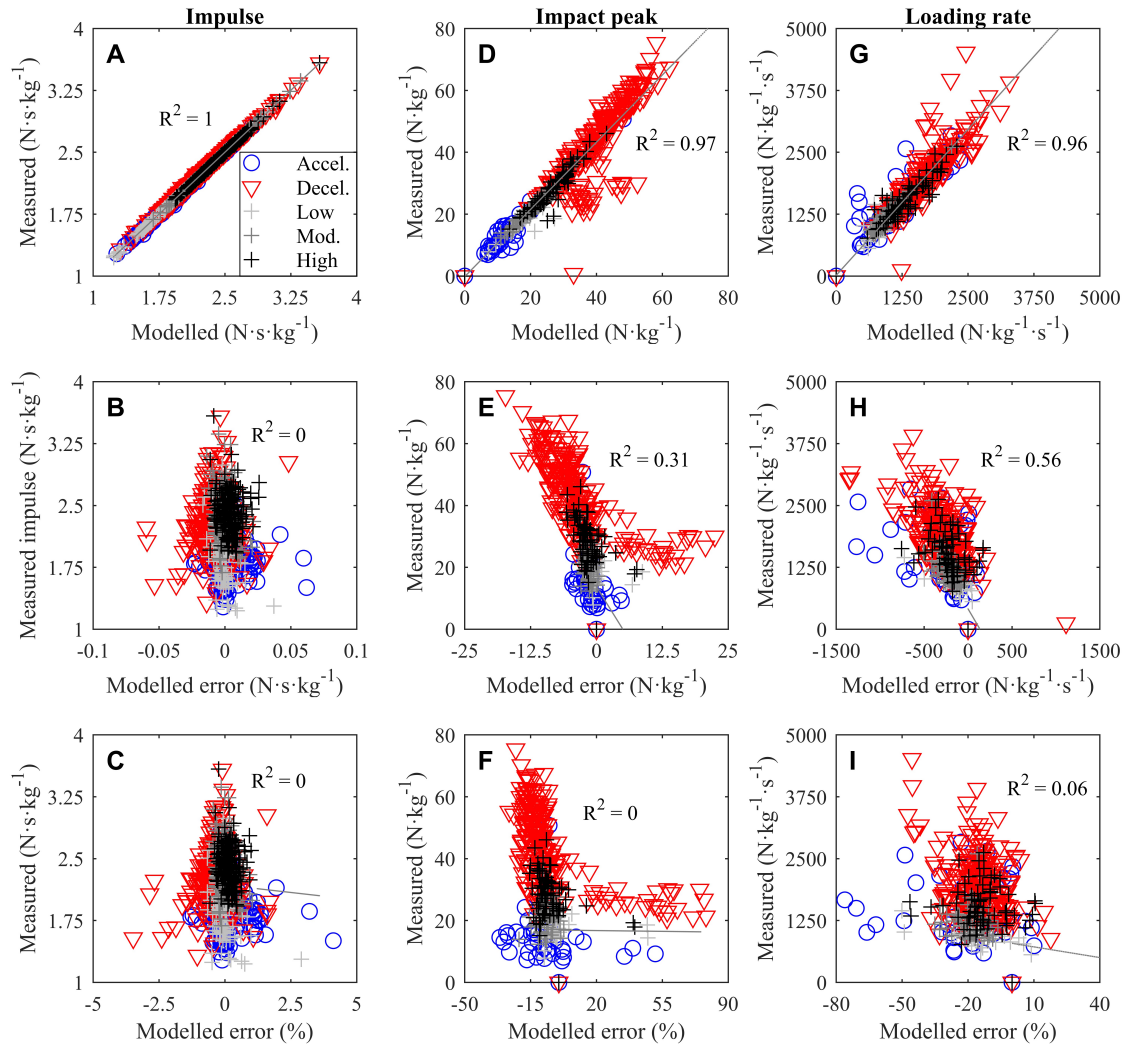


**Figure 3.2** Measured, modelled and error values for the impulses, impact peaks and loading rates. Negative and positive errors are a respective underestimation and overestimation of the measured value.

For all eight model parameters and across tasks, standard deviations of the parameter values were large (table 3.2, figure 3.3). For deceleration trials especially, the five mass related parameters (i.e. initial positions  $p_1/p_2$  and velocities  $v_1/v_2$  of the two masses, as well as the mass ratio  $\lambda$ ) were highly variable (figure 3.3). The natural spring frequencies  $\omega_1$  and  $\omega_2$  varied the most across all different tasks. Although the damping ratio  $\zeta$  was less variable between tasks, the standard deviations and variability within tasks was still large.

**Table 3.2** Mean  $\pm$  standard deviation values for the eight model parameters for the different tasks

	$p_1$ (m)	$p_2$ (m)	$v_1$ ( $m \cdot s^{-1}$ )	$v_2$ ( $m \cdot s^{-1}$ )	$\omega_1$ ( $N \cdot m^{-1} \cdot kg^{-1}$ )	$\omega_2$ ( $N \cdot m^{-1} \cdot kg^{-1}$ )	$\lambda$ (au)	$\zeta$ (au)
Accelerations	0.09 $\pm 8.2$	-0.7 $\pm 5.5$	16.5 $\pm 146$	0.37 $\pm 5$	32 $\pm 27$	102 $\pm 155$	0.4 $\pm 2.3$	0.9 $\pm 3.9$
Decelerations	12.97 $\pm 26.4$	-0.33 $\pm 1.2$	81 $\pm 184.7$	45.87 $\pm 132.3$	24 $\pm 32$	114 $\pm 91$	161.4 $\pm 474$	0.4 $\pm 0.5$
Constant speed running								
Low (2-3 $m \cdot s^{-1}$ )	0.63 $\pm 3.1$	0.07 $\pm 1.2$	-2.9 $\pm 56.2$	-0.12 $\pm 1.2$	31 $\pm 28$	72 $\pm 78$	5.87 $\pm 5.9$	0.9 $\pm 2.4$
Mod. (4-5 $m \cdot s^{-1}$ )	0.91 $\pm 5.2$	0.09 $\pm 0.8$	12.67 $\pm 137$	-0.2 $\pm 1.1$	37 $\pm 35$	101 $\pm 106$	4.16 $\pm 6.3$	0.6 $\pm 1.1$
High ( $>6 m \cdot s^{-1}$ )	-2.21 $\pm 13.4$	-1.74 $\pm 10.31$	-1.83 $\pm 115$	0.98 $\pm 12.6$	34 $\pm 35$	134 $\pm 148$	1.93 $\pm 5$	1.9 $\pm 7$
All tasks	-4 $\pm 17.1$	-0.57 $\pm 5.3$	28.49 $\pm 146.9$	13.71 $\pm 74.9$	31 $\pm 32$	109 $\pm 129$	49.38 $\pm 267$	0.9 $\pm 3.7$

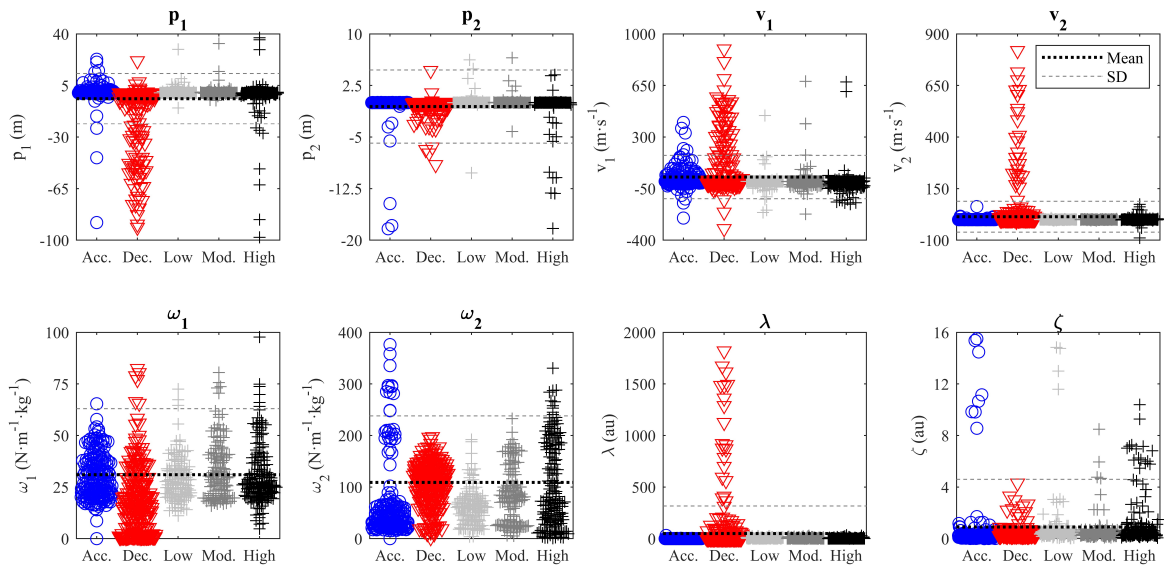


**Figure 3.3** Model parameter values for the different tasks including means (black dotted line) and standard deviations (SD; grey dashed line) for accelerations, decelerations, and low, moderate and high-speed running. For visualisation purposes, extreme individual outliers have been removed from the plots.

---

### 3.4 Discussion

The purpose of this investigation was to determine whether a two mass-spring-damper model can be used to accurately reproduce GRF profiles for a range of high-intensity running tasks. Average modelled curve errors (RMSE) were low to moderate for accelerations, decelerations and running at various constant speeds. The slightly higher errors observed in modelled deceleration curves, was likely due to the distinct GRF profile. The model typically underestimated the rapidly increasing forces after touch-down (i.e. high impact peak and loading rate) but overestimated the much lower second (active) peak (figure 3.1 C and D). Similar to these findings, Nedergaard (2017) reported the modelled GRF curve errors to be significantly higher in 45 and 90 degree side-cutting tasks, which typically have a similar high impact peak to decelerations. In addition, Derrick et al. (2000) also reported strongly increased GRF errors for a single participant who had substantially higher impact peaks during straight constant speed running. Nedergaard (2017) suggested increased curve errors in side-cutting tasks to be due to lower values for the natural frequencies of the upper ( $\omega_1$ ) and lower spring ( $\omega_2$ ), which reduces the magnitude of the impact peak (Derrick et al., 2000; Nedergaard, 2017). In a parameter sensitivity analysis with a two mass-spring-damper model, Derrick et al. (2000) showed that in order to increase the impact peak, the two mass-spring-damper model requires increased spring stiffness  $\omega_1$ ,  $\omega_2$ , initial position of the upper mass  $v_1$  and mass ratio  $\lambda$ , as well as a reduced damping ratio  $\zeta$ . In this study, mean values for  $v_1$  and  $\lambda$  were indeed substantially higher for decelerations than for other tasks, but  $\omega_1$ ,  $\omega_2$  and  $\zeta$  were in a similar range as for the other tasks (table 3.2; figure 3.3). It might be that for GRF profiles with higher impact peaks, the model needs to adjust as many parameters as possible to replicate this first peak, while maintaining an accurate representation of the rest of the curve characteristics (e.g. active peak, stance time).

The impulse (area under the GRF curve) was modelled with very high accuracy (absolute error  $\approx 0.01 \text{ N}\cdot\text{s}\cdot\text{kg}^{-1}$ ) and had a perfect correlation ( $R^2=1$ ) with the measured impulse. These results are in accordance with errors ( $\approx 0.01 \text{ N}\cdot\text{s}\cdot\text{kg}^{-1}$ ) and extremely strong correlations ( $R^2=0.98-1$ ) found by Nedergaard (2017) for straight running and side-cutting tasks, but much lower than Derrick et al. (2000) who reported impulse errors of 5.5-8.5  $\text{N}\cdot\text{s}$  ( $\approx 0.08-0.12 \text{ N}\cdot\text{s}\cdot\text{kg}^{-1}$ ) for

---

straight running at a moderate speed. Since the latter study only included  $\omega_1$ ,  $\omega_2$  and  $p_2$  in their optimisation routine, the better results in the present study are likely due to the inclusion of all model parameters in the optimisation process. Another explanation of the accurate results for the impulse is that overall curve errors (RMSE) average out when examining the impulse. If for example, the impact peak was slightly underestimated, but the active peak was overestimated, the impulse error was only affected minimally. Therefore, the two mass-spring-damper model was able to reproduce highly accurate estimates of whole-body loading (i.e. impulse) across tasks.

In contrast to overall loading, the more subtle GRF loading characteristics, impact peak and loading rate, were modelled less accurately. Moreover, the model was not able to reproduce the initial impact peak for a number of trials. The impact peak represents the end of the sharp force increase due to the lower limb colliding with the ground (Clark et al., 2017), and is typically followed by a slight decrease in GRF before gradually increasing to the active peak caused by the rest of the body (Bobbert et al., 1991). For accelerations and constant speed running this decrease in GRF is small and forms only a small part of the whole curve. Since the curve gradient and RMSE were used as optimisation criteria for the model parameters, a continuously rising curve from touch-down to mid-stance (i.e. ignoring the impact peak) only affected these criteria minimally. This explains why in decelerations, in which the impact peak comprises a much larger part of the GRF curve, for 99% of the trials an impact peak was modelled, compared to only 34-48% for accelerations and constant speed running. Moreover, the model typically underestimated the impact peak (and consequently loading rate) and errors increased as the impact peak increased (figure 3.1 C and D; figure 3.2 E and H). In general, differences between the magnitude of impact and active peaks was also higher for higher impact peaks, e.g. in decelerations with a high impact peak the second peak was typically much lower (figure 3.1 D). Since most model parameters that affected the impact peak also influenced the active peak (Derrick et al., 2000), this difference could not be effectively modelled. Hence, the model typically underestimated the impact peak more as the magnitude increased, to limit the overestimation of the second peak.

---

Despite the slightly higher errors for impact peaks and loading rates there were extremely strong correlations ( $R^2=0.96-0.97$ ) between the measured and modelled values (figure 3.2 E and H). Udofa et al. (2016), who used a similar (two mass) model to replicate GRF found a correlation of  $R^2=0.82$  between measured and modelled impact peaks, across different running speeds and loading conditions. For future research or potential application in the field, the extremely strong linear relationship observed in this study might be used to recalculate and improve the modelled impact peaks and loading rates to achieve more accurate estimates of these characteristics.

A limitation of the two mass-spring-damper model used in this study is the assumption of spring-like behaviour of the body, meaning constant stiffness of the springs (i.e. muscle-tendon units) throughout the stance phase. Moreover, during the first half of stance the model's damper absorbs energy while the model does not include elements that produce energy (e.g. muscle work) during the second half of stance. It is, however, known that the leg is stiffer during landing than take-off (Blickhan, 1989), and that the muscle-tendon units produce more work during the push-off phase compared to landing (Cavagna, 2006). Derrick et al. (2000) acknowledged this problem and increased the modelled GRF by 10% at every time point on the curve, resulting in substantial reductions of modelled curve and impulse errors. Given the accuracy of RMSE and impulse in the present study it is questionable whether such an approach would improve the results. Since increased leg stiffness has been shown to reduce energy requirements (Dutto and Smith, 2002; McMahon and Cheng, 1990) it is likely that the model overcompensates the absence of active energy supply by increasing its stiffness (i.e. higher  $\omega_1$  and  $\omega_2$ ). This might explain that on average stiffness was higher for accelerations and constant speed running, where the muscles need to produce more energy, compared to decelerations, where energy is primarily absorbed (table 3.2).

Another limitation of this study is the complexity of the model parameter combination. As described above, different parameters represent multiple physical aspects (e.g. leg stiffness) and affect various GRF characteristics (e.g. impact peak, stance time) at the same time (Derrick et al., 2000). During the optimisation process, the numerical solvers search for an optimal modelled

---

GRF solution in the eight-dimensional parameter space. Because of the complexity of this search space, multiple local minima might be found that give similarly good solutions for the modelled GRF curve, which is likely to be the main reason for the high parameter variability and physically unrealistic parameter values observed in this study (table 3.2). For example, many modelled GRF solutions had mass ratios larger than 20, meaning that for those trials the lower mass (support leg) was negligible relative to the rest of the body. One should, therefore, be careful to not over interpret the physical meaning of model parameters found in this study.

In this study, the modelled GRF was estimated by adjusting the model parameters to fit the GRF measured from a ground embedded force platform. However, outside of laboratory settings (e.g. running track, football pitch), force platforms and measured GRF are not typically available and other methods are required for estimating the model parameters to predict GRF. Since the motion of the two mass-spring-damper model is described by the acceleration of its two masses, body-worn accelerometry might be a potential candidate. For example, trunk-mounted accelerometers are currently widely used in sports to evaluate different training load characteristics in the field (Akenhead and Nassis, 2016; Camomilla et al., 2018; Cardinale and Varley, 2017). If these trunk accelerations can be used to predict the model parameters, the two mass-spring-damper model might be used to estimate GRF in non-laboratory settings. This approach could help researchers and practitioners to understand the biomechanical demands of training and/or competition in greater detail.

### **3.5 Conclusion**

This study shows that a simple two mass-spring-damper model can accurately reproduce overall GRF curves for a range of high-intensity running tasks. These tasks account for the majority of biomechanical loads experienced during running-based sports and predicting GRF for these tasks in the field could help to better understand the biomechanical demands of training and/or competition. If information from body-worn sensors (e.g. accelerations of the upper trunk) can be used to estimate the two mass-spring-damper model parameters, this approach might open the door for predicting GRF in non-laboratory settings.

---

## **Chapter 4: Predicting ground reaction forces from trunk accelerations with a two mass-spring-damper model**

---

*Abstract:* During running-based sports, athletes are exposed to substantial musculoskeletal stresses. Although whole-body biomechanical loads, which are the external ground reaction forces (GRFs), can be measured precisely in a laboratory, valid methods for accurately estimating GRF in the field are currently unavailable. Mass-spring models have been used to predict various biomechanical aspects (including GRF) from popular body-worn accelerometers, but these simple models are known to not accurately predict the task-specific GRF profiles for different running activities. Therefore, this study investigated if GRF can be predicted from a two mass-spring-damper model by adjusting its eight model parameters to replicate measured trunk accelerations for rapid accelerations and decelerations, constant speed running and maximal sprints. The resulting parameters were then used to predict GRF directly, or indirectly using a relationship with parameter values required to reproduce GRF. Measured trunk acceleration signals could be replicated well, with low to moderate errors across the different tasks. However, the following GRF predictions were very poor regardless of which method (either direct or indirect) was used. These results show that GRF cannot be predicted from trunk accelerations using a two mass-spring-damper model, suggesting that accelerations of the trunk alone are unlikely to be sufficient to accurately predict GRF in running-based sports. Therefore, additional information (e.g. accelerations of other segments) is likely required to measure and monitor whole-body biomechanical loads in non-laboratory settings.

---

## 4.1 Introduction

In running-based sports, athletes perform a large range of sport- and situation-specific movements including steady running, sprinting, accelerating, decelerating, cutting, turning and jumping. These actions expose the hard- and soft-tissues of the body to a substantial amount of musculoskeletal stresses. Internal biomechanical stresses are partly the result of the external whole-body loads, which are the ground reaction forces (GRF) and can be measured precisely in a laboratory environment using force platforms. In combination with kinematic information from motion capture systems, the internal stresses, such as muscle forces (Hamner et al., 2010; Hamner and Delp, 2013) and joint forces (Harrison et al., 1986), can be calculated. Force platforms and motion capture technologies are, however, not typically available in non-laboratory settings and biomechanical loads are thus hard to measure directly in every-day training environments.

Given the direct relationship between the acceleration of the body's centre of mass (CoM) and GRF ( $F=m \cdot a$ ), body-worn accelerometers have been used to evaluate whole-body biomechanical loads. These measures (e.g. New Body Load, Dynamic Stress Load, PlayerLoad, Force Load) are typically derived from trunk accelerometry and assume the trunk to adequately represent the body's CoM (Boyd et al., 2011; Colby et al., 2014; Ehrmann et al., 2016; Gaudino et al., 2015; Page et al., 2015). It has, however, been shown that individual segmental accelerations cannot accurately represent whole-body CoM accelerations and/or directly predict GRF (Edwards et al., 2018; Nedergaard et al., 2017; Pavei et al., 2017a; Raper et al., 2018; Vanrenterghem et al., 2010; Wundersitz et al., 2013). Other studies have used trunk-mounted accelerometers to predict and examine simple estimates of GRF, as well as vertical and leg stiffness, from a mass-spring model (Buchheit et al., 2015; Gaudino et al., 2013; Girard et al., 2011; Morin et al., 2006). This simple model is, however, known to not accurately predict the actual GRF of running (Alexander et al., 1986; Bullimore and Burn, 2007; Clark and Weyand, 2014). Therefore, more complex multi-body mass-spring-damper models (e.g. the two mass-spring-damper model), which have been shown to accurately represent the GRF for different running tasks and are typically

---

described by the acceleration of the masses, are required to accurately predict GRF from body-worn accelerometry.

The two mass-spring-damper model has been shown to be able to accurately reproduce overall GRF profiles for constant speed running (Derrick et al., 2000; Nedergaard, 2017), changes of direction (Nedergaard, 2017), and a range of high-intensity running tasks (chapter 3). Unlike other more simplistic mass-spring models, the masses in a two mass-spring-damper model represent the different parts of the body. In this model, the lower mass, spring and damper, represent the support leg, while the upper mass and spring represent the rest of the body (Alexander et al., 1986; Derrick et al., 2000). Based on this assumption, the upper mass acceleration is determined by the combined movements of the swinging leg, arms, head and trunk during ground contact. Since the trunk is the heaviest of these segments (Dempster, 1955) and believed to be a major contributor to GRF (Bobbert et al., 1991), trunk accelerometry might be used to represent the acceleration of the model's upper mass. If so, the eight model parameters required to reproduce GRF might be estimated from acceleration signals measured at the trunk and used to predict GRF. Therefore, this study investigated whether a two mass-spring-damper model can be used to predict GRF from trunk accelerations (TA). The aims of this investigation were to examine 1) whether model parameters required to replicate trunk accelerometry with a two mass-spring-damper model can be used to directly predict GRF, and 2) whether a relationship between parameter values required to reproduce TA or GRF exists, to indirectly predict GRF.

## **4.2 Methods**

### *4.2.1 Participants and protocol*

Fifteen team sport athletes performed a variety of high-intensity running tasks frequently performed in running-based sports, including accelerations, decelerations and running at constant speeds ranging from 2 m·s<sup>-1</sup> to maximal sprinting, while GRF and trunk accelerations were synchronously recorded.

---

#### 4.2.2 Kinetic and accelerometry data collection

GRF data were collected for a single step on a force platform (9287B, 90x60 cm, Kistler Holding AG, Winterthur, Switzerland) at a sampling frequency of 3000 Hz. TA data were collected with a tri-axial accelerometer built into a commercial GPS device (OptimEye S5, Catapult Innovations, Scoresby, Australia) at a sampling frequency of 100 Hz. Participants wore the GPS device in a pocket of a tight-fitting vest on the back of the upper trunk between the Scapulae throughout the whole session (figure 2.2 A). GRF and TA data were exported to Matlab (version R2016a, The MathWorks, Inc., Natick, MA, USA) and filtered at 50 and 20 Hz respectively, after which the resultant GRF and TA were calculated from the three individual force and acceleration components respectively for each step. A more detailed description of the data collection protocol and procedures is provided in the methods section of chapter 3.

#### 4.2.3 Directly predicting ground reaction forces from trunk accelerations

A two mass-spring-damper model (appendix A) was used to replicate the measured TA signal for each individual step (figure 4.1) (Nedergaard et al., 2018). TA curves were replicated by adjusting the eight natural model parameters ( $p_1$ ,  $v_1$ ,  $p_2$ ,  $v_2$ ,  $\lambda$ ,  $\omega_1$ ,  $\omega_2$  and  $\zeta$ ) to fit the model's upper mass acceleration ( $a_1$ ) to the measured TA according to equation 4.1.

$$a_1 = -\omega_1^2 \cdot (p_1 - p_2) + g \quad (4.1)$$

In which  $\omega_1$  is the upper spring's natural frequency,  $p_1$  and  $p_2$  are the relative positions of the upper and lower mass respectively, and  $g$  is the gravitational acceleration ( $-9.81 \text{ m}\cdot\text{s}^{-2}$ ). The best combination of model parameters to fit  $a_1$  to the TA was determined by minimising the root mean square error (RMSE; equation 4.2) between modelled  $a_1$  and measured TA.

$$\text{RMSE} = \sqrt{\frac{\sum_{t=0}^n (a_{1\text{modelled}}(t) - \text{TA}_{\text{measured}}(t))^2}{n}} \quad (4.2)$$

In which  $t$  is each individual time point of the GRF curve and  $n$  the total duration of stance. A purpose-written Python code (Python, 2017) using an openly available numerical optimisation algorithm (SciPy, 2017) was used to find the solution with the lowest RMSE via a numerical optimisation method (appendix B). This optimal set of model parameters was then used to calculate the predicted GRF according to equation 4.3.

$$\text{GRF}_{\text{predicted}} = -\frac{\text{BM} \cdot \omega_2}{1 + \lambda} \cdot (\omega_2 \cdot p_2 + 2 \cdot \zeta \cdot v_2) \quad (4.3)$$

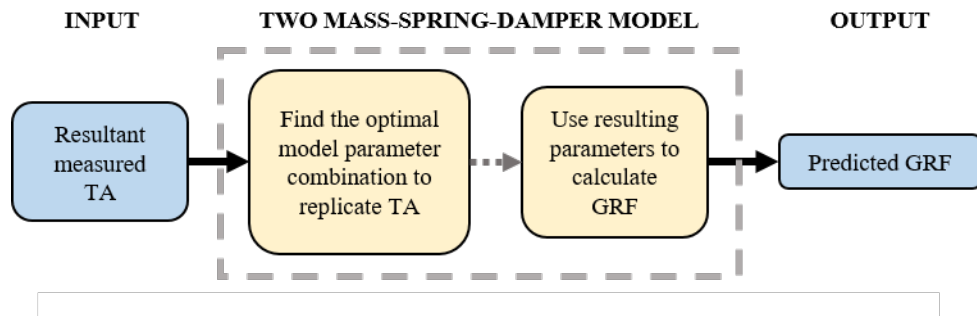


**Figure 4.1** Diagram of how measured trunk accelerations (TA) were used to directly predict ground reaction forces (GRF) with the two mass-spring-damper model.

#### 4.2.4 Indirectly predicting ground reaction forces from trunk accelerations

The model parameters following from reproducing GRF and replicating TA as described in chapter 3 and 4.2.1 of respectively, were used for a parameter regression analysis (figure 4.2). For each parameter, the relationship between values required to replicate GRF and TA were investigated across all trials, as well as for each task separate. Optimal parameter values following from modelling GRF and TA were plotted per task in a scatter plot for each parameter, for all individual trials. Parameter-specific linear model fits were then calculated using the TA and GRF parameters as the predictor and response variables respectively. If a moderate linear regression was found for a parameter (i.e.  $R^2 > 0.3$  (Hopkins et al., 2009)), this regression was then used to recalculate the parameter value that followed from replicating TA before calculating the predicted GRF.

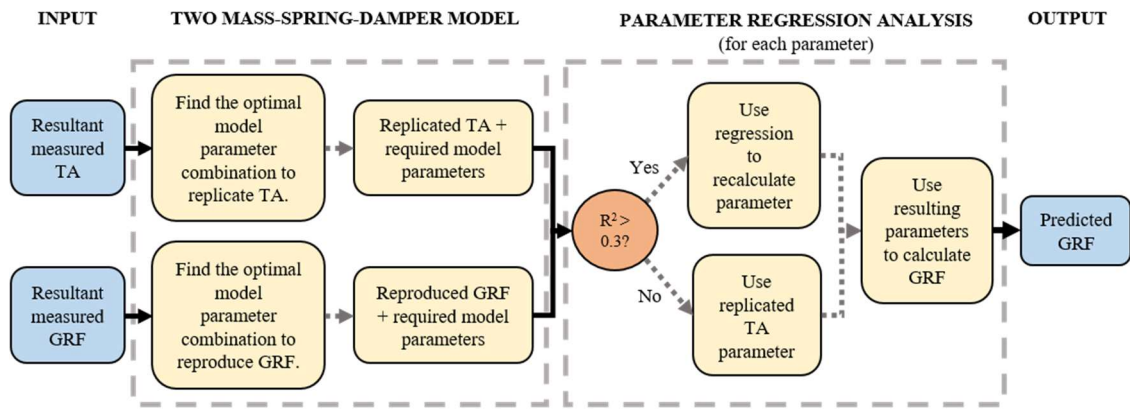


**Figure 4.2** Diagram of how measured trunk accelerations (TA) were used to indirectly predict ground reaction force (GRF) via a regression analysis. If there was a correlation between the modelled upper mass acceleration  $a_1$  (replicated TA) and GRF parameter values, this relationship was used to recalculate the parameter before calculating the predicted GRF profiles.

#### 4.2.5 Data processing and analysis

Measured GRF, as well as direct or indirect predicted GRF curves, were normalised to the participant's body mass. Accuracy of the modelled  $a_1$  (replicated TA) and predicted GRF profiles was evaluated by the curve RMSE during stance relative to the measured TA and GRF respectively. RMSE was averaged across all trials and participants for each task, i.e. accelerations, decelerations, and running at constant low ( $2-3 \text{ m}\cdot\text{s}^{-1}$ ), moderate ( $4-5 \text{ m}\cdot\text{s}^{-1}$ ) and high ( $>6 \text{ m}\cdot\text{s}^{-1}$ ) speeds. The RMSE magnitudes for modelled  $a_1$  and predicted GRF was rated as being very low ( $<1 \text{ m}\cdot\text{s}^{-2}$ ;  $<1 \text{ N}\cdot\text{kg}^{-1}$ ), low ( $1-5 \text{ m}\cdot\text{s}^{-2}$ ;  $1-2 \text{ N}\cdot\text{kg}^{-1}$ ), moderate ( $5-10 \text{ m}\cdot\text{s}^{-2}$ ;  $2-3 \text{ N}\cdot\text{kg}^{-1}$ ), high ( $10-15 \text{ m}\cdot\text{s}^{-2}$ ;  $3-4 \text{ N}\cdot\text{kg}^{-1}$ ) or very high ( $>15 \text{ m}\cdot\text{s}^{-2}$ ;  $>4 \text{ N}\cdot\text{kg}^{-1}$ ).

### 4.3 Results

#### 4.3.1 Direct ground reaction force predictions

Across tasks, the two mass-spring-damper model could replicate measured TA curves with low to moderate errors (table 4.1 and figure 4.3). Mean RMSEs of replicated TA curves were low ( $<5 \text{ m}\cdot\text{s}^{-2}$ ) for accelerations and running at constant speeds, but moderate ( $<10 \text{ m}\cdot\text{s}^{-2}$ ) for deceleration trials. The general shape of the TA profiles could be replicated well, but rapid or modest fluctuations in the TA signals were often slightly smoothed in the modelled  $a_1$  curves

(figure 4.2 A and E). In addition, sharp and high peaks in the acceleration signals were typically underestimated in the modelled curves (figure 4.2 B and G).

In contrast to modelled  $a_1$ , directly predicted GRF profiles from the following model parameters were very poor (figure 4.3). A total number of 53 trials (37 accelerations, 7 decelerations, 1 moderate and 8 high-speed running trials), for which RMSE was  $>1000 \text{ N}\cdot\text{kg}^{-1}$ , was discarded before calculating the mean RMSE per task. Despite excluding trials with extremely high errors, mean RMSE for predicted GRF profiles was still very high ( $>4 \text{ N}\cdot\text{kg}^{-1}$ ) across the different tasks (table 4.1). Predicted GRF errors increased with running speed and were the highest for running at high speeds, accelerations and decelerations.

**Table 4.1** Modelled upper mass acceleration and ground reaction force errors

	$a_1 \text{ (m}\cdot\text{s}^{-2}\text{)}$		GRF ( $\text{N}\cdot\text{kg}^{-1}$ )	
	Mean	SD	Mean	SD
Accelerations (n=189)	3.94	$\pm 1.75$	78.19	$\pm 176.30$
Decelerations (n=240)	7.02	$\pm 3.03$	38.19	$\pm 79.58$
Constant speed running				
Low (2-3 $\text{m}\cdot\text{s}^{-1}$ ; n=126)	4.02	$\pm 1.71$	9.43	$\pm 10.03$
Moderate (4-5 $\text{m}\cdot\text{s}^{-1}$ ; n=126)	4.77	$\pm 1.65$	21.33	$\pm 67.64$
High ( $>6 \text{ m}\cdot\text{s}^{-1}$ ; n=176)	4.59	$\pm 1.89$	88.45	$\pm 186.52$
All tasks (n=857)	5.07	$\pm 2.52$	49.08	$\pm 128.72$

Root mean square errors (RMSE) between the measured trunk acceleration and ground reaction force (GRF) or modelled upper mass acceleration ( $a_1$  in  $\text{m}\cdot\text{s}^{-2}$ ) and GRF (in  $\text{N}\cdot\text{kg}^{-1}$ ) respectively. Values are means  $\pm$  standard deviations (SD) for each task. For GRF, trials with RMSE  $>1000 \text{ N}\cdot\text{kg}^{-1}$  were discarded, with a total of 53 trials, before calculating mean and SD values per task.

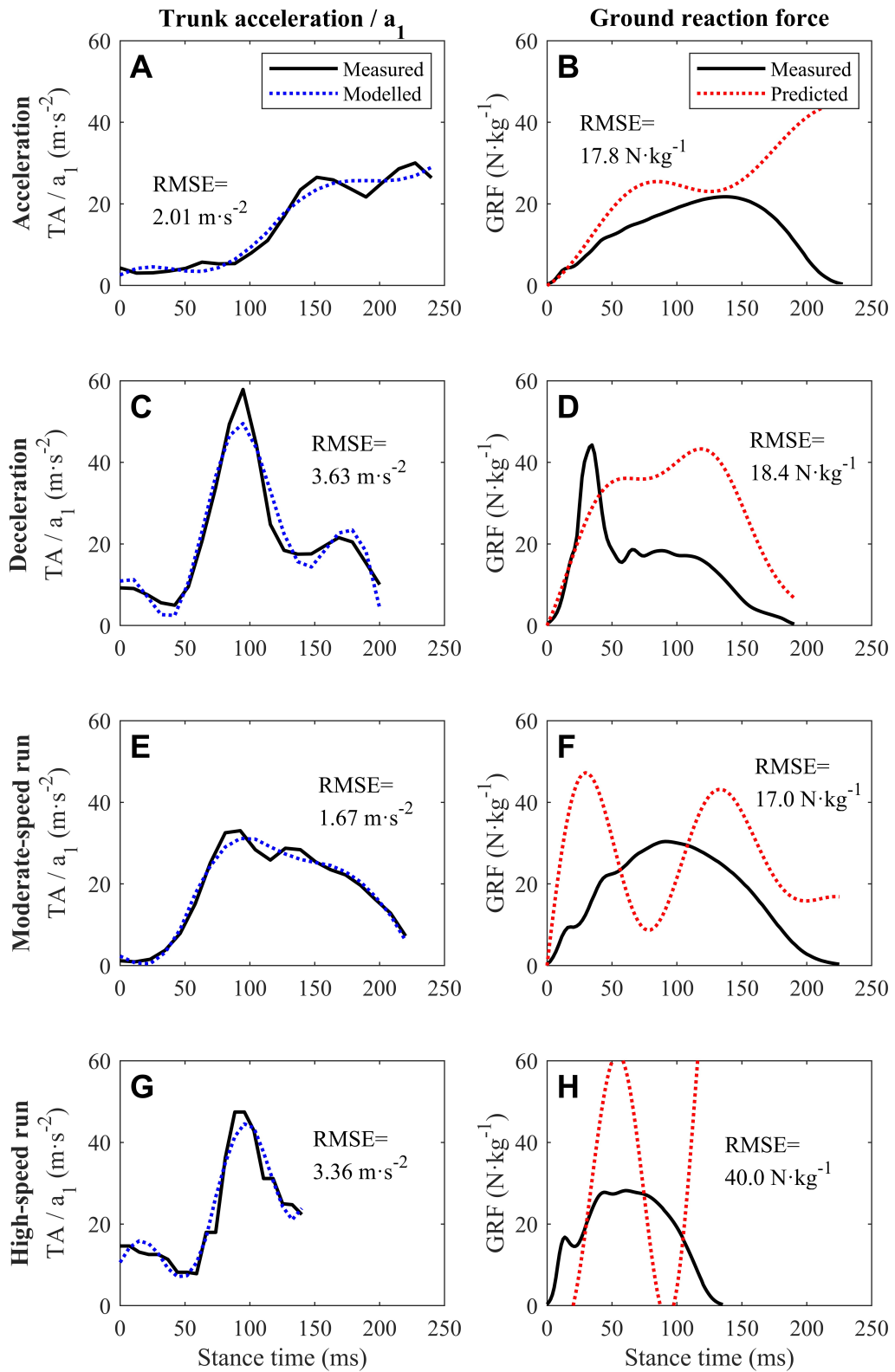


**Figure 4.3** Representative examples of measured trunk accelerations (TA; black solid line) with modelled  $a_1$  curves (blue dotted line) on the left, and the measured ground reaction force (GRF; black solid line) and directly predicted GRF profiles (red dotted line) on the right, including the root mean square error (RMSE) between both curves.

### 4.3.2 Indirect ground reaction force predictions

Although the two mass-spring-damper model could replicate measured TA and GRF profiles well on their own, the parameters required to accurately replicate TA strongly differed from the parameters required to reproduce measured GRF curves (figure 4.4). If parameter values required to reproduce GRF were low for a specific trial, the value required to replicate TA were typically very high and vice versa. This was the case for all eight parameters and was independent of task. Moreover, there was no consistency in parameter values within any of the tasks. Due to the difference between modelled  $a_1$  and GRF parameter values, there was no relationship found between the two sets of parameters, regardless of task (table 4.2). Since the largest  $R^2$  value was 0.05 and thus none of the parameters had  $R^2$  values larger than 0.3 (moderate correlation), the linear regressions were regarded as being too small to be used to recalculate any of the parameter values.

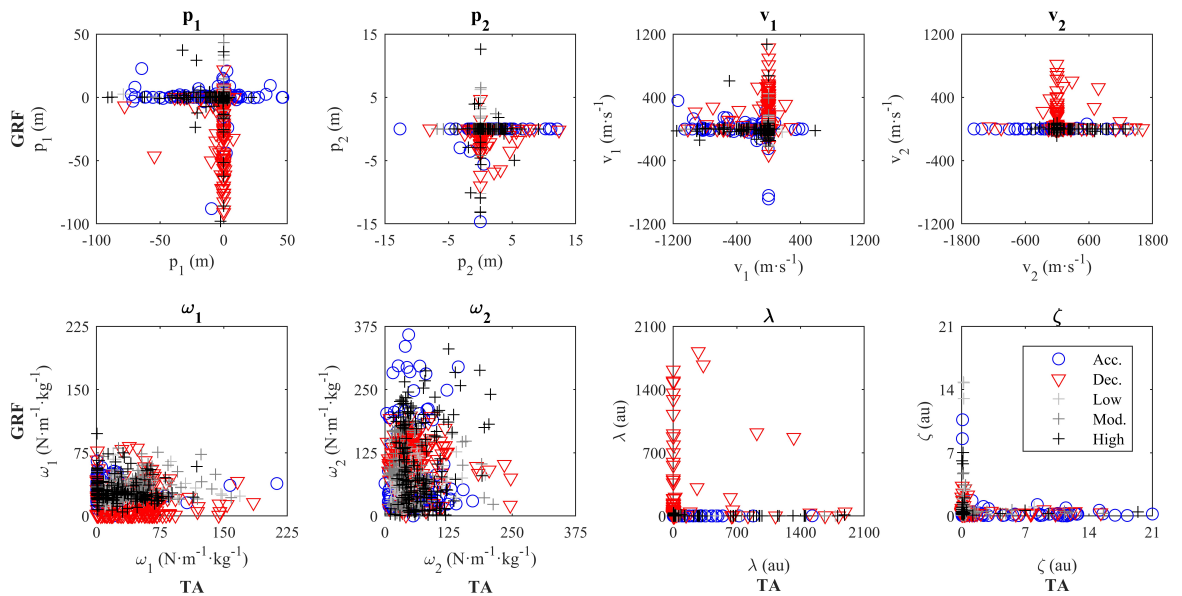


**Figure 4.4** Scatter plots of the eight model parameters for each individual acceleration (blue circles), deceleration (red triangles) and low, moderate and high-speed running (light grey, dark grey and black crosses respectively) trial. Parameter values required to model trunk accelerations (TA) or ground reaction force (GRF) are plotted on the x-axes and y-axes respectively.

	<b>p<sub>1</sub></b> <b>(m)</b>	<b>p<sub>2</sub></b> <b>(m)</b>	<b>v<sub>1</sub></b> <b>(m·s<sup>-1</sup>)</b>	<b>v<sub>2</sub></b> <b>(m·s<sup>-1</sup>)</b>	<b>ω<sub>1</sub></b> <b>(N·m<sup>-1</sup>·</b> <b>kg<sup>-1</sup>)</b>	<b>ω<sub>2</sub></b> <b>(N·m<sup>-1</sup>·</b> <b>kg<sup>-1</sup>)</b>	<b>λ</b> <b>(au)</b>	<b>ζ</b> <b>(au)</b>
Accelerations (n=189)	0.04	0.05	0.36	1.35	0.09	0.03	0	0.04
Decelerations (n=240)	0.08	0.07	0.08	0.33	0.16	0.9	1	0.05
Constant speed running								
Low (2-3 m·s <sup>-1</sup> ; n=126)	0.21	0	0.03	0.14	0.03	0.38	2.45	5.51
Mod. (4-5 m·s <sup>-1</sup> ; n=126)	0.1	0.2	0.05	0.39	1.69	0	1.2	0.4
High (>6 m·s <sup>-1</sup> ; n=176)	0.67	0.11	0.06	0.43	0.09	4.19	0.07	0.17
All tasks (n=857)	0.06	0.01	0.04	0.08	0	0.22	0.11	0

$R^2$  values ( $\cdot 10^{-2}$ ) of the linear regressions between parameter values required to model trunk accelerations or ground reaction forces, for the eight model parameters. Regressions were performed for each task separately, as well as for all tasks and trials combined. Only if  $R^2 > 0.3$  ( $=30 \cdot 10^{-2}$ ) the regression equation was used to recalculate the parameter.

#### 4.4 Discussion

This study aimed to predict GRF from accelerations measured at the upper trunk, either directly or indirectly, using a two mass-spring-damper model. Despite the model's ability to accurately replicate measured TA curves across the different tasks, direct GRF predictions following from the modelled  $a_1$  parameters were very poor. Furthermore, a relationship between trunk motion and GRF (Bobbert et al., 1991) was not reflected in the relationship between model parameters required to reproduce TA or GRF profiles, and could thus not be used to indirectly predict GRF from TA more accurately. In this discussion, several limitations of both approaches used in this study will be highlighted and a number of solutions to systematically improve the quality of GRF predictions will be described with reference to appendix C (direct method) and appendices D-F (indirect method). Furthermore, the value of using TA for biomechanical load monitoring purposes will be discussed.

##### 4.4.1 Directly predicting ground reaction forces from trunk accelerations

An essential assumption made in this study is that the model's upper mass acceleration  $a_1$  is correctly represented by the measured TA. However, since the upper mass represents multiple other segments (swinging leg, arms and head) besides the trunk (Alexander et al., 1986; Derrick et al., 2000), TA is known to be a surrogate measure of the combined motion of the model's

---

upper mass segments. This discrepancy might explain why GRF could not be directly predicted from replicated TA parameters. In addition, the measured TA signal is also known to not be an accurate representation of the trunk's CoM acceleration. First, the GPS device in which the accelerometer is embedded is worn on the back of the upper trunk between the Scapulae and thus not on, or close to the trunk's CoM. Secondly, despite carefully fitting this GPS unit in a tight vest, the measured TA signal is likely to include considerable noise due to wobbling of the unit in the pocket of the vest, as well as on the trunk. As a result of these limitations, the measured TA signal is likely to considerably differ from the actual acceleration of the trunk segment and consequently, from the combined upper mass segments movement. Appendix C shows that the measured TA signal indeed substantially deviated from the model's upper mass acceleration  $a_1$  required to accurately predict GRF. Despite these serious limitations, the unit's attachment to the trunk makes it likely that the measured TA signal contains the trunk's general motion, which might be a better reflection of the model's upper mass acceleration required to accurately predict GRF. However, appendix C also shows that extracting the general trunk motion by fitting a simple quadratic function to the measured TA signal and using this as input for the model's upper mass acceleration  $a_1$  could not lead to improved GRF predictions. The substantial differences between the measured TA and the model's upper mass acceleration were, therefore, considered to be a major reason why GRF could not be predicted from TA directly, using the two mass-spring-damper model.

#### *4.4.2 Indirectly predicting ground reaction forces from trunk accelerations*

As described in chapter 3 and the results of this chapter, for each individual trial a combination of model parameters was found to accurately model either GRF or TA profiles. Parameter values required to replicate TA were, however, not linearly related to the parameters required to reproduce GRF and could thus not be used to predict GRF using an indirect approach. There are, however, several limitations to this approach, including 1) task specificity, 2) the parameter search window, 3) the model's freedom, and 4) accuracy of the measured TA signal. These issues will here be discussed in more detail, while potential solutions will be suggested and explained with reference to appendices D-F.

---

First of all, since this investigation aimed to examine the model's ability to predict GRF for a range of activities that are frequently performed during running-based sports, a variety of different tasks was included. Figure 4.4 shows that different movements might require different ranges of values for certain parameters. For example, to reproduce GRF for deceleration trials the initial position of the model's upper mass  $p_1$  tended to be much lower and a higher initial velocity of the lower mass  $v_2$  and mass ratio  $\lambda$  were typically required, compared to other tasks (figure 4.4). Therefore, the weak relationships between modelled TA and GRF parameters could be due to the inclusion of all trials in the regression analysis. These relationships might be stronger when task-specific regression analyses are performed, rather than all movements combined. Although task-specific parameter regressions were indeed slightly stronger compared to those for a combination of all trials,  $R^2$  values were still trivial and too small to be used for recalculating any of the model parameters and achieve better GRF predictions.

Secondly, from figure 4.4 it appeared that parameter values required to replicate TA typically fell in a different range compared to those required to reproduce GRF. For example, for the majority of trials TA could be replicated with a natural frequency of the lower spring  $\omega_2$  between 0 and  $125 \text{ N}\cdot\text{m}^{-1}\cdot\text{kg}^{-1}$ , while  $\omega_2$  values required to reproduce GRF typically ranged between 0 and  $250 \text{ N}\cdot\text{m}^{-1}\cdot\text{kg}^{-1}$  (figure 4.4). As a result, regressions between both sets of parameters were very weak. In addition, parameter values often fell outside a physically meaningful range for both sets of parameters. The mass ratio  $\lambda$  for example, had values much larger than 10 for a large number of trials, which means that the support leg would represent less than 9% of the total body mass. Therefore, limiting the search window for parameter values (i.e. set an upper and lower bound to the parameters when modelling TA and GRF) might lead to a stronger relationship between both parameter sets. If for instance, equally good solutions for replicated TA and reproduced GRF exist within a physically meaningful range of parameter values, the relationship between both parameter sets might be improved. However, although the parameter space could be restricted to a physically meaningful range while maintaining reproduced GRF accuracy, this was highly detrimental for replicated TA curves and relationships between both parameter sets were still very weak (appendix D).

---

Thirdly, another possible explanation for the absence of a relationship between both sets of parameters could be the amount of freedom in the two mass-spring-damper model. All eight model parameters are closely related, highly dependent on each other and can adopt a substantial range of different values. As a result, it is likely that several combinations of parameters can give similarly good results when modelling TA and/or GRF profiles (e.g. as observed for reproduced GRF in appendix D). Therefore, restricting the number of free model parameters to limit the model's freedom might improve the relationships for the remaining free parameters. For example, if the upper spring's natural frequency  $\omega_1$  would be fixed at a constant value, the model's vertical stiffness would be determined by the natural frequency of the lower spring  $\omega_2$  only. Minor regression increases between both parameter sets were indeed observed when fixing either single or multiple parameters at a constant value (appendix E). However, the relationships were still very weak and could thus not be used to recalculate parameter values and achieve better indirect GRF predictions from TA.

Finally, the results in this chapter and chapter 3 show that the two mass-spring-damper model can accurately reproduce measured TA and GRF profiles when modelled separately. However, this chapter also shows that the model cannot be used to predict GRF from TA, either directly or indirectly. As discussed above, this discrepancy is likely to be the result of the difference between the measured TA signal and the model's upper mass acceleration  $a_1$  required for accurate GRF predictions (appendix C). Since multiple combinations of model parameters can, however, lead to similarly accurate modelled GRF (appendix D), it is possible that the model can use a single set of parameters to simultaneously reproduce measured TA and GRF profiles. If this is indeed the case, and the detrimental effects on the modelled TA and GRF curves are minimal, this might allow for bridging the dissimilarities between the measured TA and required  $a_1$ . Appendix F, however, shows a single set of model parameters that precisely replicated TA while maintaining an accurate GRF did not exist (appendix F), i.e. measured TA and GRF profiles could not both be modelled accurately at the same time. It was, therefore, concluded that GRF cannot be predicted from TA using a two mass-spring-damper model.

---

#### 4.4.3 *Using trunk accelerations for biomechanical load monitoring purposes*

The outcomes of this study have shown that predicting GRF from TA with a simple biomechanical model is not straight forward, despite its ability to accurately model a given TA or GRF profile. In most running-based sports, TA derived load measures, such as New Body Load, Dynamic Stress Load, Forceload and PlayerLoad have been suggested and used to assess the whole-body biomechanical loads of training and/or competition (Boyd et al., 2011; Colby et al., 2014; Ehrmann et al., 2016; Gaudino et al., 2015; Page et al., 2015). Although these measures have been suggested to be strongly related to e.g. total distance covered (Casamichana et al., 2013; Scott et al., 2013), an underpinning for their biomechanical meaning is yet lacking. TA derived measures are based on the assumption that TA is a good representation of the whole-body CoM acceleration, as well as the assumption that the trunk is the dominant contributor to GRF (Bobbert et al., 1991). Accelerations from trunk-mounted accelerometers have, however, been shown to poorly represent the whole-body CoM acceleration (Edwards et al., 2018; Nedergaard et al., 2017; Wundersitz et al., 2013). Moreover, it is established that the high-frequency impacts of landing are reduced in the upper body due to shock attenuation via active strategies (e.g. lower limb joint orientation and stiffness regulation) (Arampatzis et al., 1999; Bobbert et al., 1992; Lindsay et al., 2014), as well as the shock absorption of the passive structures in the musculoskeletal system (Hamill et al., 1995; Lafortune et al., 1996). The trunk's large contributions to GRF are thus likely due to its large mass rather than high accelerations. Information required to precisely predict GRF is, therefore, only partly described by the TA signal and additional segmental accelerations (e.g. shank and thigh accelerations) are probably required to estimate GRF from body-worn accelerometers. Future research should, therefore, investigate whether information about other segmental accelerations (which allows for alternative approaches to be explored) could be used to predict GRF more accurately. Moreover, one should be very cautious when interpreting acceleration signals of the trunk and derived load measures as an accurate estimate of biomechanical loading, as these metrics are unlikely to truly reflect the overall external forces experienced by the body.

---

#### 4.4.4 *Limitations*

For the studies described in chapters 3 and 4, a cohort of team sport athletes was recruited with varying sports backgrounds, training status and sex. This variability could form a limitation to the results observed. For example, participants could differ in skill or familiarity with the various running activities, fatigue prior to or during the session, training status and background (e.g. strength vs. endurance trained) and/or sex-dependent muscle-tendon properties. These factors may have affected an individual's movement execution and physical behaviour during the tasks performed. However, since GRF predictions from the two mass-spring-damper model were trial specific, it is unlikely that these factors have affected the GRF predictions. In fact, successful trial-specific GRF predictions would allow for the further examination of the effects of e.g. muscle-tendon properties or training status on movement strategies and overall loading of the body. Participants were thus deliberately recruited without a tight control for the factors mentioned above, to eventually allow for within- and between-participant investigations.

The approach described in this chapter used an accelerometer built into a commercial GPS device to predict GRF for various running tasks. The validity of this approach (and other similar methods) is, however, dependent on the validity and reliability of the accelerometer used. Although an accelerometer validation was beyond the scope of this study, previous research has demonstrated good reliability and accuracy of commercial wearable accelerometers (including the one used in the present study) for a range of sport-specific movements (Boyd et al., 2011; Scott et al., 2015; Simons and Bradshaw, 2016) (see chapter 2.2.2 for a more detailed discussion of accelerometer validity and reliability). Nevertheless, studies aiming to estimate biomechanical loading from body-worn accelerometers should consider the validity and reliability, either within or between units, as a potential source of inaccuracy for the quantified loads.

#### **4.5 Conclusion**

This study shows that the two mass-spring-damper model could replicate measured TA well, but direct and indirect GRF predictions were poor. Since GRF (which is determined by complex

---

multi-segmental movements) cannot be predicted from TA with a two mass-spring-damper model, accelerations of the trunk alone are probably insufficient to accurately predict GRF in running-based sports. Therefore, additional information (e.g. accelerations of other segments) is likely required to measure and monitor whole-body biomechanical loading in non-laboratory settings.

---

## **Chapter 5: Validating ground reaction forces estimated from multiple segmental accelerations**

---

*Abstract:* Chapter 4 has shown that acceleration signals from the trunk alone are unlikely to be sufficient to accurately predict ground reaction forces (GRFs). Since body-worn accelerometers are commonly used in sports to measure accelerations of various body segments, an alternative expression of Newton's second law might be used to estimate GRF from multiple segmental accelerations. However, it is unknown whether this approach can be used to accurately estimate GRF for activities that are frequently undertaken during running-based sports and/or what the minimal required number of segments is. Therefore, this study aimed to estimate GRF from multiple segmental accelerations for dynamic and high-intensity running tasks and determine the minimal number of segments required. GRF profiles for accelerations, decelerations, 90° cuts and running at constant low, moderate and high speeds were estimated as the sum of the product of all fifteen segmental masses and accelerations, or a reduced number of segments. Errors for GRF profiles and loading characteristics estimated from fifteen segmental accelerations varied from low to very high between the different tasks. Moreover, errors substantially increased for all tasks when the number of segments was reduced. These results show that it is unlikely that one or several segmental accelerations can provide accurate and meaningful estimates of whole GRF waveforms to assess whole-body biomechanical load across various dynamic and high-intensity activities, using a direct mechanical approach.

*This study was published in the Journal of Science and Medicine in Sports (Verheul et al., 2018).*

---

## 5.1 Introduction

Accelerometers embedded in commercial trunk-worn GPS devices are popular for assessing biomechanical training and competition loads in running-based sports. Based on the assumption that accelerations of the trunk are a good representation of whole-body centre of mass (CoM) accelerations, trunk accelerometry derived load measures (e.g. New Body Load, Dynamic Stress Load, PlayerLoad, Force Load) have been used to quantify and evaluate whole-body biomechanical loading (Boyd et al., 2011; Colby et al., 2014; Ehrmann et al., 2016; Gaudino et al., 2015; Page et al., 2015). However, evidence relating accelerations of the trunk to ground reaction forces (GRF), a well-established measure of whole-body load, is lacking. In fact, it has been shown that accelerations of individual segments (including the trunk) cannot accurately represent whole-body CoM accelerations and/or directly predict GRF during straight running at constant speeds (Edwards et al., 2018; Nedergaard et al., 2017; Pavei et al., 2017a; Raper et al., 2018; Wundersitz et al., 2013) and side-cutting (Nedergaard et al., 2017; Vanrenterghem et al., 2010; Wundersitz et al., 2013). Moreover, chapter 4 has shown that trunk accelerometry cannot be used to drive a two mass-spring-damper model to predict GRF, partly due to its deviations from the model's upper mass acceleration required for accurate GRF predictions. Acceleration signals from the trunk or other individual segments, therefore, appear to be insufficient to accurately estimate GRF.

Body-worn accelerometers are commonly used in sports to measure accelerations of various body segments (Camomilla et al., 2018; Chambers et al., 2015). Since GRF can be defined as the sum of the product of segmental mass and CoM accelerations of all body segments, multiple simultaneously measured segmental accelerations might be used to estimate GRF. Such an approach could provide a way by which the contribution of multiple segmental accelerations to the GRF can be examined systematically. Previous studies have indeed shown that this method can be used to estimate GRF for constant speed running from seven (Bobbert et al., 1991) or eleven (Pavei et al., 2017b) segmental accelerations derived from marker trajectory data measured with a laboratory-based motion capture system. However, it is yet completely unknown whether GRF for other activities that are frequently undertaken in running-based sports

---

(e.g. rapidly accelerating, decelerating, cutting, sprinting (Vigh-Larsen et al., 2018)) can be accurately estimated from segmental accelerations and/or what the minimal required number of segments is.

If simultaneously measured segmental accelerations can be used to estimate GRF, this might eventually allow GRF to be estimated from body-worn accelerometers in non-laboratory settings and provide a meaningful measure of whole-body biomechanical loading. Therefore, the aims of this study were 1) to investigate whether GRF can be estimated from multiple segmental accelerations for a variety of dynamic and high-intensity tasks frequently performed during running-based sports, and 2) to determine the minimal number of segments required.

## **5.2 Methods**

Ethical approval for this study was granted by Liverpool John Moores University ethics committee, with reference number 17/SPS/043. Data from the cohort and data collection described below were used for the studies described in this chapter, as well as chapter 6.

### *5.2.1 Participants and protocol*

Fifteen team sports athletes participated in this study (12 males and 3 females, age  $23 \pm 4$  yrs, height  $178 \pm 9$  cm, body mass  $73 \pm 10$  kg). All participants were healthy at the time of testing and were physically active for at least three hours per week (sports participation  $7.5 \pm 4.5$  hrs per wk). Prior to data collection, participants provided written informed consent according to Liverpool John Moores University ethics regulations.

After a standardised warm-up, participants performed a variety of dynamic and high-intensity running tasks including accelerations, decelerations,  $90^\circ$  cuts, and running at different constant speeds ranging from  $2 \text{ m} \cdot \text{s}^{-1}$  to maximal sprinting ( $\sim 7\text{-}9 \text{ m} \cdot \text{s}^{-1}$ ; participant-specific). Participants were instructed to land with one foot on a force platform embedded in the ground, and every task was performed five times for each leg. Participants were instructed to land with either their right or left foot on the force platform for a single step during each trial, but trials in which participants excessively targeted the force platform were excluded. Acceleration trials were performed from standstill to sprinting speed, while decelerations were performed from sprinting

---

to immediate standstill. For the 90° cutting tasks, participants approached the force platform at a self-selected moderate running speed and sharply cut to the side under a 90° angle on the force platform. Running trials were performed at a constant low (2-3 m·s<sup>-1</sup>), moderate (4-5 m·s<sup>-1</sup>) or high running speed (>6 m·s<sup>-1</sup>), including maximal sprinting. Running speeds were measured with photocell timing gates (Brower Timing Systems, Draper, UT, USA) which were positioned 3 m apart at 1.5 m before and after the force platform. Running speed were controlled by giving verbal feedback to speed up or slow down after each trial. Only trials within a ± 5% range of the target speed were included.

### 5.2.2 *Kinematic and kinetic data collection*

During the trials, full-body kinematic data were collected using a seventy-six retro-reflective marker set attached to anatomical landmarks on the body (figure 5.1 A; appendix G). Three-dimensional kinematic and kinetic data were synchronously recorded with ten infrared cameras (Qqus 300+, Qualisys Inc., Gothenburg, Sweden) sampling at 250 Hz, in combination with a force platform (9287B, 90x60 cm, Kistler Holding AG, Winterthur, Switzerland) embedded in the ground, sampling at 1500 Hz. Marker positions and ground reaction forces (GRF) were recorded and tracked using Qualisys Track Manager Software (QTM version 2.16, Qualisys Inc., Gothenburg, Sweden) (figure 5.1 B). A static calibration was recorded of participants standing in the anatomical position at the start of each session. After tracking, kinematic and kinetic data were exported to Visual3D (v6.01.06, C-Motion, Germantown, MD, USA) where static calibration trials were used to build a fifteen segment (head, trunk, pelvis, upper arms, forearms, hands, thighs, shanks and feet) six-degree-of-freedom model (figure 5.1 C). Local segment coordinate systems and joint centres were determined with a Visual3D in-built algorithm (Schwartz and Rozumalski, 2005). Segment dimension and inertial properties were based on Dempster's regression equations (Dempster, 1955) and represented as geometric volumes (Hanavan, 1964) (figure 5.1 C). This model was then applied to all the running trials and data were processed in Visual3D, as well as exported to Matlab (version R2017b, The MathWorks, Inc., Natick, MA, USA) for further processing and analysis.

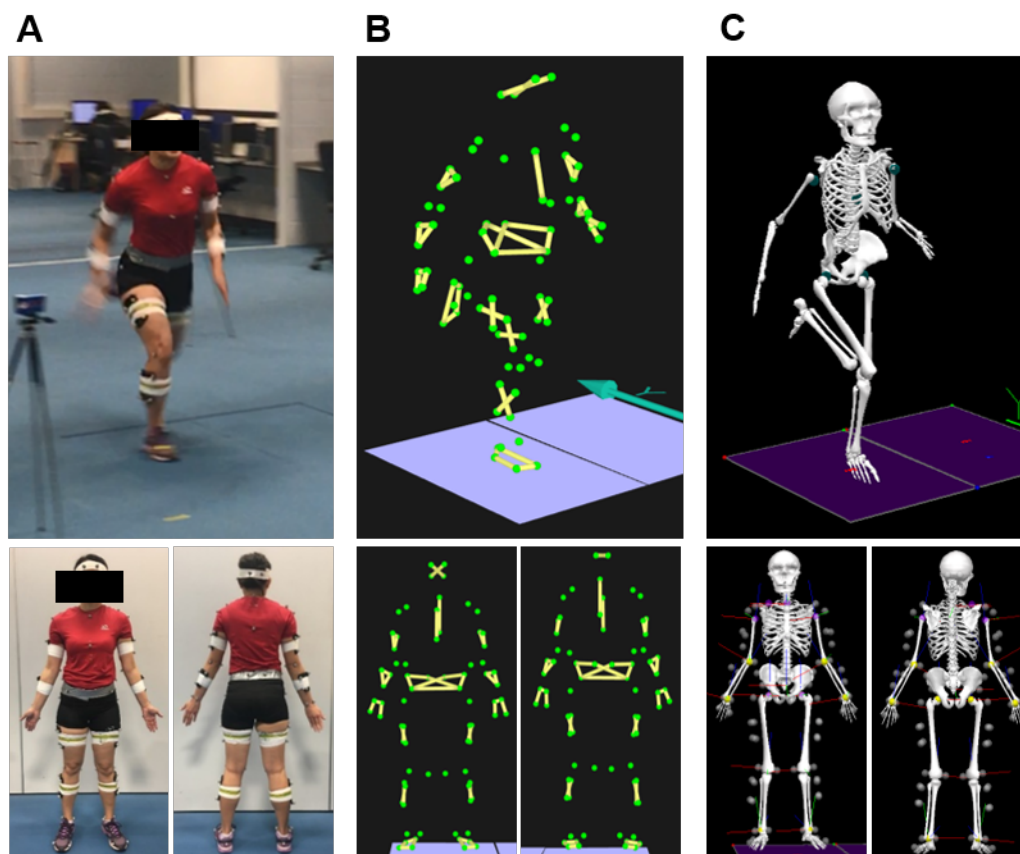


**Figure 5.1** *A*: A seventy-six retroreflective marker set was attached to anatomical landmarks and marker trajectories were recorded during the trials. *B*: Tracked marker trajectories in the Qualisys Tracking Manager (QTM) software for an example running trial (top) and static calibration trial (bottom). *C*: Marker trajectories were used to build a fifteen-segment kinematic model in Visual3D.

### 5.2.3 Data processing and analysis

Marker trajectories and force platform data were filtered with a 2<sup>nd</sup> order Butterworth low-pass filter at 20 Hz and 50 Hz respectively. Trunk defining marker trajectories were, however, filtered at 10 Hz based on a sensitivity analysis for optimal GRF prediction (appendix H). For each trial, touch-down and take-off from the force platform were identified by a 20 N threshold of the vertical GRF and resultant GRF was calculated from the three individual force components ( $F_x$ ,  $F_y$ ,  $F_z$ ). Centre of mass (CoM) position for each segment was used to define segment movements. Segmental accelerations were calculated as the double differentiation of CoM motion along the

three axes of the lab (x-y-z). Resultant GRF curves were then estimated as the sum of the product of each segmental mass and CoM acceleration in the three directions, according to equation 5.1.

$$GRF_{estimated} = \sqrt{\left(\sum_{n=1}^{1,2,\dots,15} (a_{n,x} \cdot m_n)\right)^2 + \left(\sum_{n=1}^{1,2,\dots,15} (a_{n,y} \cdot m_n)\right)^2 + \left(\sum_{n=1}^{1,2,\dots,15} (a_{n,z} \cdot m_n) + g \cdot BM\right)^2} \quad (5.1)$$

In which a is the segmental acceleration in x, y or z direction, m the segmental mass, n the number of segments included, g the gravitational acceleration ( $-9.81 \text{ m}\cdot\text{s}^{-2}$ ) and BM the total body mass. To determine the minimal number of segments required to accurately estimate GRF, all different segment combinations (per given number of segments) were used to estimate GRF data. A total of 32,676 unique combinations were analysed with a minimum of one and a maximal of fifteen segments. For combinations with less than all fifteen segments, masses of the segments not included were added to the other segments according to figure 5.2 to maintain total body mass. For each of the 32,676 combinations, the mean root mean square error (RMSE) of estimated GRFs for all participants, tasks and trials was calculated. The combination with the lowest mean RMSE across all tasks and trials for a given number of segments was then selected and used for further analysis.

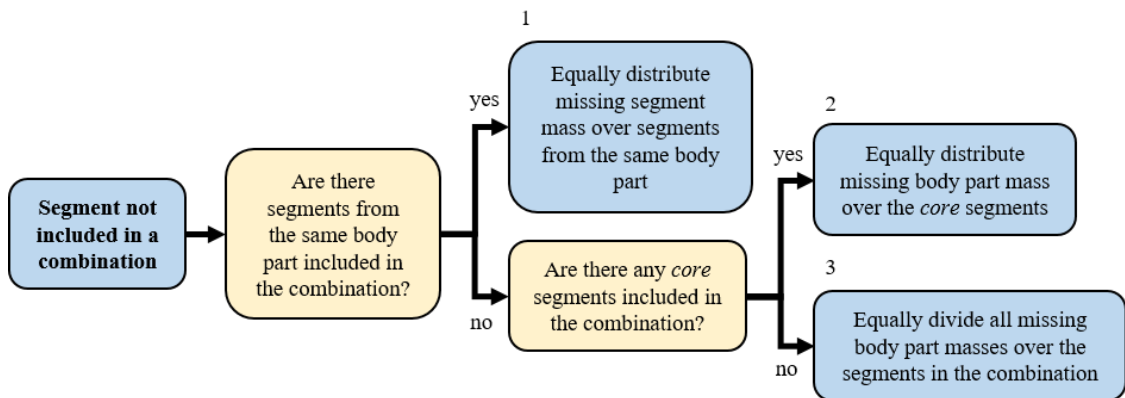


**Figure 5.2** To maintain total body mass, segment masses not included in a combination were redistributed. Body parts were defined as the core (head, trunk, pelvis), the left and right arm (hand, forearm, upper arm), and the left and right leg (foot, shank, thigh). For example, if a combination did not include the shank, its mass was equally distributed over the foot and thigh

(1), core segments if neither the thigh or foot were included (2), or all segments in the combination if no core segments were included either (3).

---

Measured and estimated GRF curves were normalised to each participant's body mass. Accuracy of the estimated GRF profiles was evaluated as the curve RMSE according to equation 5.2.

$$\text{RMSE} = \sqrt{\frac{\sum_{t=0}^n (\text{GRF}_{\text{estimated}}(t) - \text{GRF}_{\text{measured}}(t))^2}{n}} \quad (5.2)$$

In which  $t$  is each individual time point of the GRF curve and  $n$  the total duration of stance. In addition, relative RMSEs (as well as GRF loading characteristics) were determined according to equation 5.3 to allow for comparison between tasks with different GRF magnitudes.

$$\text{RMSE}_{\text{relative}} = \sqrt{\frac{\sum_{t=0}^n \left( \frac{\text{GRF}_{\text{estimated}}(t) - \text{GRF}_{\text{measured}}(t)}{\text{GRF}_{\text{measured}}(t)} \right)^2}{n}} \cdot 100\% \quad (5.3)$$

In addition, relevant GRF loading characteristics impulse, impact peak and loading rate were used to assess estimated GRF curve accuracy, as described in chapter 3.2. Since marker vibrations caused multiple smaller peaks after touch-down for some trials, only impact peaks >500 N were included in the analysis. Estimated curve RMSE and GRF loading characteristic errors were then averaged across all trials and participants for each task. RMSE was rated as being very low (<1 N·kg<sup>-1</sup>), low (1-2 N·kg<sup>-1</sup>), moderate (2-3 N·kg<sup>-1</sup>), high (3-4 N·kg<sup>-1</sup>) or very high (>4 N·kg<sup>-1</sup>). RMSE values were analysed for all possible combinations of segments per task, as well as all trials combined, to determine the best combination (i.e. lowest mean RMSE across trials) for each number of segments. Based on meaningful performance or injury related differences (Bazuelo-Ruiz et al., 2018; Bezodis et al., 2017; Hunter et al., 2005), the magnitude of GRF loading characteristic errors was rated as being very low (<5%), low (5-10%), moderate (10-15%), high (15-20%) or very high (>20%). Linear correlation analyses were performed to examine the relationship between estimated and measured impulses, impact peaks and loading rates per task, as well as all trials combined to examine the generalisability of GRF estimates across tasks. Correlations were rated as very weak ( $R^2 < 0.1$ ), weak ( $R^2 = 0.1-0.3$ ), moderate ( $R^2 = 0.3-0.5$ ), strong ( $R^2 = 0.5-0.7$ ), very strong ( $R^2 = 0.7-0.9$ ) or extremely strong ( $R^2 = 0.9-1$ ) (Hopkins et al., 2009). In addition, Bland-Altman analyses (Bland and Altman, 2010) were

performed across tasks to explore the bias (mean difference) and 95% limits of agreement between the estimated and measured GRF loading characteristics.

### 5.3 Results

#### 5.3.1 Estimated ground reaction force from fifteen segments

Accuracy of estimated GRF profiles from fifteen segmental accelerations (full-body) varied across tasks (figure 5.3; table 5.1). Overall estimated curve errors (RMSE) were low for running at low speeds and moderate for accelerations, 90° cuts and moderate-speed running. However, mean RMSE was very high for decelerations and high-speed running.

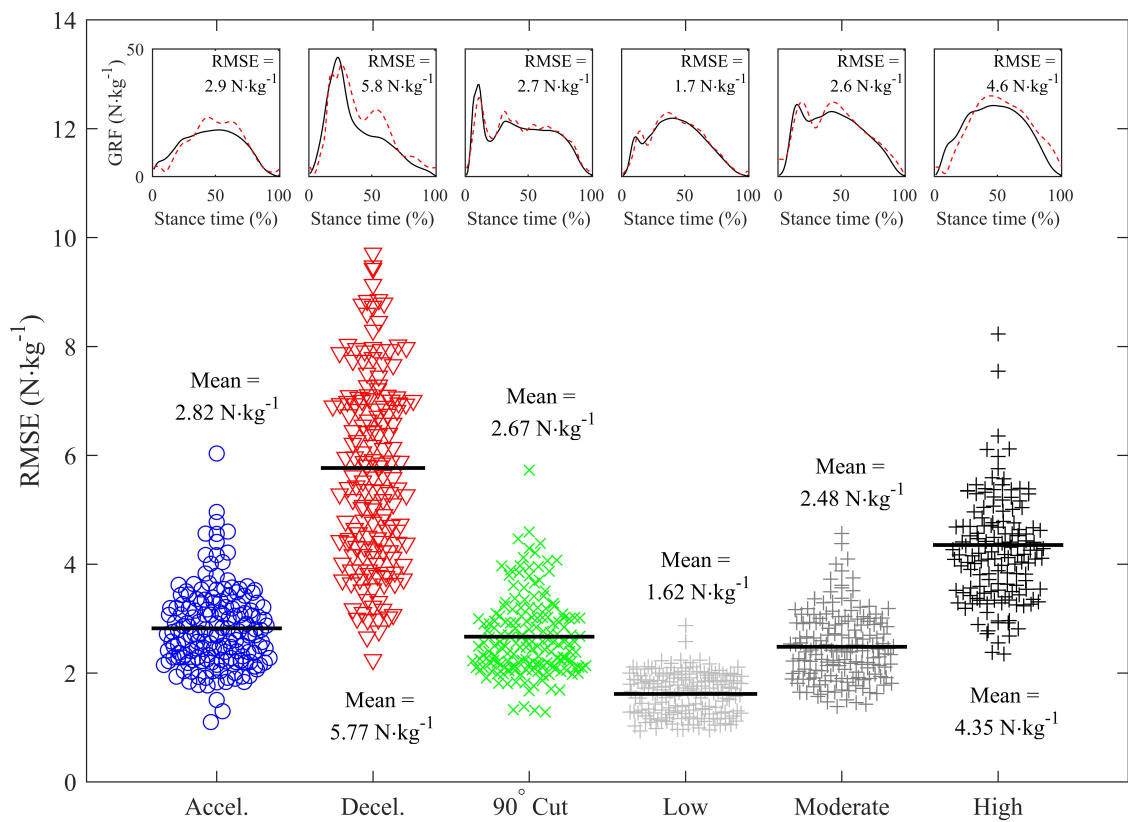


**Figure 5.3** Swarm plot of the root mean square errors (RMSE) for ground reaction force (GRF) curves estimated from fifteen segmental accelerations. *Inset:* representative measured (black solid line) and estimated (red dashed line) GRF profiles, together with RMSE values for all acceleration (n=167), deceleration (n=162), 90° cut (n=171), low (n=158), moderate (n=157) and high-speed running (n=141) trials.

Accuracy of estimated GRF loading characteristics varied between the different variables and tasks (table 5.1). Impulses were accurately estimated with very low errors for 90° cuts and running at constant low and moderate speeds, low errors for accelerations, and moderate errors for decelerations and running at high speeds. Similarly, impact peaks were estimated with low to moderate (9.2-15%) errors for all tasks, except accelerations, which had very high (28.5%) impact peak errors. Loading rate errors however, were very high (20.1-42.8%) across all tasks. Correlations and agreements between measured and estimated GRF loading characteristics were dependent on task. Impulses had extremely strong correlations, with a small bias and 95% confidence interval of the limits of agreement (-0.04 to 0.45 N·s·kg<sup>-1</sup>) (figure 5.4 A and D; table 5.1). For impact peaks however, there was a large variation of the differences with limits of agreement ranging from -12.6 to 8.4 N·kg<sup>-1</sup>, despite the very strong correlation and small bias (figure 5.4 B and E). Furthermore, measured and estimated loading rates had a strong correlation ( $R^2 = 0.68$ ) but a large bias and limits of agreement (-985 to 397 N·kg<sup>-1</sup>·s<sup>-1</sup>) (figure 5.4 C and F).

**Table 5.1** Estimated ground reaction force curve and loading characteristics errors

	RMSE		Impulse error			Impact peak error			Loading rate error		
	N·kg <sup>-1</sup>	%	N·s·kg <sup>-1</sup>	%	R <sup>2</sup>	N·kg <sup>-1</sup>	%	R <sup>2</sup>	N·kg <sup>-1</sup> ·s <sup>-1</sup>	%	R <sup>2</sup>
Accelerations (n=166)	2.82 ±0.7	8.4 ±14	0.25 ±0.1	9.1 ±4	0.89	3.27 ±2.8	28.5 ±33	0.21	229 ±264	33.2 ±27	0.36
Decelerations (n=161)	5.77 ±1.8	6.1 ±8.8	0.26 ±0.1	11.1 ±6	0.94	7.68 ±5.5	15 ±9	0.73	380 ±404	20.1 ±16	0.49
90° Cuts (n=171)	2.67 ±0.7	3.3 ±4.1	0.21 ±0.1	3.8 ±2	0.98	3.33 ±2.9	9.8 ±8	0.75	234 ±210	24.5 ±18	0.60
Constant speed running											
Low (2-3 m·s <sup>-1</sup> ; n=157)	1.62 ±0.4	1.8 ±2	0.09 ±0.06	2.3 ±2	0.96	2.22 ±2.3	13.8 ±22	0.64	173 ±101	33 ±13	0.42
Mod. (4-5 m·s <sup>-1</sup> ; n=157)	2.48 ±0.6	3.1 ±5.7	0.16 ±0.1	4.6 ±2	0.93	1.96 ±1.5	9.2 ±8	0.85	281 ±174	34 ±14	0.53
High (>6 m·s <sup>-1</sup> ; n=141)	4.35 ±1.3	6.4 ±7.6	0.26 ±0.2	10.4 ±12	0.77	3.52 ±3.5	11.9 ±13	0.56	661 ±419	42.8 ±21	0.12
All tasks (n=953)	3.26 ±1.7	4.8 ±8.3	0.20 ±0.1	6.8 ±7	0.99	4.00 ±4.1	13.1 ±15	0.88	323 ±326	29.3 ±19	0.68

Root mean square error (RMSE), impulse, impact peak and loading rate errors of the ground reaction force (GRF) estimated from fifteen segmental accelerations, for the different tasks. Values are means ± standard deviations and either absolute or relative errors compared to the measured GRF. Correlations ( $R^2$ ) were determined per task as well as for all trials combined.

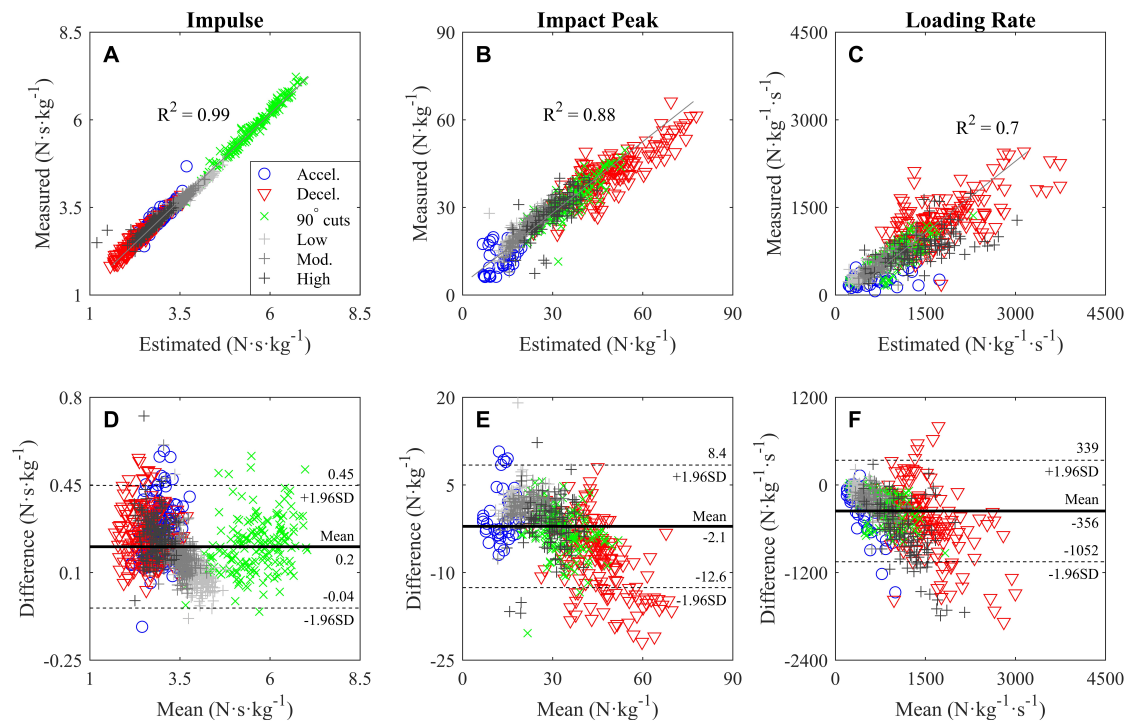


**Figure 5.4** Correlation (A-C) and Bland-Altman (D-F) plots between measured and estimated GRF loading characteristics impulse, impact peak and loading rate, from fifteen segments.

### 5.3.2 Segment reductions

The best combinations of segments across all tasks for each given number of segments are shown in table 5.2. Although GRF estimated from a single segment was the best across tasks from trunk accelerations, mean RMSEs were very high. Furthermore, the trunk was part of all combinations of segments, and thus the main contributor to overall GRF, followed by the thighs, head, shanks, arms, feet and pelvis (in descending order of importance).

Reducing the number of segmental accelerations to estimate GRF substantially increased RMSE and loading characteristics errors for all tasks (figure 5.5; table 5.2). To achieve estimated GRF errors that were moderate or better ( $<3 N \cdot kg^{-1}$ ) for at least 50% of the trials, a minimum of two and three segments was required for running at low and moderate speeds respectively. For more dynamic tasks however, a minimum of eleven (accelerations) and eight (90° cuts) segments was needed to estimate GRF with moderate errors for at least half the trials. In addition, for the high-intensity tasks (decelerations and running at high speeds) the majority of trials and combinations resulted in very high errors, regardless of the number of segments used. Likewise, impulse,

impact peak and loading rate errors substantially increased for all tasks when the number of segmental accelerations was reduced (figure 5.5).

**Table 5.2** Combinations of segments with the lowest root mean square errors for each number of segments

#	Segments in the combination	RMSE (N·kg <sup>-1</sup> )	
		Mean	SD
1	Trunk	6.76	±3.62
2	Trunk + thigh	5.91	±3.17
3	Trunk + thighs	4.54	±2.48
4	Trunk + thighs + pelvis	4.36	±2.47
5	Trunk + thighs + pelvis + head	4.00	±1.94
6	Trunk + thighs + pelvis + shanks	3.76	±1.81
7	Trunk + thighs + shanks + head + upper arm	3.61	±1.66
8	Trunk + thighs + shanks + head + upper arm + forearm	3.49	±1.73
9	Trunk + thighs + shanks + head + upper arms + forearm	3.42	±1.75
10	Trunk + thighs + shanks + head + upper arms + forearms	3.37	±1.74
11	Trunk + thighs + shanks + head + upper arms + forearms + hand	3.31	±1.73
12	Trunk + thighs + shanks + head + upper arms + forearms + hand + foot	3.28	±1.72
13	Trunk + thighs + shanks + head + upper arms + forearms + hand + feet	3.26	±1.71
14	Trunk + thighs + shanks + head + upper arms + forearms + hands + feet	3.26	±1.71
15	Trunk + thighs + shanks + head + upper arms + forearms + hands + feet + pelvis	3.26	±1.72

Combinations of segments with the lowest mean root mean square errors (RMSE) across participants, tasks and trials, for each number of segments. If only one of two segments was included in a combination (e.g. thigh or foot rather than thighs or feet), this was the segment on the side of the support leg.

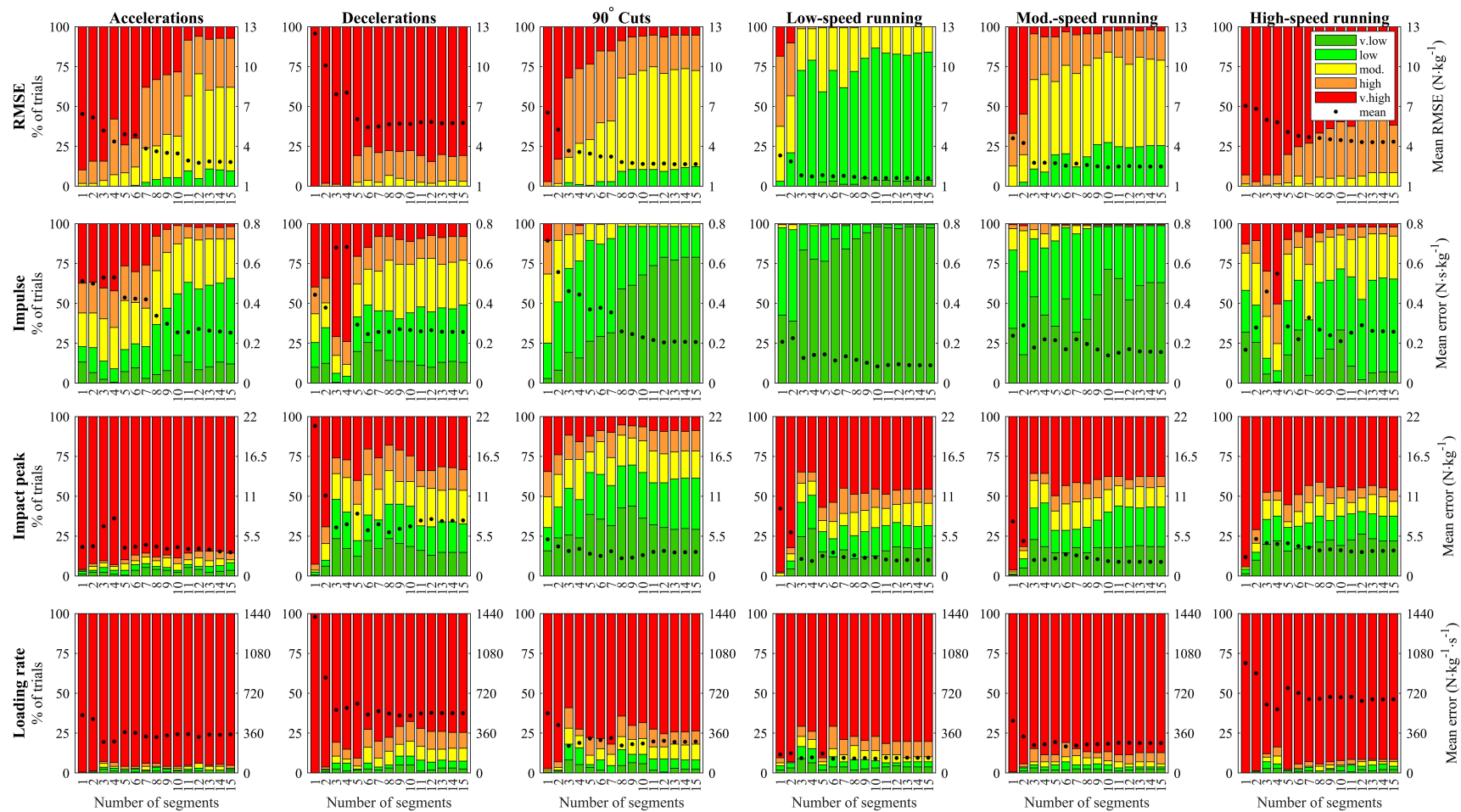


**Figure 5.5** Root mean square errors (RMSE), impulse, impact peak and loading rate errors for estimated GRF profiles for each task. Bars represent the percentage of trials (primary y-axis) within the very low ( $<1 \text{ N}\cdot\text{kg}^{-1}$ ), low ( $1\text{-}2 \text{ N}\cdot\text{kg}^{-1}$ ), moderate ( $2\text{-}3 \text{ N}\cdot\text{kg}^{-1}$ ), high ( $3\text{-}4 \text{ N}\cdot\text{kg}^{-1}$ ) or very high ( $>4 \text{ N}\cdot\text{kg}^{-1}$ ) error boundaries, and black dots represent the mean errors (secondary y-axis), for each given number of segments.

---

## 5.4 Discussion

### 5.4.1 Estimating ground reaction forces from fifteen segments

The aim of this study was to estimate whole GRF waveforms from segmental accelerations for a variety of dynamic and high-intensity running tasks that are frequently performed during running-based sports. From all fifteen body segments, overall GRF profiles as well as specific loading characteristics were estimated with varying accuracy across tasks. Overall loading errors (RMSE and impulse) for example, were considerably lower for running at low and moderate speeds (~2-5%) compared to the higher intensity tasks (decelerations, high-speed running) (~6-12%). Similarly, impact peak and loading rate errors ranged from ~9% for the lower intensity tasks to >40% for higher intensity tasks (figure 5.4 E and F). Meaningful performance or injury related differences in loading characteristics can, however, be as small as ~3-10% (Bazuelo-Ruiz et al., 2018; Bezodis et al., 2017; Hunter et al., 2005). Errors of the magnitude observed in this study might, therefore, already rule out certain applications of monitoring GRF estimated from full-body segmental accelerations. The mechanical approach to estimate GRF used in this study, therefore, has limited validity to assess whole-body biomechanical loading for dynamic and high-intensity activities.

Estimated GRF results in this study are comparable to other laboratory-based studies aiming to predict GRFs from marker trajectory data using a mechanical approach. The low impulse errors for running at low and moderate speeds (<5%) for example, are similar to the low vertical impulse errors of <1% for running at 1.94-5.56 m·s<sup>-1</sup> reported by Pavei et al. (2017b), who estimated GRFs from whole-body CoM accelerations estimated from marker trajectory data using an eleven-segment kinematic model. Likewise, the estimated impact peak errors of ~9.2% for constant moderate-speed running are comparable to the <10% impact peak errors for running at 3.6-5.3 m·s<sup>-1</sup> reported by Bobbert et al. (1991), who estimated GRF from a seven-segment model and used the same mechanical approach as this study. Moreover, Udofa et al. (2016) modelled GRF from marker trajectory data using a two-mass model and found a correlation of R<sup>2</sup>=0.82 between measured and modelled impact peaks for running at speeds ranging from 3 to 6 m·s<sup>-1</sup>, similar to the very strong to extremely strong correlations (R<sup>2</sup>=0.77-0.96 for low-high-

---

speed running) found in the current study. Despite these similarities, however, this study extends beyond other studies in that similar results can also be achieved for a range of high-intensity and dynamic running activities frequently undertaken during running-based sports. In addition, previous studies did not include the mediolateral and anteroposterior components of acceleration and GRF (Bobbert et al., 1991; Udofa et al., 2016), utilised small sample sizes of one or a few participants (Bobbert et al., 1991; Pavei et al., 2017b; Udofa et al., 2016) and/or investigated running on a treadmill rather than overground (Pavei et al., 2017b; Udofa et al., 2016), all of which limits their ability to translate their findings from the lab to an applied sport setting.

Estimated GRF errors in this study are solely due to measurement and methodological inaccuracies. The differences in estimated GRF accuracy observed between tasks in this study (figures 5.2 and 5.4; table 5.1) might thus be explained by the substantially higher impacts of landing in decelerations and high-intensity running. The hard collisions with the ground experienced during these tasks likely cause considerable marker movement and vibrations due to soft-tissue artefact (Camomilla et al., 2017), leading to increased over- or underestimation of the actual segmental CoM accelerations. For high-intensity tasks especially, the rapid accelerations of the body segments just after touch-down (for the lower limbs especially) are substantial, leading to considerable marker movement and vibrations. During less intense tasks, such as low-speed running however, impact accelerations are much less severe and thus less likely to cause excessive marker movement. Consequently, marker trajectory-based segment positions and derived accelerations, as well as resulting GRF estimates, are more accurate for these lower intensity tasks. This could explain the relatively low RMSE and GRF loading characteristics errors for low and moderate-speed running observed in the present study, compared to the substantially higher errors for decelerations and high-speed running.

In most running-based sports, the dynamic and high-intensity movements examined in this study are regularly performed (Dalen et al., 2016; Datson et al., 2018; Vigh-Larsen et al., 2018). The musculoskeletal demands of these tasks are high (Akenhead et al., 2013; Harper and Kiely, 2018; Kyröläinen et al., 2005) and thus comprise a large amount of the total biomechanical loads

---

experienced during training and competition. Therefore, highly accurate estimates of GRF loading characteristics across different tasks (including decelerations and running at high speeds) are essential to explore and understand the biomechanical demands of training in greater detail. As discussed above however, the loading characteristics errors observed in this study might already rule out several performance and injury related applications of monitoring GRF. Therefore, the strong to extremely strong correlations between estimated and measured GRF characteristics found in this study (figure 5.4; table 5.1) could be used to recalculate and improve the estimated loading characteristics to quantify the biomechanical loads of training more accurately.

#### 5.4.2 *Segment reductions*

As simultaneously measuring the accelerations of fifteen segments outside laboratory settings is currently unlikely to be feasible, this study examined the effects of reducing the number of segments and the minimal number of segments required to accurately estimate GRF. When the number of segmental accelerations was reduced to ten segments (i.e. excluding hands, feet and pelvis), errors already substantially increased for all tasks (figure 5.5). Previous studies have reported similar findings of considerably decreased accuracy in whole-body CoM estimates (and thus GRF) for constant speed running (Gill et al., 2017; Pavei et al., 2017a), side-cutting (Vanrenterghem et al., 2010), and jumping, kicking and throwing (Jamkrajang et al., 2017), when the number of segments was only slightly reduced. Furthermore, the very high errors observed in this study for GRF estimated from one segment (i.e. the trunk) are in line with other studies which reported that individual segmental accelerations cannot be used to accurately estimate GRF for straight running at constant speeds (Nedergaard et al., 2017; Pavei et al., 2017a; Raper et al., 2018) and side-cutting (Nedergaard et al., 2017; Vanrenterghem et al., 2010). Given the mixed results for GRF profiles estimated from fifteen segments in this study, as well as the increased errors from a reduced number of segments observed, it is unlikely that a reduced number of segmental accelerations can be used to accurately estimate GRF across various dynamic and high-intensity running tasks. Consequently, practically all segmental accelerations are required to measure and monitor the whole-body biomechanical loads of training.

---

#### 5.4.3 *Using accelerometers to estimate ground reaction forces*

A limitation of this study is that segmental accelerations used to estimate GRF were derived from marker trajectory data recorded with a three-dimensional motion capture system. Similar to force platforms, such systems are not typically available in the field and if they are, data collection is laborious and unpractical. In contrast to force platform and motion capture technologies however, inertial measurement units (IMUs), such as accelerometers, are commonly used in the field. These units are applied in most sports to measure and monitor various training load metrics (Cardinale and Varley, 2017), and have been widely used to identify sport-specific movements and evaluate performance (Blair et al., 2018; Camomilla et al., 2018; Chambers et al., 2015). Moreover, technological improvement have allowed for accelerometers to be embedded into body-worn devices, such as watches (Adams et al., 2016), eyeglasses (Amft, 2017), GPS devices (Boyd et al., 2011) and even garments (Amft, 2017; Dürking et al., 2016). Given their widespread use and relatively easy accessibility, accelerometers might, therefore, offer a potential way to simultaneously measure multiple segmental accelerations required to estimate GRF in non-laboratory setting, providing signals accurately reflect the actual segmental accelerations.

An important requirement for GRF to be accurately estimated from segmental accelerations is that measured signals correctly represent the actual segment CoM accelerations. If not, GRF cannot be estimated accurately and errors will increase with increasing accelerometry inaccuracies. Segment CoM accelerations are, however, known to be difficult to measure accurately, even from ‘gold-standard’ motion capture, as evidenced by the findings in this study. These inaccuracies can mainly be attributed to the limitations of motion capture techniques (e.g. marker movement and vibrations due to soft tissue artefacts) and incorrect estimates of segmental inertial properties, such as standardised segment dimensions and masses based on cadaver experiments (Dempster, 1955). Although the effects of such individual factors may only be minimal, an accumulation of errors can lead to considerable inaccuracies. Likewise, accelerometry signals are likely to deviate substantially from the actual segment’s CoM acceleration due to their positioning away from the segment’s CoM, soft tissue artefacts and,

---

with dimensions of current devices being ~50-90 mm and weighing ~50-150 g, wobbling of the units themselves. For example, accumulated trunk-accelerometry derived loads of running, agility and tackling activities have been shown to be largely dependent on the means of accelerometer attachment to the trunk (McLean et al., 2018). In addition, exploratory work with data from this study showed that acceleration signals measured with accelerometers placed on the shank, thigh and pelvis deviated substantially from segmental CoM accelerations derived from marker trajectory data (appendix I). These results support previous findings of deviations between accelerometry and motion capture derived segmental accelerations (Edwards et al., 2018; Wundersitz et al., 2015a, 2015b). Future work should, therefore, investigate whether these limitations can be overcome (e.g. by improving unit placement or fitting) and more accurate measurements of segmental CoM accelerations can be achieved. Until such research has been performed though, body-worn accelerometers are unlikely to provide valid estimates of whole GRF waveforms for dynamic and high-intensity tasks frequently performed in running-based sports, using a direct mechanical approach.

## **5.5 Conclusion**

This study shows that the accuracy of GRF profiles and loading characteristics estimated from full-body segmental accelerations is dependent on the type of task examined and the number of segments used. It is, therefore, unlikely that one or several segmental accelerations can provide accurate and meaningful estimates of whole GRF waveforms across tasks for biomechanical load monitoring purposes, using a direct mechanical approach. More complex analyses are, therefore, likely required to provide further insight in the feasibility of using segmental accelerations to assess external whole-body loads in running-based sports.

---

## **Chapter 6: Identifying key segmental contributions to ground reaction force features**

---

*Abstract:* Chapter 5 has shown that one or several segmental accelerations are unlikely to be sufficient for estimating whole ground reaction force (GRF) waveforms, across dynamic and high-intensity running tasks. Nevertheless, identifying acceleration characteristics associated with specific GRF features could provide further insight in the feasibility of using segmental accelerations to assess whole-body biomechanical loading. Therefore, this study used principal component analysis (PCA) to identify key segmental contributions to GRF. A combined PCA was performed on segmental accelerations of all fifteen body segments, for accelerations, decelerations, 90° cuts and running at constant low, moderate and high speeds. Segmental accelerations were then reconstructed and GRFs calculated from each principal component (PC). The first PC primarily explained between-task magnitude variability of segmental acceleration and GRF impulse, while the second PC highlighted magnitude and timing differences across tasks in high-frequency acceleration and GRF characteristics. Although the first five PCs described the most important GRF features, higher PCs primarily explained segmental contributions to the overall GRF magnitude. These findings show that key segmental contributions to specific GRF features, as well as the relative importance of these characteristics in different running activities, are highly complex and task-specific. Therefore, the value of using segmental accelerations, or even distinct components, to assess whole-body biomechanical loads across tasks frequently performed during running-based sports, is likely limited.

---

## 6.1 Introduction

Chapter 5 has shown some potential of using full-body segmental accelerations to estimate whole GRF waveforms, using a direct mechanical approach. However, simultaneously measuring fifteen segmental accelerations in the field on a daily basis is currently unlikely to be feasible. Moreover, estimating GRF profiles and loading characteristics from less than fifteen segments (chapter 5), as well as measuring segmental centre of mass (CoM) accelerations from body-worn accelerometers instead of a ‘gold-standard’ motion capture system (appendix I), were shown to substantially reduce the accuracy of GRF estimates. These findings suggest that whole GRF profiles are unlikely to be estimated with accuracies sufficient for biomechanical load monitoring purposes in the field, across different tasks that are frequently performed during running-based sports. However, the different approaches described in the previous chapters aimed to estimate complete GRF waveforms from a number of segmental acceleration signals but could not identify segmental contributions to specific GRF features (i.e. only during a certain part of the stance phase). Since human running is the result of a complex combination of segmental movements, which simultaneously contribute to multiple specific GRF features, more complex analyses are probably required to provide further explanation of different GRF profiles and loading characteristics.

Principal component analysis (PCA) has been used to reduce the amount of redundant information and extract key characteristics of highly-dimensional biomechanical data. For example, PCA has been used to analyse gait patterns (Daffertshofer et al., 2004; Federolf et al., 2013a; Troje, 2002) and postural control (Federolf, 2016; Federolf et al., 2013b), differentiate between pathological groups (Deluzio et al., 1997; Federolf et al., 2013a; Wrigley et al., 2005), or quantify and evaluate sports technique (Boyer et al., 2014; Federolf et al., 2014; Gløersen et al., 2018). For such applications of PCA to waveform data, PCA has been shown to be able of identifying and describing three different modes of variation (Brandon et al., 2013; Wrigley et al., 2005); 1) magnitude variability, which explains differences in waveform amplitudes within a specific time window, 2) difference features, which describe variation in sign or direction, and 3) phase shift characteristics, which describe changes in the relative timing of events within

---

waveforms. Therefore, PCA might be used to identify key elements of magnitude, variation and timing of segmental accelerations and describe their relative contribution to the GRF for different running tasks.

A mass-spring-damper model approach (chapter 4) and a direct mechanical method (chapter 5) have shown that whole GRF waveforms can unlikely be predicted from segmental acceleration profiles, across different tasks. However, these methods could not distinguish between key segmental acceleration features and describe the relative contribution of these characteristics to the overall GRF profile. If specific features of the GRF are related to identifiable acceleration characteristics, this could provide further insight in the feasibility of using body-worn accelerometry to assess external whole-body loads experienced during running-based sports. Therefore, this study used PCA to identify key segmental contributions to GRF features that might be used to evaluate biomechanical loading.

## **6.2 Methods**

### *6.2.1 Data*

Segmental CoM accelerations and GRF were collected for fifteen segments from fifteen team sports athletes (12 males and 3 females, age  $23 \pm 4$  yrs, height  $178 \pm 9$  cm, body mass  $73 \pm 10$  kg, sports participation  $7.5 \pm 4.5$  hrs per wk) who performed a variety of dynamic and high-intensity running tasks (accelerations, decelerations,  $90^\circ$  cuts and running at different constant speeds ranging from  $2 \text{ m}\cdot\text{s}^{-1}$  to maximal sprinting). For the purpose of this study, only data for ground contacts of the right foot were included. Further details on the protocol, as well as data collection and processing are described in the methods section of chapter 5.

### *6.2.2 Normalisation and scaling*

Processing of segmental acceleration data before performing the PCA was based on previously described applications of PCA for biomechanical data (Daffertshofer et al., 2004; Federolf, 2016; Gløersen et al., 2018; Troje, 2002). Segmental CoM accelerations in the mediolateral (x), anteroposterior (y) and vertical (z) direction during ground contact, together with GRF curves, were normalised to 101 data points for each trial in Visual3D (v6.01.06, C-Motion,

Germantown, MD, USA) and exported to Matlab (version R2017b, The MathWorks, Inc., Natick, MA, USA). The three-dimensional segmental accelerations for all fifteen segments were expressed as acceleration vectors  $\mathbf{a}$  for every time point  $t$  (equation 6.1) (note: vectors and matrices will be referred to by using bold lowercase or capital letters respectively).

$$\mathbf{a}(t) = [ax_1(t), ay_1(t), az_1(t), ax_2(t), \dots, az_{15}(t)] \quad (6.1)$$

The combination of acceleration vectors for each trial thus formed a  $101 \cdot 45$  acceleration matrix  $\mathbf{A}^{\text{trial}}$ . The trial-specific acceleration matrices were then combined in participant- and task-specific matrices  $\mathbf{A}^{\text{part,task}}$  by vertically stacking each trial matrix  $\mathbf{A}^{\text{trial}}$  per participant and task. The combined accelerations matrices  $\mathbf{A}^{\text{part,task}}$  were normalised and scaled to 1) assure that every participant equally contributed to the variance of the total acceleration matrix, 2) reduce the anthropometric differences between participants, 3) preserve the relative segmental acceleration amplitudes and 4) correctly represent the portion of the total body mass of each segment (Federolf, 2016). First for normalisation, a participant- and task-specific mean acceleration vector  $\overline{\mathbf{a}^{\text{part,task}}}$  was calculated and subtracted from each acceleration vector  $\mathbf{a}$  (equation 6.2), to assure that the first principal component (PC) described the direction of maximum variance in the segmental acceleration data.

$$\mathbf{A}^{\text{part,task}'}(t) = \begin{bmatrix} (ax_1(t) - \overline{ax_1^{\text{part,task}}}), (ay_1(t) - \overline{ay_1^{\text{part,task}}}), \dots, \\ (az_{15}(t) - \overline{az_{15}^{\text{part,task}}}) \end{bmatrix} \quad (6.2)$$

The normalised acceleration matrix  $\mathbf{A}^{\text{part,task}'}$  thus represented the acceleration deviations from the participant's mean segmental acceleration for each task. Secondly, the acceleration vectors for each participant were divided by the mean Euclidean norm  $\overline{\text{euc}_{\text{norm}}^{\text{part,task}}}$  of all acceleration vectors (equation 6.3), to ensure that participants equally contributed to the variance of the total acceleration matrix and minimise segmental acceleration amplitude differences due to anthropometric differences (Federolf et al., 2013b; Gløersen et al., 2018).

$$\mathbf{A}^{\text{part,task}''}(t) = \frac{\mathbf{A}^{\text{part,task}'}(t)}{\overline{\text{euc}_{\text{norm}}^{\text{part,task}}}} \quad (6.3)$$

---

Thirdly, to further account for anthropometric differences between segments, each acceleration vector was normalised for the relative segmental masses. Acceleration vectors were multiplied by a weight vector  $\mathbf{w}$  (equation 6.4), which contained the mass ratio of each segment relative to the total body mass (Dempster, 1955).

$$\mathbf{A}^{\text{part,task}}(t) = \mathbf{w} \cdot \mathbf{A}^{\text{part,task}}(t) \quad (6.4)$$

Finally, the participant- and task-specific acceleration matrices for each participant  $\mathbf{A}^{\text{part,task}}$  were combined in one 48783·45 (15 participants · 6 tasks · number of trials per task (483 in total) · 101 data points per trial) acceleration matrix  $\mathbf{A}$ .

### 6.2.3 Principal component analysis

A principal component analysis (PCA) was performed in Matlab on the normalised and combined acceleration matrix  $\mathbf{A}$ . The 45·45 covariance matrix of acceleration matrix  $\mathbf{A}$ , the eigenvector matrix  $\mathbf{EV}$  and eigenvalue matrix  $\lambda$  of the covariance matrix, and a time evolution coefficient matrix  $\mathbf{C}$  were calculated. The eigenvector matrix  $\mathbf{EV}$  consisted of 45 orthogonal eigenvectors  $\mathbf{ev}_k$ , in which each vector  $k$  indicated the largest variance in segmental acceleration for all segments. The eigenvalue matrix  $\lambda$  contained the eigenvalues  $\lambda_k$  which quantified the amount of variability described by each eigenvector  $\mathbf{ev}_k$ , with a strict decrease in the amount of variability with increasing  $k$ . The eigenvectors can also be referred to as the ‘principal component vectors’ or ‘principal acceleration vectors’. The time evolution coefficient matrix  $\mathbf{C}$  (also referred to as the ‘score matrix’) was calculated by projecting each original normalised and scaled acceleration vectors  $\mathbf{a}$  onto each PC  $k$  of the eigenvector matrix (Federolf, 2016; Moran et al., 2014), according to equation 6.5.

$$\mathbf{c}_k(t) = \mathbf{a}(t) \cdot \mathbf{ev}_k \quad (6.5)$$

The score matrix  $\mathbf{C}$  described how the original segmental acceleration data evolved along the new principal acceleration axes. Finally, participant- and task-specific principal acceleration (PA) matrices  $\mathbf{PA}^{\text{part,task}}$  were reconstructed for each individual PC  $k$  (single component reconstruction; equation 6.6) (Brandon et al., 2013; Ramsay and Silverman, 1997) to investigate how distinct features of segmental accelerations contribute to the specific GRF features, or the

sum of the first k PCs (equation 6.7) to examine the number of PCs required to adequately describe the whole GRF waveform. The PCs (i.e. eigenvectors) were expressed in the original segmental acceleration space by decomposing the reconstructed accelerations matrices into participant- and task-specific matrices, after which the normalisation and scaling steps were retraced.

$$\mathbf{PA}_k^{\text{subj,task}}(t) = \overline{\mathbf{a}^{\text{part,task}}} + \overline{\text{euc}_{\text{norm}}^{\text{part,task}}} \cdot \mathbf{w}^{-1} \cdot [\mathbf{C}_k \cdot \mathbf{ev}_k]^{\text{part,task}} \quad (6.6)$$

$$\mathbf{PA}_{1-k}^{\text{subj,task}}(t) = \overline{\mathbf{a}^{\text{part,task}}} + \overline{\text{euc}_{\text{norm}}^{\text{part,task}}} \cdot \mathbf{w}^{-1} \cdot \left[ \sum_{k=1}^{1,2,\dots,45} \mathbf{C}_k \cdot \mathbf{ev}_k \right]^{\text{part,task}} \quad (6.7)$$

#### 6.2.4 Principal accelerations and principal ground reaction forces

Since the reconstructed PAs are consistent with the laws of Newtonian mechanics, the principal segmental acceleration vectors  $\mathbf{pa}$  can be used to calculate principal GRF (PGRF) profiles. Resultant PGRF curves were calculated as the sum of the product of each segmental mass and principal CoM acceleration in the three directions, from each individual PC k (equation 6.8), or from the sum of PAs reconstructed from the first k PCs (equation 6.9).

$$\mathbf{PGRF}_k = \sqrt{\left( \sum_{n=1}^{15} (\mathbf{pa}_{k,n,x} \cdot m_n) \right)^2 + \left( \sum_{n=1}^{15} (\mathbf{pa}_{k,n,y} \cdot m_n) \right)^2 + \left( \sum_{n=1}^{15} (\mathbf{pa}_{k,n,z} \cdot m_n) + g \cdot \text{BM} \right)^2} \quad (6.8)$$

$$\mathbf{PGRF}_{1-k} = \sum_{pc=1}^k \left[ \sqrt{\left( \sum_{n=1}^{15} (\mathbf{pa}_{k,n,x} \cdot m_n) \right)^2 + \left( \sum_{n=1}^{15} (\mathbf{pa}_{k,n,y} \cdot m_n) \right)^2 + \left( \sum_{n=1}^{15} (\mathbf{pa}_{k,n,z} \cdot m_n) + g \cdot \text{BM} \right)^2} \right] \quad (6.9)$$

In which k is the PC number,  $\mathbf{pa}$  the principal segmental acceleration in x, y or z direction, m the segmental mass, n the number of segments (n=15) and g the gravitational acceleration (-9.81 m·s<sup>-2</sup>). Measured and calculated PGRF curves were normalised to each participant's body mass, while accuracy of the calculated PGRF profiles was evaluated as the curve RMSE relative to the measured GRF (see the methods sections in chapter 5 for more details). RMSE was rated as being very low (<1 N·kg<sup>-1</sup>), low (1-2 N·kg<sup>-1</sup>), moderate (2-3 N·kg<sup>-1</sup>), high (3-4 N·kg<sup>-1</sup>) or very high (>4 N·kg<sup>-1</sup>).

### 6.3 Results

The normalised eigenvalues  $\lambda_k$  of the first fifteen PCs explained 95.8% of the variance in the segmental acceleration data across all tasks. However, visual screening revealed that principal segmental accelerations related to distinct GRF features were primarily explained by the first five PCs. The first five PAs (cumulative  $\lambda_{1-5}=77.8\%$ ) were, therefore, used for further qualitative analysis. An example of the first five individual PGRFs profiles and how these were added as the summed PGRFs, is shown in figure 6.1.

**Table 6.1** Principal components and ground reaction forces for the different tasks

	Principal components (k)					
	1	2	3	4	5	45
$\lambda_k$ (%)	48.57	12.43	8.56	4.44	3.78	0
Cumulative $\lambda$ (%)	48.57	60.99	69.55	73.99	77.77	100
	PGRF RMSE (N·kg <sup>-1</sup> )					
Accelerations (n=80)	4.46 ±1.3	5.37 ±1.5	5.09 ±1.5	4.93 ±1.5	3.88 ±1.2	2.89 ±0.7
Decelerations (n=83)	10.69 ±3.1	6.18 ±2.3	6.44 ±2.4	6.11 ±2.2	5.88 ±2	5.97 ±1.8
90° Cuts (n=88)	5.11 ±1.3	3.77 ±0.9	3.79 ±0.9	3.65 ±0.8	3.61 ±0.7	2.66 ±0.7
Constant speed running						
Low (2-3 m·s <sup>-1</sup> ; n=81)	2.53 ±0.5	1.89 ±0.4	1.93 ±0.5	1.92 ±0.5	1.87 ±0.5	1.65 ±0.4
Moderate (4-5 m·s <sup>-1</sup> ; n=80)	3.74 ±1.1	2.70 ±0.8	2.82 ±0.9	2.72 ±0.8	2.66 ±0.7	2.51 ±0.6
High (>6 m·s <sup>-1</sup> ; n=71)	5.67 ±2	4.14 ±1.2	5.03 ±1.2	4.71 ±1.2	4.84 ±1.1	4.34 ±1.3
All tasks (n=483)	5.38 ±3.1	4.01 ±2	4.17 ±2.1	4.00 ±1.9	3.78 ±1.8	3.33 ±1.8

Summed principal ground reaction force (PGRF) error results from the first k principal components (PCs), as well as all 45 PCs (i.e. original data). Eigenvalues  $\lambda_k$  represent the normalised amount of segmental acceleration variance explained by each PC k. PGRF root mean square errors (RMSE) are mean ± standard deviation values for each task, per PC k.

PC<sub>1</sub> explained 48.6% of the segmental CoM accelerations of all segments in three directions. The PGRF<sub>1</sub> following from the first PC, accounted for the majority of the overall GRF impulse for all the different tasks (figure 6.2; table 6.1). For decelerations and running at constant low, moderate and high speeds, most segments showed a similar segmental PA<sub>1</sub> profile with the

---

majority of acceleration (and subsequent GRF) occurring between ~10-70% of stance (figure 6.3 and 6.4). However, for acceleration trials, PC<sub>1</sub> was related to a large overall GRF impulse later during stance (~30-90%). For 90° cuts and running at slower speeds, segmental PAs from PC<sub>1</sub> generally had a lower magnitude, but showed a very similar and consistent acceleration profile throughout stance for all segments. The largest accelerations for PC<sub>1</sub> were typically observed for the forearms and hands, although the PA<sub>1</sub> profiles for these segments followed those of the other upper body segments.

When the second PC was included, summed PGRF errors were reduced by 25.5% across tasks (table 6.1). PC<sub>2</sub> primarily explained a distinct contribution of segmental accelerations to the impact peak (figure 6.2), for all tasks except accelerations. PAs of the right thigh, shank and foot (stance leg segments), together with the pelvis, were the dominant contributors to PGRF<sub>2</sub>. For accelerations, however, these segments predominantly contributed to a GRF peak between ~50-90% of stance.

Segmental accelerations from PC<sub>3</sub> were associated with two distinct GRF features for running at constant speeds, but not for the other tasks. PGRF<sub>3</sub> included a small amount of impact peak forces during the first ~20-30% of stance, while there was a general contribution of PGRF<sub>3</sub> to the overall GRF impulse during the second half of stance (figure 6.2). The magnitude for both GRF features increased with running speed and were mainly related to the PA<sub>3</sub> profiles of the support and swing leg segments, together with the arms (figure 6.4).

Compared to the first three PCs, the fourth and fifth PC explained considerably less of the variance in the segmental CoM acceleration data (table 6.1), while contributions to the GRF were less distinct. For accelerations, these PCs included a constant (but relatively small) contribution to overall GRF from ~10-80% (PGRF<sub>4</sub>) and ~0-50% (PGRF<sub>5</sub>) of stance. For the other tasks, PC<sub>4</sub> primarily included PAs that explained relatively small contributions to GRF during the first ~40% of stance. For running at high speeds, PGRF<sub>5</sub> included a considerable contribution to overall GRF impulse, but not for the other tasks. Across tasks, GRF features in PC<sub>4</sub> and PC<sub>5</sub> were mainly associated with PAs of the upper body and swing leg.

Including higher PCs (i.e.  $k > 5$ ) steadily and consistently reduced the error between the summed PGRF and measured GRF profiles. These PCs contained relatively constant PAs of the arm and leg segments throughout the stance phase. The higher PAs primarily increased the overall magnitude of the summed PGRF, rather than influence specific GRF features. To achieve mean summed PGRF errors within 10% of the mean RMSE for GRF from all 45 PCs (i.e. the original data), a total of 18 (accelerations), 2 (decelerations), 15 ( $90^\circ$  cuts), 7 (low-speed running), 4 (moderate-speed running) and 18 (high-speed running) PCs were required respectively.

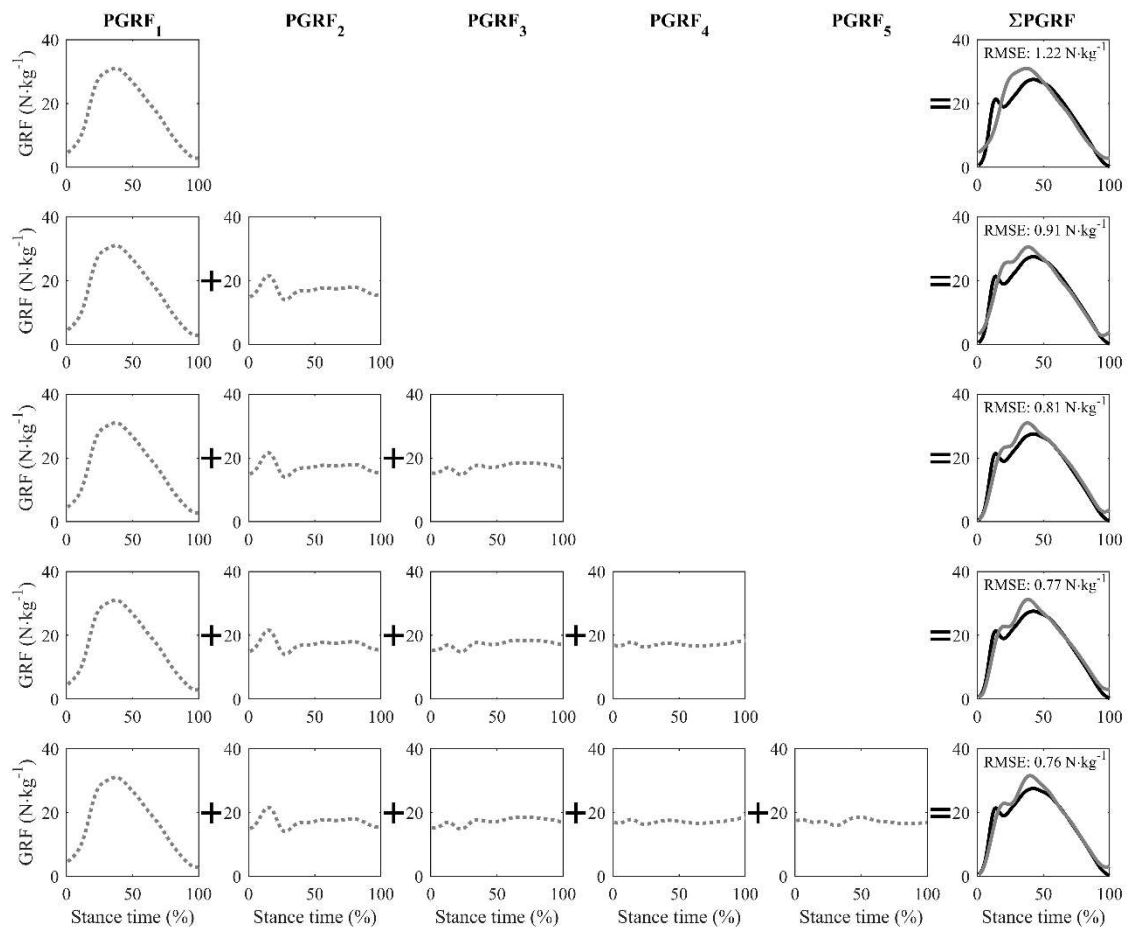


**Figure 6.1** Representative example of individual and summed ground reaction force (GRF) profiles reconstructed from the first five principal components (PCs), for a single participant running at a constant moderate speed. Individual principal GRFs (PGRFs; grey dotted lines) were added together as the summed PGRFs ( $\Sigma$ PGRFs; grey solid lines) for the first  $k$  PCs and compared to the measured GRF (black solid line) by the curve root mean square error (RMSE).

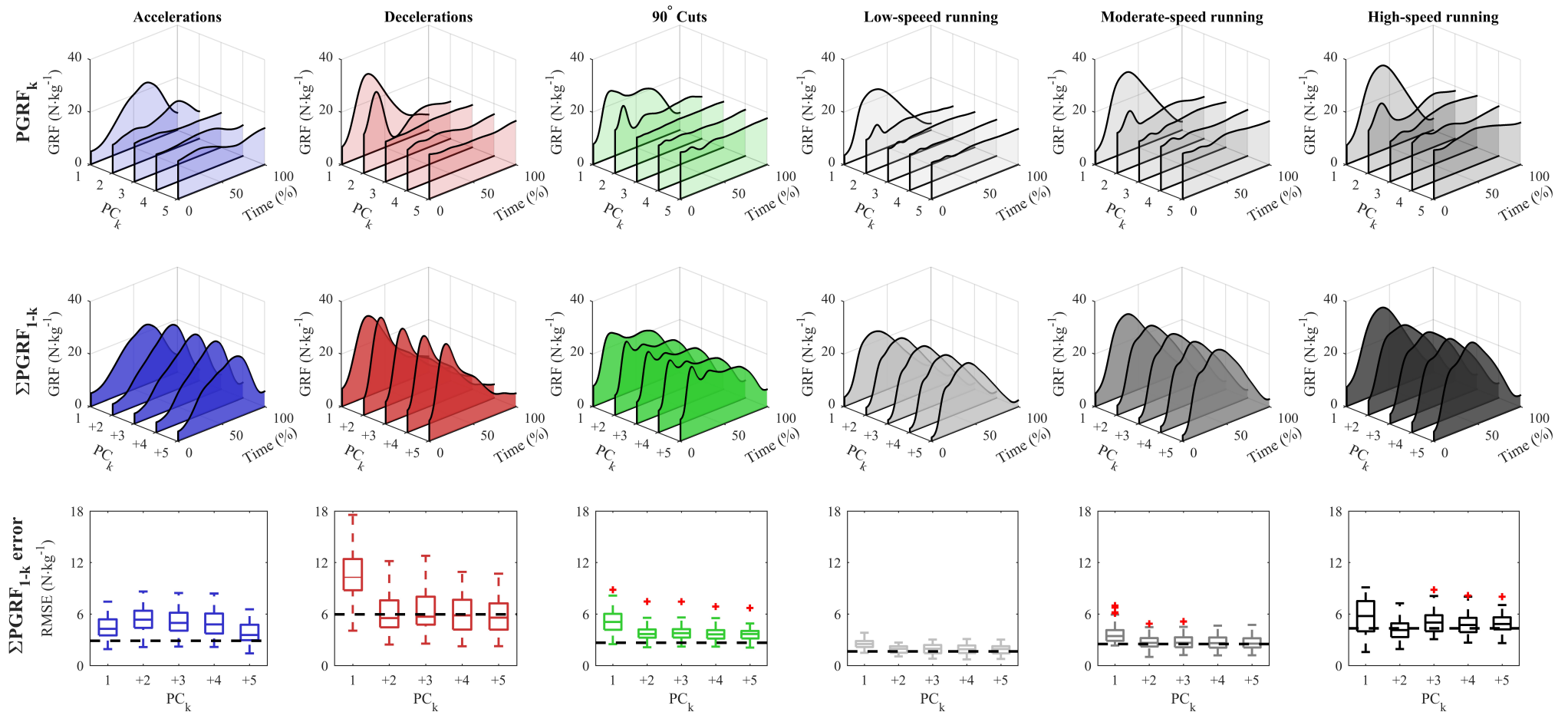


**Figure 6.2** Mean principal ground reaction forces (PGRFs) calculated from the first five principal components (PCs), for each task. PGRFs were calculated from principal accelerations (PAs) reconstructed from either the  $k^{\text{th}}$  PC (top row), or the sum of the first  $k$  PCs ( $\Sigma PGRF_{1-k}$ ; middle row). Root mean square errors (RMSE; bottom row) are mean errors for the  $\Sigma PGRF$  profiles and the horizontal black line represents the RMSE for  $\Sigma PGRFs$  from all 45 PCs (i.e. the original data).

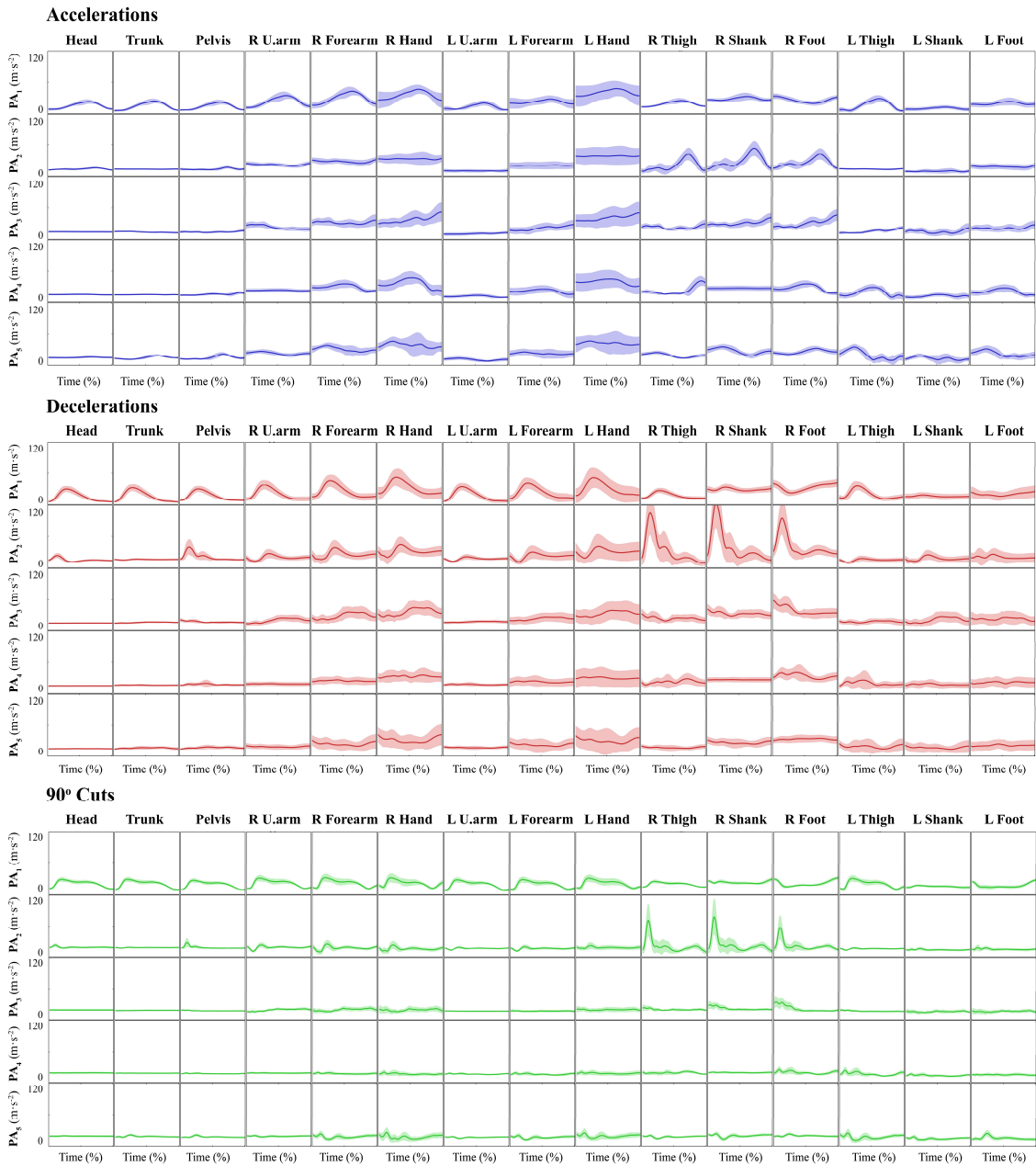


**Figure 6.3** Principal accelerations (PAs) from the first five principal components (rows) for accelerations (blue), decelerations (red) and 90° cuts (green). PA profiles are mean  $\pm$  standard deviation (shaded) curves from 0-100% of stance, for all fifteen segments (columns).

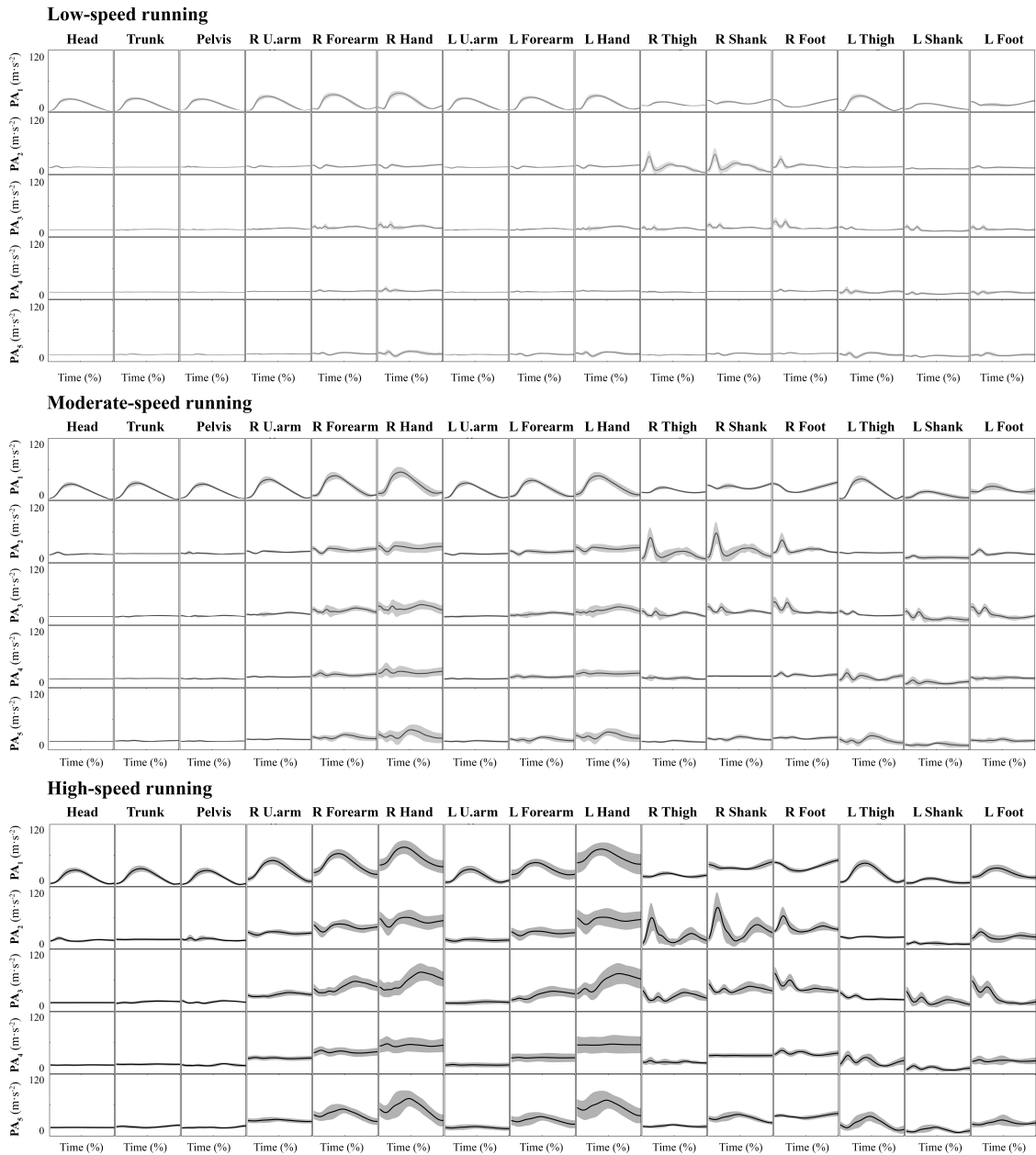


**Figure 6.4** Principal accelerations (PAs) from the first five principal components (rows) for running at constant low (light grey), moderate (grey) and high speeds (black). PA profiles are mean  $\pm$  standard deviation (shaded) curves from 0-100% of stance, for all fifteen segments (columns).

---

## 6.4 Discussion

The aim of this study was to identify key elements of segmental accelerations and their contribution to specific resultant GRF features, using a PCA method. The three primary modes of variation described by PCA; a magnitude operator, a difference operator and a phase shift (Brandon et al., 2013; Wrigley et al., 2005), were evident in the first five PAs and PGRFs. First, segmental acceleration magnitude differences associated with the majority of the GRF impulse (i.e. overall loading of the body) and the impact peak were captured by the first and second PC respectively. Substantial variation in PA and PGRF profiles (i.e. amplitude variability of acceleration and force) between tasks showed that the magnitude of these GRF characteristics was strongly dependent on task (figure 6.2). Secondly, the third and fifth PC highlighted clear difference operator features. In acceleration trials for instance, PGRF<sub>3</sub> and PGRF<sub>5</sub> mainly contributed to the overall GRF for the first half of stance but explained a much lower amount of force during push-off, while for running at constant speeds this was the other way around. Thirdly, clear phase shift characteristics were also manifested in the first two PCs. The impulse peak in PGRF<sub>1</sub> for example, appeared during the second half of stance for accelerations, but the first half of stance for the other tasks. Similarly, the high-frequency accelerations associated with the impact of landing appeared in the first ~20-30% of stance in the PA<sub>2</sub> and PGRF<sub>2</sub> profiles for decelerations, 90° cuts and running at all constant speeds, but much later for the acceleration trials. These results are consistent with previously described variability features (Brandon et al., 2013; Deluzio et al., 1997; Wrigley et al., 2005), and show that PCA can identify important task-specific GRF and associated segmental acceleration characteristics, as well as highlight the relative importance of these features in different running tasks.

The second PC primarily contained acceleration and force features related to the impact peak of the resultant GRF profile, for all tasks except accelerations. The impact peaks in PGRF<sub>2</sub> during the first ~20-30% of stance were mostly the result of high PA<sub>2</sub> peaks of the foot, shank and thigh segment of the support leg, as well as the pelvis to a lesser extent (figure 6.3 and 6.4). This supports previous suggestions that the impact peak is predominantly associated with the accelerations of the stance leg segments (Bobbert et al., 1992, 1991; Clark et al., 2017; Shorten

---

and Mientjes, 2011). Moreover, it has been shown that despite the visual absence of impact peaks in the GRF waveforms for non-rearfoot running gaits (e.g. sprinting), force frequencies associated with these initial force peaks are still present (Gruber et al., 2017, 2015; Hamill and Gruber, 2017). Indeed, for running at high speeds, during which runners typically switched to a forefoot landing technique which caused a visual impact peak in the resultant GRF profiles to be absent, a clear impact force peak was observed in PGRF<sub>2</sub> (figure 6.2). These findings thus support suggestions of the likely presence of an impact peak, despite their visual absence in the resultant GRF waveform.

As described above, PC<sub>2</sub> was mainly associated with the high-frequency impact accelerations and forces due to landing. For acceleration trials, however, PA<sub>2</sub> profiles of the foot, shank and thigh segments of the support leg were mainly related to a force peak later during stance (figure 6.2). This shows that in contrast to the other tasks, which typically include a high-frequency impact peak during the first ~20-30% of stance, acceleration movements contain a large support leg acceleration component later during stance, i.e. when pushing off. Furthermore, the smoother impacts of landing during acceleration activities were better explained by PC<sub>5</sub> and, therefore, of less importance for the overall biomechanical load on the body in these trials. This phase shift feature highlights the importance of force production during the second half of stance for acceleration tasks, compared to the other tasks in which the braking aspect is emphasised more. Using a PCA approach to evaluate segmental acceleration data can thus not only identify important characteristics of the acceleration profiles, but also explain their contribution and relative importance to resultant GRF profiles for different running tasks.

#### *6.4.1 Implications for load monitoring purposes*

The results of the PCA approach described in this study highlighted different key magnitude, difference and phase shift characteristics of segmental accelerations, and their specific contributions to the overall GRF waveforms. However, these results have also emphasised that GRF and segmental acceleration features are highly task-specific, as described above. These findings could explain why individual models of any given number of segments, as considered

---

in chapter 5, could not lead to accurate estimates of whole GRF waveforms across different tasks. For example, a combination of specific segmental accelerations might be appropriate to estimate GRF profiles for sprinting well, while the same segments are not so suitable to describe the GRF for decelerations. This further supports the suggestion made in chapter 5, that it is unlikely that GRF waveforms can be estimated accurately from less than all fifteen segments, across different dynamic and high-intensity tasks frequently performed during running-based sports. Therefore, one should be very careful when using a generic biomechanical model or approach, to estimate and evaluate external biomechanical loads from segmental accelerations across several different tasks.

Trunk accelerometry is a commonly (and arguably the most often) used acceleration signal for assessing biomechanical loads in different sports (Akenhead et al., 2017; Buchheit et al., 2015; Colby et al., 2014; Gaudino et al., 2013). Although the trunk has been suggested to be the main contributor to GRF (Bobbert et al., 1991; also see chapter 2 and 4), trunk PAs from PC<sub>1</sub> (which described the majority of the overall resultant GRF impulse) showed very similar acceleration profiles compared to other segments, for all tasks (figure 6.3 and 6.4). Moreover, the higher PCs (i.e.  $k > 1$ ) did not explain any considerable additional trunk acceleration features. These findings further support the suggestion made in chapter 4, that the trunk's large contributions to GRF are likely due to its large mass rather than high accelerations. The value of trunk acceleration signals for biomechanical load monitoring purposes is thus probably limited and one should be very cautious when using trunk accelerations alone to evaluate whole-body biomechanical loading.

Across the different PCs and tasks, PAs for the arm segments (forearms and hands especially) typically had a high magnitude of acceleration (figure 6.3 and 6.4). This is likely the result of the relatively large amplitude of movement (and consequent acceleration) of these segments for each stride, compared to other segments. Nevertheless, the high PAs of the arm segments didn't substantially affect any distinct features of the whole GRF profiles, which is likely due to their relatively low segmental mass. Errors for summed PGRFs did, however, gradually decrease when more PCs were included (figure 6.2), mainly due to arm segmental accelerations (but also

---

swing leg accelerations) explained by the higher PCs. Moreover, for decelerations and running at low to moderate speeds, mean errors for the summed PGRF profiles were slightly lower from the first five PCs relative to all 45 PCs, while considerably less PCs were required to achieve mean summed PGRF errors within 10% of the mean RMSE value from all 45 PCs. These results are likely caused by the more profound and complex arm movements during acceleration, 90° cutting and sprinting tasks. Therefore, although arm and swing leg motion are not the primary contributors to GRF, their segmental accelerations do account for a considerable part of the overall GRF impulse. These findings thus highlight the importance of considering all segments for evaluating overall whole-body loading in the field, especially for sports in which dynamic and high-intensity tasks are frequently performed.

The reconstructed PAs described and interpreted in this study are no real acceleration signals, i.e. body segments do not really accelerate according to the individual PAs. Measuring these PAs, as well as qualitatively describing and visually interpreting the resulting PGRFs for load monitoring purposes, is thus impossible. Consequently, the present findings cannot directly be applied to estimate biomechanical loading (features) from segmental accelerations. Furthermore, each PA can represent a combination of multiple key acceleration characteristics. For example, PC<sub>2</sub> emphasised the importance of the timing of high-frequency accelerations of the stance foot, shank and thigh segment for the GRF impact peak, but at the same time described considerable amplitude differences of these peaks between the different tasks. Although PCA can reduce the complexity and extract important characteristics of high-dimensional biomechanical data sets, individual PCs can thus still contain multiple key elements of the original data. This complexity of segmental contributions to GRF observed, further emphasises that estimating and assessing whole-body biomechanical loading from segmental accelerations is not straightforward. One should, therefore, be very cautious when interpreting segmental acceleration signals as a measure of biomechanical load, especially across different tasks.

---

#### 6.4.2 *Limitations*

For the purpose of this study, PCA was performed on a data set that deliberately combined segmental accelerations for multiple participants and tasks. The results of this study are thus a general representation of key segmental acceleration elements that explain GRF profiles (i.e. whole-body loading), across tasks typically performed during running-based sports. A limitation of this combined analysis is that unique loading features or requirements for individual athletes or tasks might not be highlighted. Moreover, the relative number of trials for each task could cause the overall PCA results to be dominated by task-specific features. However, although subtle differences could be highlighted by task-specific PCAs, the outcomes were highly comparable to the combined PCA described in this study (appendix J). Furthermore, the variation in the number of trials for the different tasks included ( $81 \pm 5$  trials) was deemed sufficiently small to be an equal and appropriate representation of all tasks. Therefore, the combined PCA approach was considered appropriate for the purposes of this study.

The use of resultant accelerations and GRFs could form a limitation for the interpretation of the PCA results. Direction specific segmental accelerations and related GRF features might not be identified by the resultant waveforms. However, the aim of this study was to evaluate overall biomechanical loading of the body and associated segmental accelerations. Moreover, since body-worn accelerometers cannot typically distinguish between global x-y-z directions, using resultant accelerations is thus more feasible for eventual translations of findings for biomechanical load estimation in the field.

Before performing the PCA, segmental acceleration data for all participants were normalised by a weighting vector based on a standardised mass distribution (Dempster, 1955). Due to the anthropometric variability between the participants in this study (see the methods section), defining and applying an individualised mass distribution could improve the results. Although this was beyond the scope of the present study, future work should consider whether normalising data according to personalised mass distributions might be beneficial.

---

The methods described in this study used a classical PCA on a set of measured segmental acceleration signals. PCs resulting from this technique include a set of scores in the temporal domain that evaluate along the newly defined eigenvector axes (see section 6.2) but can be difficult to interpret biomechanically. Therefore, functional principal component analysis (fPCA), in which PCs are represented by functions in the original domain and thus allow for the direct interpretation of the fPCA outcomes, has been used (Ryan et al., 2006; Warmenhoven et al., 2017). In this study however, PCs were projected back from the temporal domain to the original segmental acceleration domain by reconstructing participant- and task-specific accelerations matrices which allowed for a clear biomechanical interpretation of each PC (i.e. PAs; see section 6.2.4). Furthermore, the segmental acceleration signal used in the PCAs typically contained high-frequency content. Fitting and smoothing basis functions (e.g. B-splines, Fourier components, Gaussians) required for fPCA is likely to over-smooth acceleration signals and thus remove potentially important segment acceleration features. fPCA was therefore deemed inappropriate for the purposes of this study.

## **6.5 Conclusion**

Since it is unlikely that whole GRF waveforms can be estimated from one or several segmental accelerations, this study aimed to identify key segmental accelerations associated with specific GRF features that might be used to assess whole-body biomechanical loads. However, the present findings show that segmental contributions to GRF, as well as the relative importance of these characteristics in different running activities, are highly complex and task-specific. Therefore, the value of using segmental accelerations, or even distinct components, to assess whole-body biomechanical loads across tasks frequently performed during running-based sports, is likely limited.

---

## **Chapter 7: General discussion**

---

The aim of this discussion is to provide an interpretation of the outcomes of the different studies described in this thesis. First, the biomechanical and practical interpretations of the various results will be discussed, as well as the implications for current research and training load monitoring practice. Based on these interpretations and implications, several recommendations for researchers and practitioners will be made. Secondly, a critical reflection on the value of using ground reaction forces (GRFs) as a measure of external whole-body biomechanical load will be provided. The potential strengths, possible limitations and future challenges of GRF as a biomechanical load measure will be evaluated, and further informed by the findings of the different studies. Thirdly, several potential applications of segmental accelerations for biomechanical load monitoring purposes will be introduced. Different opportunities for the future use of current body-worn sensors, as well as other technologies, for evaluating biomechanical loads will be suggested. In addition, specific recommendations and suggestions for future research, as well as notions of caution when estimating and assessing biomechanical loads in the field, will be made throughout this general discussion chapter. Finally, based on the outcomes and conclusions following from the different studies, an overall conclusion of this thesis will be provided.

---

## 7.1 Introduction

The overall aim of this thesis was to investigate whether ground reaction forces (GRFs) can be estimated from segmental accelerations, especially for dynamic and high-intensity running tasks that are frequently performed during running-based sports. The main findings were that:

- 1) A two mass-spring-damper model can be used to accurately reproduce overall GRF profiles and impulses measured with a force platform for a range of high-intensity running tasks, but this model could not be used to predict GRF from trunk accelerations measured with a trunk-mounted accelerometer.
- 2) Using a direct mechanical approach, GRF profiles and loading characteristics can be estimated with reasonable accuracy across various dynamic and high-intensity running tasks from fifteen segmental accelerations measured with a motion capture system, but errors substantially increased when the number of segments was reduced.
- 3) A principal component analysis can be used to identify key segmental contributions to specific GRF features for different dynamic and high-intensity running activities, but these characteristics and their relative importance were highly complex and task-specific.

These outcomes have important implications for current research and training load monitoring practice. Moreover, the findings in this thesis provide valuable insight into previous research findings, can be used to inform future work that aims to use GRF as a measure of whole-body biomechanical load, and demonstrate some possible applications for current body-worn sensors, as well as potential opportunities for future technologies. Therefore, the aim of this general discussion is to discuss the various implications, applications and opportunities following from the studies described in this thesis.

## 7.2 Implications for biomechanical load monitoring practice

In the introduction of this thesis, biomechanical load monitoring was described as a multi-layered sphere of which researchers and practitioners should aim to reach the core (chapter 1).

---

The outcomes of the different studies have important implications for current research and training load monitoring practice and can further inform this biomechanical load sphere concept. This section will discuss the implications of the different findings for researchers and practitioners, as well as identify their position within the biomechanical load sphere (figure 7.1).

### *7.2.1 The two mass-spring-damper model approach*

Chapter 3 has shown that the two mass-spring-damper can be used to accurately reproduce overall GRF profiles for high-intensity running tasks. This study was the first attempt to use a two mass-spring-damper model to replicate and predict GRF for tasks other than steady running at slow or moderate speeds. Although the model's ability to accurately model a variety of GRF curves did not lead to eventually predicting GRF from trunk accelerations (chapter 4), the modelled GRFs could potentially be used to investigate how human locomotion, as well as physical and anatomical characteristics, relate to GRF during tasks other than steady running. Previous studies have for instance used the two mass-spring-damper model, as well as comparable models, to investigate various kinematic, kinetic or external variables (see chapter 2.4 for a detailed overview of several applications of mass-spring(-damper) models). For such analyses to be biomechanically relevant, model parameters are required to remain constant between similar tasks and/or trials and vary only within a physically meaningful range of parameter values. However, the results of chapter 3 have shown that the required model parameters to reproduce measured GRF strongly varied between trials of the same task and had minimal physical meaning. Researchers should, therefore, be very careful when using the two mass-spring-damper model (and other similar models) to investigate locomotion during high-intensity running, as these models are possibly unable to truthfully describe the biomechanical aspects of such tasks.

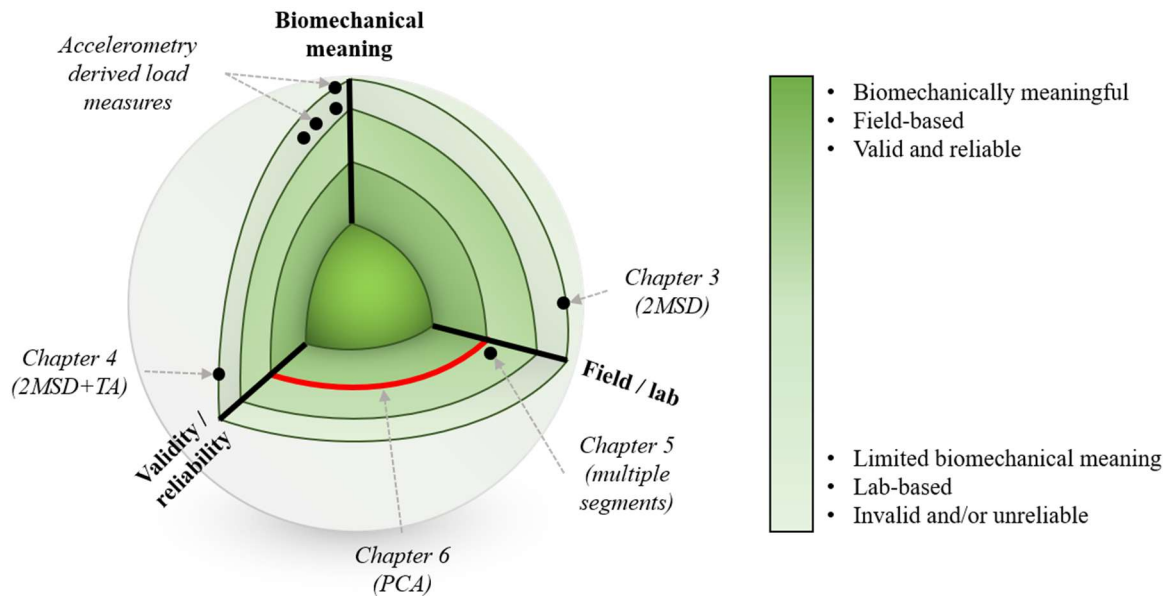


**Figure 7.1** The multi-layered biomechanical load sphere. While the two mass-spring-damper model (2MSD) studies were located towards the surface of the sphere, ground reaction forces estimated from multiple segments demonstrated the potential for moving towards the core of the sphere. The complexity revealed by the principal component analysis (PCA) highlights the difficulty of moving towards the core.

Chapter 3 has shown that reproducing GRF with a two mass-spring-damper model is valid and reliable, but this approach is purely lab based and its biomechanical meaning is thus possibly limited. This study can, therefore, be located on the surface of the biomechanical load sphere (figure 7.1). To move closer towards a field application of the two mass-spring-damper model, chapter 4 investigated if this model could be driven by commonly used trunk accelerations to predict GRF. However, the findings of this study showed that this method could not lead to valid and/or reliable GRF predictions. Therefore, despite the big leap towards a field-based measure of biomechanical loading, chapter 4 should still be located on the surface of the sphere (although in a different location) (figure 7.1).

### 7.2.2 Trunk accelerations to assess biomechanical loading?

Commonly applied and popular methods to assess the biomechanical loads athletes are exposed to, rely heavily on accelerometry derived training load measures. These metrics such as PlayerLoad (Barrett et al., 2014; Boyd et al., 2011; Scott et al., 2013), (New) Body Load

---

(Ehrmann et al., 2016; Lovell et al., 2013; McLean et al., 2018; Weaving et al., 2014), Force Load (Colby et al., 2014) and Dynamic Stress Load (Gaudino et al., 2015) are typically based on a single (trunk) acceleration signal and characterise a general ‘shaking up’ of the body. However, a biomechanical underpinning that relates these measures to established parameters of biomechanical load is still lacking. In fact, the ability of PlayerLoad (which is arguably the most widely used accelerometry-based load metric) to distinguish between different activities has been shown to be poor, suggesting PlayerLoad to be more related to the overall workload (e.g. total distance covered, duration) rather than biomechanical loads experienced (Green, 2018). Moreover, it has been shown that cumulative PlayerLoad can vary between accelerometers worn on the trunk or the pelvis (Barrett et al., 2014), while the accumulation of Body Load (a similar metric) has been shown to be strongly dependent on accelerometer fitting in either a vest or a jersey (McLean et al., 2018). Furthermore, the validity of absolute acceleration magnitudes from commercial accelerometer units has been found to be poor and device dependent (Kelly et al., 2015; Nicolella et al., 2018), and even depends on operating range (Mitschke et al., 2018). These findings make the construct validity of accelerometry derived load measures to assess the external biomechanical loading of the body questionable.

In line with the above described findings, the results in chapter 4 have shown that trunk accelerometry could not be used to drive a two mass-spring-damper model to predict GRF. Moreover, chapter 5 has shown that accelerations of most body segments are required to achieve meaningful GRF estimates using a direct mechanical approach, while chapter 6 has shown that trunk accelerations were predominantly described by a single principal component and are not related to any specific GRF features. These findings show that it is not straightforward to associate accelerations of the trunk or other individual segments to GRF, thus making it unlikely that acceleration signals from individual segments provide an accurate measure of whole-body biomechanical loading. Despite their field-based nature, these measures are thus located towards the surface of the biomechanical load sphere (figure 7.1). Given the importance of a full understanding of load measures before embedding them into monitoring programs (Burgess, 2017), these outcomes have important implications for current training load monitoring practices

---

using trunk accelerometers. More specifically, researchers and practitioners should exercise caution when interpreting acceleration signals and accelerometry derived load metrics from a single unit as measures of whole-body biomechanical load.

Chapter 5 introduced a direct mechanical approach to estimate GRF and has shown that GRF can be estimated from multiple segmental accelerations with reasonable accuracy. Although this study was laboratory based, these findings highlighted the potential of this approach for moving biomechanical load monitoring practice towards the centre of the sphere. Providing valid and reliable measures of multiple segmental accelerations can be obtained in the field (see section 7.4 for a more detailed discussion on this), this approach could offer a way towards a more field-based measure of biomechanical load. Scoring well for accuracy and biomechanical meaning, chapter 5 can thus be located slightly further to the centre of the sphere (figure 7.1). However, chapter 6 has revealed the complex variety of segmental contributions to GRF within and between different running tasks. This complexity highlights that biomechanical load monitoring is not straightforward and can thus be seen as a tough layer in the multi-layered sphere, explaining the difficulty experienced when moving closer towards the core (figure 7.1). These conclusions further emphasise the highly complex nature of biomechanical load monitoring in the field and support the recommendations for caution made above.

### **7.3 The value of ground reaction force as a biomechanical load measure**

An important assumption made in this thesis and rationale for investigating if GRF can be estimated from segmental accelerations is that GRF is a meaningful measure of biomechanical load. Following on from the initial interpretations provided above it is useful to critically reflect on this assumption, to put these findings, as well as suggestions for future research, in a broader perspective. Therefore, this section will (informed by the outcomes of the previous chapters) discuss the value of GRF for biomechanical load monitoring in running-based sports, the required accuracy of GRF estimates, how GRF relates to other measures of biomechanical loading.

---

### 7.3.1 *Ground reaction forces in running-based sports*

Since the impacts of landing during running (i.e. GRF) are absorbed and returned by the different hard- and soft-tissues of the body, GRF is believed to be related to performance determining factors, as well as injuries (see chapter 2.3 for more a more detailed explanation). For example, several studies have shown that GRF components can be used to evaluate and improve sprint performance in different athlete populations (Bezodis et al., 2017; Hunter et al., 2005; Nagahara et al., 2017; Rabita et al., 2015). Likewise, musculoskeletal overuse injuries have been suggested to be related to several specific characteristics of the GRF such as the impact peak and the loading rate (e.g. Hreljac, 2004; Hreljac et al., 2000; Milner et al., 2006), which might be directly affected by fatigue (Bazuelo-Ruiz et al., 2018; Christina et al., 2001; Degache et al., 2016; Lazzer et al., 2015; Morin et al., 2011). However, other studies have found different results and suggested that vertical GRF profiles might not differ for athletes with lower-limb stress fractures (Zadpoor and Nikooyan, 2011a), while impact peaks may not significantly contribute to running injuries (Nigg et al., 2015; van der Worp et al., 2016). Peak vertical GRF and loading rates have even been found to be higher in uninjured runners compared to injured runners (Duffey et al., 2000; Messier et al., 2018). In addition, fatigue related changes in GRF have been suggested to be ambiguously small (Bazuelo-Ruiz et al., 2018; Nikooyan and Zadpoor, 2012; Paquette and Melcher, 2017), while injury and/or performance related aspects of the GRF are likely to be age- (Paquette et al., 2018) and sex-specific (Bazuelo-Ruiz et al., 2018; Bredeweg et al., 2013; Messier et al., 2018; Milner et al., 2006; Napier et al., 2018). These contrasting findings indicate that using GRF for performance optimisation or injury prevention purposes is not straightforward and performance- or injury-related differences might be very subtle and individual-specific. Therefore, the question can be asked how accurate GRF measurements need to be, to be used as a valid and reliable tool for training load monitoring, as well as if there are other, more appropriate measures of biomechanical load to evaluate injury risk and performance.

### 7.3.2 *How good is good enough?*

Potential injury-related changes in GRF within, and differences between populations have been shown to be small and indefinite. Meaningful performance- or injury-related differences in GRF

---

loading characteristics can even be as small as ~3-10% (Bazuelo-Ruiz et al., 2018; Bezodis et al., 2017). It may thus be critical to achieve highly accurate estimates of GRF for valid, reliable and meaningful external biomechanical load monitoring. Therefore, the varying accuracy of estimated GRF characteristics (errors of ~2-40%) from fifteen segmental accelerations found in chapter 5 (i.e. the most accurate GRF estimates in this thesis) might already rule out the usefulness of this approach for certain biomechanical load monitoring purposes. However, although errors of estimated impact peaks and loading rates typically ranged between ~13-29% across the different tasks, estimated impulse errors were only ~7%. Since this overall loading magnitude (i.e. impulse), rather than vertical loading rates, has been suggested to be the primary cause of mechanical fatigue of bone (Loundagin et al., 2018), monitoring the accumulation of overall GRF impulse might be used to assess potential cumulative overloading and investigate injury mechanisms. Impulses of the accuracy found in chapter 5 could thus still be used a valuable tool for quantifying and evaluating the overall external biomechanical load on the body. Moreover, all estimated GRF errors observed in chapter 5 are solely the result of measurement and methodological inaccuracies (e.g. marker placement inaccuracies, soft-tissue artefacts, assumed standardised segmental properties). Future research could, therefore, examine if dynamically consistent models (e.g. by using residual reduction algorithms; (Delp et al., 2007; Faber et al., 2018)) or new technologies (e.g. implantable accelerometers or markerless motion capture; see section 7.4) could overcome these limitations and reduce measurement errors. If so, the accuracy of GRF estimates might be improved and allow for other loading characteristics (e.g. impact peak, loading rate) to be used. Therefore, although further research is required to improve GRF estimates, the mechanical approach described in chapter 5 can form a valuable tool for biomechanical load monitoring in the field and open the door for a more detailed understanding of the external loading of the body during different tasks.

The aim of this thesis was to estimate GRF to ultimately evaluate the overall external biomechanical loading of the body from body-worn accelerometers in the field. However, most accelerometers cannot typically distinguish between a global mediolateral, anteroposterior and vertical orientation and hence, using resultant segmental accelerations is more feasible for

---

practical reasons. Therefore, the different studies described have all aimed to estimate and use resultant segmental accelerations and GRF, rather than their three individual components. Although resultant forces are a measure of the total external load, however, their use can be a limitation for load monitoring purposes. For example, resultant GRF does not allow to distinguish between the different force components, which could be important to assess the risk for specific injuries (Gottschall and Kram, 2005; Zadpoor and Nikooyan, 2011b) or evaluate performance (Bezodis et al., 2017; Kugler and Janshen, 2010). Although the investigation of separate acceleration and force components was beyond the scope of this thesis, measuring and assessing individual acceleration and GRF components may provide a more complete picture of the relationships between external load and e.g. specific injuries. Therefore, future research should investigate how separate segmental acceleration and GRF directions are related for different tasks.

### *7.3.3 External vs internal biomechanical loads*

How GRF is related to injury is still not well understood, as described above. However, overuse injuries can be defined as structural failure when the continuous and repetitive stresses exceed the structure-specific load capacity (Bertelsen et al., 2017; Edwards, 2018). Since GRF is known to not always be an appropriate reflection of these internal stresses working on the different body structures, the value of GRF (or GRF loading characteristics) as a measure of biomechanical loading in relation to injuries could be questioned. For example, forces experienced by the ankle joint and lower leg during running (~10-14 times body weight) have been shown to be primarily due to self-inflicted muscle contractions rather than the forces resulting from collisions with the ground (~2-3 times body weight) (Scott and Winter, 1990). Measuring and evaluating forces acting on internal structural tissues (e.g. a specific joint, muscle, tendon, bone loads etc.) might, therefore, provide more meaningful and valuable information for biomechanical training load monitoring than GRF. On the other hand, GRF indirectly drives and contributes to internal stresses on the different hard- and soft-tissues of the body, as described in chapter 2.3, and may thus be used to partially describe these internal loads. Furthermore, in combination with kinematic measurements in the field (e.g. from accelerometry suits or markerless motion capture

---

systems as described in chapter 7.3), GRF could be used to determine and evaluate the internal structure-specific loads in more detail. Although GRF measurements might thus have limitations in its ability to directly assess injury-risk and should be evaluated and interpreted carefully alongside other available information, monitoring GRF in the field would be an important first step towards investigating internal biomechanical stresses in more detail.

The different studies described in this thesis have focused on using segmental accelerations to estimate GRF. An important rationale for this was to ultimately use currently popular body-worn accelerometers to more accurately assess external whole-body biomechanical loading. However, internal structure-specific loading might provide more valuable information regarding specific injuries, as described above. Despite available methods to calculate these internal loads such as joint and muscle forces (Damsgaard et al., 2006; Delp et al., 2007; Seth et al., 2018), detailed kinetic and kinematic input not typically available in the field are required. Therefore, if body-worn accelerometers could be used to directly assess biomechanical loading at an organ level, this would overcome the need for other biomechanical measurements. However, evidence relating individual segmental accelerations to internal biomechanical forces is yet lacking. For example, despite suggestions that tibial accelerations are related to stress and strain experienced by the tibia, this has not been proven (Sheerin et al., 2019). Therefore, besides using accelerometry to estimate and assess GRF as a measure of whole-body biomechanical load, future research should also aim to identify meaningful structure-specific loads and investigate if these internal biomechanical loads can be accurately estimated from body-worn accelerometry.

#### *7.3.4 Cumulative biomechanical loading*

As discussed above, the value of GRF profiles or specific loading characteristics in relation to injuries is still unclear. This ambiguity further emphasises that meaningful biomechanical load monitoring (and training load monitoring in general) in running-based sport is not straightforward. However, the majority of studies investigating GRF related load parameters in relation to injury use relatively small sample sizes of ~20-60 participants (van der Worp et al., 2015; Zadpoor and Nikooyan, 2011a), who typically perform a limited number of trials in an

---

unnatural laboratory environment. Moreover, these lab-based studies only examine GRF profiles at a specific point in time and do not typically account for the temporal nature of injury-risk factors (Verhagen et al., 2018), or the cumulative nature of injuries (Bertelsen et al., 2017; Edwards, 2018). For example, it has been shown that isolated tibial and femoral bone samples can withstand ~12,000-16,500 cycles of a typical running GRF profile before failure (Loundagin et al., 2018), which highlights the importance of monitoring the accumulation of biomechanical loads over time. The mentioned limitations of previous lab-based studies might thus partly explain the current lack of solid evidence for a relation between GRF (loading characteristics) and injuries. However, GRF measurements without the need for force platforms could provide a large amount of GRF data for consecutive ground contacts and enable biomechanical studies to be performed on a bigger scale than currently usual (i.e. more participant and ground contacts collected over time in natural training and/or competition environments). Such a substantial increase in available GRF information could allow for identifying general trends of injury-related GRF characteristics, as well as investigating the effects of the accumulation of external forces working on the body. Future research should, however, investigate if GRF measured on a large scale can be used to identify potential injury mechanisms and/or risk factors. Nevertheless, assessing the value of GRF as a biomechanical training load measure should not solely be based on laboratory studies relating individual GRF features to running related (overuse) injuries, but also consider the accumulation of these loads (which are typically poorly quantified in lab-based studies) as a major cause for such injuries.

#### **7.4 Future applications and technologies**

Although several outcomes of this thesis have highlighted that care should be taken when using accelerometry data, this thesis has also demonstrated some potential applications of segmental accelerations. Therefore, this section will discuss several opportunities for the use of current body-worn accelerometers, future implantable sensors, markerless motion capture technologies or machine learning techniques for biomechanical load monitoring purposes. These techniques might ultimately open the door to GRF measurements that are field based and thus closer to the core of the biomechanical load sphere.

---

#### 7.4.1 *Body-worn accelerometers*

Chapter 5 has demonstrated different potential applications of currently popular body-worn accelerometers. This chapter demonstrated that GRF profiles and loading characteristics for different high-intensity and dynamic running tasks can be estimated reasonably well from fifteen segmental accelerations, measured from a laboratory-based motion capture system. If accelerometers could provide full-body segmental accelerations, this direct mechanical approach might open the door for estimating GRF in applied sport settings (e.g. running tracks, football pitches, tennis courts). Full-body wireless accelerometry suits have already been shown to be a reliable and valid method to simultaneously measure kinematic information of all body segments for motion capture purposes outside the laboratory (e.g. Xsens MVN (Roetenberg et al., 2013)), and have even been used to estimate GRF and moments during walking (Karatsidis et al., 2017). Although these systems allow the measurement and analysis of movement in virtually any environment, their application to predict GRF or other biomechanical load variables in sport settings has not been investigated yet. The direct mechanical approach described in chapter 5 could thus provide a simple method to estimate GRF using existing full-body accelerometry technologies. Moreover, accurate GRF estimation in combination with the already available kinematic measures could allow for further information on several internal biomechanical stresses, such as muscle forces and joint moments. Therefore, future research is recommended on whether these existing accelerometry systems can be used to estimate and monitor GRF in the field.

Although full-body accelerometry techniques have the potential to estimate GRF as described above, it is questionable whether such systems can be used to monitor loads of training and/or competition on a daily basis. Since the use of full-body suits is often invasive and time consuming, accelerometry suits are unlikely to be a feasible means for day-to-day biomechanical load monitoring. In team sports especially, where a relatively large number of athletes typically train multiple times a day, these practical issues might form a serious limitation. Moreover, accelerometry suits can highly compromise comfort and restrict movement during sports, which can considerably affect an athlete's performance or induce injury related biomechanics. Using

---

accelerometers that are implemented into other body-worn devices or items is, therefore, desirable to enhance usability. Examples include accelerometers embedded in watches (Adams et al., 2016), eyeglasses (Amft, 2017), trunk-mounted GPS devices (Boyd et al., 2011) and even garments (Amft, 2017; Düking et al., 2016). However, it is unlikely that such units can simultaneously provide accelerations of all body segments, while the measured acceleration signals probably deviate from the actual segmental CoM accelerations, as shown in appendix I. It is, therefore, unlikely that a few of these integrated body-worn accelerometers can be used to accurately measure and monitor subtle GRF loading characteristics such as impact peaks and loading rates, across a range of different running tasks. Nevertheless, the results in chapter 5 have also shown that GRF impulses, which are the overall whole-body loads experienced by the body, could be estimated with low to moderate errors across various dynamic and high-intensity tasks. Moreover, impulse errors were relatively robust against the reduction of segments. Although further work on this is required, impulses may thus have the potential to be measured from a limited number of body-worn accelerometers and could potentially be used to monitor the general cumulative quantity of whole-body loading experienced during training and/or competition.

#### *7.4.2 Implantable sensors*

The overall aim and methods throughout this thesis have primarily assumed the use of current, externally worn inertial sensors to eventually predict GRF. Although body-worn devices are currently a popular means to quantify and assess training loads and health status (Thompson, 2018, 2017, 2016, 2015), the reliability and validity of wearables for use in various sport and fitness contexts has also been questioned (Düking et al., 2016; Peake et al., 2018; Sperlich and Holmberg, 2016). Moreover, it has been suggested that technological developments might in the future replace wearable sensors by other techniques such as implantable units (Catherwood et al., 2015; Sperlich et al., 2017). Implantable accelerometers for example, have already been used to provide accurate continuous diagnostic information such as blood pressure (Theodor et al., 2014) and heart rate (variability) (Hawkins et al., 2016; Perego et al., 2008), and have for instance been applied successfully to predict and prevent heart failure (Hawkins et al., 2016;

---

Perego et al., 2008). In a sport and training load monitoring context, implantable accelerometers could overcome several issues of the current externally worn units. Implantables are virtually unnoticeable, minimise movement relative to the segment it is implanted in and can be placed close to a segment's CoM. These advantages might allow for more precise measurements of multiple (full-body) segmental CoM accelerations, and as a result, open the door for more accurate predictions of GRF from segmental accelerations, e.g. following the approach described in chapter 5. On the other hand, initial placement of implantable devices is currently invasive and might raise a number of ethical problems (Catherwood et al., 2015; Sperlich et al., 2017). Depending on unit location, placement requires minor or major surgery, limiting e.g. user-friendly hard- and software updates or replacement. Moreover, implanted devices could raise concerns around ethical issues such as an athlete's long-term health risks (Catherwood et al., 2015) or data accessibility and ownership (Sperlich et al., 2017). Therefore, although it is not unthinkable that implantables can be applied for training load monitoring purposes in the future, several hurdles need to be overcome for implantable devices to become as widely used as the current generation of wearables.

#### *7.4.3 Markerless motion capture*

Despite the relatively easy in-field use of wearable (or implantable) sensors, these methods also have some serious limitations. Individual body-worn devices or full-body suits are often invasive in one way or another and can considerably affect an athlete's movement during sports. Therefore, if other methods to measure segmental accelerations besides body-worn accelerometers would become available in the future, this could increase the usability for GRF estimations. Markerless motion capture for example, has been suggested to be a potential future method for non-invasively measuring different biomechanical variables in the field (Alderson, 2015; Corazza et al., 2006). Examples of markerless motion capture applications include the analysis of tennis serves (Abrams et al., 2014), tracking golf swing motion (Fung et al., 2014), the assessment of BMX starts (Grigg et al., 2018), measurements of flight time and height during vertical jumps (Balsalobre-Fernández et al., 2014), and kinematic assessments of walking and running (Padulo et al., 2015), and squatting (Perrott et al., 2017; Saylor et al., 2017). Similarly,

---

markerless measurements of whole-body movements in different sport settings (e.g. running tracks, football pitches, tennis courts) might be used to measure segmental accelerations and estimate GRF according to the methods described in chapter 5. Moreover, similar to the above described full-body accelerometry suits, markerless motion capture systems can provide readily available kinematic information which, in combination with GRF, allows for further investigation of biomechanical loads on the internal structures. Therefore, if markerless motion capture technologies become available which can provide valid and reliable real-time measures of segmental displacements and accelerations in the field, this might eventually be used to substantially enhance biomechanical load monitoring of training and/or competition in different sports.

#### 7.4.4 *Machine learning*

An important finding of the studies described in this thesis was that GRF cannot be predicted from one or multiple segmental accelerations, following different mechanical approaches. However, other methods, such as machine learning, have emerged in medical sciences and also gained popularity in human movement biomechanics (Halilaj et al., 2018). More specifically, several studies have aimed to use machine learning methods to predict GRF from commonly used types of kinematic data. For example, based on the GRF and accelerometry data described in chapter 3 and 4, Pogson et al. (2018) used a neural network method to predict GRF from a trunk-accelerometer and found very strong correlations ( $R^2 > 0.9$ ) between measured and predicted GRF curves, across a variety of different high-intensity running tasks (Pogson et al., n.d.). Similarly, machine learning has successfully been used to predict GRF from one or multiple body-worn accelerometers in walking (Guo et al., 2017; Karatsidis et al., 2017) and steady running (Wouda et al., 2018). In addition, other studies using neural networks models have accurately predicted GRF and moments, as well as joint forces and moments, from marker trajectory data for walking and sidestepping (Johnson et al., 2018b, 2018a; Oh et al., 2013). Although these studies have reported promising results, there are also disadvantages of using computational approaches to estimate GRF for load monitoring purposes. For example, underlying physical mechanisms of the predicted variable (e.g. GRF, joint moments) are often

---

difficult to explore (Halilaj et al., 2018). Therefore, despite ongoing research into the interpretability of machine learning (Doshi-Velez and Kim, 2017), these methods may still be limited in their application for e.g. explaining injury mechanisms or performance enhancing criteria. Machine learning could thus offer a powerful and simple alternative for mechanical approaches to predict GRF in non-laboratory settings, providing that no further exploration of underlying physical mechanisms is required.

---

## **Chapter 8: Conclusion**

---

---

This thesis has aimed to estimate GRF from segmental accelerations to ultimately provide researchers and practitioners with a biomechanically sound and meaningful measure of external whole-body biomechanical loading. The outcomes of the different studies have shown that it is not straightforward to predict GRF from accelerometers embedded in current trunk-worn GPS devices, or even multiple segmental accelerations measured with a three-dimensional motion capture system. Moreover, the key segmental contributions to specific GRF features were highly complex and specific to different tasks frequently performed during running-based sports. Together, these findings show that accurately estimating a well-established measure of whole-body biomechanical load from segmental accelerations is difficult, especially across a range of tasks that are frequently performed during running-based sports. Consequently, the construct validity of using single accelerometer units and accelerometry derived load measures to assess the external biomechanical loads in the field, is likely to be poor. Researcher and practitioners should, therefore, be very cautious when using these methods to measure, monitor and evaluate external whole-body biomechanical loads.

---

## **Appendices**

---

## Appendix A: The two mass-spring-damper model

This appendix aims to describe the two mass-spring-damper model (chapter 3 and 4) and explain how the eight natural model parameters of this model were derived. The model consists of a lower mass on a spring and damper, representing the support leg, with an upper mass on a spring on top, representing the rest of the body (figure A.1). The positions of the upper ( $m_1$ ) and lower mass ( $m_2$ ) without any external load are described by  $x_1$  and  $x_2$ , while  $l_1$  and  $l_2$  are the natural lengths of the upper and lower springs respectively. The linear spring stiffness constants for the upper and lower spring are defined by  $k_1$  and  $k_2$ , while  $c$  is the damper's damping coefficient.

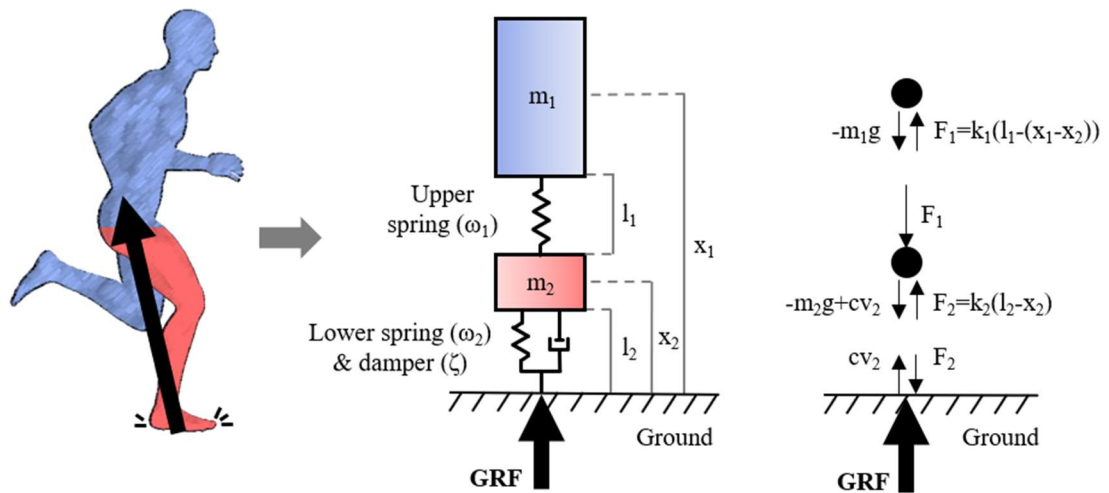


**Figure A.1** The two mass-spring-damper model.

From these nine model parameters the eight natural model parameters were derived according to equations A.1.1-8. These eight natural model parameters were then used to describe the accelerations of the upper ( $a_1$ ) and lower mass ( $a_2$ ) according to equations A.1.9-10, in which  $g$  is the gravitational acceleration ( $-9.81 \text{ m}\cdot\text{s}^{-2}$ ) and  $BM$  the total body mass. Finally, the modelled ground reaction force (GRF) was calculated according to equation A.1.11.

<b>Table A.1</b> Equations describing the eight natural parameters of the two mass-spring-damper model		
Initial position of the upper mass	$p_1 = x_1 - l_1 - l_2$	Eq. A.1.1
Initial position of the lower mass	$p_2 = x_2 - l_2$	Eq. A.1.2
Initial velocity of the upper mass	$v_1 = \dot{p}_1$	Eq. A.1.3
Initial velocity of the lower mass	$v_2 = \dot{p}_2$	Eq. A.1.4
Mass ratio	$\lambda = \frac{m_1}{m_2}$	Eq. A.1.5
Natural frequency of the upper spring	$\omega_1 = \sqrt{\frac{k_1}{m_1}} = \sqrt{\frac{(1 + \lambda) \cdot k_1}{\lambda \cdot BM}}$	Eq. A.1.6
Natural frequency of the lower spring	$\omega_2 = \sqrt{\frac{k_2}{m_2}} = \sqrt{\frac{(1 + \lambda) \cdot k_2}{BM}}$	Eq. A.1.7
Damping ratio of the damper	$\zeta = \frac{c}{2 \cdot \sqrt{k_2 \cdot m_2}}$	Eq. A.1.8
Acceleration of the upper mass	$a_1 = -\omega_1^2 \cdot (p_1 - p_2) + g$	Eq. A.1.9
Acceleration of the lower mass	$a_2 = -\omega_2^2 \cdot p_2 + \omega_1^2 \cdot \lambda \cdot (p_1 - p_2) - 2 \cdot \zeta \cdot \omega_2 \cdot v_2 + g$	Eq. A.1.10
Ground reaction force	$GRF = -\frac{BM \cdot \omega_2}{1 + \lambda} \cdot (\omega_2 \cdot p_2 + 2 \cdot \zeta \cdot v_2)$	Eq. A.1.11

---

## Appendix B: Comparing solving methods: gradient descent vs. numerical optimisation

---

### *B.1 Objective*

Solving procedures for finding the two mass-spring damper model parameters (appendix A) required to accurately model ground reaction force (GRF) profiles can lead to multiple local optimal solutions in the eight-parameter search windows. Therefore, the aim of this appendix was to determine the best method to solve the model's equations and reproduce measured GRF profiles most accurately. Parameter optimisations were performed by using two distinct methods; 1) a gradient descent optimisation routine (Nedergaard, 2017; Nedergaard et al., 2018) and 2) a numerical optimisation method.

### *B.2 Methods*

Measured GRF profiles were reproduced with a two mass-spring-damper (see the methods section in chapter 3 for more details). A gradient descent optimisation routine was performed using a purpose written Matlab code (version R2015a, The MathWorks, Inc., Natick, MA, USA) (Nedergaard, 2017). The two 2<sup>nd</sup> order differential equations for the upper and lower mass accelerations  $a_1$  and  $a_2$  (appendix A) were transformed to four 1<sup>st</sup> order differential equations. This new set of equations was then solved with a 4<sup>th</sup> order Runge Kutta method and the resulting parameters were used to calculate the modelled GRF according to equation A1.11. For each trial, a unique optimal set of the eight model parameters was defined based on the lowest value of the RMSE between the measured and modelled GRF curves.

For the numerical method, a purpose written Python code (Python, 2017) based on a numerical optimisation library (SciPy, 2017) was used. For this method, the gradient of the GRF profiles was included as an extra error metric besides RMSE. The best combination of model parameters was selected based on the combination of the lowest RMSE and gradient error between the modelled and measured GRF curves during ground contact. Multiple different in-built Python solvers (BFGS, CG, COBYLA, L-BFGS-B, Nelder-Mead, Powell, SLSQP, and TNC) were run

---

simultaneously to solve the model equations and the solution with the best modelled GRF was chosen for each individual trial. For more details on the solving processes, see chapter 3.2.

### *B.3 Results*

The gradient descent optimisation routine was not able to find a combination of parameters to model GRF for 29 trials (3.4%), while modelled GRF curves showed large oscillations and unrealistic solutions for 27 trials (3.2%). These trials were, therefore, not included in the analysis and the results for the gradient descent optimisation method only included 93.5% of the trials. The numerical method on the other hand, could solve the model's equations for 100% of the data and resulting modelled GRF curves were all realistic. Therefore, for the numerical method all the trials were included in the analysis.

When using a gradient descent method, RMSE of the modelled GRF was the lowest for accelerations and running at low speeds but increased with increasing running speed (table B.1). However, the numerical method modelled GRF with substantially lower errors for these tasks. The least accurate modelled GRF profiles were for deceleration trials which had a very high RMSE ( $>4 \text{ N}\cdot\text{kg}^{-1}$ ) using gradient descent, but moderate ( $2\text{-}3 \text{ N}\cdot\text{kg}^{-1}$ ) for the numerical method. Similarly, impulse errors were very low ( $<5\%$ ) across all tasks for both optimisation methods, but impulses were more accurate using the numerical method.

For both methods, impact peaks observed in the measured GRF could not always be modelled. For the gradient descent optimisation, impact peaks were visible in the modelled curves for 28%, 100% and 51% of the acceleration, deceleration and constant speed running trials respectively, while the numerical method could model these peaks for 34%, 99% and 48% for the same tasks respectively. The gradient descent method modelled impact peaks with moderate to high (11.7-17.8%) errors for running at a constant low or moderate speed, but very high ( $>20\%$ ) for accelerations, decelerations and running at high speeds. In addition, loading rate errors were very high ( $>20\%$ ) across all tasks. The numerical method, however, modelled the impact peaks with low to moderate errors (7.5-11%) for constant speed running, but high to very high for accelerations and decelerations (table B.1). Similarly, modelled loading rate values were high to

very high across tasks. However, both the impact peak and loading rate errors were substantially lower across tasks for the numerical method compared to the gradient descent method (table B.1).

**Table B.1** Modelled ground reaction force curve and loading characteristics errors

<b>Gradient descent method</b>								
	<b>RMSE</b>		<b>Impulse error</b>		<b>Impact peak error</b>		<b>Loading rate error</b>	
	$\text{N}\cdot\text{kg}^{-1}$	%	$\text{N}\cdot\text{s}\cdot\text{kg}^{-1}$	%	$\text{N}\cdot\text{kg}^{-1}$	%	$\text{N}\cdot\text{kg}^{-1}\cdot\text{s}^{-1}$	%
Accelerations	1.49	40.3	0.06	2.3	4.49	30.4	848	62.1
Decelerations	5.78	124.8	0.09	3	10.95	25.2	1178	51.5
Constant speed running								
Low ( $2\text{-}3\text{ m}\cdot\text{s}^{-1}$ )	1.26	44.7	0.09	2.4	1.87	11.7	148	28.2
Mod. ( $4\text{-}5\text{ m}\cdot\text{s}^{-1}$ )	1.81	57	0.02	0.7	3.15	17.8	221	23.7
High ( $>6\text{ m}\cdot\text{s}^{-1}$ )	2.82	64.3	0.05	2	5.40	23.6	800	51.3
All tasks	3.02	73	0.07	2.3	8.98	24.2	1003	49.1
<b>Numerical method</b>								
	<b>RMSE</b>		<b>Impulse error</b>		<b>Impact peak error</b>		<b>Loading rate error</b>	
	$\text{N}\cdot\text{kg}^{-1}$	%	$\text{N}\cdot\text{s}\cdot\text{kg}^{-1}$	%	$\text{N}\cdot\text{kg}^{-1}$	%	$\text{N}\cdot\text{kg}^{-1}\cdot\text{s}^{-1}$	%
Accelerations	0.70	9.9	0.01	0.6	2.43	18.9	487	31.3
Decelerations	2.48	33.9	0.01	0.7	7.43	20.6	431	18.7
Constant speed running								
Low ( $2\text{-}3\text{ m}\cdot\text{s}^{-1}$ )	0.48	7.6	0.01	0.4	1.53	10.2	200	19.1
Mod. ( $4\text{-}5\text{ m}\cdot\text{s}^{-1}$ )	0.78	9.4	0.01	0.3	1.54	7.5	254	20.8
High ( $>6\text{ m}\cdot\text{s}^{-1}$ )	1.21	13.6	0.01	0.3	2.99	11	287	18.5
All tasks	1.28	17	0.01	0.5	5.74	17.4	385	20.3

Mean values for root mean square errors (RMSE), impulse, impact peak and loading rate errors of the modelled GRF profiles for different tasks. Results are for either a gradient descent optimisation routine (top), or a numerical optimisation method (bottom). Values are either absolute or relative errors compared to the measured GRF. Green shaded error values represent the lowest error values of the two methods.

From the eight different numerical solving methods used in the Python code, five gave the best GRF solutions for individual trials (table B.2). The BFGS solver found the best solution for the majority of all trials (61%), while three solving methods (CG, COBYLA and TNC) did not find a best solution for any of the trials.

<b>Optimiser name</b>	<b>Number of trials (#)</b>	<b>Percentage of all trials (%)</b>
BFGS	518	61
CG	0	0
COBYLA	0	0
L-BFGS-B	173	20
Nelder-Mead	98	11
Powell	27	3
SLSQP	40	5
TNC	0	0
Total	856	100

The eight numerical solvers used in the purpose written Python code, which found the best solutions for individual trials.

#### *B.4 Conclusion*

This investigation shows that a gradient descent and numerical optimisation method can both find acceptable results for modelled GRF profiles. However, the gradient descent method could not always find a (realistic) solution and the modelled GRF profiles and loading characteristics were most accurate when using a numerical method. Therefore, the numerical optimisation method was used in chapter 3 (and 4) to determine the best combination of the two mass-spring-damper model's eight parameters to accurately replicate GRF.

---

## **Appendix C: The relationship between measured trunk accelerations and the two mass-spring-damper model's upper mass acceleration**

---

### *C.1 Objective*

The results in chapter 4 have shown that trunk accelerations (TA) cannot be used to predict ground reaction forces (GRF) using a two mass-spring-damper model, either directly or indirectly. Since chapter 3 has shown that this model is able to accurately reproduce GRF for various tasks, it is likely that the measured TA substantially deviates from the model's upper mass acceleration  $a_1$  required to accurately predict GRF. This appendix, therefore, aimed to explore 1) how the measured TA is related to the model's upper mass acceleration required to accurately model GRF and 2) whether this relationship can be used to predict GRF from TA more accurately.

### *C.2 Trunk and upper mass accelerations*

Measured TA signals were compared to the model's upper mass acceleration  $a_1$  for the tasks described in chapter 4. As expected, TA indeed substantially deviated from the upper mass acceleration required to accurately model GRF across the different tasks (figure C.1). Differences were mainly apparent in the shapes of the acceleration profiles, as well as magnitudes. In contrast to the required  $a_1$ , which had smooth sinusoidal shaped acceleration profiles, the measured TA curves contained multiple rapid oscillations and sharp peaks (figures C1 A, C, E and G). Moreover, the magnitude of TA peaks was typically larger than the maximal accelerations in the  $a_1$  profiles. For deceleration trials, the required  $a_1$  profiles typically had a maximal peak earlier during stance compared to the TA. This earlier modelled  $a_1$  peak is in accordance with the impact peaks just after touch-down usually observed in GRF profiles for decelerations (figures C1 C and D). Due to the discrepancies between the TA and  $a_1$  curves across tasks, it was concluded that the measured TA did not represent the required  $a_1$  well enough to be used to accurately predict GRF.

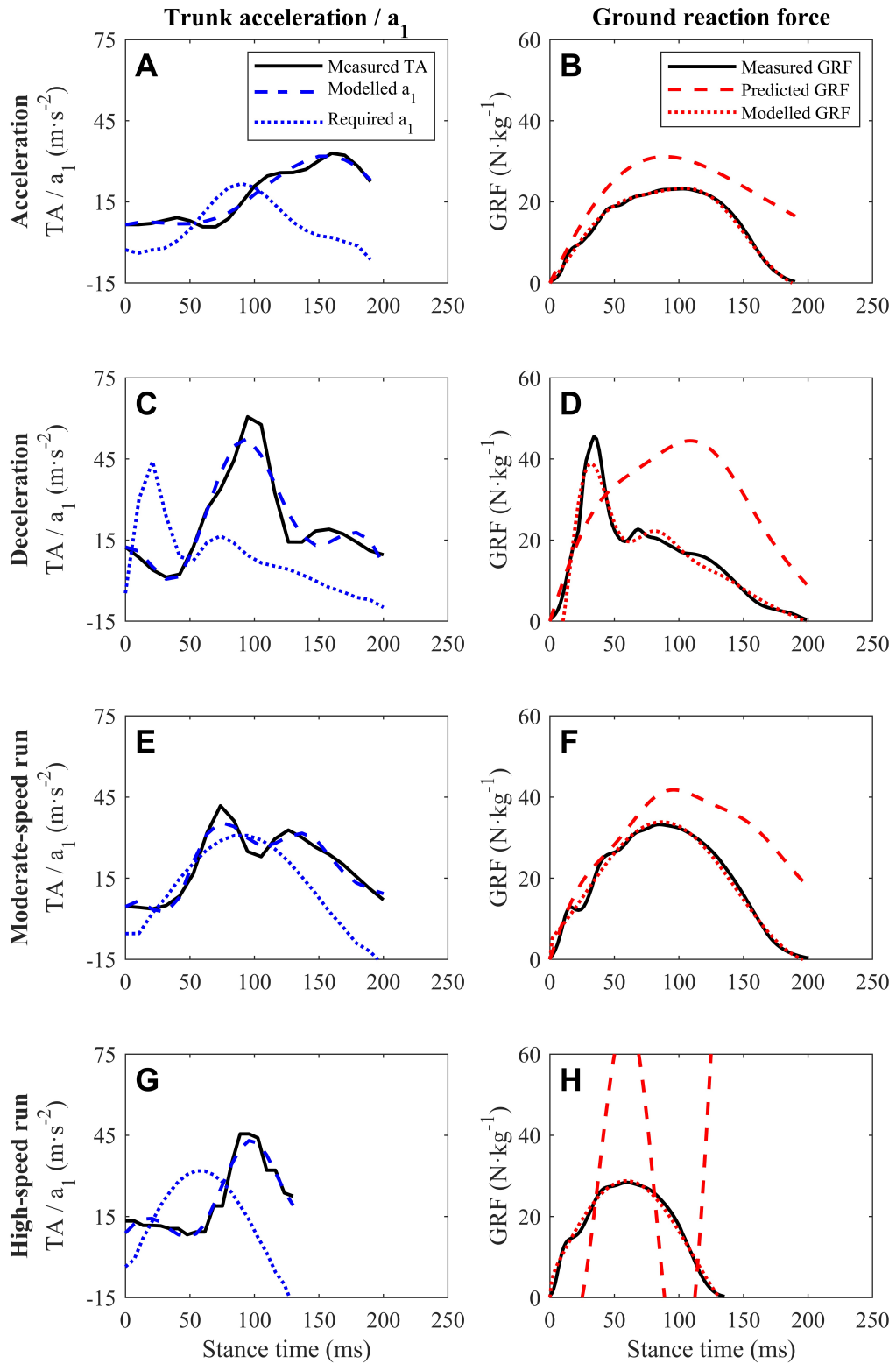


**Figure C.1** Representative examples of trunk accelerations (TA) and upper mass accelerations ( $a_1$ ), and measured, predicted and modelled ground reaction forces (GRF) for different tasks. Although TA could be replicated well by the model's  $a_1$  (blue dashed line), the predicted GRFs (red dashed line) were poor. Required  $a_1$  (blue dotted line) to accurately model GRF (red dotted line) strongly deviated from the TA for all tasks.

---

### C.3 *Modifying trunk accelerations*

The above described differences between the measured TA and  $a_1$  needed for precise GRF estimates could possibly be related to the quality of the measured TA signal. Even though the GPS device in which the accelerometer was embedded was carefully fitted in the pocket of a tight vest, several wobbling factors are likely to distort the TA signal. For example, wobbling of the GPS unit in the pocket of the vest and movement of the shirt and skin can introduce substantial noise in the measured acceleration signal. In addition, the GPS device was attached to the back of the upper trunk and thus away from its centre of mass. The measured TA is thus unlikely to be an accurate reflection of the actual movement of the trunk segment. Nevertheless, the GPS-embedded accelerometer was attached to the trunk segment and the measured signal will thus be dominated by the general motion of trunk. If this general trunk movement can be extracted from the measured TA signal, this might be a better representation of the required  $a_1$  to accurately predict GRF.

To extract the general trunk motion from the measured TA, quadratic functions were fitted to each individual TA signal. The aim of fitting these simple functions was to remove (or at least reduce) the noise due to above described factors from the TA. The quadratic fitted TA signals ( $TA_Q$ ) were replicated by adjusting the eight model parameters to fit the model's upper mass acceleration  $a_1$  to  $TA_Q$ , after which GRF was calculated from the following set of parameters. A more detailed description of this process is provided in chapter 4.2.

Between the different tasks, a general difference in quadratic fitted TA curve shapes was observed (figure C.2 A, D G, J). Acceleration trials typically had an (roughly linearly) increasing  $TA_Q$  profile, while decelerations and running at a constant speed had a more sinusoidal shaped  $TA_Q$ . Sharp peaks and rapid oscillations in the measured TA signals, which are likely due to wobbling of the unit relative to the trunk, were effectively eliminated. Across trials, the maximal  $TA_Q$  peaks were the highest for decelerations and running at high speeds.

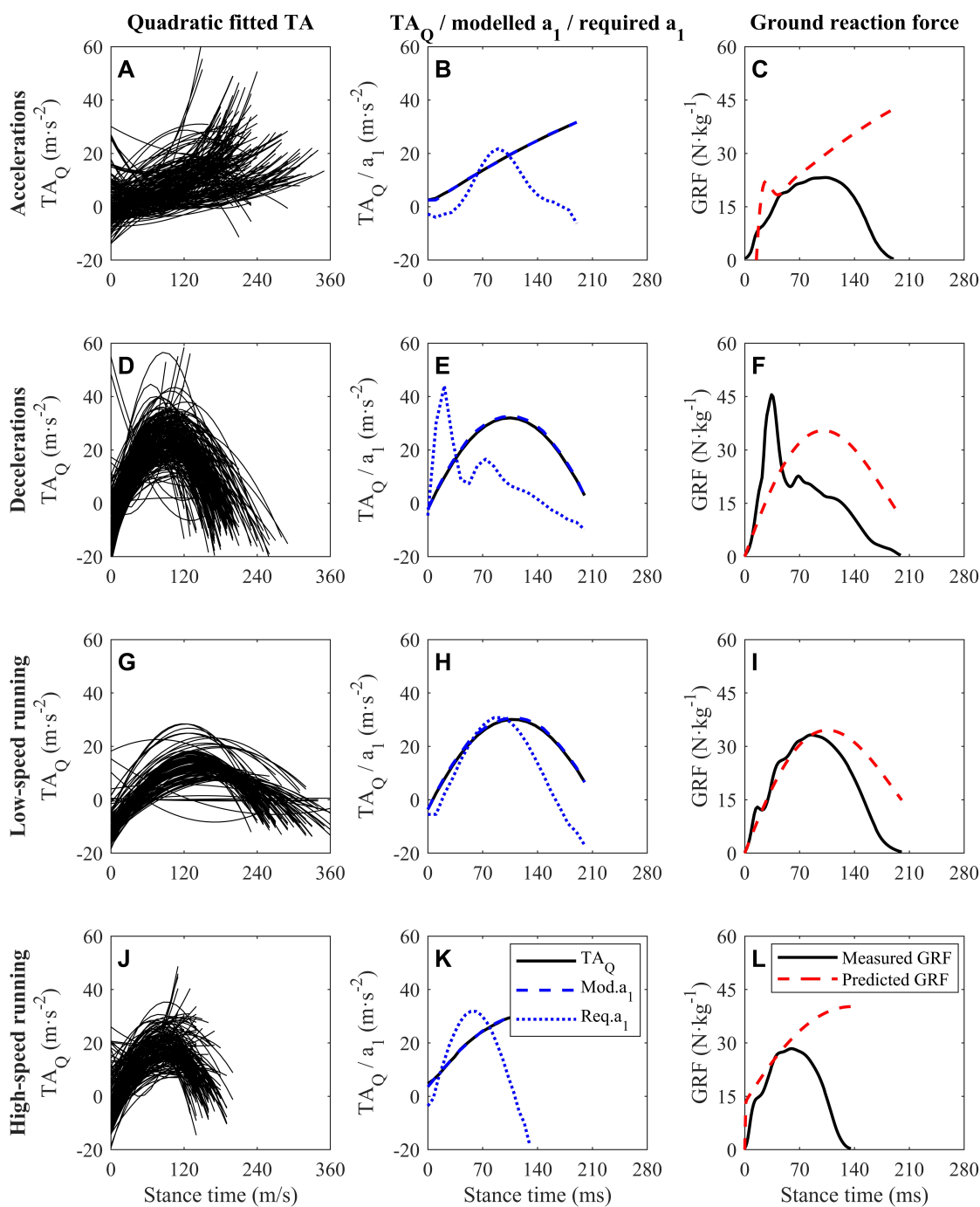


**Figure C.2** Quadratic fitted trunk acceleration (TA<sub>Q</sub>) signals were used as input for the model's upper mass acceleration (a<sub>1</sub>) to predict GRF. General TA curve shapes showed different shapes between the different tasks (A, D, G, J). Although the model was able to accurately fit the modelled a<sub>1</sub> to the TA<sub>Q</sub> (B, E, H, K), predicted GRF was still very poor (C, F, I, L).

---

Fitting simple quadratic functions to the measured TA signals did not lead to a better representation of the upper mass acceleration  $a_1$  required to accurately predict GRF. Despite the considerably simplified  $TA_Q$  profiles and likely removal of the majority of wobbling effects from the TA,  $TA_Q$  profiles still substantially differed from the required  $a_1$  for the majority of trials and tasks (figure C.2 B, E, H, K). Therefore, although the  $TA_Q$  could be replicated by the model's upper mass with very high accuracy, this did not lead to more accurate GRF predictions (figure C.2 C, F, I, L). Hence, modifying the measured TA could not lead to a sufficiently close representation of the required upper mass acceleration.

#### *C.4 Conclusion*

Acceleration signals measured with a trunk-mounted accelerometer considerably deviate from the upper mass acceleration in a two mass-spring-damper model required to accurately model GRF. Although the effects of factors such as unit wobbling relative to the trunk could be reduced, this did not lead to a more accurate representation of the required  $a_1$ . The substantial differences between the measured TA and the model's upper mass acceleration were, therefore, considered to be a major reason why GRF cannot be predicted from TA using a two mass-spring-damper model.

---

## Appendix D: Bounding the two mass-spring-damper model's parameter search spaces

---

### *D.1 Objective*

The two mass-spring-damper model parameter values required to replicate trunk accelerations (TA) typically fell in a different range compared to those required to reproduce ground reaction forces (GRF; chapter 3 and 4). Furthermore, parameter values had little physical meaning for the majority of trials. The difference between modelled TA and GRF parameter ranges, as well as the lack of physical meaning of the parameters, likely affects the regressions between both sets of parameters. If equally good solutions exist to replicate TA and reproduce GRF within a physically meaningful range of parameter values, the relationship between both parameter sets might be improved. Therefore, the aim of this appendix was to investigate whether acceptable modelled TA and GRF curves can be found within a similar and physically meaningful parameter space for both signals.

### *D.2 Methods*

The parameters resulting from replicating TA (chapter 4) and reproducing GRF (chapter 3) were taken as a starting point. The eight model parameter value spaces were then bound in four steps:

1. Model parameter values required to replicate TA and reproduce GRF were plotted for each individual trial in a regression plot for each parameter.
2. Parameter regression plots were visually appraised, and bounds were defined for each parameter based on similarity between modelled TA and GRF parameter ranges, as well as the  $R^2$  values of the regressions. In addition, physical parameter meaning was considered when defining bounds for each parameter (e.g. a mass ratio  $\lambda > 10$  is not realistic and was thus used as an upper bound).
3. The model was then used to re-model TA and GRF, using the parameter upper and lower bounds as defined in step (2).
4. Steps 1 to 3 were repeated until the modelled TA and GRF parameter values were within a similar range, and within physically sensible values.

---

### D.3 Results

Bounding the upper and lower spring natural frequencies  $\omega_1$  and  $\omega_2$  was highly detrimental to the modelled TA and GRF curves. Therefore, these parameters were only given a lower limit of 0 (i.e. spring stiffness  $k_{1,2} > 0 \text{ kN}\cdot\text{m}^{-1}$ ) while the upper limits were left free. When the parameter bounding steps were repeated, however,  $\omega_1$  and  $\omega_2$  naturally moved towards a similar range of values for both the modelled TA and GRF. After the third iteration of the bounding procedure RMSE values substantially increased and the process was stopped. The lower and upper limits for each parameter ( $p_2$  was calculated from  $v_2$ ,  $\omega_2$  and  $\lambda$  as described in chapter 3.2.4) after the third iteration were:

- $p_1 = -0.4 - 0.1 \text{ m}$
- $v_1 = -3 - 1 \text{ m}\cdot\text{s}^{-1}$
- $v_2 = -0.5 - 2 \text{ m}\cdot\text{s}^{-1}$
- $\omega_1 = 0 - \infty \text{ N}\cdot\text{m}^{-1}\cdot\text{kg}^{-1}$
- $\omega_2 = 0 - \infty \text{ N}\cdot\text{m}^{-1}\cdot\text{kg}^{-1}$
- $\lambda = 0.5 - 6 \text{ au}$
- $\zeta = 0.1 - 1.5 \text{ au}$

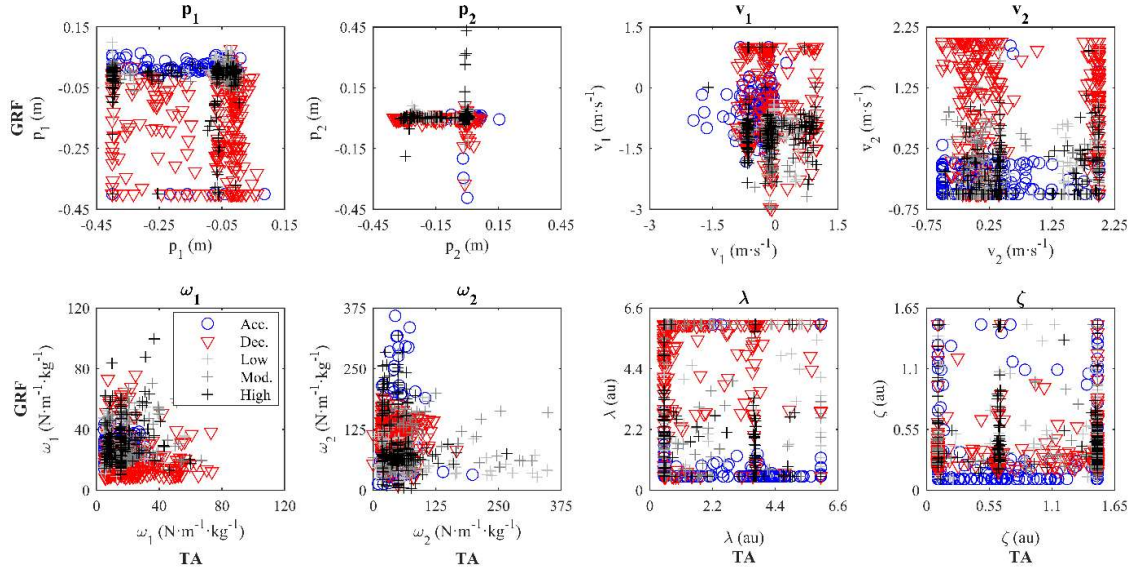


**Figure D.1** Scatter plots of the eight model parameters for each individual acceleration (blue circles), deceleration (red triangles) and low, moderate and high-speed running (light grey, dark grey and black crosses respectively) trial. Parameter values required to model trunk accelerations (TA) or ground reaction force (GRF) are plotted on the x-axes and y-axes respectively.

**Table D.1** Modelled trunk acceleration and ground reaction force curve errors using a free and bound parameter search space

	TA ( $\text{m}\cdot\text{s}^{-2}$ )				GRF ( $\text{N}\cdot\text{kg}^{-1}$ )			
	Free parameters		Bound parameters		Free parameters		Bound parameters	
	Mean	SD	Mean	SD	Mean	SD	Mean	SD
Accelerations	3.9	$\pm 1.8$	7.1	$\pm 12$	0.69	$\pm 0.46$	0.98	$\pm 0.60$
Decelerations	7	$\pm 3$	17.9	$\pm 14.6$	2.48	$\pm 1.17$	2.96	$\pm 2.04$
Constant speed running								
Low ( $2\text{-}3 \text{ m}\cdot\text{s}^{-1}$ )	4	$\pm 1.7$	10.6	$\pm 14.3$	0.48	$\pm 0.22$	0.55	$\pm 0.25$
Mod. ( $4\text{-}5 \text{ m}\cdot\text{s}^{-1}$ )	4.8	$\pm 1.7$	8.2	$\pm 5.2$	0.78	$\pm 0.25$	0.87	$\pm 0.26$
High ( $>6 \text{ m}\cdot\text{s}^{-1}$ )	4.6	$\pm 1.9$	21.5	$\pm 19.8$	1.21	$\pm 0.56$	1.26	$\pm 0.62$
All tasks	5.1	$\pm 2.5$	13.7	$\pm 15.5$	1.28	$\pm 1.06$	1.52	$\pm 1.49$

Root mean square errors (RMSE) between the replicated and measured trunk acceleration (TA in  $\text{m}\cdot\text{s}^{-2}$ ), and reproduced and measured ground reaction force (GRF in  $\text{N}\cdot\text{kg}^{-1}$ ). Results are for modelled curves using a free parameter search space or a bound parameter space (grey shaded). Values are mean errors  $\pm$  standard deviations (SD) for each task.

---

After bounding the model parameter spaces, the two mass-spring-damper model could model the measured TA and GRF profiles within a similar range of model parameters (figure D.1). Despite the substantial restrictions put on the maximal and minimal values for five parameters (the upper bounds for  $\omega_1$  and  $\omega_2$  were left free, and  $p_2$  was calculated from  $v_2$ ,  $\omega_2$  and  $\lambda$ ) the detrimental effects on the RMSE for reproduced GRF curves were small (table D.1). Errors were very low ( $<1 \text{ N}\cdot\text{kg}^{-1}$ ) for accelerations and running at low and moderate speeds, and low ( $1\text{-}2 \text{ N}\cdot\text{kg}^{-1}$ ) and moderate ( $2\text{-}3 \text{ N}\cdot\text{kg}^{-1}$ ) for high-speed running and decelerations respectively. TA on the other hand, could not be replicated well when the model parameter search space was restricted. Modelled TA errors substantially increased (table D.1) and RMSEs were low ( $<5 \text{ m}\cdot\text{s}^{-2}$ ) and moderate ( $5\text{-}10 \text{ m}\cdot\text{s}^{-2}$ ) for accelerations and running at a moderate speed, high ( $10\text{-}15 \text{ m}\cdot\text{s}^{-2}$ ) for running at low speeds, but very high ( $>15 \text{ m}\cdot\text{s}^{-2}$ ) for running at high speeds and decelerations.

From figure D.1 it appeared that there was no relationship between the two parameter sets. Parameter values varied throughout the bound search spaces for both the modelled TA and GRF. Moreover, the absence of a relationship between both parameter sets was independent of task, i.e. there was no consistency within or between tasks.

#### *D.4 Conclusion*

This investigation shows that multiple combinations of model parameters can lead to similarly good solutions to reproduce measured GRF profiles. Bounding the parameter search space was, however, highly detrimental for replicated TA curves. In addition, there was no relationship between any of the parameters required to model TA or GRF. It was, therefore, concluded that bounding model parameters could not lead to better relationships between parameters required to model TA and GRF and could thus not improve indirect GRF predictions from TA.

---

## **Appendix E: Fixing the two mass-spring-damper model's parameter values**

---

### *E.1 Objective*

The two mass-spring-damper model has a large amount of freedom with interdependency between, and variability within, its eight model parameters. As a result, it is likely that several combinations of parameters can give similarly good results when modelling trunk accelerations (TA) and/or ground reaction force (GRF) profiles (e.g. as observed for reproduced GRF in appendix D). Restricting the number of free model parameters to limit the model's freedom might, therefore, improve the relationships for the remaining free parameters. Therefore, the aim of this appendix was to investigate whether fixing single or multiple parameters at a constant value to limit the model's freedom could improve the linear relationships of other model parameters.

### *E.2 Methods*

To limit the freedom of the model's parameter spaces, the upper and lower parameter value limits following from appendix D were used for this analysis. First, single model parameters were fixed at a constant value while the seven remaining parameters were optimised to model GRF and TA (see the methods section of chapter 3 and 4 for more detail). Values at which the parameters were fixed were determined by visually evaluating the regression plots in figures 4.4 and D1. Fixed parameter values were chosen to represent the majority of the trials, for TA as well as GRF parameters. In addition, GRF and TA were also modelled with several combinations of either two or three parameters fixed simultaneously. Fixed values for single, or a combination of parameters were:

---

#### Single fixed parameters

- $p_1 = -0.1 \text{ m}$
- $v_1 = -0.5 \text{ m}\cdot\text{s}^{-1}$
- $v_2 = 0.5 \text{ m}\cdot\text{s}^{-1}$
- $\omega_1 = 22.5 \text{ N}\cdot\text{m}^{-1}\cdot\text{kg}^{-1}$
- $\omega_2 = 100 \text{ N}\cdot\text{m}^{-1}\cdot\text{kg}^{-1}$
- $\lambda = 3 \text{ au}$
- $\zeta = 0.5 \text{ au}$

#### Two fixed parameters

- $\omega_1 = 22.5 \text{ N}\cdot\text{m}^{-1}\cdot\text{kg}^{-1}; \lambda = 3 \text{ au}$
- $\omega_2 = 100 \text{ N}\cdot\text{m}^{-1}\cdot\text{kg}^{-1}; \lambda = 3 \text{ au}$

#### Three fixed parameters

- $\omega_1 = 22.5 \text{ N}\cdot\text{m}^{-1}\cdot\text{kg}^{-1}; \omega_2 = 100 \text{ N}\cdot\text{m}^{-1}\cdot\text{kg}^{-1}; \lambda = 3 \text{ au}$

After re-modelling the measured TA and GRF profiles, a new parameter regression analysis was performed (see chapter 4 for more detail). Linear regressions were performed for all tasks and trials combined. Only if  $R^2$  values were larger than 0.3 (i.e. a moderate correlation of  $R^2 > 0.3$  (Hopkins et al., 2009)) the regression equation was used to recalculate the parameter value before calculating the predicted GRF.

### *E.3 Results*

Fixing parameters considerably affected the distribution of model parameters required to model TA and GRF (figure E.1). When fixing either single or multiple parameters the free parameters were shifted to a narrower range. This reduction in parameter variation was mainly observed for replicated TA, and mass-related parameters ( $p_1$ ,  $p_2$ ,  $v_1$ ,  $v_2$  and  $\lambda$ ) especially. It is likely that the free mass-related parameters could not account for the rapid acceleration changes typically observed in the measured TA profiles and, therefore, only showed minor variability when replicating TA. In addition, visually screening the modelled curves revealed that limiting the model's freedom was highly detrimental for the replicated TA, as well as reproduced GRF accuracy.

**Table E.1** Linear regressions for the eight model parameters with free, bound and fixed parameters

	Free params	Bound params	Bound + fixed parameter combinations									
			$p_1$	$v_1$	$v_2$	$\omega_1$	$\omega_2$	$\lambda$	$\zeta$	$\omega_1, \lambda$	$\omega_2, \lambda$	$\omega_1, \omega_2, \lambda$
$p_1$	0.06	0.36	-	4.28	4.65	1.01	3.89	0.46	4.22	9.09	2.58	0.02
$p_2$	0.01	0.00	0.02	0.26	0.58	0.15	4.89	0.54	3.13	8.10	1.99	0.43
$v_1$	0.04	1.06	1.34	-	0.13	0.00	0.00	0.17	0.59	0.23	0.00	15.77
$v_2$	0.08	1.79	1.99	3.31	-	2.58	0.99	0.96	2.25	1.37	1.23	0.00
$\omega_1$	0.00	0.01	0.70	1.47	0.05	-	1.84	0.55	0.37	-	0.04	-
$\omega_2$	0.22	0.26	2.13	0.24	0.38	8.43	-	0.01	0.16	4.49	-	-
$\lambda$	0.11	1.72	0.49	1.41	1.04	3.68	0.10	-	2.35	-	-	-
$\zeta$	0.00	0.39	0.03	0.00	9.64	1.12	0.92	0.13	-	0.44	2.01	2.52

$R^2$  values ( $\cdot 10^{-2}$ ) of the linear regression between parameter values required to model trunk accelerations and ground reaction forces for the eight model parameters. Parameter search spaces were either left free, bound according to the upper and lower limits described in appendix D, or bound in combination with one, two or three parameters fixed at a constant value. Regression results are for all tasks and trials combined. Dark green shading indicates an increased  $R^2$  value of the bound relative to the free parameter space. Light green shading represents higher  $R^2$  values relative to the bound parameter space without fixed parameters. Only if  $R^2 > 0.3$  (i.e.  $30 \cdot 10^{-2}$ ) the regression equation was used to recalculate the parameter.

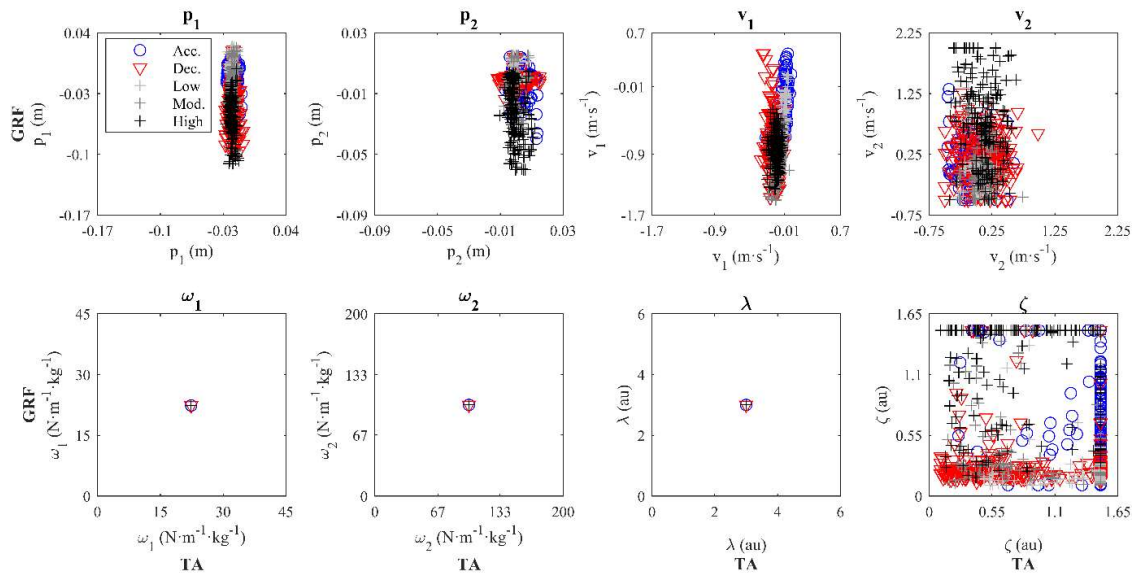


**Figure E.1** Example of scatter plots of the eight model parameter values required to model TA and GRF when three parameters ( $\omega_1$ ,  $\omega_2$ ,  $\lambda$ ) were fixed at a constant value. Scatter plots include each individual acceleration (blue circles), deceleration (red triangles) and low-, moderate- and high-speed (light grey, dark grey and black crosses respectively) trial. Parameter values required to model trunk accelerations (TA) or ground reaction force (GRF) are plotted on the x-axes and y-axes respectively.

---

By fixing model parameter values the relationships between modelled TA and GRF parameter sets could be slightly improved for the majority of parameters (table E.1). Compared to the bound search spaces as described in appendix D, parameter regression values slightly increased when fixing individual parameters or a combination of parameter values. The best relationship observed was  $R^2 = 0.16$  (but  $< 0.3$ ) for the upper mass velocity  $v_1$  when fixing three other parameters (figure E.1; table E.1). Despite these improvements, however, the regressions were still very weak for most parameters and could thus not be used to recalculate parameters to achieve more accurate GRF predictions.

#### *E.4 Conclusion*

This investigation shows that by fixing either individual or multiple parameters at a constant value, relationships between modelled TA and GRF parameters sets could be slightly improved. However, for the majority of parameters these improvements were negligible, and the regression values were still very weak. It was, therefore, concluded that fixing model parameters could not lead to substantially stronger relationships between parameters required to model TA and GRF and therefore, could not lead to better indirect GRF predictions from TA.

---

## Appendix F: Simultaneously modelling trunk accelerations and ground reaction forces

---

### *F.1 Objective*

Although the two mass-spring-damper model can be used to accurately reproduce measured trunk acceleration (TA) and ground reaction force (GRF) profiles separately, TA cannot be used to predict GRF with this model, either directly or indirectly. Appendix C has shown that this discrepancy is likely to be the result of the difference between the measured TA signal and the model's upper mass acceleration  $a_1$  required for accurate GRF predictions. However, multiple combinations of model parameters can lead to similarly accurate modelled GRF (appendix D), and it is possible that the model can use a single set of parameters to simultaneously reproduce measured TA and GRF profiles. If this is indeed the case, and the detrimental effects on the modelled TA and GRF curves are minimal, this might allow for bridging the dissimilarities between the measured TA and required  $a_1$ . This appendix, therefore, aimed to investigate whether the differences between TA and  $a_1$  can be minimised by simultaneously modelling measured TA and GRF with the two mass-spring-damper model.

### *F.2 Methods*

Measured TA and GRF signals were modelled simultaneously with the two mass-spring-damper model (figure F.1). For each trial, the eight model parameters were optimised to fit the model's upper mass acceleration  $a_1$  to the measured TA, while the resulting GRF was fitted to the measured GRF (see the methods section in chapter 3 and 4 for more detail). The best set of model parameters was determined by minimising the root mean square errors (RMSE) of the modelled  $a_1$  and GRF curves relative to the measured TA and GRF respectively. Since the aim of this study was to find the best solution for TA and GRF, RMSE of both curves were given an equal weighting during the parameter optimisation process.

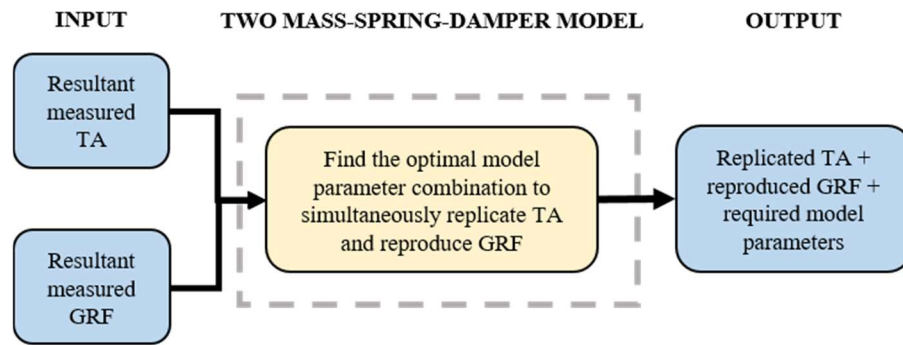


**Figure F.1** Diagram of how measured trunk accelerations (TA) and ground reaction forces (GRF) were simultaneously modelled with the two mass-spring-damper model.

### F.3 Results

Across the different tasks, TA and GRF could not both be modelled well at the same time using a single set of model parameters (figure F.2). Reproduced TA ( $a_1$ ) and GRF errors both substantially increased when simultaneously modelled, compared to TA and GRF modelled separately (table F.1). For TA, RMSE increased to moderate ( $5\text{-}10\text{ m}\cdot\text{s}^{-2}$ ) for accelerations and running at a low and moderate speeds, but high errors ( $10\text{-}15\text{ m}\cdot\text{s}^{-2}$ ) for decelerations and running at high speeds. Similarly, mean RMSE for modelled GRF curves increased across tasks to low ( $1\text{-}2\text{ N}\cdot\text{kg}^{-1}$ ; low-speed running), moderate ( $2\text{-}3\text{ N}\cdot\text{kg}^{-1}$ ; accelerations, moderate and high-speed running) or very high ( $>4\text{ N}\cdot\text{kg}^{-1}$ ; decelerations).

**Table F.1** Modelled curve errors for  $a_1$  and ground reaction force

	TA ( $\text{m}\cdot\text{s}^{-2}$ )				GRF ( $\text{N}\cdot\text{kg}^{-1}$ )			
	Separate		Simultaneous		Separate		Simultaneous	
	Mean	SD	Mean	SD	Mean	SD	Mean	SD
Accelerations	3.94	$\pm 1.8$	8.79	$\pm 3.8$	0.69	$\pm 0.46$	2.25	$\pm 1.3$
Decelerations	7.02	$\pm 3$	12.48	$\pm 4.1$	2.48	$\pm 1.17$	6.33	$\pm 2.34$
Constant speed running								
Low ( $2\text{-}3\text{ m}\cdot\text{s}^{-1}$ )	4.02	$\pm 1.7$	7.34	$\pm 2.5$	0.48	$\pm 0.22$	1.18	$\pm 0.61$
Moderate ( $4\text{-}5\text{ m}\cdot\text{s}^{-1}$ )	4.77	$\pm 1.6$	9.22	$\pm 2.7$	0.78	$\pm 0.25$	2.04	$\pm 0.97$
High ( $>6\text{ m}\cdot\text{s}^{-1}$ )	4.59	$\pm 1.9$	10.38	$\pm 3.8$	1.21	$\pm 0.56$	2.43	$\pm 1.53$
All tasks	5.07	$\pm 2.5$	10	$\pm 4$	1.28	$\pm 1.06$	3.24	$\pm 2.54$

Root mean square errors (RMSE) of the modelled relative to the measured trunk acceleration (TA) and ground reaction force (GRF) profiles. Values are mean errors  $\pm$  standard deviations (SD) for each task, compared between separately or simultaneously modelled TA and GRF.

---

Despite the substantial detrimental effects on the modelled TA and GRF profiles, reproduced GRFs were generally more accurate than TA ( $a_1$ ; figure F.2). Visual inspection revealed that rapid changes (i.e. sharp peaks) in the measured signals could not be replicated well and were typically over-smoothed. High acceleration peaks in the TA signal (figure F.2 C and G) and the distinct impact peaks in the GRF curve (figure F.2 D and H) especially, were modelled very poorly or not at all.

#### *F.4 Conclusion*

The two mass-spring-damper model could not accurately replicate measured TA profiles, while maintaining an accurate GRF. Errors of modelled TA and GRF profiles were too large to satisfy the accuracy requirements for both curves simultaneously. Therefore, it was concluded that the two mass-spring-damper model cannot be used to accurately reproduce measured TA and GRF profiles using a single set of model parameters.

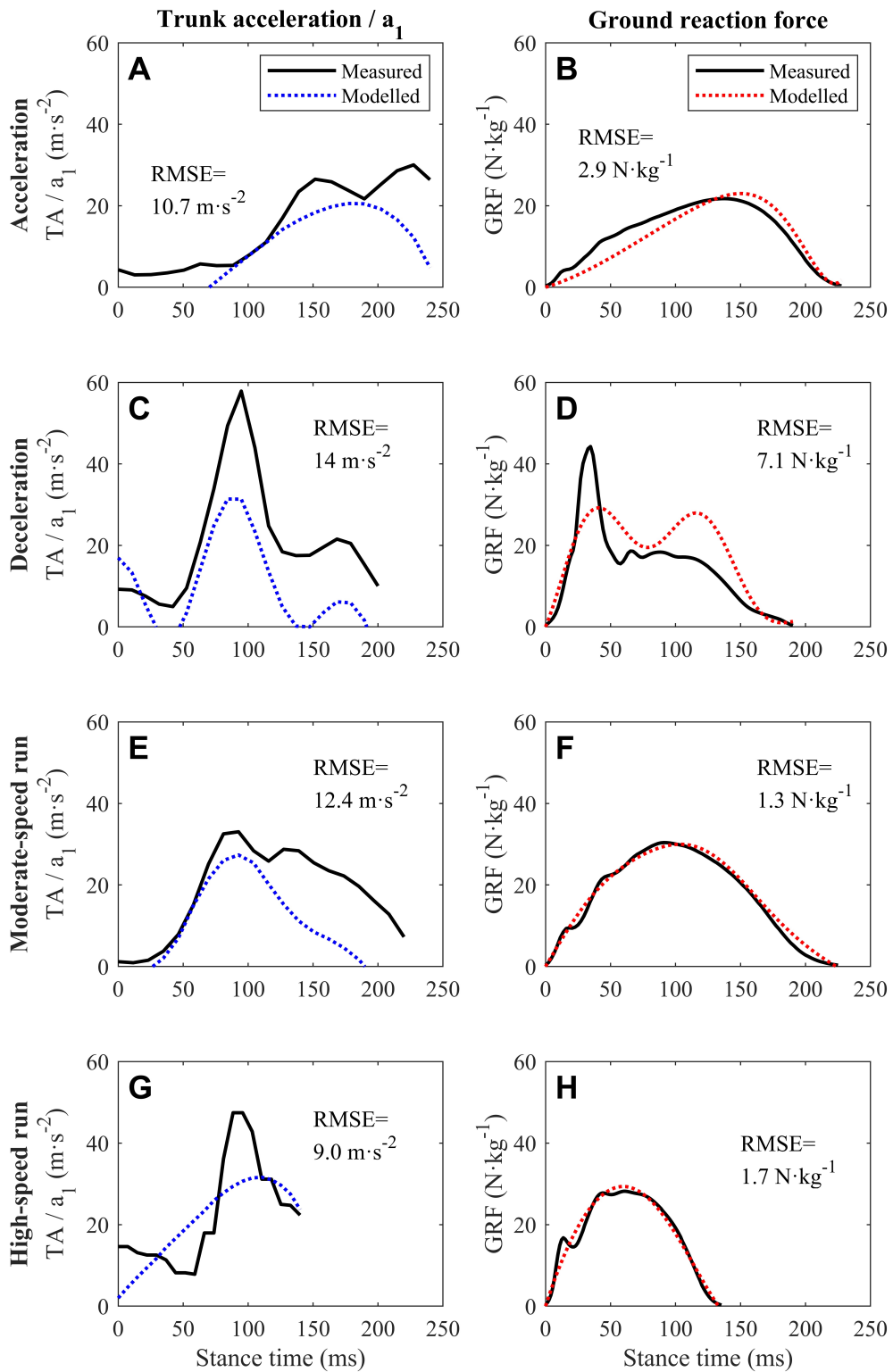


**Figure F.2** Representative examples of measured trunk accelerations (TA; black solid line) and modelled  $a_1$  (blue dotted line) on the left, and the measured ground reaction force (GRF; black solid line) and predicted GRF (red dotted line) on the right, when simultaneously modelled. Across the different tasks TA and GRF could not both be reproduced well at the same time, using the same set of model parameters.

---

## Appendix G: Marker attachment locations

---

Full-body kinematic data in chapter 5 were collected using a seventy-six retro-reflective marker set attached to anatomical landmarks of the body. The aim of this appendix is to clarify the attachment locations of segment defining and segment tracking markers (figure G.1). Markers for segment definition (of which some were also used for segment tracking; see figure G.1) were attached to the Calcaneus, lateral Calcaneus, first and fifth Metatarsus head, lateral/medial Malleolus, lateral/medial Epicondyle of the Femur, Femur greater Trochanter, anterior/posterior Superior Iliac Spine, Iliac Crest, Acromion, anterior/posterior head, shoulder, lateral/medial Epicondyle of the Humerus, Styloid process of the Radius and Ulna, lateral/medial Metacarpal head (all left and right), Cervical vertebrae 7, Thoracic vertebrae 8, and the Jugular notch and Xiphoid process of the Sternum. In addition, marker clusters for segment tracking were attached to the lateral sides of the shanks and thighs (four markers per cluster), as well as the forearms and upper arms (three markers per cluster).

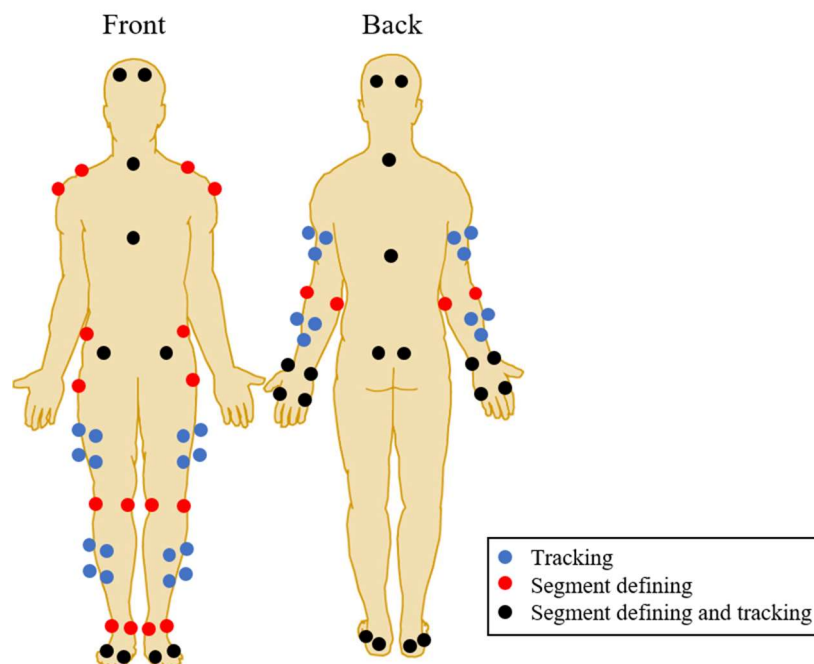


**Figure G.1** Attachment locations of segment tracking markers (blue), segment defining markers (red) and markers used for both (black).

---

## Appendix H: Marker trajectory filter cut-off frequencies

---

### *H.1 Objective*

Segmental accelerations used to estimate ground reaction forces (GRFs) in chapter 5 were derived from motion capture-based marker trajectories. Accuracy of estimated GRF profiles is thus dependent on marker trajectory processing before calculating the segmental centre of mass (CoM) accelerations. The aim of this appendix was, therefore, to investigate what filter cut-off frequency lead to the most accurate GRF estimates.

### *H.2 Methods*

Kinematic and kinetic data for ten participants (7 males and 3 females, age  $24 \pm 5$  yrs, height  $176 \pm 8$  cm, mass  $72 \pm 9$  kg) was used (see the methods section of chapter 5 for more detail on the data collection and processing). Marker trajectories were filtered with a 2<sup>nd</sup> order Butterworth low-pass filter using four different cut-off frequencies (25 Hz, 20 Hz, 15 Hz and 10 Hz), while force data were filtered at 50 Hz. Visual screening of the data revealed relatively large trunk marker vibrations compared to the other markers, which was likely due to marker attachment to the shirt rather than the skin. Therefore, combinations of filter cut-off frequencies (20-15 Hz, 20-10 Hz and 15-10 Hz) were also examined, i.e. markers defining the trunk segment were filtered at a lower cut-off frequency than the other markers. Trunk defining markers that were filtered at a lower cut-off frequency were those attached to the left and right Iliac Crest and Acromion, Cervical vertebrae 7, Thoracic vertebrae 8, and the Jugular notch and Xiphoid process of the Sternum.

### *H.3 Results*

Estimated GRF errors typically decreased for lower cut-off frequencies (table H.1). For higher frequencies (25 Hz, 20 Hz) the estimated GRF profiles included more oscillations compared to the lower cut-off frequencies (15 Hz, 10 Hz) (figure H.1). Consequently, RMSEs were lower across all tasks when marker data were filtered at 15 Hz, compared to 25 and 20 Hz. However, only for accelerations and constant speed running, errors were further reduced when a 10 Hz filter was applied, while over-smoothing of estimated GRF profiles resulted in the loss of

important GRF characteristics (e.g. impact peak) for the other tasks (figure H.1 C, D, E). When a combination of two cut-off frequencies (20-15, 20-10 and 15-10 Hz) was used, however, RMSE values were further reduced. For most tasks separately, as well as all trials combined, a combination where the trunk was filtered at 10 Hz resulted in the most accurate GRF estimates (table H.1; figure H.1).

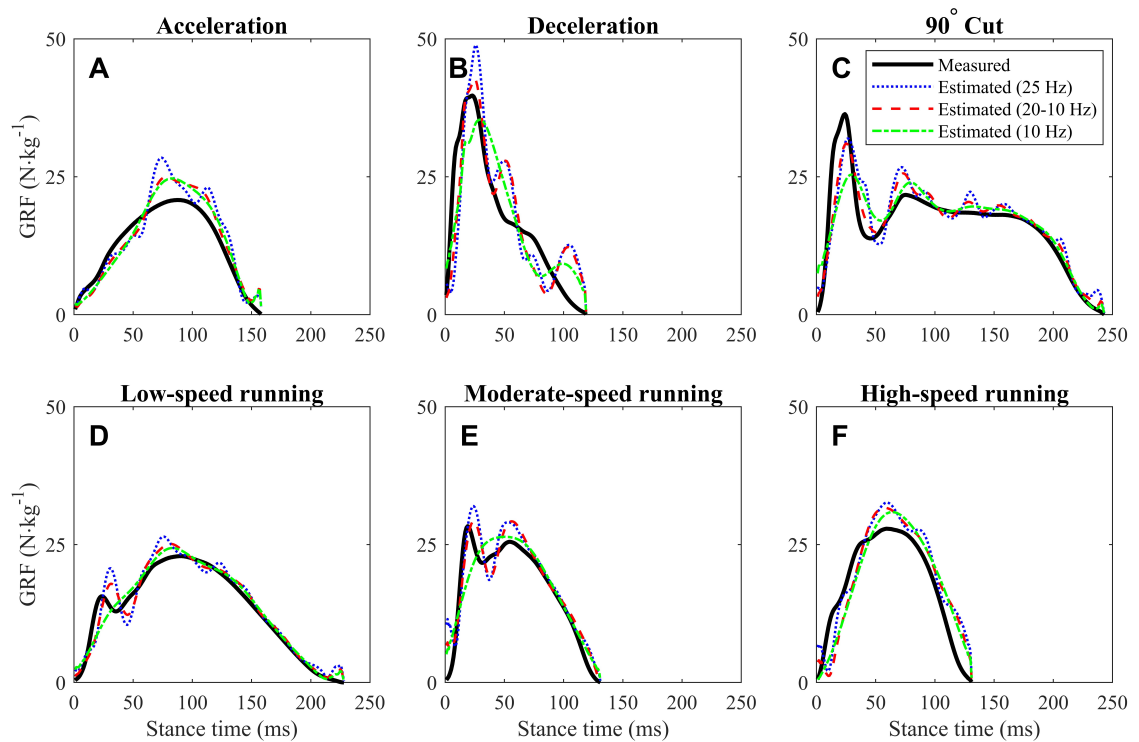


**Figure H.1** Representative examples of measured ground reaction force (GRF; black solid line) profiles and GRF estimated from marker trajectories filtered at 25 Hz (blue dotted line), 20-10 Hz (red dashed line) or 10 Hz (green dashed line), for each task.

<b>Table H.1</b> Marker trajectory filter cut-off frequency comparison							
	25 Hz	20 Hz	20-15 Hz	20-10 Hz	15 Hz	15-10 Hz	10 Hz
Accelerations	3.7±1	3.4±0.9	3.1±0.8	2.8±0.7	3±0.8	2.6±0.6	2.4±0.6
Decelerations	7.7±2.4	7.4±2.3	6.8±2	6±1.8	7.3±2.2	6.4±1.9	8±2.5
90° Cuts	3.4±0.8	3.2±0.8	3±0.7	2.7±0.7	3.1±0.8	2.8±0.7	3.4±0.9
Constant speed running							
Low (2-3 m·s <sup>-1</sup> )	2.3±0.6	2.1±0.6	1.9±0.5	1.7±0.4	1.9±0.5	1.6±0.4	1.7±0.5
Moderate (4-5 m·s <sup>-1</sup> )	3.3±0.9	3.1±0.8	2.9±0.7	2.6±0.6	3±0.8	2.6±0.6	2.9±0.7
High (>6 m·s <sup>-1</sup> )	5.4±1.3	5.1±1.3	4.8±1.2	4.4±1	4.9±1.2	4.4±1	4.7±1.3
All tasks	4.3±2.2	4.1±2.1	3.8±2	3.4±1.7	3.9±2.2	3.4±1.9	3.9±2.5

Root mean square errors (RMSE) for each (combination of) filter cut-off frequencies. Values are means ± standard deviation per task, as well as all tasks combined. The best cut-off frequency per task is highlighted in green shading.

#### H.4 Conclusions

Estimated GRF profiles were more accurate across tasks when a combination of different cut-off frequencies was used for different markers. More specifically, the best results were obtained when marker trajectories were filtered at a 20 Hz cut-off frequency, with trunk defining markers filtered at 10 Hz. These cut-off frequencies were, therefore, used to filter marker trajectory data before further processing.

---

## **Appendix I: Measuring segmental accelerations: motion capture vs. accelerometers**

---

### *I.1 Objective*

Accurately estimating ground reaction forces (GRFs) from segmental accelerations as described in chapter 5, requires measured accelerations to correctly represent the actual segmental centre of mass (CoM) acceleration. If not, estimated GRF profiles will differ from the real GRF, with higher errors as acceleration inaccuracies increase. Therefore, the aim of this appendix was to investigate how well segmental acceleration signals measured with body-worn accelerometers can represent the actual segmental CoM accelerations.

### *I.2 Methods*

Segmental accelerations measured with body-worn accelerometers were compared to ‘gold-standard’ segmental accelerations derived from marker trajectory data, for a single participant (male, age 22 yrs, height 183 cm, mass 70.7 kg). Five tri-axial wireless accelerometers (DTS 3D accelerometer 518, 5.7 g, L:19 mm, W:14.2 mm, H:6.3 mm, Noraxon Inc, Scottsdale, AZ, USA) sampling at 500 Hz, were attached to the medial side of both shanks and thighs, and the back of the pelvis (figure I.1). Accelerometry and marker trajectory data were synchronously recorded using Qualisys Track Manager Software (QTM version 2.16, Qualisys Inc., Gothenberg, Sweden). Marker trajectory based resultant segmental CoM accelerations were estimated from a six-degree-of-freedom model (see the methods section of chapter 5 for more details) and compared to resultant segmental acceleration measured from accelerometers during each ground contact phase.

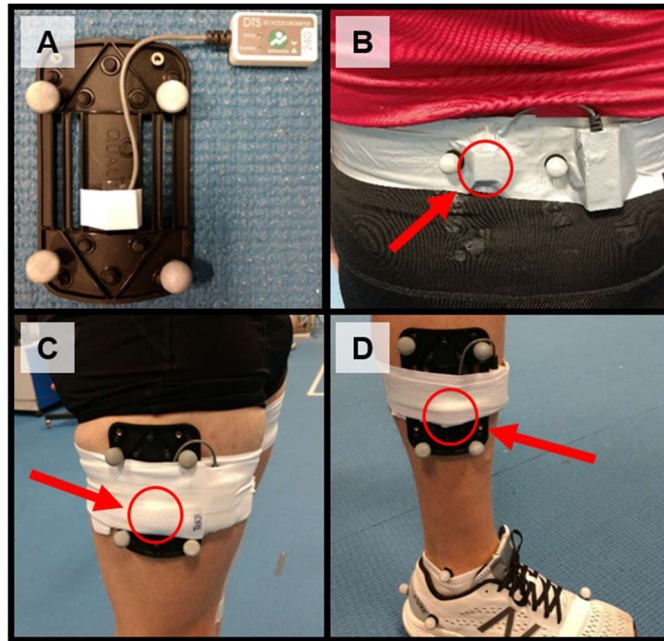


**Figure I.1** Attachment of the Noraxon DTS 3D accelerometer to the marker cluster plate (A), back of the pelvis (B), and medial side of the thigh (C) and shank (D).

### *I.3 Results*

Segmental acceleration signals of the shanks, thighs and pelvis from body-worn accelerometers, represented the general segmental acceleration profiles measured with a motion capture system (figure I.2). However, accelerometers considerably over- and underestimated the marker trajectory based segmental accelerations for all tasks. Moreover, substantial differences were found between both methods in the timing segmental acceleration peaks. Both methods were most similar for the lower intensity tasks (i.e. accelerations and running at low speeds) but deviated more for decelerations and at higher running speeds (figure I.2). In general, oscillations and segmental acceleration differences between methods were the largest for the thighs, possibly due to the relatively large muscles and associated soft-tissue artefacts.

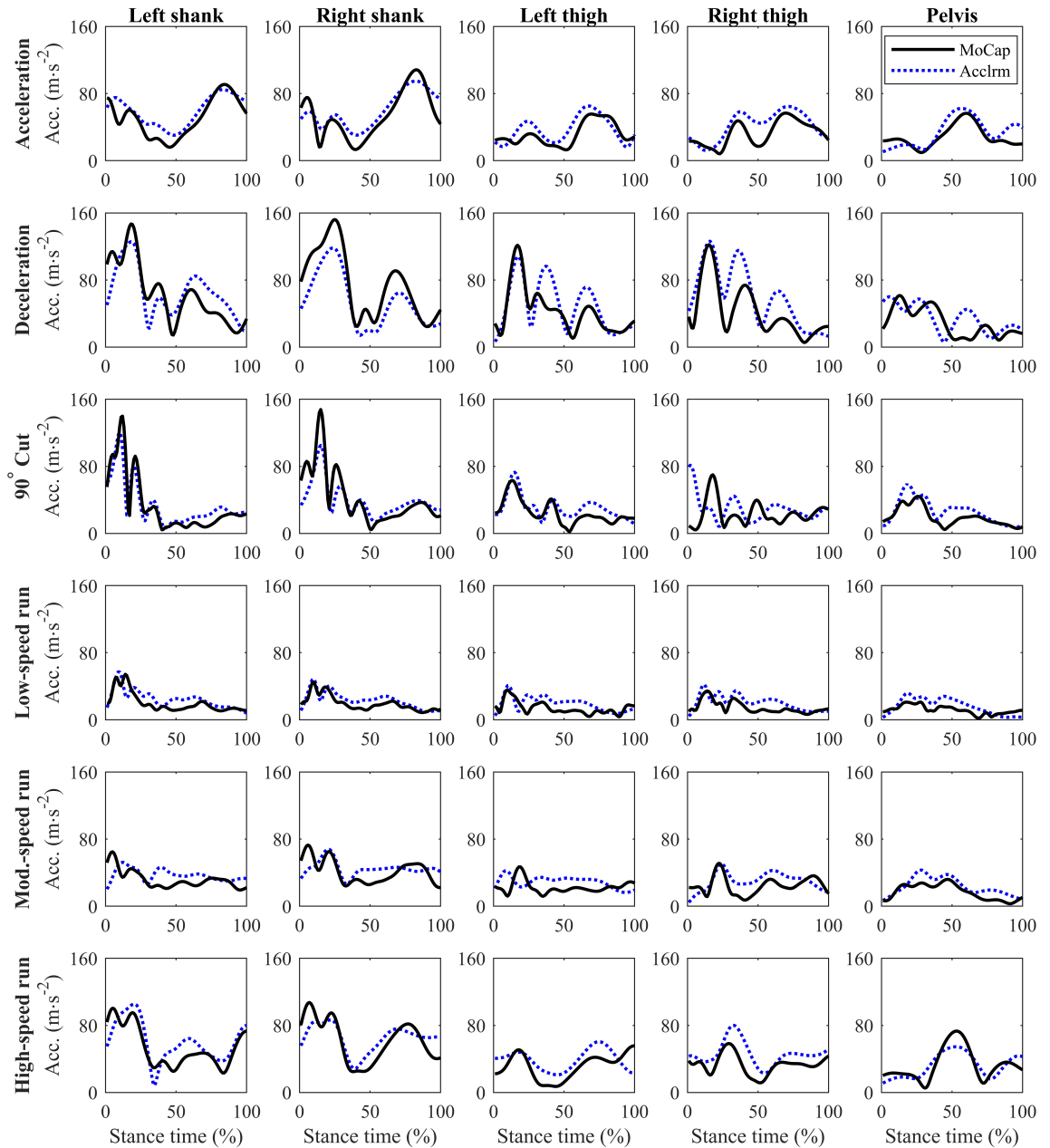


**Figure I.2** Representative examples of segmental accelerations from motion capture-based marker trajectories (MoCap; black solid line) and accelerometry (Acclrm; blue dotted line). Columns represent the segmental accelerations of the left/right shank and thigh, and pelvis, while rows represent the different tasks.

---

#### *I.4 Conclusions*

Acceleration signals from body-worn accelerometers substantially deviated from segmental CoM accelerations derived from marker trajectory data measured with a motion capture system. If segmental accelerations are used to estimate GRF as described in chapter 5, an accumulation of measurement errors for each segment is likely to lead to considerable errors in the estimated GRF profiles. Future work should, therefore, investigate whether limitations of accelerometry can be overcome (e.g. by improving unit placement) and a more accurate measurements of segment CoM accelerations from accelerometers can be achieved.

---

## Appendix J: Task specific principal component analysis

---

### *J.1 Objective*

The principal component analysis (PCA) described in chapter 6 was performed on a combination of segmental accelerations for multiple participants and tasks. However, unique segmental contributions to task-specific ground reaction force (GRF) features might not be highlighted by such a combined analysis. Therefore, this appendix aimed to examine if a task-specific PCA could reveal additional information about key segmental accelerations and associated GRF features.

### *J.2 Methods*

Data were processed, normalised and scaled as described in the methods section of chapter 6. However, participant- and task-specific acceleration matrices for each participant  $\mathbf{A}^{\text{subj,task}}$  were combined in six task-specific segmental acceleration matrices  $\mathbf{A}^{\text{task}}$ , rather than a single matrix for all tasks. The PCA was then performed on each task-specific matrix  $\mathbf{A}^{\text{task}}$ , and further processed and analysed as described in the methods section of chapter 6.

### *J.3 Results*

Similar to the combined PCA, the first principal component (PC) from task-specific PCAs primarily explained the majority of the overall GRF impulse for all the different tasks, while the second principal GRF (PGRF) contained clear impact peak features for decelerations, 90° cuts and running at low and moderate speeds (figure J.1). For accelerations and high-speed running tasks however, high-frequency GRF (and segmental accelerations) characteristics associated with the impacts of landing were primarily explained by PC<sub>3</sub>, emphasising the relatively smaller importance of impact features in these tasks. Furthermore, across tasks PC<sub>4</sub> and PC<sub>5</sub> mainly explained minor contributions to the impact features of the GRF profile during the first half of stance.

When higher PCs were included (i.e.  $k > 5$ ), summed PGRF errors steadily and consistently decreased (figure J.2). As for the combined PCA, these PCs contained relatively constant PAs

---

of the arm and leg segments throughout the stance phase and primarily increased the overall magnitude of the summed PGRF, rather than influence specific GRF features. For accelerations and high-speed running however, errors decreased more rapidly for a task-specific PCA, when the number of PCs was increased. This discrepancy was likely the result of the more profound arm-swing in these tasks, which could be explained better by the first few PCs of a task-specific PCA. To achieve mean summed PGRF errors within 10% of the mean RMSE for GRF from all 45 PCs (i.e. the original data), a total of 4 (accelerations), 2 (decelerations), 15 (90° cuts), 3 (low-speed running), 5 (moderate-speed running) and 4 (high-speed running) PCs were required respectively, which was slightly lower compared to the combined PCA for all tasks except 90° cuts (no change).

#### *J.4 Conclusions*

The relative importance of landing associated GRF features and errors for summed PGRF profiles were slightly different for acceleration tasks and high-speed running, when task-specific PCAs was used. However, differences were small and overall results from task-specific PCAs were highly comparable to the outcomes of the PCA for all tasks combined, as described in chapter 6. Therefore, although subtle differences between tasks can be highlighted using task-specific PCA analyses, a combined PCA was deemed acceptable for the purposes of chapter 6.

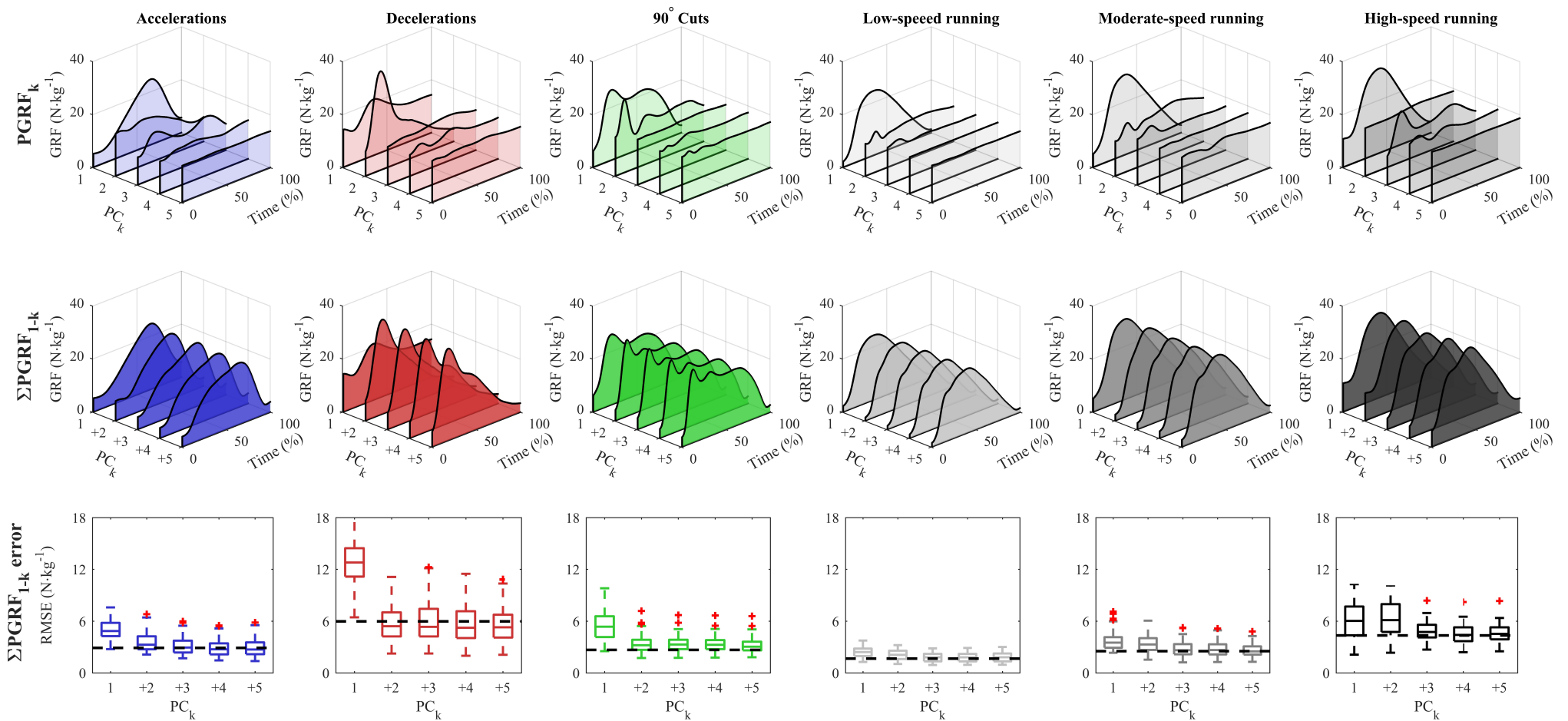


**Figure J.1** Mean principal ground reaction forces (PGRFs) calculated from the first five principal components (PCs), for each task. PGRFs were calculated from principal accelerations (PAs) reconstructed from either the  $k^{\text{th}}$  PC (top row), or the sum of the first  $k$  PCs ( $\Sigma\text{PGRF}_{1-k}$ ; middle row). Root mean square errors (RMSE; bottom row) are mean errors for the  $\Sigma\text{PGRF}$  profiles and the horizontal black line represents the RMSE for  $\Sigma\text{PGRFs}$  from all 45 PCs (i.e. the original data).

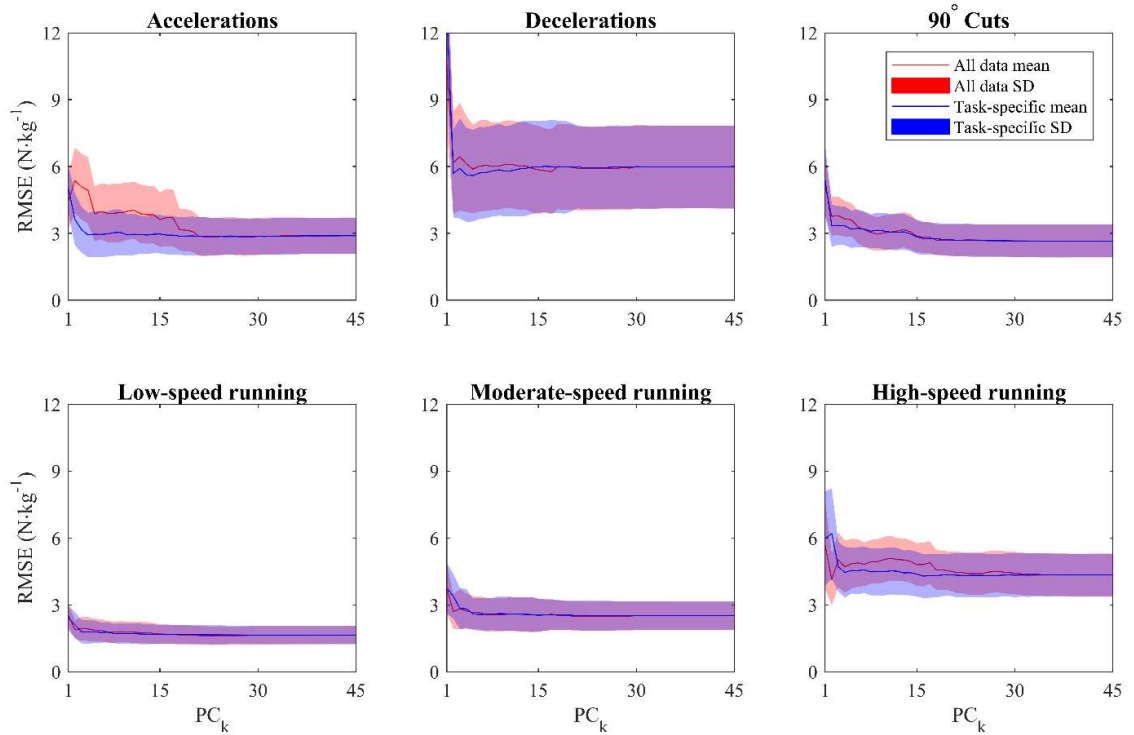


**Figure J.2** Root mean square error (RMSE) values for ground reaction forces (GRFs) reconstructed from  $k$  summed principal components ( $\text{PC}_k$ ). Mean and standard deviations (SD) of RMSEs for summed principal GRFs were compared between the task-specific (blue solid line and shaded area) principal component analysis (PCA) or a PCA on all data combined (red solid line and shaded area).

---

## References

---

- 
- Abrams, G.D., Harris, A.H.S., Andriacchi, T.P., Safran, M.R., 2014. Biomechanical analysis of three tennis serve types using a markerless system. *Br. J. Sports Med.* 48, 339–342. doi:10.1136/bjsports-2012-091371
- Adams, D., Pozzi, F., Carroll, A., Rombach, A., Zeni, J., 2016. Validity and Reliability of a Commercial Fitness Watch for Measuring Running Dynamics. *J. Orthop. Sport. Phys. Ther.* 46, 471–476. doi:10.2519/jospt.2016.6391
- Ahmadi, A., Rowlands, D., James, D.A., 2009. Towards a wearable device for skill assessment and skill acquisition of a tennis player during the first serve. *Sport. Technol.* 2, 129–136. doi:10.1002/jst.112
- Akenhead, R., French, D., Thompson, K.G., Hayes, P.R., 2014. The acceleration dependent validity and reliability of 10Hz GPS. *J. Sci. Med. Sport* 17, 562–566. doi:10.1016/j.jsams.2013.08.005
- Akenhead, R., Hayes, P.R., Thompson, K.G., French, D., 2013. Diminutions of acceleration and deceleration output during professional football match play. *J. Sci. Med. Sport* 16, 556–561. doi:10.1016/j.jsams.2012.12.005
- Akenhead, R., Marques, J.B., Paul, D.J., 2017. Accelerometer load: a new way to measure fatigue during repeated sprint training? *Sci. Med. Footb.* 1, 151–156. doi:10.1080/24733938.2017.1330550
- Akenhead, R., Nassis, G.P., 2016. Training load and player monitoring in high-level football: Current practice and perceptions. *Int. J. Sports Physiol. Perform.* 11, 587–593. doi:10.1123/ijsp.2015-0331
- Akubat, I., Barrett, S., Abt, G., 2013. Integrating the internal and external training load in soccer. *Int. J. Sports Physiol. Perform.* 9, 457–462. doi:10.1123/ijsp.2012-0347
- Alderson, J., 2015. A markerless motion capture technique for sport performance analysis and injury prevention: Toward a ‘big data’, machine learning future. *J. Sci. Med. Sport* 19S, e79. doi:10.1016/j.jsams.2015.12.192
- Alexander, R.M., Bennett, M.B., Ker, R.F., 1986. Mechanical properties and function of the paw pads of some mammals. *J. Zool.* 209, 405–419.
- Almeida, M.O., Davis, I.S., Lopes, A.D., 2015. Biomechanical Differences of Foot Strike Patterns During Running: A Systematic Review With Meta-Analysis. *J. Orthop. Sports Phys. Ther.* 45, 738–755. doi:10.2519/jospt.2015.6019
- Amar, J., 1920. *The Human Motor*. George Routledge and Sons, Ltd., London.
- Amft, O., 2017. Smart Eyeglasses, e-Textiles, and the Future of Wearable Computing. *Adv. Sci. Technol.* 100, 141–150. doi:10.4028/www.scientific.net/AST.100.141
- Arampatzis, A., Brüggemann, G.-P., Metzler, V., 1999. The effect of speed on leg stiffness and joint kinetics in human running. *J. Biomech.* 32, 1349–1353.
- Ardern, C.L., Glasgow, P., Schneiders, A., Witvrouw, E., Clarsen, B., Cools, A., Gojanovic, B., Griffin, S., Khan, K.M., Moksnes, H., Mutch, S.A., Phillips, N., Reurink, G., Sadler, R., Silbernagel, K.G., Thorborg, K., Wangensteen, A., Wilk, K.E., Bizzini, M., 2016. 2016 Consensus statement on return to sport from the First World Congress in Sports Physical Therapy, Bern. *Br. J. Sports Med.* 50, 853–864. doi:10.1136/bjsports-2016-096278
- Balsalobre-Fernández, C., Tejero-González, C.M., del Campo-Vecino, J., Bavaresco, N., 2014. The Concurrent Validity and Reliability of a Low-Cost, High-Speed Camera-Based Method for Measuring the Flight Time of Vertical Jumps. *J. Strength Cond. Res.* 28, 528–533.
- Bangsbo, J., Mohr, M., Krstrup, P., 2006. Physical and metabolic demands of training and

- 
- match-play. *J. Sport. Sci.* El Reilly Thomas 24, 665–674. doi:10.1080/02640410500482529
- Banister, E.W., Calvert, I.W., Savage, M.V., Bach, I.M., 1975. A system model of training for athletic performance. *Aust. J. Sport. Med.* 7, 75–61.
- Barrett, S., Midgley, A., Lovell, R., 2014. PlayerLoad™: Reliability, convergent validity, and influence of unit position during treadmill running. *Int. J. Sports Physiol. Perform.* 9, 945–952. doi:10.1123/ijsp.2013-0418
- Barrett, S., Midgley, A., Reeves, M., Joel, T., Franklin, E., Heyworth, R., Garrett, A., Lovell, R., 2016. The within-match patterns of locomotor efficiency during professional soccer match play: Implications for injury risk? *J. Sci. Med. Sport* 19, 810–815. doi:10.1016/j.jsams.2015.12.514
- Barrett, S., Midgley, A.W., Towson, C., Garrett, A., Portas, M., Lovell, R., 2015. Within-match playerload patterns during a simulated soccer match: potential implications for unit positioning and fatigue management. *Int. J. Sports Physiol. Perform.* 10, 135–140.
- Bazuelo-Ruiz, B., Durá-Gil, J. V., Palomares, N., Medina, E., Llana-Belloch, S., 2018. Effect of fatigue and gender on kinematics and ground reaction forces variables in recreational runners. *PeerJ* 6, e4489. doi:10.7717/peerj.4489
- Beanland, E., Main, L.C., Aisbett, B., Gastin, P., Netto, K., 2014. Validation of GPS and accelerometer technology in swimming. *J. Sci. Med. Sport* 17, 234–238. doi:10.1016/j.jsams.2013.04.007
- Bertelsen, M.L., Hulme, A., Petersen, J., Brund, R.K., Sørensen, H., Finch, C.F., Parner, E.T., Nielsen, R.O., 2017. A framework for the etiology of running-related injuries. *Scand. J. Med. Sci. Sport.* 27, 1170–1180. doi:10.1111/sms.12883
- Bezodis, N.E., North, J.S., Razavet, J.L., 2017. Alterations to the orientation of the ground reaction force vector affect sprint acceleration performance in team sports athletes. *J. Sports Sci.* 35, 1817–1824. doi:10.1080/02640414.2016.1239024
- Blair, S., Duthie, G., Robertson, S., Hopkins, W., Ball, K., 2018. Concurrent validation of an inertial measurement system to quantify kicking biomechanics in four football codes. *J. Biomech.* 73, 24–32. doi:10.1016/j.jbiomech.2018.03.031
- Blanch, P., Gabbett, T.J., 2016. Has the athlete trained enough to return to play safely? The acute:chronic workload ratio permits clinicians to quantify a player's risk of subsequent injury. *Br. J. Sports Med.* 50, 471–475. doi:10.1136/bjsports-2015-095445
- Bland, J.M., Altman, D.G., 2010. Statistical methods for assessing agreement between two methods of clinical measurement. *Int. J. Nurs. Stud.* 47, 931–936. doi:10.1016/j.ijnurstu.2009.10.001
- Blickhan, R., 1989. The Spring-Mass model for running and hopping. *J. Biomech.* 22, 1217–1227.
- Bloomfield, J., Polman, R., O'Donoghue, P., 2007. Physical demands of different positions in FA Premier League soccer. *J. Sport. Sci. Med.* 6, 63–70.
- Bobbert, M.F., Schamhardt, H.C., Nigg, B.M., 1991. Calculation of vertical ground reaction force estimates during running from positional data. *J. Biomech.* 24, 1095–1105. doi:10.1016/0021-9290(91)90002-5
- Bobbert, M.F., Yeadon, M.R., Nigg, B.M., 1992. Mechanical analysis of the landing phase in heel-toe running. *J. Biomech.* 25, 223–234. doi:10.1016/0021-9290(92)90022-S
- Bohm, S., Mersmann, F., Arampatzis, A., 2015. Human tendon adaptation in response to mechanical loading: a systematic review and meta-analysis of exercise intervention studies

---

on healthy adults. *Sport. Med. - Open* 1, 7. doi:10.1186/s40798-015-0009-9

- Bompa, T.O., Buzzichelli, C., 2019. *Periodization: Theory and Methodology of Training*, 6th ed. Human Kinetics.
- Bourdon, P.C., Cardinale, M., Murray, A., Gastin, P., Kellmann, M., Varley, M.C., Gabbett, T.J., Coutts, A.J., Burgess, D.J., Gregson, W., Cable, N.T., 2017. Monitoring Athlete Training Loads: Consensus Statement. *Int. J. Sport. Physiol. Performance* 12, S2-161-S2-170. doi:10.1123/IJSPP.2017-0208
- Bouten, C. V., Westerterp, K.R., Verduin, M., Janssen, J.D., 1994. Assessment of energy expenditure for physical activity using a triaxial accelerometer. *Med. Sci. Sports Exerc.* 26, 1516–1523.
- Boyd, L.J., Ball, K., Aughey, R.J., 2011. The reliability of minimaxX accelerometers for measuring physical activity in Australian football. *Int. J. Sports Physiol. Perform.* 6, 311–321.
- Boyer, K.A., Silvernail, J.F., Hamill, J., 2014. The Role of Running Mileage on Coordination Patterns in Running. *J. Appl. Biomech.* 30, 649–654. doi:10.1123/JAB.2013-0261
- Bradley, P.S., Sheldon, W., Wooster, B., Olsen, P., Boanas, P., Krustup, P., 2009. High-intensity running in English FA Premier League soccer matches. *J. Sports Sci.* 27, 159–168. doi:10.1080/02640410802512775
- Brandon, S.C.E., Graham, R.B., Almosnino, S., Sadler, E.M., Stevenson, J.M., Deluzio, K.J., 2013. Interpreting principal components in biomechanics: Representative extremes and single component reconstruction. *J. Electromyogr. Kinesiol.* 23, 1304–1310. doi:10.1016/j.jelekin.2013.09.010
- Bredeweg, S.W., Kluitenberg, B., Bessem, B., Buist, I., 2013. Differences in kinetic variables between injured and noninjured runners: A prospective cohort study. *J. Sci. Med. Sport* 16, 205–210. doi:10.1016/j.jsams.2012.08.002
- Buchheit, M., Gray, A., Morin, J.-B., 2015. Assessing stride variables and vertical stiffness with GPS-embedded accelerometers: preliminary insights for the monitoring of neuromuscular fatigue on the field. *J. Sport. Sci. Med.* 698–701.
- Buchheit, M., Simpson, B.M., 2017. Player-tracking technology: Half-full or half-empty glass? *Int. J. Sports Physiol. Perform.* 12, S2-35-S2-41. doi:10.1123/ijsp.2016-0499
- Bullimore, S.R., Burn, J.F., 2007. Ability of the planar spring-mass model to predict mechanical parameters in running humans. *J. Theor. Biol.* 248, 686–695. doi:10.1016/j.jtbi.2007.06.004
- Burgess, D.J., 2017. The research doesn't always apply: Practical solutions to evidence-based training-load monitoring in elite team sports. *Int. J. Sports Physiol. Perform.* 12, 136–141. doi:10.1123/ijsp.2016-0608
- Busso, T., 2003. Variable dose-response relationship between exercise training and performance. *Med. Sci. Sports Exerc.* 35, 1188–1195. doi:10.1249/01.MSS.0000074465.13621.37
- Calvert, T.W., Banister, E.W., Savage, M. V., Bach, T., 1976. A Systems Model of the Effects of Training on Physical Performance. *IEEE Trans. Syst. Man Cybern.* SMC-6, 94–102. doi:10.1109/TSMC.1976.5409179
- Camomilla, V., Bergamini, E., Fantozzi, S., Vannozzi, G., 2018. Trends Supporting the In-Field Use of Wearable Inertial Sensors for Sport Performance Evaluation: A Systematic Review. *Sensors* 18, 873. doi:10.3390/s18030873
- Camomilla, V., Dumas, R., Cappozzo, A., 2017. Human movement analysis: The soft tissue

- 
- artefact issue. *J. Biomech.* 62, 1–4. doi:10.1016/j.jbiomech.2017.09.001
- Cardinale, M., Varley, M.C., 2017. Wearable Training-Monitoring Technology: Applications, Challenges, and Opportunities. *Int. J. Sports Physiol. Perform.* 12, 55–62.
- Casamichana, D., Castellano, J., Calleja-Gonzalez, J., San Roman, J., Castagna, C., 2013. Relationship Between Indicators of Training Load in Soccer Players. *J. Strength Cond. Res.* 27, 369–374. doi:10.1519/JSC.0b013e3182610b7d
- Catherwood, P.A., Finlay, D.D., McLaughlin, J.A.D., 2015. Subcutaneous body area networks: A SWOT analysis. 2015 IEEE Int. Symp. Technol. Soc. 1–8. doi:10.1109/ISTAS.2015.7439414
- Cavagna, G.A., 2006. The landing-take-off asymmetry in human running. *J. Exp. Biol.* 209, 4051–60. doi:10.1242/jeb.02344
- Cavagna, G.A., Saibene, F.P., Margaria, R., 1964. Mechanical work in running. *J. Appl. Physiol.* 19, 249–256.
- Cavagna, G.A., Saibene, F.P., Margaria, R., 1961. A three-directional accelerometer for analyzing body movements. *J. Appl. Physiol.* 16, 191.
- Cavanagh, P.R., Lafortune, M.A., 1980. Ground reaction forces in distance running. *J. Biomech.* 13, 397–406. doi:10.1016/0021-9290(80)90033-0
- Chambers, R., Gabbett, T.J., Cole, M.H., Beard, A., 2015. The Use of Wearable Microsensors to Quantify Sport-Specific Movements. *Sport. Med.* 45, 1065–1081. doi:10.1007/s40279-015-0332-9
- Christina, K.A., White, S.C., Gilchrist, L.A., 2001. Effect of localized muscle fatigue on vertical ground reaction forces and ankle joint motion during running. *Hum. Mov. Sci.* 20, 257–276. doi:10.1016/S0167-9457(01)00048-3
- Clansey, A.C., Hanlon, M., Wallace, E.S., Nevill, A., Lake, M.J., 2014. Influence of Tibial shock feedback training on impact loading and running economy. *Med. Sci. Sports Exerc.* 46, 973–981. doi:10.1249/MSS.0000000000000182
- Clark, K.P., Ryan, L.J., Weyand, P.G., 2017. A general relationship links gait mechanics and running ground reaction forces. *J. Exp. Biol.* 220, 247–258. doi:10.1242/jeb.138057
- Clark, K.P., Ryan, L.J., Weyand, P.G., 2014. Foot speed, foot-strike and footwear: linking gait mechanics and running ground reaction forces. *J. Exp. Biol.* 217, 2037–2040. doi:10.1242/jeb.099523
- Clark, K.P., Weyand, P.G., 2014. Are running speeds maximized with simple-spring stance mechanics? *J. Appl. Physiol.* 117, 604–615. doi:10.1152/jappphysiol.00174.2014
- Clement, D.B., Taunton, J.E., 1981. A guide to the prevention of running injuries. *Aust. Fam. Physician* 10, 156–161.
- Colby, M.J., Dawson, B., Heasman, J., Rogalski, B., Gabbett, T.J., 2014. Accelerometer and GPS-Derived Running Loads and Injury Risk in Elite Australian Footballers. *J. Strength Cond. Res.* 28, 2244–2252.
- Connaghan, D., Kelly, P., O'Connor, N.E., Gaffney, M., Walsh, M., O'Mathuna, C., 2011. Multi-sensor classification of tennis strokes. *Proc. IEEE Sensors* 1437–1440. doi:10.1109/ICSENS.2011.6127084
- Corazza, S., Mündermann, L., Chaudhari, A.M., Demattio, T., Cobelli, C., Andriacchi, T.P., 2006. A markerless motion capture system to study musculoskeletal biomechanics: Visual hull and simulated annealing approach. *Ann. Biomed. Eng.* 34, 1019–1029. doi:10.1007/s10439-006-9122-8

- 
- Coutts, A.J., Duffield, R., 2010. Validity and reliability of GPS devices for measuring movement demands of team sports. *J. Sci. Med. Sport* 13, 133–135. doi:10.1016/j.jsams.2008.09.015
- Cummins, C., Orr, R., O'Connor, H., West, C., 2013. Global positioning systems (GPS) and microtechnology sensors in team sports: A systematic review. *Sport. Med.* 43, 1025–1042. doi:10.1007/s40279-013-0069-2
- Daffertshofer, A., Lamoth, C.J.C.C., Meijer, O.G., Beek, P.J., 2004. PCA in studying coordination and variability: A tutorial. *Clin. Biomech.* 19, 415–428. doi:10.1016/j.clinbiomech.2004.01.005
- Dalen, T., Jørgen, I., Gertjan, E., Havard, H.G., Ulrik, W., 2016. Player load, Acceleration, and Deceleration during 45 Competitive Matches of Elite Soccer. *J. Strength Cond. Res.* 30, 351–359.
- Dalleau, G., Belli, A., Bourdin, M., Lacour, J.-R., 1998. The spring-mass model and the energy cost of treadmill running. *Eur. J. Appl. Physiol.* 77, 257–263. doi:10.1007/s004210050330
- Damsgaard, M., Rasmussen, J., Christensen, S.T., Surma, E., de Zee, M., 2006. Analysis of musculoskeletal systems in the AnyBody Modeling System. *Simul. Model. Pract. Theory* 14, 1100–1111. doi:10.1016/j.simpat.2006.09.001
- Daniels, J.T., Yarbrough, R.A., Foster, C., 1978. Changes in VO<sub>2</sub> max and Running Performance with Training. *Eur. J. Appl. Physiol.* 39, 249–254.
- Datson, N., Drust, B., Weston, M., Gregson, W., 2018. Repeated high-speed running in elite female soccer players during international competition. *Sci. Med. Footb.* 1–7. doi:10.1080/24733938.2018.1508880
- Davis, I.S., Bowser, B.J., Mullineaux, D.R., 2016. Greater vertical impact loading in female runners with medically diagnosed injuries: A prospective investigation. *Br. J. Sports Med.* 50, 887–892. doi:10.1136/bjsports-2015-094579
- Degache, F., Morin, J., Oehen, L., Guex, K., Giardini, G., Schena, F., Millet, G.Y., Millet, G.P., 2016. Running Mechanics During the World's Most Challenging Mountain Ultramarathon. *Int. J. Sports Physiol. Perform.* 11, 608–614.
- Dellaserra, C.L., Gao, Y., Ransdell, L., 2014. Use of integrated technology in team sports: a review of opportunities, challenges, and future directions for athletes. *J. Strength Cond. Res.* 28, 556–573. doi:10.1519/JSC.0b013e3182a952fb
- Delp, S.L., Anderson, F.C., Arnold, A.S., Loan, P., Habib, A., John, C.T., Guendelman, E., Thelen, D.G., 2007. OpenSim: Open-Source Software to Create and Analyze Dynamic Simulations of Movement. *IEEE Trans. Biomed. Eng.* 54, 1940–1950.
- Deluzio, K.J., Wyss, U.P., Zee, B., Costigan, P.A., Sorbie, C., 1997. Principal component models of knee kinematics and kinetics: Normal vs. pathological gait patterns. *Hum. Mov. Sci.* 16, 201–217. doi:10.1016/S0167-9457(96)00051-6
- Dempster, W.T., 1955. Space requirements of the seated operator: Geometrical, Kinematic, and Mechanical Aspects of the Body With Special Reference to the Limbs. WADC Tech. Rep. 55–159.
- Derrick, T.R., Caldwell, G.E., Hamill, J., 2000. Modeling the stiffness characteristics of the human body while running with various stride lengths. *J. Appl. Biomech.* 16, 36–51.
- Di Salvo, V., Gregson, W., Atkinson, G., Tordoff, P., Drust, B., 2009. Analysis of high intensity activity in premier league soccer. *Int. J. Sports Med.* 30, 205–212. doi:10.1055/s-0028-1105950
- Dickinson, J.A., Cook, S.D., Leinhardt, T.M., 1985. The measurement of shock waves following heel strike while running. *J. Biomech.* 18, 415–422. doi:10.1016/0021-9290(85)90276-3

- 
- Doshi-Velez, F., Kim, B., 2017. Towards A Rigorous Science of Interpretable Machine Learning. ArXiv Prepr. 1702.08608.
- Drew, M.K., Finch, C.F., 2016. The Relationship Between Training Load and Injury, Illness and Soreness: A Systematic and Literature Review. *Sport. Med.* doi:10.1007/s40279-015-0459-8
- Duffey, M.J., Martin, D.F., Cannon, D.W., Craven, T., Messier, S.P., 2000. Etiologic factors associated with anterior knee pain in distance runners. *Med. Sci. Sport. Exerc.* 32, 1825–1832. doi:10.1097/00005768-200011000-00003
- Duhig, S., Shield, A.J., Opar, D., Gabbett, T.J., Ferguson, C., Williams, M., 2016. Effect of high-speed running on hamstring strain injury risk. *Br. J. Sports Med.* 50, 1536–1540. doi:10.1136/bjsports-2015-095679
- Düking, P., Hotho, A., Holmberg, H.C., Fuss, F.K., Sperlich, B., 2016. Comparison of non-invasive individual monitoring of the training and health of athletes with commercially available wearable technologies. *Front. Physiol.* 7. doi:10.3389/fphys.2016.00071
- Dutto, D.J., Smith, G. a, 2002. Changes in spring-mass characteristics during treadmill running to exhaustion. *Med. Sci. Sport. Exerc.* 34, 1324–1331.
- Eckard, T.G., Padua, D.A., Hearn, D.W., Pexa, B.S., Frank, B.S., 2018. The Relationship Between Training Load and Injury in Athletes: A Systematic Review, *Sports Medicine*. Springer International Publishing. doi:10.1007/s40279-018-0951-z
- Edwards, S., White, S., Humphreys, S., Robergs, R., O’Dwyer, N., 2018. Caution using data from triaxial accelerometers housed in player tracking units during running. *J. Sports Sci.* 1–9. doi:10.1080/02640414.2018.1527675
- Edwards, W.B., 2018. Modeling Overuse Injuries in Sport as a Mechanical Fatigue Phenomenon. *Exerc. Sport Sci. Rev.* 46, 224–231. doi:10.1249/JES.000000000000163
- Eggers, T.M., Massard, T.I., Clothier, P.J., Ric, L., 2018. Measuring Vertical Stiffness in Sport With Accelerometers: Exercise Caution! *J. Strength Cond. Res.* 32, 1919–1922.
- Ehrmann, F.E., Duncan, C.S., Sindhusake, D., Franzsen, W.N., Greene, D.A., 2016. GPS and Injury Prevention in Professional Soccer. *J. Strength Cond. Res.* 30, 360–367.
- Faber, H., Van Soest, A.J., Kistemaker, D.A., 2018. Inverse dynamics of mechanical multibody systems: An improved algorithm that ensures consistency between kinematics and external forces. *PLoS One* 13, e0204575. doi:10.1371/journal.pone.0204575
- Farley, C.T., González, O., 1996. Leg stiffness and stride frequency in human running. *J. Biomech.* 29, 181–186. doi:10.1016/0021-9290(95)00029-1
- Federolf, P.A., 2016. A novel approach to study human posture control: “Principal movements” obtained from a principal component analysis of kinematic marker data. *J. Biomech.* 49, 364–370.
- Federolf, P.A., Boyer, K.A., Andriacchi, T.P., 2013a. Application of principal component analysis in clinical gait research: Identification of systematic differences between healthy and medial knee-osteoarthritic gait. *J. Biomech.* 46, 2173–2178. doi:10.1016/j.jbiomech.2013.06.032
- Federolf, P.A., Reid, R., Gilgien, M., Haugen, P., Smith, G., 2014. The application of principal component analysis to quantify technique in sports. *Scand. J. Med. Sci. Sports* 24, 491–499. doi:10.1111/j.1600-0838.2012.01455.x
- Federolf, P.A., Roos, L., Nigg, B.M., 2013b. Analysis of the multi-segmental postural movement strategies utilized in bipedal, tandem and one-leg stance as quantified by a principal component decomposition of marker coordinates. *J. Biomech.* 46, 2626–2633.

---

doi:10.1016/j.jbiomech.2013.08.008

- Fenn, W.O., 1930. Work against gravity and work due to velocity changes in running: movements of the center of gravity within the body and foot pressure on the ground. *Am. J. Physiol.* 93, 433–462.
- Fenn, W.O., 1924. The relation between the work performed and the energy liberated in muscular contraction. *J. Physiol.* 58, 373–395.
- Ferris, D.P., Louie, M., Farley, C.T., 1998. Running in the real world: Adjusting leg stiffness for different surfaces. *Proc. R. Soc. London B* 265, 989–994. doi:10.1098/rspb.1998.0388
- Firminger, C.R., Edwards, W.B., 2016. The influence of minimalist footwear and stride length reduction on lower-extremity running mechanics and cumulative loading. *J. Sci. Med. Sport* 19, 975–979. doi:10.1016/j.jsams.2016.03.003
- Forner Cordero, A., Koopman, H.J.F.M., Van Der Helm, F.C.T., 2004. Use of pressure insoles to calculate the complete ground reaction forces. *J. Biomech.* 37, 1427–1432. doi:10.1016/j.jbiomech.2003.12.016
- Foster, C., Florhaug, J. a, Franklin, J., Gottschall, L., Hrovatin, L. a, Parker, S., Doleshal, P., Dodge, C., 2001. A new approach to monitoring exercise training. *J. strength Cond. Res.* 15, 109–115. doi:10.1519/1533-4287(2001)015<0109:ANATME>2.0.CO;2
- Foster, C., Rodriguez-Marroyo, J.A., Koning, J.J. De, 2017. Monitoring Training Loads : The Past , the Present , and the Future. *Int. Journals Sport. Physiol. Perform.* 12, S2–S8.
- Frost, H.M., 1987. Bone “mass” and the “mechanostat”: A proposal. *Anat. Rec.* 219, 1–9. doi:10.1002/ar.1092190104
- Fung, S.K., Sundaraj, K., Ahamed, N.U., Kiang, L.C., Nadarajah, S., Sahayadhas, A., Ali, A., Islam, A., Palaniappan, R., 2014. Hybrid markerless tracking of complex articulated motion in golf swings. *J. Bodyw. Mov. Ther.* 18, 220–227. doi:10.1016/j.jbmt.2013.05.011
- Gabbett, T., Jenkins, D., Abernethy, B., 2010. Physical collisions and injury during professional rugby league skills training. *J. Sci. Med. Sport* 13, 578–583. doi:10.1016/j.jsams.2010.03.007
- Gabbett, T.J., 2013. Quantifying the Physical Demands of Collision Sports. *J. Strength Cond. Res.* 27, 2319–2322. doi:10.1519/JSC.0b013e318277fd21
- Gabbett, T.J., Ullah, S., 2012. Relationship between running loads and soft-tissue injury in elite team sport athletes. *J. Strength Cond. Res.* 26, 953–960.
- Gallo, T., Cormack, S., Gabbett, T., Williams, M., Lorenzen, C., 2015. Characteristics impacting on session rating of perceived exertion training load in Australian footballers. *J. Sports Sci.* 33, 467–475. doi:10.1080/02640414.2014.947311
- Gastin, P.B., McLean, O.C., Breed, R.V., Spittle, M., 2014. Tackle and impact detection in elite Australian football using wearable microsensor technology. *J. Sports Sci.* 32, 947–953. doi:10.1080/02640414.2013.868920
- Gaudino, P., Alberti, G., Iaia, F.M., 2014. Estimated metabolic and mechanical demands during different small-sided games in elite soccer players. *Hum. Mov. Sci.* 36, 123–133. doi:10.1016/j.humov.2014.05.006
- Gaudino, P., Gaudino, C., Alberti, G., Minetti, A.E., 2013. Biomechanics and predicted energetics of sprinting on sand: Hints for soccer training. *J. Sci. Med. Sport* 16, 271–275. doi:10.1016/j.jsams.2012.07.003
- Gaudino, P., Iaia, F.M., Strudwick, A.J., Hawkins, R.D., Alberti, G., Atkinson, G., Gregson, W., 2015. Factors Influencing Perception of Effort (Session-RPE) During Elite Soccer

- 
- Training. *Int. J. Sports Physiol. Perform.* 10, 860–864. doi:10.1123/ijsp.2014-0518
- Geyer, H., Seyfarth, A., Blickhan, R., 2006. Compliant leg behaviour explains basic dynamics of walking and running. *Proc. R. Soc. B-Biological Sci.* 273, 2861–2867. doi:10.1098/rspb.2006.3637
- Gill, N., Preece, S.J., Young, S., Bramah, C., 2017. Are the arms and head required to accurately estimate centre of mass motion during running? *Gait Posture* 51, 281–283. doi:10.1016/j.gaitpost.2016.11.001
- Girard, O., Brocherie, F., Morin, J.B., Millet, G.P., 2017. Mechanical alterations during interval-training treadmill runs in high-level male team-sport players. *J. Sci. Med. Sport* 20, 87–91. doi:10.1016/j.jsams.2016.05.002
- Girard, O., Brocherie, F., Tomazin, K., Farooq, A., Morin, J.B., 2016. Changes in running mechanics over 100-m, 200-m and 400-m treadmill sprints. *J. Biomech.* 49, 1490–1497. doi:10.1016/j.jbiomech.2016.03.020
- Girard, O., Micallef, J.P., Millet, G.P., 2011. Changes in spring-mass model characteristics during repeated running sprints. *Eur. J. Appl. Physiol.* 111, 125–134. doi:10.1007/s00421-010-1638-9
- Gløersen, Ø., Myklebust, H., Hallén, J., Federolf, P.A., 2018. Technique analysis in elite athletes using principal component analysis. *J. Sports Sci.* 36, 229–237. doi:10.1080/02640414.2017.1298826
- Gottschall, J.S., Kram, R., 2005. Ground reaction forces during downhill and uphill running. *J. Biomech.* 38, 445–452. doi:10.1016/j.jbiomech.2004.04.023
- Green, M., 2018. The Relevance of Potential Indicators of External Load for Movement Evaluation in Elite Football Training.
- Grigg, J., Haakonssen, E., Rathbone, E., Orr, R., Keogh, J.W.L., 2018. The validity and intra-tester reliability of markerless motion capture to analyse kinematics of the BMX Supercross gate start. *Sport. Biomech.* 17, 383–401. doi:10.1080/14763141.2017.1353129
- Grimston, S.K., Nigg, B.M., Fisher, V., Ajemian, S. V., 1994. External loads throughout a 45 minute run in stress fracture and non-stress fracture runners. *J. Biomech.* 27, 668.
- Grimston, S.K., Nigg, B.M., Fisher, V., Ajemian, S. V., 1993. External loads throughout a 45 minute run in stress fracture and non-stress fracture runners, in: *International Society of Biomechanics XIV Congress*. p. 668.
- Gruber, A.H., Edwards, W.B., Hamill, J., Derrick, T.R., Boyer, K.A., 2017. A comparison of the ground reaction force frequency content during rearfoot and non-rearfoot running patterns. *Gait Posture*. doi:10.1016/j.gaitpost.2017.04.037
- Gruber, A.H., Edwards, W.B., Hamill, J., Derrick, T.R., Boyer, K.A., 2015. Ground Reaction Forces In Rearfoot And Forefoot Running Assessed By A Continuous Wavelet Transform. *Med. Sci. Sport. Exerc.* 47, 710.
- Guo, Y., Storm, F., Zhao, Y., Billings, S., Pavic, A., Mazzà, C., Guo, L.-Z., 2017. A New Proxy Measurement Algorithm with Application to the Estimation of Vertical Ground Reaction Forces Using Wearable Sensors. *Sensors* 17, 2181. doi:10.3390/s17102181
- Gurchiek, R.D., McGinnis, R.S., Needle, A.R., McBride, J.M., van Werkhoven, H., 2017. The use of a single inertial sensor to estimate 3-dimensional ground reaction force during accelerative running tasks. *J. Biomech.* 61, 263–268. doi:10.1016/j.jbiomech.2017.07.035
- Halabi, R., Diab, M., Badaoui, M. el, Moslem, B., Guillet, F., 2017. Vertical Ground Reaction Force Spectral Analysis for Fatigue Assessment, in: *Fourth International Conference on Advances in Biomedical Engineering*.

- 
- Halilaj, E., Rajagopal, A., Fiterau, M., Hicks, J.L., Hastie, T.J., Delp, S.L., 2018. Machine Learning in Human Movement Biomechanics: Best Practices, Common Pitfalls, and New Opportunities. *J. Biomech.* doi:10.1016/j.jbiomech.2018.09.009
- Hamill, J., Bates, B.T., Knutzen, K.M., Sawhill, J.A., 1983. Variations in ground reaction force parameters at different running speeds. *Hum. Mov. Sci.* 2, 47–56. doi:10.1016/0167-9457(83)90005-2
- Hamill, J., Derrick, T.R., Holt, K.G., 1995. Shock attenuation and stride frequency during running. *Hum. Mov. Sci.* 14, 45–60. doi:10.1016/0167-9457(95)00004-C
- Hamill, J., Gruber, A.H., 2017. Is changing footstrike pattern beneficial to runners? *J. Sport Heal. Sci.* 6, 146–153. doi:10.1016/j.jshs.2017.02.004
- Hamill, J., Gruber, A.H., Derrick, T.R., 2014. Lower extremity joint stiffness characteristics during running with different footfall patterns. *Eur. J. Sport Sci.* 14, 130–136. doi:10.1080/17461391.2012.728249
- Hamner, S.R., Delp, S.L., 2013. Muscle contributions to fore-aft and vertical body mass center accelerations over a range of running speeds. *J. Biomech.* 46, 780–787. doi:10.1016/j.jbiomech.2012.11.024
- Hamner, S.R., Seth, A., Delp, S.L., 2010. Muscle contributions to propulsion and support during running. *J. Biomech.* 43, 2709–2716. doi:10.1016/j.jbiomech.2010.06.025
- Hanavan, E.P., 1964. A mathematical model of the human body. WADC Tech. Rep. AMRL-TR-64-102, Aerosp. Med. Research Lab. Wright-Patterson Air Force Base, OH.
- Harding, J.W., Mackintosh, C.G., Hahn, A.G., James, D.A., 2008. Classification of Aerial Acrobatics in Elite Half-Pipe Snowboarding Using Body Mounted Inertial Sensors. *Proc. 7th ISEA Conf.* 7, 447–456. doi:10.1007/978-2-287-09413-2\_55
- Harper, D.J., Kiely, J., 2018. Damaging nature of decelerations: Do we adequately prepare players? *BMJ Open Sport Exerc. Med.* 4, 1–3. doi:10.1136/bmjsem-2018-000379
- Harrison, R.N., Lees, A., McCullagh, P.J.J., Rowe, W.B., 1986. A bioengineering analysis of human muscle and joint forces in the lower limbs during running. *J. Sports Sci.* 4, 201–218. doi:10.1080/02640418608732119
- Hawkins, N.M., Virani, S.A., Sperrin, M., Buchan, I.E., McMurray, J.J.V., Krahn, A.D., 2016. Predicting heart failure decompensation using cardiac implantable electronic devices: a review of practices and challenges. *Eur. J. Heart Fail.* 18, 977–986. doi:10.1002/ejhf.458
- Heiderscheit, B.C., Chumanov, E.S., Michalski, M.P., Wille, C.M., Ryan, M.B., 2011. Effects of step rate manipulation on joint mechanics during running. *Med. Sci. Sports Exerc.* 43, 296–302. doi:10.1249/MSS.0b013e3181ebedf4
- Heise, G.D., Martin, P.E., 2001. Are variations in running economy in humans associated with ground reaction force characteristics? *Eur. J. Appl. Physiol.* 84, 438–442. doi:10.1007/s004210100394
- Heise, G.D., Martin, P.E., 1998. “Leg spring” characteristics and the aerobic demand of running. *Med. Sci. Sport. Exerc.* 30, 750–754.
- Hellard, P., Avalos, M., Lacoste, L., Barale, F., Chatard, J.C., Millet, G.P., 2006. Assessing the limitations of the Banister model in monitoring training. *J. Sports Sci.* 24, 509–520. doi:10.1080/02640410500244697
- Hobara, H., Kimura, K., Omuro, K., Gomi, K., Muraoka, T., Sakamoto, M., Kanosue, K., 2010. Differences in lower extremity stiffness between endurance-trained athletes and untrained subjects. *J. Sci. Med. Sport* 13, 106–111. doi:10.1016/j.jsams.2008.08.002

- 
- Hobara, H., Sato, T., Sakaguchi, M., Sato, T., Nakazawa, K., 2012. Step frequency and lower extremity loading during running. *Int. J. Sports Med.* 33, 310–313. doi:10.1055/s-0031-1291232
- Hollville, E., Couturier, A., Guilhem, G., Rabita, G., 2016. Minimaxx Player Load As an Index of the Center of Mass Displacement? a Validation Study. *ISBS - Conf. Proc. Arch.* 33, 608–611.
- Hopkins, W.G., Marshall, S.W., Batterham, A.M., Hanin, J., 2009. Progressive statistics for studies in sports medicine and exercise science. *Med. Sci. Sports Exerc.* 41, 3–12. doi:10.1249/MSS.0b013e31818cb278
- Hreljac, A., 2004. Impact and Overuse Injuries in Runners. *Med. Sci. Sport. Exerc.* 36, 845–849. doi:10.1249/01.MSS.0000126803.66636.DD
- Hreljac, A., Marshall, R.N., Hume, P.A., 2000. Evaluation of lower extremity overuse injury potential in runners. *Med. Sci. Sport. Exerc.* 32, 1635–1641.
- Hulin, B.T., Gabbett, T.J., Lawson, D.W., Caputi, P., Sampson, J.A., 2016. The acute: Chronic workload ratio predicts injury: High chronic workload may decrease injury risk in elite rugby league players. *Br. J. Sports Med.* 50, 231–236. doi:10.1136/bjsports-2015-094817
- Hunter, J., Marshall, R., McNair, P., 2005. Relationship between ground reaction force impulse and kinematics of sprint-running acceleration. *J. Appl. Biomech.* 21, 31–43. doi:10.1123/jab.21.1.31
- Impellizzeri, F.M., Rampinini, E., Coutts, A.J., Sassi, A., Marcora, S.M., 2004. Use of RPE-based training load in soccer. *Med. Sci. Sports Exerc.* 36, 1042–1047. doi:10.1249/01.MSS.0000128199.23901.2F
- Impellizzeri, F.M., Rampinini, E., Marcora, S.M., 2005. Physiological assessment of aerobic training in soccer. *J. Sports Sci.* 23, 583–92. doi:10.1080/02640410400021278
- Jamkrajang, P., Robinson, M.A., Limroongreungrat, W., Vanrenterghem, J., 2017. Can segmental model reductions quantify whole-body balance accurately during dynamic activities? *Gait Posture* 56, 37–41. doi:10.1016/j.gaitpost.2017.04.036
- Jobson, S.A., Passfield, L., Atkinson, G., Barton, G., Scarf, P., 2009. The analysis and utilisation of cycling training data. *Sport. Med.* 39, 833–844. doi:10.2165/11317840-000000000-00000
- Johnson, W.R., Alderson, J., Lloyd, D.G., Mian, A., 2018a. Predicting Athlete Ground Reaction Forces and Moments from Spatio-temporal Driven CNN Models. *IEEE Trans. Biomed. Eng.* doi:10.1109/TBME.2018.2854632
- Johnson, W.R., Mian, A., Donnelly, C.J., Lloyd, D., Alderson, J., 2018b. Predicting athlete ground reaction forces and moments from motion capture. *Med. Biol. Eng. Comput.* 56, 1781–1792. doi:https://doi.org/10.1007/s11517-018-1802-7
- Johnston, R.J., Watsford, M.L., Kelly, S.J., Pine, M.J., Spurr, R.W., 2014. Validity and Interunit Reliability of 10 Hz and 15 Hz GPS Units for Assessing Athlete Movement Demands. *J. Strength Cond. Res.* 28, 1649–1655. doi:10.1519/JSC.0000000000000323
- Jung, Y., Jung, M., Lee, K., Koo, S., 2014. Ground reaction force estimation using an insole-type pressure mat and joint kinematics during walking. *J. Biomech.* 47, 2693–2699. doi:10.1016/j.jbiomech.2014.05.007
- Karatsidis, A., Bellusci, G., Schepers, M.H., de Zee, M., Andersen, M.S., Veltink, P.H., 2017. Estimation of Ground Reaction Forces and Moments During Gait Using Only Inertial Motion Capture. *Sensors* 17, 1–22. doi:10.3390/s17010075
- Kavanagh, J.J., Menz, H.B., 2008. Accelerometry: A technique for quantifying movement

- 
- patterns during walking. *Gait Posture* 28, 1–15. doi:10.1016/j.gaitpost.2007.10.010
- Kelly, S.J., Murphy, A.J., Watsford, M.L., Austin, D., Rennie, M., 2015. Reliability and validity of sports accelerometers during static and dynamic testing. *Int. J. Sports Physiol. Perform.* 10, 106–111. doi:10.1123/ijsp.2013-0408
- Kerdok, A.E., Biewener, A.A., McMahon, T.A., Weyand, P.G., Herr, H.M., 2002. Energetics and mechanics of human running on surfaces of different stiffnesses. *J. Appl. Physiol.* 92, 469–478. doi:10.1152/jappphysiol.01164.2000
- Kibler, B.W., Chandler, J.T., Stracener, E.S., 1992. Musculoskeletal adaptations and injuries due to overtraining. *Exerc. Sport Sci. Rev.* 20, 99–126.
- Klute, G.K., Berge, J.S., 2004. Modelling the effect of prosthetic feet and shoes on the heel – ground contact force in amputee gait. *Eng. Med.* 218, 173–182.
- Koda, H., Sagawa, K., Kuroshima, K., Tsukamoto, T., Urita, K., Ishibashi, Y., 2010. 3D Measurement of Forearm and Upper Arm during Throwing Motion using Body Mounted Sensor. *J. Adv. Mech. Des. Syst. Manuf.* 4, 167–178. doi:10.1299/jamdsm.4.167
- Kugler, F., Janshen, L., 2010. Body position determines propulsive forces in accelerated running. *J. Biomech.* 43, 343–348. doi:10.1016/j.jbiomech.2009.07.041
- Kuitunen, S., Komi, P. V., Kyröläinen, H., 2002. Knee and ankle joint stiffness in sprint running. *Med. Sci. Sports Exerc.* 34, 166–173. doi:0195-9131/02/3401-0166
- Kyröläinen, H., Avela, J., Komi, P. V., 2005. Changes in muscle activity with increasing running speed. *J. Sports Sci.* 23, 1101–1109. doi:10.1080/02640410400021575
- Kyröläinen, H., Belli, A., Komi, P. V., 2001. Biomechanical factors affecting running economy. *Med. Sci. Sports Exerc.* 33, 1330–1337. doi:10.1097/00005768-200108000-00014
- Lafortune, A., 1991. Three-Dimensional Acceleration of the Tibia During Walking and Running. *J. Biomech.* 24, 877–886.
- Lafortune, M.A., Lake, M.J., Hennig, E.M., 1996. Differential shock transmission response of the human body to impact severity and lower limb posture. *J. Biomech.* 29, 1531–1537. doi:10.1016/0021-9290(96)00092-9
- Lai, D.T.H., Hetchl, M., Wei, X.C., Ball, K., McLaughlin, P., 2011. On the difference in swing arm kinematics between low handicap golfers and non-golfers using wireless inertial sensors. *Procedia Eng.* 13, 219–225. doi:10.1016/j.proeng.2011.05.076
- Lazzer, S., Salvadego, D., Taboga, P., Rejc, E., Giovanelli, N., Di Prampero, P.E., 2015. Effects of the Etna uphill ultramarathon on energy cost and mechanics of running. *Int. J. Sports Physiol. Perform.* 10, 238–247. doi:10.1123/ijsp.2014-0057
- Lieberman, D.E., Venkadesan, M., Werbel, W.A., Daoud, A.I., D’Andrea, S., Davis, I.S., Mang’Eni, R.O., Pitsiladis, Y., 2010. Foot strike patterns and collision forces in habitually barefoot versus shod runners. *Nature* 463, 531–536. doi:10.1038/nature08723
- Lindsay, T.R., Yaggie, J.A., McGregor, S.J., 2014. Contributions of lower extremity kinematics to trunk accelerations during moderate treadmill running. *J. Neuroeng. Rehabil.* 11, 162. doi:10.1186/1743-0003-11-162
- Liu, T., Inoue, Y., Shibata, K., 2010. A wearable ground reaction force sensor system and its application to the measurement of extrinsic gait variability. *Sensors* 10, 10240–10255. doi:10.3390/s101110240
- Liu, W., Nigg, B.M., 2000. A mechanical model to determine the influence of masses and mass distribution on the impact force during running. *J. Biomech.* 33, 219–224. doi:10.1016/S0021-9290(99)00151-7

- 
- Loundagin, L.L., Schmidt, T.A., Edwards, W.B., 2018. Mechanical Fatigue of Bovine Cortical Bone Using Ground Reaction Force Waveforms in Running. *J. Biomech. Eng.* 140, 031003-1-031003-5. doi:10.1115/1.4038288
- Lovell, T.W.J., Sirotic, A.C., Impellizzeri, F.M., Coutts, A.J., 2013. Factors affecting perception of effort (session rating of perceived exertion) during rugby league training. *Int. J. Sports Physiol. Perform.* 8, 62–69. doi:10.1123/ijsp.8.1.62
- Ly, Q.H., Alaoui, A., Erlicher, S., Baly, L., 2010. Towards a footwear design tool: Influence of shoe midsole properties and ground stiffness on the impact force during running. *J. Biomech.* 43, 310–317. doi:10.1016/j.jbiomech.2009.08.029
- Marsland, F., Lyons, K., Anson, J., Waddington, G., Macintosh, C., Chapman, D., 2012. Identification of cross-country skiing movement patterns using micro-sensors. *Sensors* 12, 5047–5066. doi:10.3390/s120405047
- McGregor, S.J., Busa, M.A., Yagie, J.A., Bollt, E.M., 2009. High resolution MEMS accelerometers to estimate VO<sub>2</sub> and compare running mechanics between highly trained inter-collegiate and untrained runners. *PLoS One* 4. doi:10.1371/journal.pone.0007355
- McGuigan, M.R., Foster, C., 2004. A New Approach to Monitoring Resistance Training. *Strength Cond. J.* 26, 42–47.
- McLaren, S.J., Macpherson, T.W., Coutts, A.J., Hurst, C., Spears, I.R., Weston, M., 2018. The Relationships Between Internal and External Measures of Training Load and Intensity in Team Sports: A Meta-Analysis. *Sport. Med.* 48, 641–658. doi:10.1007/s40279-017-0830-z
- McLean, B.D., Cummins, C., Conlan, G., Duthie, G., Coutts, A.J., 2018. The Fit Matters: Influence of Accelerometer Fitting and Training Drill Demands on Load Measures in Rugby League Players. *Int. J. Sports Physiol. Perform.* doi:10.1123/ijsp.2015-0012
- McMahon, T.A., 1987. The spring in the human foot. *Nature.* doi:10.1038/325108a0
- McMahon, T.A., Cheng, G.C., 1990. The mechanics of running: How does stiffness couple with speed? *J. Biomech.* 23, 65–78. doi:10.1016/0021-9290(90)90042-2
- McNamara, D.J., Gabbett, T.J., Chapman, P., Naughton, G., Farhart, P., 2015. The validity of microsensors to automatically detect bowling events and counts in cricket fast bowlers. *Int. J. Sports Physiol. Perform.* 10, 71–75. doi:10.1123/ijsp.2014-0062
- Meeusen, R., de Pauw, K., 2013. Overtraining syndrome, in: Hausswirth, C., Mujika, I. (Eds.), *Recovery for Performance in Sport.* Human Kinetics.
- Messier, S.P., Martin, D.F., Mihalko, S.L., Ip, E., DeVita, P., Cannon, D.W., Love, M., Beringer, D., Saldana, S., Fellin, R.E., Seay, J.F., 2018. A 2-Year Prospective Cohort Study of Overuse Running Injuries: The Runners and Injury Longitudinal Study (TRAILS). *Am. J. Sports Med.* 46, 2211–2221. doi:10.1177/0363546518773755
- Milner, C.E., Ferber, R., Pollard, C.D., Hamill, J., Davis, I.S., 2006. Biomechanical factors associated with tibial stress fracture in female runners. *Med. Sci. Sports Exerc.* 38, 323–328. doi:10.1249/01.mss.0000183477.75808.92
- Mitschke, C., Kiesewetter, P., Milani, T.L., 2018. The effect of the accelerometer operating range on biomechanical parameters: Stride length, velocity, and peak tibial acceleration during running. *Sensors* 18, 1–12. doi:10.3390/s18010130
- Mizrahi, J., Susak, Z., 1982. In-vivo elastic and damping response of the human leg to impact forces. *J. Biomech. Eng.* 104, 63–66. doi:10.1115/1.3138305
- Moore, I.S., 2016. Is There an Economical Running Technique? A Review of Modifiable Biomechanical Factors Affecting Running Economy. *Sport. Med.* 0. doi:10.1007/s40279-

- Moran, K., Richter, C., O'Connor, N.E., 2014. Letter to the editor regarding "Application of principal component analysis in clinical gait research" by Federolf and colleagues. *J. Biomech.* 47, 1554–1555. doi:10.1016/j.jbiomech.2014.01.057
- Morin, J.-B., Dalleau, G., Kyröläinen, H., Jeannin, T., Belli, A., 2005. A simple method for measuring stiffness during running. *J. Appl. Biomech.* 21, 167–180. doi:10.1519/JSC.0b013e318260edad
- Morin, J.B., Jeannin, T., Chevallier, B., Belli, A., 2006. Spring-mass model characteristics during sprint running: Correlation with performance and fatigue-induced changes. *Int. J. Sports Med.* 27, 158–165. doi:10.1055/s-2005-837569
- Morin, J.B., Samozino, P., Millet, G.Y., 2011. Changes in running kinematics, kinetics, and spring-mass behavior over a 24-h run. *Med. Sci. Sports Exerc.* 43, 829–836. doi:10.1249/MSS.0b013e3181fec518
- Morton, R.H., Fitz-Clarke, J.R., Banister, E.W., 1990. Modeling human performance in running. *J. Appl. Physiol.* 69, 1171–1177.
- Mujika, I., 2017. Quantification of training and competition loads in endurance sports: Methods and applications. *Int. J. Sports Physiol. Perform.* 12, 9–17. doi:10.1123/ijsp.2016-0403
- Mujika, I., 2013. The alphabet of sport science research starts with Q. *Int. J. Sports Physiol. Perform.* 8, 465–466. doi:10.1123/ijsp.8.5.465
- Munro, C.F., Miller, D.I., Fuglevand, A.J., 1987. Ground Reaction Forces in Running: A Reexamination. *J. Biomech.* 20, 147–155.
- Murray, A.M., Ryu, J.H., Sproule, J., Turner, A.P., Graham-Smith, P., Cardinale, M., 2017. A pilot study using entropy as a non-invasive predictor in running. *Int. J. Sports Physiol. Perform.* 12, 1119–1122. doi:10.1002/elan.
- Nagahara, R., Mizutani, M., Matsuo, A., Kanehisa, H., Fukunaga, T., 2017. Association of sprint performance with ground reaction forces during acceleration and maximal speed phases in a single sprint. *J. Appl. Biomech.* 1–20. doi:10.1123/jab.2016-0356
- Nagel, A., Fernholz, F., Kibele, C., Rosenbaum, D., 2008. Long distance running increases plantar pressures beneath the metatarsal heads. A barefoot walking investigation of 200 marathon runners. *Gait Posture* 27, 152–155. doi:10.1016/j.gaitpost.2006.12.012
- Napier, C., MacLean, C.L., Maurer, J., Taunton, J.E., Hunt, M.A., 2018. Kinetic Risk Factors of Running-Related Injuries in Female Recreational Runners. *Scand. J. Med. Sci. Sports* 0–2. doi:10.1111/sms.13228
- Nedergaard, N.J., 2017. Whole-body biomechanical load monitoring from accelerometry in team sports. PhD Thesis. Liverpool John Moores University, Liverpool.
- Nedergaard, N.J., Kersting, U., Lake, M., 2014. Using accelerometry to quantify deceleration during a high-intensity soccer turning manoeuvre. *J. Sports Sci.* 32, 1897–1905. doi:10.1080/02640414.2014.965190
- Nedergaard, N.J., Robinson, M.A., Eusterwiemann, E., Drust, B., Lisboa, P.J., Vanrenterghem, J., 2017. The relationship between whole-body external loading and body-worn accelerometry during team sports movement. *Int. J. Sports Physiol. Perform.* 12, 18–26.
- Nedergaard, N.J., Verheul, J., Drust, B., Etchells, T., Lisboa, P.J., Robinson, M.A., Vanrenterghem, J., 2018. The feasibility of predicting ground reaction forces during running from a trunk accelerometry driven mass-spring-damper model. *PeerJ* 6, e6105.
- Neugebauer, J.M., Collins, K.H., Hawkins, D.A., 2014. Ground reaction force estimates from

- 
- ActiGraph GT3X+ hip accelerations. *PLoS One* 9, e99023. doi:10.1371/journal.pone.0099023
- Nicolella, D.P., Torres-Ronda, L., Saylor, K.J., Schelling, X., 2018. Validity and reliability of an accelerometer-based player tracking device. *PLoS One* 13, 1–13. doi:10.1371/journal.pone.0191823
- Nigg, B., Baltich, J., Hoerzer, S., Enders, H., 2015. Running shoes and running injuries: mythbusting and a proposal for two new paradigms: ‘preferred movement path’ and ‘comfort filter.’ *Br. J. Sports Med.* 49, 1290–1294. doi:10.1136/bjsports-2015-095054
- Nigg, B.M., Bahlsen, H.A., Luethi, S.M., Stokes, S., 1987. The influence of running velocity and midsole hardness on external impact forces in heel-toe running. *J. Biomech.* 20, 951–959.
- Nigg, B.M., Liu, W., 1999. The effect of muscle stiffness and damping on simulated impact force peaks during running. *J. Biomech.* 32, 849–856. doi:10.1016/S0021-9290(99)00048-2
- Nigg, B.M., Wakeling, J.M., 2001. Impact forces and muscle tuning: a new paradigm. *Exerc. Sport Sci. Rev.* 29, 37–41. doi:10.1097/00003677-200101000-00008
- Nikooyan, A.A., Zadpoor, A.A., 2012. Effects of muscle fatigue on the ground reaction force and soft-tissue vibrations during running: A model study. *IEEE Trans. Biomed. Eng.* 59, 797–804. doi:10.1109/TBME.2011.2179803
- Nikooyan, A.A., Zadpoor, A.A., 2011. Mass-spring-damper modeling of the human body to study running and hopping: an overview. *Proc. Inst. Mech. Engineers Part H J. Eng. Med.* 225, 1121–1135. doi:10.1177/0954411911424210
- Nilsson, J., Thorstensson, A., 1989. Ground reaction forces at different speeds of human walking and running. *Acta Physiol. Scand.* 136, 217–227. doi:10.1111/j.1748-1716.1989.tb08655.x
- Noakes, T.D., 2000. Physiological models to understand exercise fatigue and the adaptations that predict or enhance athletic performance. *Scand. J. Med. Sci. Sports* 10, 123–145. doi:10.1034/j.1600-0838.2000.010003123.x
- Oh, S.E., Choi, A., Mun, J.H., 2013. Prediction of ground reaction forces during gait based on kinematics and a neural network model. *J. Biomech.* 46, 2372–2380. doi:10.1016/j.jbiomech.2013.07.036
- Ozgülven, H.N., Berme, N., 1988. An experimental and analytical study of impact forces during human jumping. *J. Biomech.* 21, 1061–6.
- Padulo, J., Vando, S., Chamari, K., Chaouachi, A., Bagnò, D., Pizzolato, F., 2015. Validity of the MarkWiiR for kinematic analysis during walking and running gaits. *Biol. Sport* 32, 53–58. doi:10.5604/20831862.1127282
- Page, R.M., Marrin, K., Brogden, C.M., Greig, M., 2015. Biomechanical and physiological response to a contemporary soccer match-play simulation. *J. Strength Cond. Res.* 29, 2860–2866.
- Pappas, P., Paradisis, G., Tsolakis, C., Smirniotou, A., Morin, J.-B., 2014a. Reliabilities of leg and vertical stiffness during treadmill running. *Sport. Biomech.* 13, 391–399. doi:10.1080/14763141.2014.981853
- Pappas, P., Paradisis, G., Tsolakis, C., Smirniotou, A., Morin, J.B., 2014b. Reliabilities of leg and vertical stiffness during treadmill running. *Sport. Biomech.* 13. doi:10.1080/14763141.2014.981853
- Paquette, M.R., Devita, P., Williams III, D.S.B., 2018. Biomechanical Implications of Training Volume and Intensity in Aging Runners. *Med. Sci. Sport. Exerc.* 50, 510–515.

---

doi:10.1249/MSS.0000000000001452

- Paquette, M.R., Melcher, D.A., 2017. Impact of a long run on injury-related biomechanics with relation to weekly mileage in trained male runners. *J. Appl. Biomech.* 33, 216–221. doi:10.1123/jab.2016-0170
- Park, J., Na, Y., Gu, G., Kim, J., 2016. Flexible insole ground reaction force measurement shoes for jumping and running. *Proc. IEEE RAS EMBS Int. Conf. Biomed. Robot. Biomechatronics 2016–July*, 1062–1067. doi:10.1109/BIOROB.2016.7523772
- Pavei, G., Seminati, E., Cazzola, D., Minetti, A.E., 2017a. On the estimation accuracy of the 3D body center of mass trajectory during human locomotion: Inverse vs. forward dynamics. *Front. Physiol.* 8, 1–13. doi:10.3389/fphys.2017.00129
- Pavei, G., Seminati, E., Storniolo, J.L.L., Peyré-Tartaruga, L.A., 2017b. Estimates of running ground reaction force parameters from motion analysis. *J. Appl. Biomech.* 33, 69–75. doi:10.1123/jab.2015-0329
- Peake, J.M., Kerr, G., Sullivan, J.P., 2018. A Critical Review of Consumer Wearables, Mobile Applications, and Equipment for Providing Biofeedback, Monitoring Stress, and Sleep in Physically Active Populations. *Front. Physiol.* 9, 1–9. doi:10.3389/fphys.2018.00743
- Perego, G.B., Landolina, M., Vergara, G., Lunati, M., Zanotto, G., Pappone, A., Lonardi, G., Speca, G., Iacopino, S., Varbaro, A., Sarkar, S., Hettrick, D.A., Denaro, A., 2008. Implantable CRT device diagnostics identify patients with increased risk for heart failure hospitalization. *J. Interv. Card. Electrophysiol.* 23, 235–242. doi:10.1007/s10840-008-9303-5
- Perrott, M.A., Pizzari, T., Cook, J., McClelland, J.A., 2017. Comparison of lower limb and trunk kinematics between markerless and marker-based motion capture systems. *Gait Posture* 52, 57–61. doi:10.1016/j.gaitpost.2016.10.020
- Pogson, M., Verheul, J., Robinson, M.A., Vanrenterghem, J., Lisboa, P.J., n.d. Estimating mechanical load in running activities: A neural network method to predict task- and step-specific ground reaction forces from trunk acceleration Under review.
- Polglaze, T., Dawson, B., Hiscock, D.J., Peeling, P., 2015. A comparative analysis of acceleromter and time motion data in elite mens hockey training and competition. *Int. J. Sports Physiol. Perform.* 10, 446–451. doi:10.1123/ijsp.2014-0233
- Python, 2017. Python Software Foundation, 2017, Python Language Reference, version 2.7. Available at <http://www.python.org>.
- Rabita, G., Dorel, S., Slawinski, J., Sàez-de-Villarreal, E., Couturier, A., Samozino, P., Morin, J.B., 2015. Sprint mechanics in world-class athletes: A new insight into the limits of human locomotion. *Scand. J. Med. Sci. Sports* 25, 583–594. doi:10.1111/sms.12389
- Ramirez-Bautista, J.A., Huerta-Ruelas, J.A., Chaparro-Cárdenas, S.L., Hernández-Zavala, A., 2017. A Review in Detection and Monitoring Gait Disorders Using In-Shoe Plantar Measurement Systems. *IEEE Rev. Biomed. Eng.* 10, 299–309. doi:10.1109/RBME.2017.2747402
- Rampinini, E., Alberti, G., Fiorenza, M., Riggio, M., Sassi, R., Borges, T.O., Coutts, A.J., 2015. Accuracy of GPS devices for measuring high-intensity running in field-based team sports. *Int. J. Sports Med.* 36, 49–53. doi:10.1055/s-0034-1385866
- Ramsay, J.O., Silverman, B.W., 1997. *Functional data analysis*. Springer, New York.
- Raper, D.P., Witchalls, J., Philips, E.J., Knight, E., Drew, M.K., Waddington, G., 2018. Use of a tibial accelerometer to measure ground reaction force in running: A reliability and validity comparison with force plates. *J. Sci. Med. Sport* 21, 84–88.

---

doi:10.1016/j.jsams.2017.06.010

- Reenalda, J., Maartens, E., Homan, L., Buurke, J.H., 2016. Continuous three dimensional analysis of running mechanics during a marathon by means of inertial magnetic measurement units to objectify changes in running mechanics. *J. Biomech.* 49, 3362–3367. doi:10.1016/j.jbiomech.2016.08.032
- Roetenberg, D., Luinge, H., Slycke, P., 2013. Xsens MVN: Full 6DOF Human Motion Tracking Using Miniature Inertial Sensors, Xsens Technologies. doi:10.1.1.569.9604
- Rosa, N., Simoes, R., Magalhães, F.D., Marques, A.T., 2015. From mechanical stimulus to bone formation: A review. *Med. Eng. Phys.* 37, 719–728. doi:10.1016/j.medengphy.2015.05.015
- Rowlands, A.V., Stiles, V.H., 2012. Accelerometer counts and raw acceleration output in relation to mechanical loading. *J. Biomech.* 45, 448–454. doi:10.1016/j.jbiomech.2011.12.006
- Ryan, W., Harrison, A., Hayes, K., 2006. Functional data analysis of knee joint kinematics in the vertical jump. *Sport. Biomech.* 5, 121–138. doi:10.1080/14763141.2006.9628228
- Santello, M., 2005. Review of motor control mechanisms underlying impact absorption from falls. *Gait Posture* 21, 85–94. doi:10.1016/j.gaitpost.2004.01.005
- Saunders, M., Inman, V.T., Eberhart, H.D., 1953. The major determinant in normal and pathological gait. *J. Bone Jt. Surg.* 35, 543–558. doi:10.1007/978-1-4471-5451-8\_102
- Saylor, K., Nicolella, D., Chambers, D., Swenson, B., 2017. Markerless biomechanics analysis for optimization of soldier physical performance. *J. Sci. Med. Sport* 20S, S119. doi:10.1016/j.jsams.2017.09.431
- Schütte, K.H., Maas, E.A., Exadaktylos, V., Berckmans, D., 2015. Wireless Tri-Axial Trunk Accelerometry Detects Deviations in Dynamic Center of Mass Motion Due to Running-Induced Fatigue 1–12. doi:10.1371/journal.pone.0141957
- Schwartz, M.H., Rozumalski, A., 2005. A new method for estimating joint parameters from motion data. *J. Biomech.* 38, 107–116. doi:10.1016/j.jbiomech.2004.03.009
- SciPy, 2017. SciPy 0.19.1, Available at <https://scipy.org>.
- Scott, B., Lockie, R., Knight, T., Clark, A., Janse de Jonge, X., 2013. A comparison of methods to quantify the in-season training load of professional soccer players. *Int. J. Sports Physiol. Perform.* 8, 195–202. doi:10.1111/j.1475-097X.2009.00899.x
- Scott, M.T.U., Scott, T.J., Kelly, V.G., 2015. The Validity and Reliability of Global Positioning Systems in Team Sport: A Brief Review. *J. Strength Cond. Res.* 30, 1470–1490. doi:10.1519/JSC.0000000000001221
- Scott, S.H., Winter, D.A., 1990. Internal forces at chronic running injury sites. *Med. Sci. Sport. Exerc.* 22, 357–369.
- Seel, T., Raisch, J., Schauer, T., 2014. IMU-Based Joint Angle Measurement for Gait Analysis. *Sensors* 14, 6891–6909. doi:10.3390/s140406891
- Seth, A., Hicks, J.L., Uchida, T.K., Habib, A., Dembia, C.L., Dunne, J.J., Ong, C.F., DeMers, M.S., Rajagopal, A., Millard, M., Hamner, S.R., Arnold, E.M., Yong, J.R., Lakshmikanth, S.K., Sherman, M.A., Ku, J.P., Delp, S.L., 2018. OpenSim: Simulating musculoskeletal dynamics and neuromuscular control to study human and animal movement. *PLoS Comput. Biol.* 14, e1006223. doi:10.1371/journal.pcbi.1006223
- Sheerin, K.R., Reid, D., Besier, T.F., 2019. The measurement of tibial acceleration in runners. A review of the factors that can affect tibial acceleration during running and evidence based

- 
- guidelines for its use. *Gait Posture* 67, 12–24. doi:10.1016/j.gaitpost.2018.09.017
- Shorten, M., Mientjes, M.I.V., 2011. The “heel impact” force peak during running is neither “heel” nor “impact” and does not quantify shoe cushioning effects. *Footwear Sci.* 3, 41–58. doi:10.1080/19424280.2010.542186
- Simons, C., Bradshaw, E.J., 2016. Reliability of accelerometry to assess impact loads of jumping and landing tasks. *Sport. Biomech.* 1–10. doi:10.1080/14763141.2015.1091032
- Soligard, T., Schweltnus, M., Alonso, J.M., Bahr, R., Clarsen, B., Dijkstra, H.P., Gabbett, T., Gleeson, M., Hägglund, M., Hutchinson, M.R., Janse Van Rensburg, C., Khan, K.M., Meeusen, R., Orchard, J.W., Pluim, B.M., Raftery, M., Budgett, R., Engebretsen, L., 2016. How much is too much? (Part 1) International Olympic Committee consensus statement on load in sport and risk of injury. *Br. J. Sports Med.* 50, 1030–1041. doi:10.1136/bjsports-2016-096581
- Sperlich, B., Düking, P., Holmberg, H.-C., 2017. A SWOT Analysis of the Use and Potential Misuse of Implantable Monitoring Devices by Athletes. *Front. Physiol.* 8, 1–3. doi:10.3389/fphys.2017.00629
- Sperlich, B., Holmberg, H.-C., 2016. Wearable, yes, but able...?: it is time for evidence-based marketing claims! *Br. J. Sports Med.* 51, 1240–1240. doi:10.1136/bjsports-2016-097295
- Stamm, A., James, D.A., Burkett, B.B., Hagem, R.M., Thiel, D. V., 2013. Determining maximum push-off velocity in swimming using accelerometers. *Procedia Eng.* 60, 201–207. doi:10.1016/j.proeng.2013.07.067
- Tao, W., Liu, T., Zheng, R., Feng, H., 2012. Gait analysis using wearable sensors. *Sensors* 12, 2255–2283. doi:10.3390/s120202255
- Taylor, M.J.D., Beneke, R., 2012. Spring mass characteristics of the fastest men on earth. *Int. J. Sports Med.* 33, 667–670. doi:10.1055/s-0032-1324404
- Theodor, M., Fiala, J., Ruh, D., Förster, K., Heilmann, C., Beyersdorf, F., Manoli, Y., Zappe, H., Seifert, A., 2014. Implantable accelerometer system for the determination of blood pressure using reflected wave transit time. *Sensors Actuators A Phys.* 206, 151–158. doi:10.1016/j.sna.2013.12.006
- Thompson, W., 2018. Worldwide Survey of Fitness Trends for 2019. *ACSMs. Health Fit. J.* 22, 10–17. doi:10.1249/FIT.0000000000000252
- Thompson, W.R., 2017. Worldwide Survey of Fitness Trends for 2018. *ACSMs. Health Fit. J.* 21, 10–19. doi:10.1249/FIT.0000000000000164
- Thompson, W.R., 2016. Worldwide Survey of Fitness Trends for 2017. *ACSMs. Health Fit. J.* 20, 8–17. doi:10.1249/FIT.0000000000000164
- Thompson, W.R., 2015. Worldwide Survey of Fitness Trends for 2016: 10th Anniversary Edition. *ACSMs. Health Fit. J.* 19, 9–18.
- Timmins, R.G., Shield, A.J., Williams, M.D., Lorenzen, C., Opar, D.A., 2016. Architectural adaptations of muscle to training and injury: a narrative review outlining the contributions by fascicle length, pennation angle and muscle thickness. *Br. J. Sports Med.* 50, 1467–1472. doi:10.1136/bjsports-2015-094881
- Tran, J., Netto, K.J., Aisbett, B., Gastin, P.B., 2010. Validation of accelerometer data for measuring impacts during jumping and landing tasks, in: *Proceedings of the 28th International Conference on Biomechanics in Sports.* pp. 1–4. doi:10.1675/1524-4695(2008)31
- Troiano, R.P., McClain, J.J., Brychta, R.J., Chen, K.Y., 2014. Evolution of accelerometer methods for physical activity research. *Br. J. Sports Med.* 48, 1019–1023.

---

doi:10.1136/bjsports-2014-093546

- Troje, N.F., 2002. Decomposing biological motion: A framework for analysis and synthesis of human gait patterns. *J. Vis.* 2, 371–387.
- Udofa, A.B., Clark, K.P., Ryan, L.J., Weyand, P.G., 2017. Does symmetry matter for speed? Study finds Usain Bolt may have asymmetrical running gait [WWW Document]. URL <http://blog.smu.edu/research/2017/06/27/does-symmetry-matter-for-speed-study-finds-usain-bolt-may-have-asymmetrical-running-gait/>
- Udofa, A.B., Ryan, L.J., Weyand, P.G., 2016. Impact Forces During Running: Loaded Questions, Sensible Outcomes, in: *IEEE 13th International Conference on Wearable and Implantable Body Sensor Networks (BSN)*. pp. 371–376.
- van der Worp, H., Vrieling, J.W., Bredeweg, S.W., 2016. Do runners who suffer injuries have higher vertical ground reaction forces than those who remain injury-free? A systematic review and meta-analysis. *Br. J. Sports Med.* 50, 450–7. doi:10.1136/bjsports-2015-094924
- van der Worp, M.P., ten Haaf, D.S.M., van Cingel, R., de Wijer, A., Nijhuis-van der Sanden, M.W.G., Staal, J.B., 2015. Injuries in Runners; A Systematic Review on Risk Factors and Sex Differences. *PLoS One* 10, e0114937. doi:10.1371/journal.pone.0114937
- Vanrenterghem, J., Gormley, D., Robinson, M., Lees, A., 2010. Solutions for representing the whole-body centre of mass in side cutting manoeuvres based on data that is typically available for lower limb kinematics. *Gait Posture* 31, 517–521. doi:10.1016/j.gaitpost.2010.02.014
- Vanrenterghem, J., Nedergaard, N.J., Robinson, M.A., Drust, B., 2017. Training Load Monitoring in Team Sports: A Novel Framework Separating Physiological and Biomechanical Load-Adaptation Pathways. *Sport. Med.* 47, 2135–2142. doi:10.1007/s40279-017-0714-2
- Varley, M.C., Fairweather, I.H., Aughey, R.J., 2012. Validity and reliability of GPS for measuring instantaneous velocity during acceleration, deceleration, and constant motion. *J. Sports Sci.* 30, 121–127. doi:10.1080/02640414.2011.627941
- Verhagen, E., Van Dyk, N., Clark, N., Shrier, I., 2018. Do not throw the baby out with the bathwater; Screening can identify meaningful risk factors for sports injuries. *Br. J. Sports Med.* 52, 1223–1224. doi:10.1136/bjsports-2017-098547
- Verheul, J., Clancy, A.C., Lake, M.J., 2017. Adjustments with running speed reveal neuromuscular adaptations during landing associated with high mileage running training. *J. Appl. Physiol.* 122, 653–665.
- Verheul, J., Gregson, W., Lisboa, P.J., Vanrenterghem, J., Robinson, M.A., 2018. Whole-body biomechanical load in running-based sports: The validity of estimating ground reaction forces from segmental accelerations. *J. Sci. Med. Sport.*
- Verheul, J., Nedergaard, N.J., Pogson, M., Lisboa, P.J., Gregson, W., Vanrenterghem, J., Robinson, M.A., 2019. Biomechanical loading during running: can a two mass-spring-damper model be used to evaluate ground reaction forces for high-intensity tasks? *Sport. Biomech.*
- Vigh-Larsen, J.F., Dalgas, U., Andersen, T.B., 2018. Position-Specific Acceleration and Deceleration Profiles in Elite Youth and Senior Soccer Players. *J. Strength Cond. Res.* 32, 1114–1122. doi:10.1519/JSC.0000000000001918
- Wakeling, J.M., Tschanner, V. Von, Nigg, B.M., Stergiou, P., 2001. Muscle activity in the leg is tuned in response to ground reaction forces. *J. Appl. Physiol.* 91, 1307–1317.

- 
- Walker, E.J., McAinch, A.J., Sweeting, A., Aughey, R.J., 2016. Inertial sensors to estimate the energy expenditure of team-sport athletes. *J. Sci. Med. Sport* 19, 177–181. doi:10.1016/j.jsams.2015.01.013
- Wallace, L.K., Slattery, K.M., Coutts, A.J., 2009. The Ecological Validity and Application of the Session-RPE Method for Quantifying Training Loads in Swimming. *J. Strength Cond. Res.* 23, 33–38.
- Wang, T., Lin, Z., Day, R.E., Gardiner, B., Landao-Bassonga, E., Rubenson, J., Kirk, T.B., Smith, D.W., Lloyd, D.G., Hardisty, G., Wang, A., Zheng, Q., Zheng, M.H., 2013. Programmable mechanical stimulation influences tendon homeostasis in a bioreactor system. *Biotechnol. Bioeng.* 110, 1495–1507. doi:10.1002/bit.24809
- Warmenhoven, J., Cogley, S., Draper, C., Harrison, A., Bargary, N., Smith, R., 2017. Considerations for the use of functional principal components analysis in sports biomechanics: examples from on-water rowing. *Sport. Biomech.* 1–25. doi:10.1080/14763141.2017.1392594
- Weaving, D., Marshall, P., Earle, K., Nevill, A., Abt, G., 2014. Combining Internal- and External-Training-Load Measures in Professional Rugby League. *Int. J. Sports Physiol. Perform.* 9, 905–912. doi:10.1123/ijspp.2013-0444
- Weston, M., 2018. Training load monitoring in elite English soccer: a comparison of practices and perceptions between coaches and practitioners. *Sci. Med. Footb.* 00, 1–9. doi:10.1080/24733938.2018.1427883
- Weston, M., 2013. Difficulties in Determining the Dose-Response Nature of Competitive Soccer Matches. *J. Athl. Enhanc.* 2, 1–2. doi:10.4172/2324-9080.1000e107
- Weston, M., Siegler, J., Bahnert, A., McBrien, J., Lovell, R., 2015. The application of differential ratings of perceived exertion to Australian Football League matches. *J. Sci. Med. Sport* 18, 704–708. doi:10.1016/j.jsams.2014.09.001
- Williams III, D.S.B., Green, D.H., Wurzinger, B., 2012. Changes in lower extremity movement and power absorption during forefoot striking and barefoot running. *Int. J. Sports Phys. Ther.* 7, 525–532.
- Willy, R.W., Buchenic, L., Rogacki, K., Ackerman, J., Schmidt, A., Willson, J.D., 2016. In-field gait retraining and mobile monitoring to address running biomechanics associated with tibial stress fracture. *Scand. J. Med. Sci. Sports* 26, 197–205. doi:10.1111/sms.12413
- Windt, J., Gabbett, T.J., 2017. How do training and competition workloads relate to injury? The workload—*injury aetiology model*. *Br. J. Sports Med.* 51, 428–435. doi:10.1136/bjsports-2016-096040
- Winter, D.A., 2009. *Biomechanics and Motor Control of Human Movement*, 4th ed. John Wiley & Sons, Inc., Hoboken, New Jersey.
- Winter, D.A., 1983. Moments of force and mechanical power in jogging. *J. Biomech.* 16, 91–97.
- Wisdom, K.M., Delp, S.L., Kuhl, E., 2015. Use it or lose it: multiscale skeletal muscle adaptation to mechanical stimuli. *Biomech. Model. Mechanobiol.* 14, 195–215. doi:10.1007/s10237-014-0607-3
- Wood, R.E., Hayter, S., Rowbottom, D., Stewart, I., 2005. Applying a mathematical model to training adaptation in a distance runner. *Eur. J. Appl. Physiol.* 94, 310–316. doi:10.1007/s00421-005-1319-2
- Wouda, F.J., Giuberti, M., Bellusci, G., Maartens, E., Reenalda, J., van Beijnum, B.-J.F., Veltink, P.H., 2018. Estimation of Vertical Ground Reaction Forces and Sagittal Knee

- 
- Kinematics During Running Using Three Inertial Sensors. *Front. Physiol.* 9, 1–14. doi:10.3389/fphys.2018.00218
- Wrigley, A.T., Albert, W.J., Deluzio, K.J., Stevenson, J.M., 2005. Differentiating lifting technique between those who develop low back pain and those who do not. *Clin. Biomech.* 20, 254–263. doi:10.1016/j.clinbiomech.2004.11.008
- Wundersitz, D.W.T., Gastin, P.B., Richter, C., Robertson, S.J., Netto, K.J., 2015a. Validity of a trunk-mounted accelerometer to assess peak accelerations during walking, jogging and running. *Eur. J. Sport Sci.* 15, 382–390. doi:10.1080/17461391.2014.955131
- Wundersitz, D.W.T., Gastin, P.B., Robertson, S.J., Davey, P.C., Netto, K.J., 2015b. Validation of a Trunk-mounted Accelerometer to Measure Peak Impacts during Team Sport Movements. *Int. J. Sports Med.* 36, 742–746. doi:10.1055/s-0035-1547265
- Wundersitz, D.W.T., Gastin, P.B., Robertson, S.J., Netto, K.J., 2015c. Validity of a trunk-mounted accelerometer to measure physical collisions in contact sports. *Int. J. Sports Physiol. Perform.* 10, 681–686. doi:10.1123/ijsp.2014-0381
- Wundersitz, D.W.T., Josman, C., Gupta, R., Netto, K.J., Gastin, P.B., Robertson, S.J., 2015d. Classification of team sport activities using a single wearable tracking device. *J. Biomech.* 48, 3975–3981. doi:10.1016/j.jbiomech.2015.09.015
- Wundersitz, D.W.T., Netto, K.J., Aisbett, B., Gastin, P.B., 2013. Validity of an upper-body-mounted accelerometer to measure peak vertical and resultant force during running and change-of-direction tasks. *Sport. Biomech.* 12, 403–412. doi:10.1080/14763141.2013.811284
- Zadpoor, A.A., Nikooyan, A.A., 2011a. The relationship between lower-extremity stress fractures and the ground reaction force: A systematic review. *Clin. Biomech.* 26, 23–28. doi:10.1016/j.clinbiomech.2010.08.005
- Zadpoor, A.A., Nikooyan, A.A., 2011b. The relationship between lower-extremity stress fractures and the ground reaction force: a systematic review. *Clin. Biomech.* 26, 23–8. doi:10.1016/j.clinbiomech.2010.08.005
- Zadpoor, A.A., Nikooyan, A.A., 2010. Modeling muscle activity to study the effects of footwear on the impact forces and vibrations of the human body during running. *J. Biomech.* 43, 186–193. doi:10.1016/j.jbiomech.2009.09.028
- Ziebart, C., Giangregorio, L.M., Gibbs, J.C., Levine, I.C., Tung, J., Laing, A.C., 2017. Measurement of peak impact loads differ between accelerometers – Effects of system operating range and sampling rate.pdf. *J. Biomech.* 58, 222–226.